

Development of “Smart” Particles for Silencing Anti-apoptotic Bcl-2 Protein Expression in Epithelial Cancer Cells

by

Yen-Ling Lin

**A dissertation submitted in partial fulfillment
of the requirements for the degree of
Doctor of Philosophy
(Biomedical Engineering)
in the University of Michigan
2013**

Doctoral Committee:

**Assistant Professor Mohamed E.H. ElSayed, Chair
Professor David Kohn
Professor Mary-Ann Mycek
Professor Jacques E. Nör**

© Yen-Ling Lin

2013

To my loving family,

Acknowledgements

First, I would like to thank my doctoral research advisor, Dr. Mohamed E.H. ElSayed for the training, support, and direction he provided throughout my doctoral education. I'd also like to thank Dr. Jacques E. Nör for the suggestions and experimental support he provided during our research collaboration. I would also like to acknowledge the contribution of Dr. Yasemin Yuksel Durmaz who performed the chemical synthesis work on the star-shaped polymer, and the work done by Dr. Guohua Jiang who synthesized the comb-like polymer described in this thesis. I would like to thank the rest of the members of the Cellular Engineering and Nano-Therapeutic laboratory, who provided their expertise, help, and support, allowing me to overcome the challenges I encountered during my doctoral research work. Finally, I would like to thank my friends, especially Dr. Hsing-Fang Hsieh and Dr. Chi-Shan Li, for the company and encouragement they provided.

Table of Contents

Dedication	ii
Acknowledgements	iii
List of Figures	x
List of Tables.....	xvi
Abstract.....	1
Chapter 1. Introduction.....	3
1.1 Introduction to small interfering RNA therapy.....	3
1.1.1 Basic concept and mechanism of small interfering RNA (siRNA)	4
1.1.2 Challenges for delivery of naked siRNA	4
1.1.2.1 Serum/nuclease instability	5
1.1.2.2 Non-specific tissue distribution	5
1.1.2.3 Poor cell uptake/internalization	6
1.1.3 Use of non-viral carriers in delivery of siRNA	6
1.1.3.1 Lipids.....	7
1.1.3.2 Polymers	8
1.1.4 Challenges and solutions for systematic administration	9
1.1.4.1 siRNA packaging	9
1.1.4.2 Stability of particulate carriers	9
1.1.4.3 Diffusion across the endothelial barrier	10
1.1.4.4 Cellular entry	11
1.1.4.4.1 Non-specific uptake.....	11
1.1.4.4.2 Targeted uptake.....	12
1.1.4.5 Endo-lysosomal entrapment and escape.....	13
1.1.4.6 Nucleic acid/vector dissociation	13
1.1.4.7 Effective RNA interference	14
Chapter 2. Background.....	19
2.1 Challenge in Endosomal/lysosomal escape	19
2.1.1 Mechanisms of endosomal escape.....	19

2.1.1.1	“Proton sponge” effect and carriers	19
2.1.1.1.1	Polyethylenimine (PEI)	20
2.1.1.1.2	Poly (amidoamine) (PAMAM) dendrimers.....	21
2.1.1.2	Amphiphilic membrane-destabilizing effect and carriers	22
2.1.1.2.1	Amphiphilic carriers.....	23
2.1.2	Limitations of current siRNA carriers	24
2.1.3	Structural requirements of an “ideal” polymeric carrier for <i>in vivo</i> siRNA delivery	25
2.1.4	Comparison between star-shaped polymers and other non-viral vectors.....	27
2.1.4.1	Polyethyleneimine-based carriers	27
2.1.4.2	Cyclodextrin-based carriers	28
2.2	Objective and Hypothesis	29
2.3	Specific aims	30
Chapter 3.	Degradable, pH-sensitive, membrane-destabilizing, comb-like polymers for intracellular delivery of nucleic acids	35
3.1	Introduction.....	35
3.2	Materials and methods.....	42
3.2.1	Materials.....	42
3.2.2	Synthesis of poly(ethyl acrylic acid-co-alkyl methyl acrylate) copolymers ...	42
3.2.3	Synthesis of poly(ethyl acrylic acid-co-butyl methacrylate)-b-N-acryloxy succinimide copolymers	45
3.2.4	Synthesis of poly(ethyl acrylic acid-co-alkyl methyl acrylate)-b-β-benzyl L-aspartate copolymers	46
3.2.5	Graft polymerization of HMA and TMAEMA monomers via hydrazone linkages	46
3.2.6	Characterization of the diblock backbone and comb-like grafts	47
3.2.7	Evaluation of the pH-dependent membrane-destabilizing activity of comb-like polymers.....	48
3.2.8	Formulation and characterization of “smart” particles	49
3.2.9	Culture of MCF-7 cells	49
3.2.10	Cellular uptake of “smart” particles.....	50
3.2.11	In vitro transfection of MCF-7 cells	50
3.2.12	Effect of serum and nuclease enzymes on stability of “smart” particles	51
3.3	Results and Discussion	52

3.3.1	Synthesis of degradable, pH-sensitive, membrane-destabilizing, comb-like polymers.....	52
3.3.2	Membrane-destabilizing activity of comb-like polymers	57
3.3.3	Formulation of “smart” particles	61
3.3.4	Membrane-destabilizing activity of “smart” particles	63
3.3.5	Characterization of “smart” particles.....	65
3.3.6	Uptake of “smart” particles into MCF-7 breast cancer cells.....	66
3.3.7	Effect of “smart” particles on GAPDH expression	67
3.3.8	Effect of serum and nuclease enzymes on “smart” particles.....	70
3.4	Conclusions.....	72
Chapter 4.	Smart, comb-like carriers for silencing Bcl-2 expression in epithelial cancer cells	77
4.1	Introduction.....	77
4.2	Experimental Section.....	81
4.2.1	Materials.....	81
4.2.2	Formulation and characterization of “smart” particles	81
4.2.3	Culture of HeLa and UM-SCC-17B cells	82
4.2.4	Cellular uptake of “smart” particles.....	82
4.2.5	In vitro evaluation of GAPDH knockdown in HeLa and UM-SCC-17B cells	82
4.2.6	In vitro evaluation of Bcl-2 protein knockdown in HeLa and UM-SCC-17B cells	83
4.2.7	In vitro evaluation of Bcl-2 mRNA knockdown in HeLa and UM-SCC-17B cells	84
4.3	Results.....	85
4.3.1	Formulation and characterization of “smart” particles	85
4.3.2	Uptake of “smart” particles into HeLa and UM-SCC-17B cells.....	86
4.3.3	Effect of “smart” particles on GAPDH expression	87
4.3.4	Effect of “smart” particles on Bcl-2 expression	89
4.4	Discussions	92
4.5	Conclusions.....	93
Chapter 5.	Development of degradable, pH-sensitive, star vectors for cytoplasmic delivery of nucleic acids	96
5.1	Introduction.....	96

5.2	Experimental Section.....	101
5.2.1	Synthesis and characterization of degradable, pH-sensitive, star-shaped polymers.....	101
5.2.2	Formulation and characterization of “smart” particles	101
5.2.3	Cell culture	102
5.2.4	Cellular uptake of “smart” particles.....	102
5.2.5	In vitro evaluation of “smart” particles	103
5.3	Results and Discussion	104
5.3.1	Synthesis of degradable, pH-sensitive, star-shaped polymers.....	104
5.3.2	Formulation of “smart” particles	107
5.3.3	Characterization of “smart” particles.....	111
5.3.4	Uptake of “smart” particles into HeLa cervical cancer cells.....	112
5.3.5	Effect of “smart” particles on GAPDH expression	113
5.3.6	Contribution of DMAEMA monomers to carrier’s transfection capacity	116
5.3.7	Cellular uptake and activity of P1/P2 particles in MCF-10A and UM-SCC-17B cells	119
5.4	Conclusions.....	123
Chapter 6.	Synergistic inhibition of anti-apoptotic Bcl-2 activity by smart, star-shaped vector and small molecule inhibitor in head & neck cancer cells	142
6.1	Introduction.....	142
6.2	Materials and Methods	145
6.2.1	Materials.....	145
6.2.2	Culture of UM-SCC-17B cells	146
6.2.3	<i>In vitro</i> evaluation of Bcl-2 protein knockdown in UM-SCC-17B cells	146
6.2.4	<i>In vitro</i> evaluation of Bcl-2 mRNA knockdown in UM-SCC-17B cells	147
6.2.5	Determination of IC ₂₅ , IC ₅₀ , and IC ₇₅ of AT-101	147
6.2.6	Cell growth after combination treatment	148
6.2.7	Cellular apoptosis after combination treatment.....	148
6.3	Results.....	149
6.3.1	Effect of “smart” particles on Bcl-2 expression	149
6.3.2	Determination of IC ₂₅ , IC ₅₀ , and IC ₇₅ of AT-101	150
6.3.3	Effect of AT-101 on cellular apoptosis and cell cycle.....	151
6.3.4	Effect of combination treatment on cell growth.....	153

6.3.5	Effect of combination treatment on cellular apoptosis	154
6.4	Discussion	156
6.4.1	Effect of “smart” particles on Bcl-2 expression	156
6.4.2	Effect of AT-101 on cellular apoptosis and cell cycle	157
6.4.3	Effect of combination treatment on cell growth, cellular apoptosis, and cell cycle	157
6.5	Conclusions	158
Chapter 7.	Conclusions & future direction	160
7.1	Conclusions	160
7.1.1	“Smart” pH-sensitive, comb-like polymers	160
7.1.2	“Smart” pH-sensitive, star-shaped polymers	161
7.2	Future directions	162
7.2.1	Development of EGFR-targeted, PEG- β CD-P(HMA-co-DMAEMA-co-TMAEMA) polymers	164
7.2.2	Development of GE-11-targeted, PEG- β CD-P(HMA-co-DMAEMA-co-TMAEMA) polymers with Bcl-2 small molecule inhibitor inclusion	165
7.2.3	<i>In vivo</i> evaluation of “smart” particles	166
Appendix I.	Quantitative evaluation of the effect of poly (amidoamine) dendrimers on the porosity of Caco-2 cell monolayers	169
I.1	Introduction	169
I.2	Methods	174
I.2.1	The relationship between porosity and the paracellular permeability across Caco-2 cell monolayers	174
I.2.2	Calculation of porosity and Renkin function of Caco-2 cell monolayers	175
I.2.3	Calculation of porosity and Renkin function of Caco-2 cell monolayers based on PAMAM-NH ₂ permeability	177
I.3	Results and Discussion	178
I.3.1	Calculation of effective porosity of Caco-2 cell monolayers based on mannitol permeability	178
I.3.2	Calculation of porosity of Caco-2 cell monolayers based on permeability of PAMAM-NH ₂ dendrimers	184
I.4	Conclusions	186
Appendix II.	Visualizing the attack of RNase enzymes on dendriplexes and naked siRNA using atomic force microscopy	190
II.1	Introduction	190

II.2	Experimental section	193
II.2.1	Materials	193
II.2.2	Formulation of Dendriplexes	194
II.2.3	AFM Imaging of Dendriplexes and Naked siRNA	194
II.3	Results.....	195
II.3.1	Formulation of G4 and G5 Dendriplexes	195
II.3.2	Effect of RNase Enzyme on Free siRNA	196
II.3.3	Effect of RNase Enzyme on G4 Dendriplexes	197
II.3.4	Effect of RNase Enzyme on G5 Dendriplexes	201
II.4	Discussion	204
II.5	Conclusions	206

List of Figures

Figure 1.1: The mechanism of RNA interference.	4
Figure 1.2: Chemical modifications of siRNA molecules.	5
Figure 1.3: Chemical structures of some common liposome reagents.	7
Figure 1.4: Chemical structure of poly (L-lysine) (PLL).	8
Figure 1.5: A schematic drawing shows the accumulation of non-viral vectors (purple) in the tumor tissue due to the diffusion across the leaky vasculature and the poor lymphatic drainage.	11
Figure 1.6: A schematic drawing shows (A) the degradation of free siRNA in the endosomal/lysosomal trafficking.	13
Figure 2.1: A schematic drawing shows the buffering capacity of poly (amidoamine) (PAMAM) dendrimers in acidic endosomal pH.	20
Figure 2.2: Chemical structure of (A) linear and (B) branched PEI.	21
Figure 2.3: Chemical structure of poly (amidoamine) (PAMAM) dendrimer.	22
Figure 2.4: Chemical structures of some common pH-sensitive amphiphilic polymers. ...	23
Figure 2.5: (A) Protonation of the pH-sensitive carboxyl groups of poly (ethyl acrylic acid) (PEAA) at acidic pH.	24
Figure 2.6: A schematic drawing shows the design of an ideal polymeric carrier, pH-sensitive star-shaped β -CD-P(HMA-co-DMAEMA-co-TMAEMA) _n polymers.	27
Figure 3.1: A schematic drawing comparing the cellular fate of: (A) free nucleic acid molecules (e.g. siRNA) and (B) “intelligent” particles encapsulating therapeutic siRNA molecules.	38
Figure 3.2: A schematic drawing showing the chemical structure of a degradable, pH-sensitive, membrane-destabilizing, comb-like polymer.	39
Figure 3.3: A schematic drawing showing the structure of a comb-like polymer, complexation of siRNA molecules into “smart” particles, their response to acidic pH, and fragmentation of the comb-like carrier.	41

Figure 3.4: Protocol for synthesis of poly(EAA- <i>co</i> -BMA)-b-NASI-g-(HMA- <i>co</i> -TMAEMA) comb-like polymer.	44
Figure 3.5: Protocol for synthesis of poly(EAA- <i>co</i> -BMA)-b-Asp-g-(HMA- <i>co</i> -TMAEMA) and poly(EAA- <i>co</i> -HMA)-b-Asp-g-(HMA- <i>co</i> -TMAEMA) comb-like polymers.	45
Figure 3.6: A plot correlating the change in the areas under the curve for the amount of parent (A) poly(EAA- <i>co</i> -BMA)-b-NASI-g-(HMA- <i>co</i> -TMAEMA), (B) poly(EAA- <i>co</i> -BMA)-b-Asp-g-(HMA- <i>co</i> -TMAEMA), and (C) poly(EAA- <i>co</i> -HMA)-b-Asp-g-(HMA- <i>co</i> -TMAEMA) comb-like polymers and the released poly(HMA- <i>co</i> -TMAEMA) fragments.....	57
Figure 3.7: The hemolytic activity of poly(EAA- <i>co</i> -BMA) (A & B) and poly(EAA- <i>co</i> -HMA) (C) copolymers.....	59
Figure 3.8: Hemolytic activity of (A) poly(EAA- <i>co</i> -BMA)-b-NASI-g-(HMA- <i>co</i> -TMAEMA), (B) poly(EAA- <i>co</i> -BMA)-b-Asp-g-(HMA- <i>co</i> -TMAEMA) and (C) poly(EAA- <i>co</i> -HMA)-b-Asp-g-(HMA- <i>co</i> -TMAEMA) comb-like polymers.....	61
Figure 3.9: Images of the 1% w/v agarose gels stained with SYBR Green II dye showing the electrophoretic mobility of free siRNA and the particles	63
Figure 3.10: The hemolytic activity of particles 1-3	65
Figure 3.11: The size (A) and zeta potential (B) of particles 1-3.....	66
Figure 3.12: The % of MCF-7 cells that internalized free siRNA molecules, particles 1-3, and siPORT amine-based complexes	67
Figure 3.13: The effect of particles 1-3 encapsulating 100 nM of anti-GAPDH siRNA (+) or a scrambled siRNA sequence (-) on GAPDH protein expression (A) and mRNA levels (B) in MCF-7 breast cancer cells	68
Figure 3.14: The effect of particle 1 prepared by complexation of poly(EAA- <i>co</i> -BMA)-b-NASI-g-(HMA- <i>co</i> -TMAEMA) comb-like polymers with 0.57 μ g of anti-GAPDH siRNA (+) or a scrambled siRNA sequence (-) at different N/P (+/-) ratios on GAPDH protein expression (A) and mRNA levels (B) in MCF-7 breast cancer cells	70
Figure 3.15: The change in the amount of siRNA molecules encapsulated within particles 1-3 upon incubation for 6 hours at 37 °C with 10% and 25% of fetal bovine serum (FBS) compared to the particles incubated in serum-free medium	71
Figure 3.16: Image of a 1% w/v agarose gel stained with SYBR Green II dye showing the electrophoretic mobility of free siRNA molecules (0.75 μ g) and an equal amount complexed with poly(EAA- <i>co</i> -BMA)-b-NASI-g-(HMA- <i>co</i> -TMAEMA) comb-like polymer at different N/P (+/-) ratios upon incubation with RNase V1 enzyme.	72

Figure 4.1: A schematic drawing showing (A) the chemical structure of a degradable, pH-sensitive, membrane-destabilizing, comb-like polymer.	80
Figure 4.2: The size and zeta potential of siPORT amine-based complexes and particles prepared by complexation of poly(EAA-co-BMA)-b-NASI-g-(HMA-co-TMAEMA) comb-like polymers with 1.14 μ g of anti-GAPDH siRNA.	85
Figure 4.3: Percentage of HeLa cervical cancer and UM-SCC-17B head and neck cancer cells that internalize siPORT amine-based complexes and “smart” nanoparticles	86
Figure 4.4: Effect of siPORT amine-based complexes and “smart” nanoparticles prepared by complexation of poly(EAA-co-BMA)-b-NASI-g-(HMA-co-TMAEMA) comb-like polymer with 1.14 μ g of the anti-GAPDH siRNA (+) or scrambled siRNA (-) at N/P (+/-) ratios of 2.5/1, 4/1, and 6/1 (A, B) or 5/1 (C, D) on GAPDH protein (A, C) and mRNA levels (B, D) in HeLa cervical cancer cells (A, B) and in UM-SCC-17B head and neck cancer cells (C, D).	89
Figure 4.5: Effect of siPORT amine-based complexes and “smart” nanoparticles prepared by complexation of poly(EAA-co-BMA)-b-NASI-g-(HMA-co-TMAEMA) comb-like polymer with 1.14 μ g of the anti-Bcl-2 siRNA (+) or scrambled siRNA (-) at N/P (+/-) ratios of 2.5/1 and 4/1 on Bcl-2 mRNA (A) and protein (B) levels after treatment for 48 hours in HeLa cervical cancer cells	91
Figure 4.6: Effect of “smart” nanoparticles prepared by complexation of poly(EAA-co-BMA)-b-NASI-g-(HMA-co-TMAEMA) comb-like polymer with 1.14 μ g of the anti-Bcl-2 siRNA (+) or scrambled siRNA (-) at an N/P (+/-) ratio of 2.5/1 on Bcl-2 mRNA (A) and protein (B) levels at 48, 72, and 96 hours in UM-SCC-17B head and neck cancer cells	91
Figure 5.1: (A) Structure of pH-sensitive star-shaped β -CD-P(HMA-co-DMAEMA-co-TMAEMA) _n polymers.	100
Figure 5.2: Hydrolysis of hydrazone linkages incorporated in β -CD-1 to β -CD-4 polymers when dissolved in PBS (pH 5.8) and incubated at 37 °C.....	106
Figure 5.3: Images of the 1% w/v agarose gel containing ethidium bromide showing the electrophoretic mobility of free siRNA and the particles prepared by complexation of β CD-1 to β CD-8 (A-H) polymers with anti-GAPDH siRNA (0.7 μ g) at different N/P(+/-) ratios.	110
Figure 5.4: Size (A) and surface charge (B) of “smart” particles (P1-P8) prepared by complexation of β -CD-1 to β -CD-8 star polymers with anti-GAPDH siRNA (10.3 μ g) at N/P (+/-) ratios of 2.5/1 and 4/1.	111
Figure 5.5: Percentage of fluorescently-labeled HeLa cancer cells after incubating for 6 hours in a serum-free culture medium with free siRNA, siPORT amine-based complexes, and “smart” P1-P8 particles prepared by complexation of β -CD-1 to β -CD-8 polymers	

with FAM-labeled anti-GAPDH siRNA (1.14 μg) at N/P ratios of 1.5/1, 2.5/1, and 4/1. 112

Figure 5.6: Effect of “smart” particles (P1-P8) and siPORTamine-based complexes encapsulating 200 nM of (+) anti-GAPDH siRNA or (-) a scrambled siRNA sequence on GAPDH protein expression in HeLa cervical cancer cells 114

Figure 5.7: Effect of P1-DMAEMA, P1-TMAEMA, and P2-TMAEMA particles loaded with 1.14 μg of (+) anti-GAPDH siRNA or (-) a scrambled siRNA sequence on GAPDH protein (A) and mRNA (B) levels in HeLa cervical cancer cells..... 119

Figure 5.8: Percentage of fluorescently-labeled MCF-10A (A) and UM-SCC-17B (B) cells that internalize free FAM-labeled anti-GAPDH siRNA molecules, “smart” P1-P2 particles encapsulating FAM-labeled anti-GAPDH siRNA, and siPORT amine-based complexes upon incubation for 6 hours in a serum-free culture medium 121

Figure 6.1: A schematic drawing shows the “smart” particles encapsulating anti-Bcl-2 siRNA molecules and the hydrolysis of acid-labile hydrazone linkages in the endosome, leading to the fragmentation of the membrane-active P(HMA-co-TMAEMA) grafts, rupture of the endosomal membrane, and release of the siRNA cargo into the cytoplasm of cancer cells to knockdown Bcl-2 expression and trigger apoptosis of cancer cells.... 144

Figure 6.2: Effect of “smart” nanoparticles prepared by complexation of β -CD-P(HMA-co-DMAEMA-co-TMAEMA)_{4.8} star-shaped polymer with 0.57 μg of the anti-Bcl-2 siRNA (+) or scrambled siRNA (-) at an N/P (+/-) ratio of 2.5/1 on Bcl-2 mRNA (A) and protein (B) levels at 48 and 72 hours in UM-SCC-17B head and neck cancer cells.. 150

Figure 6.3: Determination of IC₂₅, IC₅₀, and IC₇₅ of Bcl-2 small molecule inhibitor, AT-101, at 48 (A) and 72 (B) hours in UM-SCC-17B head and neck cancer cells 151

Figure 6.4: Effect of AT-101 treatment on cellular apoptosis at 48 and 72 hours in UM-SCC-17B head and neck cancer cells 152

Figure 6.5: Effect of AT-101 and “smart” nanoparticles prepared by complexation of β -CD-P(HMA-co-DMAEMA-co-TMAEMA)_{4.8} star-shaped polymer with 0.57 μg of the anti-Bcl-2 siRNA (+) or scrambled siRNA (-) at an N/P (+/-) ratio of 2.5/1 on cell survival at 48 and 72 hours in UM-SCC-17B head and neck cancer cells..... 154

Figure 6.6: Effect of AT-101 and “smart” nanoparticles prepared by complexation of β -CD-P(HMA-co-DMAEMA-co-TMAEMA)_{4.8} star-shaped polymer with 0.57 μg of the anti-Bcl-2 siRNA (+) or scrambled siRNA (-) at an N/P (+/-) ratio of 2.5/1 on apoptosis at 48 and 72 hours in UM-SCC-17B head and neck cancer cells 155

Figure 7.1: Schematic drawing showing PEGylated β CD-P(HMA-co-DMAEMA-co-TMAEMA) polymers. 163

Figure 7.2: Schematic drawing showing targeted, PEG- β CD-P(HMA-co-DMAEMA-co-TMAEMA) polymers. 163

Figure 7.3: Schematic drawing showing AT-101-loaded (dark green), targeted, PEG- β CD-P(HMA-co-DMAEMA-co-TMAEMA) polymers.	166
Figure I.1: Schematic drawing showing the tree-like branching architecture of G0-G2 of PAMAM-NH ₂ dendrimers.	170
Figure I.2: Relationship between the porosity $\frac{\varepsilon}{\delta} F(\frac{r}{R})$ of unperturbed Caco-2 cell monolayers (♦) and those incubated with 0.1 mM (■), 1.0 mM (▲) and 10 mM (●) of PAMAM-NH ₂ (G0-G4) dendrimers and the incubation time.	180
Figure I.3: Relationship between the porosity $\frac{\varepsilon}{\delta} F(\frac{r}{R})$ of unperturbed Caco-2 cell monolayers (♦) and those incubated with 0.1 mM (■), 1.0 mM (▲) and 10 mM (●) of PAMAM-COOH (G-0.5-G4.5) dendrimers and the incubation time.	182
Figure I.4: Relationship between the porosity $\frac{\varepsilon}{\delta} F(\frac{r}{R})$ of unperturbed Caco-2 cell monolayers (♦) and those incubated with 0.1 mM (■), 1.0 mM (▲) and 10 mM (●) of PAMAM-OH (G2-G4) dendrimers and the incubation time.	184
Figure I.5: Relationship between the porosity $\frac{\varepsilon}{\delta} F(\frac{r}{R})$ of unperturbed Caco-2 cell monolayers (♦) and those incubated with 1.0 mM (■) and 10 mM (●) of PAMAM-NH ₂ (G0-G2) dendrimers and the incubation time.	186
Figure II.1: Image of the 1% w/v agarose gel stained with ethidium bromide showing the electrophoretic mobility of free siRNA, free G4 and G5 dendrimers, and the particles prepared by mixing G4 and G5 dendrimers with 0.7 μ g of anti-GAPDH siRNA at an N/P (+/-) ratio of 2/1 for 20 minutes or 24 hours.	195
Figure II.2: (A) AFM image of free anti-GAPDH siRNA dissolved in 1mM PBS containing 2mM MgCl ₂ after adding to the surface of freshly cleaved mica, which shows rod-, sphere-, and bead-like arrangements.	197
Figure II.3: (A) AFM image of hexagonal G4 dendriplexes prepared by mixing of G4 dendrimers with 0.7 μ g of anti-GAPDH siRNA at N/P ratio of 2/1 for 20 minutes at room temperature before loading onto the surface of freshly cleaved mica.	199
Figure II.4: (A) AFM image of G4 dendriplexes prepared by mixing of G4 dendrimers with 0.7 μ g of anti-GAPDH siRNA at N/P ratio of 2/1 for 24 hours at room temperature before loading onto the surface of freshly cleaved mica.	201
Figure II.5: (A) AFM image of hexagonal G5 dendriplexes prepared by mixing of G5 dendrimers with 0.7 μ g of anti-GAPDH siRNA at N/P ratio of 2/1 for 20 minutes at room temperature before loading onto the surface of freshly cleaved mica.	203

Figure II.6: (A) AFM image of G5 dendriplexes prepared by mixing of G5 dendrimers with 0.7 μg of anti-GAPDH siRNA at N/P ratio of 2/1 for 24 hours at room temperature before loading onto the surface of freshly cleaved mica.204

List of Tables

Table 3.1: Composition of new degradable, pH-sensitive, membrane-destabilizing, comb-like polymers	54
Table 5.1: Composition of the degradable, pH-sensitive, star-shaped β -CD-based vectors	105
Table 6.1: Cell cycle distribution and mitotic index of UM-SCC-17B cells after treatment with AT-101	153
Table 6.2: Cell cycle distribution and mitotic index of UM-SCC-17B cells after combination treatment with AT-101 and “smart” particles encapsulating anti-Bcl2 (+) or scrambled (-) siRNA molecules	156
Table I.1: The physicochemical properties of mannitol and PAMAM dendrimers.	172

Abstract

Development of “Smart” Particles for Silencing Anti-apoptotic Bcl-2 Protein Expression in Epithelial Cancer Cells

by

Yen-Ling Lin

Chair: Mohamed E.H. ElSayed

B-cell lymphoma 2 (Bcl-2) is an anti-apoptotic protein that is over-expressed in head and neck cancer cells and results in increased radio- and chemo-resistance. Short interfering RNA (siRNA) inhibits Bcl-2 expression causing enhanced cancer cell death and reduction of tumor growth. Transforming anti-Bcl-2 siRNA into a viable therapy with a defined dosage regimen requires a biocompatible carrier that can shuttle a large dose of siRNA into the cytoplasm of cancer cells. This dissertation describes the development of degradable, pH-sensitive, membrane-destabilizing, comb- and star-shaped polymers to condense anti-Bcl-2 siRNA into “smart” nanoparticles, which bypassed the endosomal membrane and delivered the cargo into the cytoplasm of cancer cells resulting in efficient

knockdown of Bcl-2 gene expression. Specifically, comb-like polymers were synthesized by grafting copolymers of cationic trimethyl aminoethyl methacrylate (TMAEMA) and hydrophobic hexyl methacrylate (HMA) monomers from a diblock linear backbone via acid-labile hydrazone linkages. Similarly, β -cyclodextrin (β -CD) was used as a core to synthesize star-shaped polymers where pH-sensitive dimethyl aminoethyl methacrylate (DMAEMA) and hydrophobic HMA monomers were grafted from the secondary face of β -CD via hydrazone linkages to form β -CD-P(HMA-co-DMAEMA) polymers. Both comb- and star-shaped polymers condensed siRNA molecules into “smart” particles that were stable at physiologic pH but rapidly degraded into membrane-active fragments in acidic endosomal pH. We systematically evaluated the effect of hydrophobic/hydrophilic balance (HMA/DMAEMA ratio), percentage of DMAEMA monomers quaternized into TMAEMA, and molecular weight of grafts on the ability of star polymers to achieve functional delivery of anti-Bcl-2 siRNA. Results show that star-shaped polymers incorporating P(HMA-co-DMAEMA-co-TMAEMA) grafts with the MW of 25 kDa, 50/50 HMA/DMAEMA monomers, and 50% of DMAEMA monomers transformed to TMAEMA exhibit the highest transfection efficiency. These star-shaped polymers delivered anti-Bcl-2 siRNA into UM-SCC-17B cells causing 50-75% reduction in Bcl-2 mRNA and protein levels. Further, combining “smart” particles loaded with anti-Bcl-2 siRNA with AT-101(a Bcl-2 small molecule inhibitor) synergistically inhibited the proliferation of cancer cells by 63% while increasing cancer cell apoptosis by 12-14%. These results confirm the successful development of a new family of degradable, pH-sensitive, membrane-destabilizing star-shaped polymers that enhance the cytoplasmic delivery of anti-Bcl-2 siRNA into head and neck cancer cells.

Chapter 1.

Introduction

1.1 Introduction to small interfering RNA therapy

Gene therapy by using plasmid DNA (pDNA), antisense oligodeoxynucleotide (ASODN), and small interfering RNA (siRNA) to regulate specific gene expression has been considered a potential method to treat genetic diseases,¹ viral infections,² or cancer³ for decades. Among them, siRNA has recently been intensively studied due to its physical stability⁴ and reduced possible adverse gene alteration.^{3a} The therapeutic potential of siRNA has been demonstrated both *in vitro* and *in vivo*.⁵ Recent progress in siRNA-based clinical trials, including treatment of age-related macular degeneration (AMD),⁶ respiratory syncytial virus infection,⁷ and solid tumors⁸ further proved that the use of siRNA molecules is an applicable method for treatment of diseases. However, so far there is still no FDA-approved siRNA-based therapeutic product, which is mostly due to the difficulties in the systemic delivery of siRNA molecules to target site. Therefore, numerous studies have focused on the design and development of carriers that can encapsulate siRNA molecules into stable particles and achieve efficient targeted siRNA delivery *in vivo*.

1.1.1 Basic concept and mechanism of small interfering RNA (siRNA)

RNA interference (RNAi) by long double-stranded RNA (dsRNA) (> 30 bp) is a natural biological mechanism, which was demonstrated in a variety of organisms, including *Caenorhabditis elegans*,⁹ insects,¹⁰ plants,¹¹ and mammalian cells.¹² It was found that in cytoplasm, the long dsRNA molecules are processed into small 21-23 nucleotide duplex by the cleavage of RNase III enzyme Dicer (Figure 1.1).^{12b} The resulting small interfering RNA (siRNA) molecules are then incorporated into the RNA-induced silencing complex

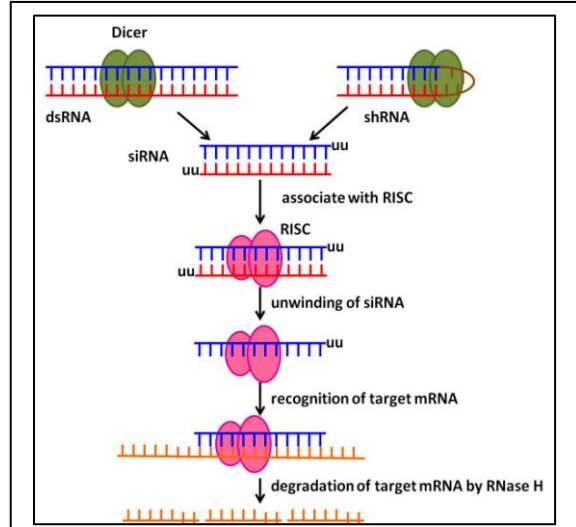


Figure 1.1: The mechanism of RNA interference. In the cytoplasm, long double-stranded RNA (dsRNA) and small hairpin RNA (shRNA) molecules are cleaved into small interfering RNA (siRNA) by the enzyme Dicer. The siRNA duplex is then incorporated with the RNA-induced silencing complex (RISC) and unwound into two single-stranded RNA (ssRNA). The anti-sense strand RNA guides the activated RISC binding to the complementary mRNA and degrading it, which leads to the silencing of the target gene.

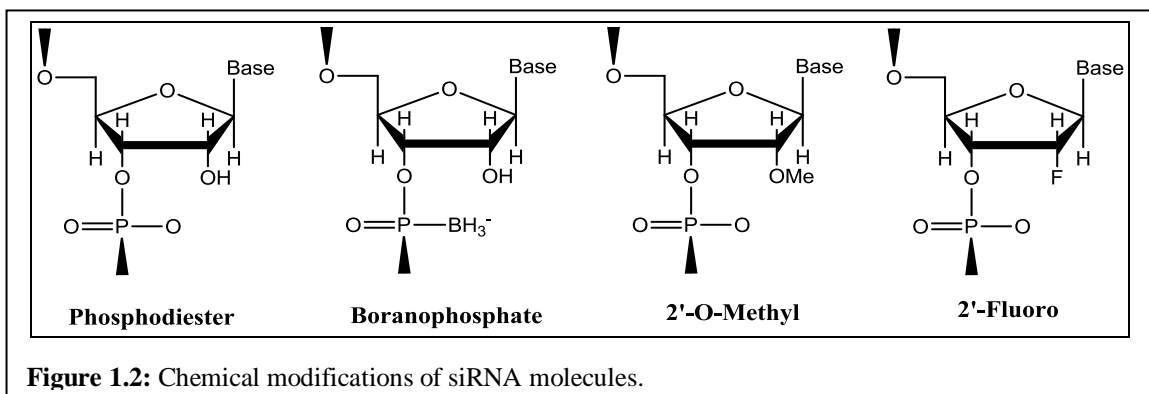
(RISC) and unwound into two single-stranded RNA (ssRNA). The sense strand ssRNA is then degraded and the activated RISC containing anti-sense ssRNA is guided to the complementary mRNA sequences and degrade target mRNA.¹³ The translation of specific protein is, therefore, inhibited.

1.1.2 Challenges for delivery of naked siRNA

Although siRNA-based therapy has been considered a promising therapeutic strategy, there are many difficulties in efficient delivery of naked siRNA molecules to the cytoplasm of target cells, owing to their low stability, non-specific tissue penetration, and poor cellular uptake.

1.1.2.1 Serum/nuclease instability

Naked siRNA molecules are highly susceptible to endogenous nuclease degradation in the serum.¹⁴ Previous studies showed that the half life of unprotected siRNAs is less than 10 minutes *in vivo*.¹⁵ To improve the stability of siRNA molecules *in vivo*, the chemical modification of siRNA has been investigated.¹⁶ Replacement of the non-bridging oxygen by a borane in siRNA becomes boranophosphate siRNA (**Figure 1.2**), which proved to be 10 times more resistant to nuclease degradation than unmodified siRNAs.¹⁷ Modification of siRNA sugar moiety at the 2' position of the ribose by linkage of O-methyl (2'-OMe) and fluoro (2'-F) (**Figure 1.2**) also showed increased plasma stability and nuclease resistancy.¹⁸ However, this increase in stability did not necessary translate into enhanced gene silencing activity in mice.¹⁹ In addition, the degradation of modified siRNA molecules may produce unsafe products in the body.



1.1.2.2 Non-specific tissue distribution

Effective siRNA-based treatment relies on the delivery of therapeutic siRNA molecules into target tissue sites. Local, direct delivery of naked siRNAs to the eye, lung, and central nervous system has been successfully tested in several studies.^{3a,20} For example, local injection of siRNA molecules targeting the vascular endothelial growth factor (VEGF) into the eye has been proved to be effective for the treatment of age-related

macular degeneration (AMD) by reducing the ocular neovascularization.²¹ Intranasal injection of siRNA targeting respiratory syncytial virus (RSV) has also been investigated for the treatment of RSV infection.²² However, majority of the treatments requires systematic delivery of siRNAs to target tissues deep within the body without uptake and clearance by non-target tissues. Previous studies have shown radio-labeled siRNA molecules rapidly accumulated in the kidney and liver after intravenous (IV) injection,²³ and then were rapidly cleared from the body through renal excretion and the reticuloendothelial system.¹⁴

1.1.2.3 Poor cell uptake/internalization

siRNA molecules are negatively charged, hydrophilic macromolecules,²⁴ so it is difficult for them to cross cellular membrane into the cytoplasm of target cells and induce effective gene inhibition.²⁵ Previous studies showed that siRNAs can access the cytoplasm by hydrodynamic injection, where large amount of siRNA molecules were rapidly injected into the body to induce transient damage to cell membranes in highly vascularized organs.²⁶ However, this method is highly dangerous and not applicable for human use. So far, no evidence shows that naked siRNA molecules can be efficiently internalized into cells after conventional IV injection.

1.1.3 Use of non-viral carriers in delivery of siRNA

In order to transform siRNA molecules into the therapeutic agents for disease treatment, therefore, we need to develop effective delivery systems, which can (i) encapsulate siRNAs into nuclease- and serum-stable particles, (ii) preferentially accumulate in diseased tissue, (iii) be efficiently taken up by target cells, and (iv) release siRNA cargo into the cytoplasm.²⁷ Although viral vectors, such as retrovirus²⁸ and adenovirus,²⁹ have

been proved to exhibit high efficiency in transferring nucleic acids into various mammalian cells. Their toxicity, immunogenicity, and high cost still remain the chief concerns, which limit their clinic application.³⁰ As a result, development of non-viral delivery systems using lipids and polymers is emerging as an alternative strategy to replace viral vectors.

1.1.3.1 Lipids

Cationic lipids have become commonly used transfection reagents for gene delivery since N-[1-(2, 3-dioleoyloxy)propyl]-N,N,N-trimethylammonium chloride (DOTMA) (**Figure 1.3**) was first used to deliver DNA molecules into cells in 1987.³¹ The cationic lipids have a cationic hydrophilic head group which is attached to a lipid hydrophobic moiety through a linker. Their amphiphilic structure allows them to spontaneously form lipid bilayers when they are dispersed in an aqueous solution. Mixture of negatively charged nucleic acids with cationic lipids spontaneously leads to the formation of lipoplexes through electrostatic interaction. Among the numerous cationic lipids that have been developed, 1,2-dioleoyl-3-trimethylammonium-propane (DOTAP) (**Figure 1.3**) showed high transfection efficiency and low toxicity, so it became one of the most widely used lipids.³²

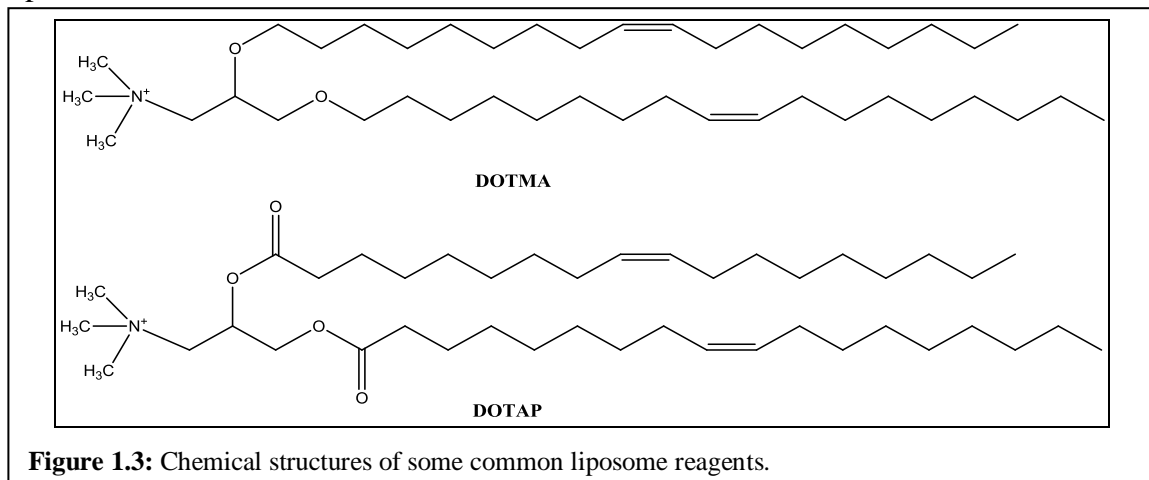
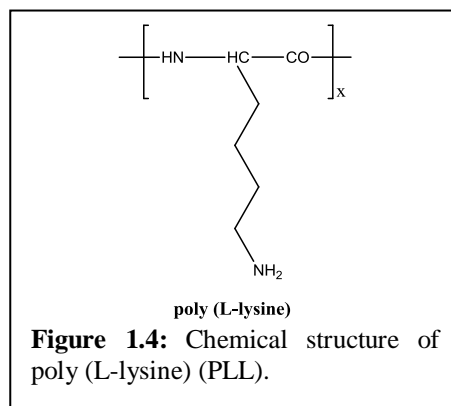


Figure 1.3: Chemical structures of some common liposome reagents.

Previous studies also showed that lipoplexes composed of DOTAP and cholesterol exhibited enhanced transfection efficiency and reduced serum degradation compared to conventional lipoplexes.³³ In addition, delivery of siRNA against hepatitis B virus (HBV) by using liver-targeted DOTAP/cholesterol lipoplexes through IV administration proved to show specific accumulation in liver and functional suppression in viral protein expression *in vivo*.³⁴ However, recent studies also reported that many cationic lipids can induce the occurrence of systemic immune responses possibly due to their surface charge.³⁵ The safety of lipid-based delivery systems needs to be further investigated and improved.

1.1.3.2 Polymers

Cationic polymers are commonly used in the intracellular delivery of siRNA molecules because they can easily form polyplexes through the electrostatic interaction. Polymeric carriers can be specifically designed and synthesized for the proposed application by the control of molecular weight, modification of functional group, and conjugation of targeting ligands, etc.³⁶ Their manufacture process is relatively easy and cheap compared to other viral and lipid vectors. Poly (L-lysine) (PLL) (**Figure 1.4**) is a cationic biodegradable polymer that has been used for non-viral gene delivery for many years due to their excellent condensing ability with anionic nucleic acids.³⁷ A varieties of PLL derivatives have been synthesized to improve stability, decrease toxicity,



and increase half-life *in vivo*.^{37a,b,38} For example, previous studies proved that graft of hydrophilic poly (ethylene glycol) (PEG) to PLL significantly increased the circulation time of the encapsulated siRNA molecules and their accumulation in tumor tissues *in vivo*.³⁸ However, PLL-based polyplexes cannot escape from endosomal/lysosomal trafficking³⁹ and rapidly release siRNA molecules to cytoplasm, so their transfection efficiency is relatively low and they are inapplicable to clinical applications.⁴⁰

1.1.4 Challenges and solutions for systematic administration

1.1.4.1 siRNA packaging

Among the numerous requirements to be addressed in the development of a safe and effective siRNA delivery system, the first is the packaging of siRNA molecules. The system should have the ability to (i) prevent charge repulsion between negatively charged siRNA duplexes and cell surface membrane by neutralization of siRNAs, (ii) shield the siRNA molecules from serum protein and nuclease degradation, and (iii) condense the siRNA molecules into nano-sized particles and facilitate their internalization into target cells.^{14,41} Due to the anionic nature of siRNA molecules, cationic lipids and polymers can easily complex siRNAs into stable particles through electrostatic interaction. These particles usually carry positive surface charge, which allows them to be taken up by cells through adsorptive endocytosis. This complexation also limits the access of nuclease enzymes to siRNA molecules and prevents the degradation.⁴²

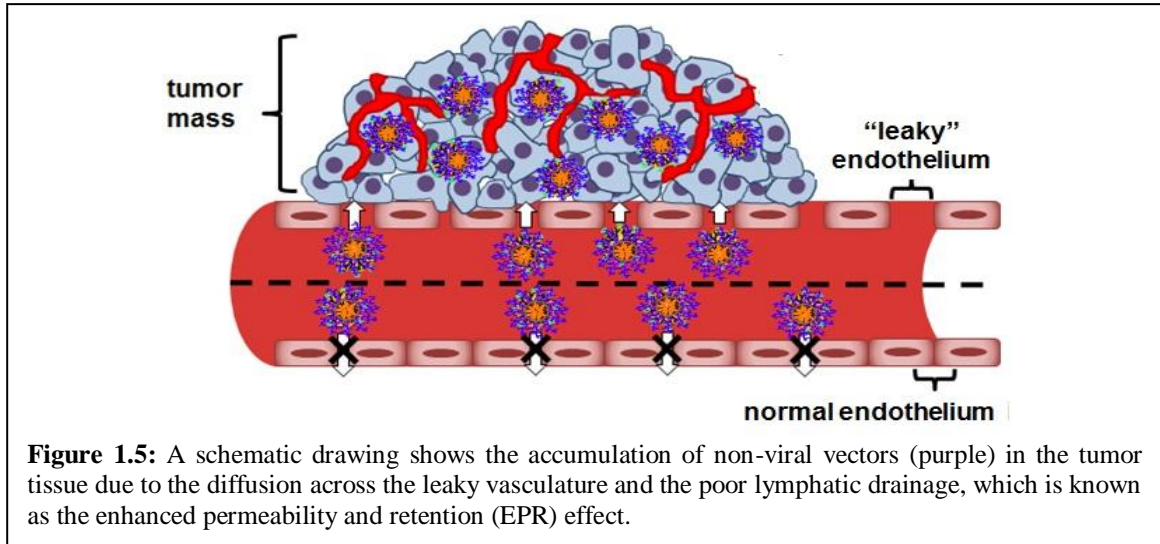
1.1.4.2 Stability of particulate carriers

Although the cationic surface charge of particles enhances cellular uptake, it also causes some problems when applied systematically. These positively charged particles can

nonspecifically interact with blood components to form large aggregates, which activate the complement system and eventually lead to rapid removal of particles from circulation through the reticular endothelial system (RES).^{36,40-41,43} It has been proved that the incorporation of hydrophilic polymers such as poly (ethylene glycol) (PEG) into non-viral carriers can mask their cationic surface charge, reduce their non-specific binding with serum proteins, and therefore prolong their circulation time.⁴⁴ The modification of carriers with PEG, however, affects their complexation with siRNA molecules, the internalization into cells, and the transfection efficiency.⁴⁵ Therefore, the molecular weight and density of the PEG incorporated in the design of carriers need to be carefully selected.⁴⁶

1.1.4.3 Diffusion across the endothelial barrier

The non-viral carriers encapsulating therapeutic siRNA molecules then need to extravasate through the vascular endothelial junctions to reach target tissues. However, the vascular permeability of particles with 5 nm or larger in size is significantly limited in normal tissues,⁴⁷ while only certain organs with an irregular fenestration, such as liver and spleen, allow the permeation of molecules up to 200 nm in diameter.⁴⁸ On the other hand, the rapid and disorganized angiogenesis in tumor tissues lead to the development of leaky and discontinuous vascular structures with poor lymphatic drainage, which results in the enhanced permeation and retention (EPR) effect (**Figure 1.5**),⁴⁹ allowing the accumulation of particles up to 500 nm in tumors.⁵⁰ It has been proved to successfully deliver non-viral complexes to tumor tissues without the incorporation of targeting ligands.⁵¹



1.1.4.4 Cellular entry

Once reaching the target cells in tumor tissue, the non-viral carrier/siRNA complexes encounter the obstacle, to traverse the cellular membrane. The cellular membrane is composed of a lipid bilayer with embedded proteins, and it is selectively permeable to ions and small hydrophobic molecules through passive diffusion.⁵² For large and charged particles, such as lipoplexes and polyplexes, previous studies have shown that most of them pass the cellular membrane through endocytic pathways, including clathrin-mediated endocytosis (adsorptive or receptor mediated), lipid-raft mediated endocytosis (caveolae mediated or not), phagocytosis (mostly happen in specialized cells), and macropinocytosis.^{25a,52-53}

1.1.4.4.1 Non-specific uptake

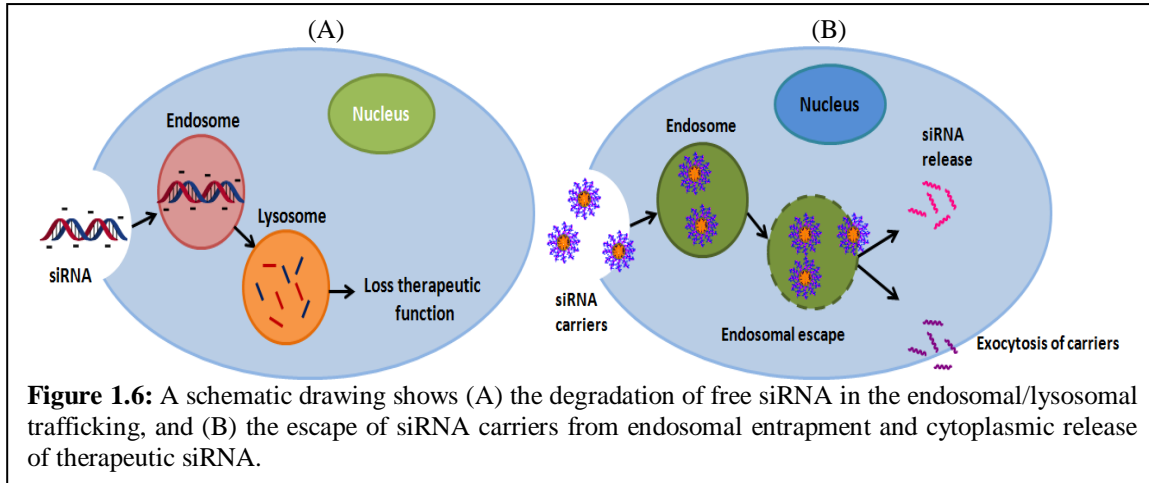
The most common route for the entry of cationic lipoplexes and polyplexes into cells is through non-specific adsorptive endocytosis followed by the clathrin-coated pit mechanism. This is due to the electrostatic interaction between positively charged particles and cellular membrane, containing negatively charged glycoproteins,

proteoglycans, and glycerophosphates.⁵⁴ The uptake of these cationic molecules into cells can be enhanced by the increase of their surface charge, which results in higher affinity to plasma membrane,⁵⁵ but this strategy is not applicable since it also increases particles' toxicity and renal clearance.³⁶ Research by Rejman et al. showed that DOTAP/DNA lipoplexes were taken up into cells only through clathrin-mediated endocytosis, while PEI/DNA polyplexes internalization was processed by both clathrin- and caveolae-mediated mechanisms.⁵⁶ However, the exact route for cationic particles to be taken up by cells varies largely between different cell types and the vectors used, and the contribution of each pathway in cellular uptake is still poorly defined.^{53b,57}

1.1.4.4.2 Targeted uptake

In order to specifically deliver therapeutic siRNA molecules to the designated target cells, non-viral vectors containing targeting ligands, which are recognized by specific cell surface receptor, have been widely investigated.^{25a,36} For example, asialoglycoprotein receptor is abundantly expressed in hepatocytes and selectively binds to asialoglycoproteins.⁵⁸ Incorporation of a sugar moiety such as asialoglycoprotein or galactose into the vectors has been proved to effectively target liver cancer cells both *in vitro* and *in vivo*.⁵⁹ Transferrin and folic acid are also commonly used targeting ligands, which can be easily conjugated to the surface of non-viral carriers and specifically bind to their receptors over-expressed in tumor cells.⁶⁰ In addition to eliminate the non-specific delivery to normal cells, the targeted non-viral vectors can also increase cellular uptake by the route of both adsorptive endocytosis and receptor-mediated endocytosis, and therefore enhance the transfection efficiency.³⁶

1.1.4.5 Endo-lysosomal entrapment and escape



After internalization into cells via endocytosis, the non-viral vectors are entrapped in the endosomes, where the pH drops from neutral (7.4) to around 5-6 due to the ATPase proton pumps.⁶¹ Then the endosomes fuse with lysosomes, which contain various degradative enzymes in more acidic pH environment.⁶¹ The encapsulated siRNA molecules, therefore, will be ultimately degraded in the lysosomes and lose their therapeutic functions (**Figure 1.6**).^{25a,61} In order to escape from enzymatic degradation, the non-viral carriers should be able to release siRNA molecules to cytoplasm at an early stage of the endo-lysosomal trafficking to preserve their therapeutic functions (**Figure 1.6**).⁶² Various approaches have been proposed to improve endosomal escape of non-viral vectors based on two main hypotheses, “proton sponge” effect and membrane-destabilizing effect.^{25a,53b,61} Detail mechanisms will be further explained in Chapter 2.

1.1.4.6 Nucleic acid/vector dissociation

Once non-viral vectors escape from endosomal entrapment, they need to rapidly dissociate from siRNA molecules and release them into cytoplasm. It has been shown that poor decomplexation of the loaded DNA/RNA molecules can lead to low

transfection efficiency.⁶³ The disassembly of the nucleic acids from the vectors can be regulated by the use of less cationic carriers^{63a,64} or the use of degradable vectors.^{41,61} For example, ester bonds and hydrazone bonds have been used as linkages for connection of cationic grafts to a polymer backbone, so the polymeric carriers become fragmented and dissociate from their cargos when hydrolysis occurs.⁶⁵ It is important to develop a vector which forms compact particles with siRNA molecules but rapidly releases them into cytoplasm upon endosomal escape.

1.1.4.7 Effective RNA interference

Unlike plasmid DNA, which can be replicated or incorporated into the host chromosome, siRNA molecules can only induce transient gene silencing effects (3-7 days) in proliferating cells.⁶⁶ The persistence of silencing in different cell types depends on the factors such as proliferation rate and transcriptional activity.⁶⁷ In addition, siRNA-induced gene silencing usually only suppresses target gene expression but not completely inhibits their translation.⁶⁸ The effective RNA interference relies on the drop of target protein level under a specific threshold to induce the desired biological effects, and this requires the successful cytoplasmic delivery of enough number of therapeutic siRNA molecules.⁶⁸

References

- (1) (a) Aiuti, A.; Cattaneo, F.; Galimberti, S.; Benninghoff, U.; Cassani, B.; Callegaro, L.; Scaramuzza, S.; Andolfi, G.; Mirolo, M.; Brigida, I.; Tabucchi, A.; Carlucci, F.; Eibl, M.; Aker, M.; Slavin, S.; Al-Mousa, H.; Al Ghoniaim, A.; Ferster, A.; Duppenthaler, A.; Notarangelo, L.; Wintergerst, U.; Buckley, R. H.; Bregni, M.; Markt, S.; Valsecchi, M. G.; Rossi, P.; Ciceri, F.; Miniero, R.; Bordignon, C.; Roncarolo, M. *New Engl J Med* **2009**, *360*, 447. (b) Gaspar, H. B.; Parsley, K. L.; Howe, S.; King, D.; Gilmour, K. C.; Sinclair, J.; Brouns, G.; Schmidt, M.; Von Kalle, C.; Barington, T.; Jakobsen, M. A.; Christensen, H. O.; Al Ghoniaim, A.; White, H. N.; Smith, J. L.; Levinsky, R. J.; Ali, R. R.; Kinnon, C.; Thrasher, A. J. *Lancet* **2004**, *364*, 2181.
- (2) (a) Dykxhoorn, D. M.; Lieberman, J. *Plos Med* **2006**, *3*, 1000. (b) Rossi, J. J. *Biotechniques* **2006**, *40*, 25.
- (3) (a) Oh, Y. K.; Park, T. G. *Adv Drug Deliver Rev* **2009**, *61*, 850. (b) Pai, S. I.; Lin, Y. Y.; Macaes, B.; Meneshian, A.; Hung, C. F.; Wu, T. C. *Gene Ther* **2006**, *13*, 464.
- (4) Bertrand, J. R.; Pottier, M.; Vekris, A.; Opolon, P.; Maksimenko, A.; Malvy, C. *Biochem Bioph Res Co* **2002**, *296*, 1000.
- (5) Xia, H. B.; Mao, Q. W.; Paulson, H. L.; Davidson, B. L. *Nat Biotechnol* **2002**, *20*, 1006.
- (6) Kaiser, P. K.; Symons, R. C. A.; Shah, S. M.; Quinlan, E. J.; Tabandeh, H.; Do, D. V.; Reisen, G.; Lockridge, J. A.; Short, B.; Guerciolini, R.; Nguyen, Q. D.; Investigators, S.-S. *Am J Ophthalmol* **2010**, *150*, 33.
- (7) (a) DeVincenzo, J.; Cehelsky, J. E.; Alvarez, R.; Elbashir, A.; Elbashir, S.; Harborth, J.; Toudjarska, I.; Nechev, L.; Murugaiah, V.; Van Vliet, A.; Vaishnav, A. K.; Meyers, R. *Antivir Res* **2008**, *77*, 225. (b) DeVincenzo, J.; Lambkin-Williams, R.; Wilkinson, T.; Cehelsky, J.; Nochur, S.; Walsh, E.; Meyers, R.; Gollob, J.; Vaishnav, A. *P Natl Acad Sci USA* **2010**, *107*, 8800.
- (8) Davis, M. E. *Mol Pharmaceut* **2009**, *6*, 659.
- (9) (a) Fire, A.; Xu, S. Q.; Montgomery, M. K.; Kostas, S. A.; Driver, S. E.; Mello, C. C. *Nature* **1998**, *391*, 806. (b) Tabara, H.; Sarkissian, M.; Kelly, W. G.; Fleenor, J.; Grishok, A.; Timmons, L.; Fire, A.; Mello, C. C. *Cell* **1999**, *99*, 123.
- (10) (a) Elbashir, S. M.; Lendeckel, W.; Tuschl, T. *Gene Dev* **2001**, *15*, 188. (b) Pal-Bhadra, M.; Bhadra, U.; Birchler, J. A. *Mol Cell* **2002**, *9*, 315.
- (11) (a) Vaucheret, H.; Fagard, M. *Trends Genet* **2001**, *17*, 29. (b) Waterhouse, P. M.; Graham, H. W.; Wang, M. B. *P Natl Acad Sci USA* **1998**, *95*, 13959.
- (12) (a) Caplen, N. J.; Parrish, S.; Imani, F.; Fire, A.; Morgan, R. A. *P Natl Acad Sci USA* **2001**, *98*, 9742. (b) Elbashir, S. M.; Harborth, J.; Lendeckel, W.; Yalcin, A.; Weber, K.; Tuschl, T. *Nature* **2001**, *411*, 494.
- (13) (a) Doi, N.; Zenno, S.; Ueda, R.; Ohki-Hamazaki, H.; Ui-Tei, K.; Saigo, K. *Curr Biol* **2003**, *13*, 41. (b) Matranga, C.; Tomari, Y.; Shin, C.; Bartel, D. P.; Zamore, P. D. *Cell* **2005**, *123*, 607. (c) Rand, T. A.; Petersen, S.; Du, F. H.; Wang, X. D. *Cell* **2005**, *123*, 621. (d) Zamore, P. D.; Tuschl, T.; Sharp, P. A.; Bartel, D. P. *Cell* **2000**, *101*, 25.

- (14) (a) Alexis, F.; Pridgen, E.; Molnar, L. K.; Farokhzad, O. C. *Mol Pharmaceut* **2008**, *5*, 505. (b) Whitehead, K. A.; Langer, R.; Anderson, D. G. *Nat Rev Drug Discov* **2009**, *8*, 129.
- (15) Soutschek, J.; Akinc, A.; Bramlage, B.; Charisse, K.; Constien, R.; Donoghue, M.; Elbashir, S.; Geick, A.; Hadwiger, P.; Harborth, J.; John, M.; Kesavan, V.; Lavine, G.; Pandey, R. K.; Racie, T.; Rajeev, K. G.; Rohl, I.; Toudjarska, I.; Wang, G.; Wuschko, S.; Bumcrot, D.; Koteliansky, V.; Limmer, S.; Manoharan, M.; Vornlocher, H. P. *Nature* **2004**, *432*, 173.
- (16) De Fougerolles, A.; Manoharan, M.; Meyers, R.; Vornlocher, H. P. *Method Enzymol* **2005**, *392*, 278.
- (17) Hall, A. H. S.; Wan, J.; Shaughnessy, E. E.; Shaw, B. R.; Alexander, K. A. *Nucleic Acids Res* **2004**, *32*, 5991.
- (18) (a) Allerson, C. R.; Sioufi, N.; Jarres, R.; Prakash, T. P.; Naik, N.; Berdeja, A.; Wanders, L.; Griffey, R. H.; Swayze, E. E.; Bhat, B. *J Med Chem* **2005**, *48*, 901. (b) Chiu, Y. L.; Rana, T. M. *Rna* **2003**, *9*, 1034.
- (19) Layzer, J. M.; McCaffrey, A. P.; Tanner, A. K.; Huang, Z.; Kay, M. A.; Sullenger, B. A. *Rna* **2004**, *10*, 766.
- (20) (a) de Fougerolles, A.; Vornlocher, H. P.; Maraganore, J.; Lieberman, J. *Nat Rev Drug Discov* **2007**, *6*, 443. (b) Shim, M. S.; Kwon, Y. J. *Febs J* **2010**, *277*, 4814.
- (21) (a) Shen, J.; Samul, R.; Silva, R. L.; Akiyama, H.; Liu, H.; Saishin, Y.; Hackett, S. F.; Zinnen, S.; Kossen, K.; Fosnaugh, K.; Vargeese, C.; Gomez, A.; Bouhana, K.; Aitchison, R.; Pavco, P.; Campochiaro, P. A. *Gene Ther* **2006**, *13*, 225. (b) Tolentino, M. J.; Brucker, A. J.; Fosnot, J.; Ying, G. S.; Wu, I. H.; Malik, G.; Wan, S.; Reich, S. J. *Retina-J Ret Vit Dis* **2004**, *24*, 660.
- (22) Bitko, V.; Musiyenko, A.; Shulyayeva, O.; Barik, S. *Nat Med* **2005**, *11*, 50.
- (23) (a) Braasch, D. A.; Paroo, Z.; Constantinescu, A.; Ren, G.; Oz, O. K.; Mason, R. P.; Corey, D. R. *Bioorg Med Chem Lett* **2004**, *14*, 1139. (b) Gao, S.; Dagnaes-Hansen, F.; Nielsen, E. J. B.; Wengel, J.; Besenbacher, F.; Howard, K. A.; Kjems, J. *Mol Ther* **2009**, *17*, 1225.
- (24) Aagaard, L.; Rossi, J. J. *Adv Drug Deliv Rev* **2007**, *59*, 75.
- (25) (a) Khalil, I. A.; Kogure, K.; Akita, H.; Harashima, H. *Pharmacol Rev* **2006**, *58*, 32. (b) Lam, J. K. W.; Liang, W.; Lan, Y.; Chaudhuri, P.; Chow, M. Y. T.; Witt, K.; Kudsiova, L.; Mason, A. J. *J Control Release* **2012**, *158*, 293.
- (26) (a) McCaffrey, A. P.; Meuse, L.; Pham, T. T. T.; Conklin, D. S.; Hannon, G. J.; Kay, M. A. *Nature* **2002**, *418*, 38. (b) Song, E. W.; Lee, S. K.; Wang, J.; Ince, N.; Ouyang, N.; Min, J.; Chen, J. S.; Shankar, P.; Lieberman, J. *Nat Med* **2003**, *9*, 347.
- (27) (a) Jere, D.; Jiang, H. L.; Arote, R.; Kim, Y. K.; Choi, Y. J.; Cho, M. H.; Akaike, T.; Chot, C. S. *Expert Opin Drug Del* **2009**, *6*, 827. (b) Lai, W. F.; Lin, M. C. *J Control Release* **2009**, *134*, 158. (c) Midoux, P.; Pichon, C.; Yaouanc, J. J.; Jaffres, P. A. *Brit J Pharmacol* **2009**, *157*, 166.
- (28) (a) Barton, G. M.; Medzhitov, R. *P Natl Acad Sci USA* **2002**, *99*, 14943. (b) McTaggart, S.; Al-Rubeai, M. *Biotechnol Adv* **2002**, *20*, 1.
- (29) Shen, C. X.; Buck, A. K.; Liu, X. W.; Winkler, M.; Reske, S. N. *Febs Lett* **2003**, *539*, 111.

- (30) (a) Favre, D.; Provost, N.; Blouin, V.; Blacho, G.; Cherel, Y.; Salvetti, A.; Moullier, P. *Mol Ther* **2001**, *4*, 559. (b) Kay, M. A.; Glorioso, J. C.; Naldini, L. *Nat Med* **2001**, *7*, 33.
- (31) Felgner, P. L.; Gadek, T. R.; Holm, M.; Roman, R.; Chan, H. W.; Wenz, M.; Northrop, J. P.; Ringold, G. M.; Danielsen, M. *P Natl Acad Sci USA* **1987**, *84*, 7413.
- (32) Simberg, D.; Weisman, S.; Talmon, Y.; Barenholz, Y. *Crit Rev Ther Drug Carrier Syst* **2004**, *21*, 257.
- (33) Cardoso, A. L. C.; Simoes, S.; de Almeida, L. P.; Pelisek, J.; Culmsee, C.; Wagner, E.; de Lima, M. C. P. *J Gene Med* **2007**, *9*, 170.
- (34) Kim, S. I.; Shin, D.; Choi, T. H.; Lee, J. C.; Cheon, G. J.; Kim, K. Y.; Park, M.; Kim, M. *Mol Ther* **2007**, *15*, 1145.
- (35) Lonz, C.; Vandenbranden, M.; Ruyschaert, J. M. *Prog Lipid Res* **2008**, *47*, 340.
- (36) Merdan, T.; Kopecek, J.; Kissel, T. *Adv Drug Deliver Rev* **2002**, *54*, 715.
- (37) (a) Inoue, Y.; Kurihara, R.; Tsuchida, A.; Hasegawa, M.; Nagashima, T.; Mori, T.; Niidome, T.; Katayama, Y.; Okitsu, O. *J Control Release* **2008**, *126*, 59. (b) Watanabe, K.; Harada-Shiba, M.; Suzuki, A.; Gokuden, R.; Kurihara, R.; Sugao, Y.; Mori, T.; Katayama, Y.; Niidome, T. *Mol Biosyst* **2009**, *5*, 1306. (c) Zauner, W.; Ogris, M.; Wagner, E. *Adv Drug Deliver Rev* **1998**, *30*, 97.
- (38) (a) Kano, A.; Moriyama, K.; Yamano, T.; Nakamura, I.; Shimada, N.; Maruyama, A. *J Control Release* **2011**, *149*, 2. (b) Sato, A.; Choi, S. W.; Hirai, M.; Yamayoshi, A.; Moriyama, R.; Yamano, T.; Takagi, M.; Kano, A.; Shimamoto, A.; Maruyama, A. *J Control Release* **2007**, *122*, 209.
- (39) Akinc, A.; Langer, R. *Biotechnol Bioeng* **2002**, *78*, 503.
- (40) Guo, J. F.; Bourre, L.; Soden, D. M.; O'Sullivan, G. C.; O'Driscoll, C. *Biotechnol Adv* **2011**, *29*, 402.
- (41) Wong, S. Y.; Pelet, J. M.; Putnam, D. *Prog Polym Sci* **2007**, *32*, 799.
- (42) Mintzer, M. A.; Simanek, E. E. *Chem Rev* **2009**, *109*, 259.
- (43) Vonarbourg, A.; Passirani, C.; Saulnier, P.; Benoit, J. P. *Biomaterials* **2006**, *27*, 4356.
- (44) (a) Klibanov, A. L.; Maruyama, K.; Torchilin, V. P.; Huang, L. *Febs Lett* **1990**, *268*, 235. (b) Mosqueira, V. C. F.; Legrand, P.; Gref, R.; Heurtault, B.; Appel, M.; Barratt, G. *J Drug Target* **1999**, *7*, 65.
- (45) Erbacher, P.; Bettinger, T.; Belguise-Valladier, P.; Zou, S. M.; Coll, J. L.; Behr, J. P.; Remy, J. S. *J Gene Med* **1999**, *1*, 210.
- (46) Petersen, H.; Fechner, P. M.; Martin, A. L.; Kunath, K.; Stolnik, S.; Roberts, C. J.; Fischer, D.; Davies, M. C.; Kissel, T. *Bioconjugate Chem* **2002**, *13*, 845.
- (47) (a) Juliano, R.; Bauman, J.; Kang, H.; Ming, X. *Mol Pharmaceut* **2009**, *6*, 686. (b) Rippe, B.; Rosengren, B. I.; Carlsson, O.; Venturoli, D. *J Vasc Res* **2002**, *39*, 375.
- (48) Scherphof, G. L. *In vivo behavior of liposomes: Interactions with the mononuclear phagocyte system and implications for drug targeting*, 1991.
- (49) Jain, R. K.; Stylianopoulos, T. *Nat Rev Clin Oncol* **2010**, *7*, 653.
- (50) (a) Jang, S. H.; Wientjes, M. G.; Lu, D.; Au, J. L. S. *Pharmaceut Res* **2003**, *20*, 1337. (b) Li, W. J.; Szoka, F. C. *Pharmaceut Res* **2007**, *24*, 438.

- (51) (a) Bartlett, D. W.; Su, H.; Hildebrandt, I. J.; Weber, W. A.; Davis, M. E. *P Natl Acad Sci USA* **2007**, *104*, 15549. (b) Shiah, J. G.; Sun, Y. G.; Peterson, C. M.; Kopecek, J. *J Control Release* **1999**, *61*, 145.
- (52) Conner, S. D.; Schmid, S. L. *Nature* **2003**, *422*, 37.
- (53) (a) Kirkham, M.; Parton, R. G. *Bba-Mol Cell Res* **2005**, *1745*, 273. (b) Morille, M.; Passirani, C.; Vonarbourg, A.; Clavreul, A.; Benoit, J. P. *Biomaterials* **2008**, *29*, 3477.
- (54) (a) Mislick, K. A.; Baldeschwieler, J. D. *P Natl Acad Sci USA* **1996**, *93*, 12349. (b) Mounkes, L. C.; Zhong, W.; Cipres-Palacin, G.; Heath, T. D.; Debs, R. J. *J Biol Chem* **1998**, *273*, 26164.
- (55) Blau, S.; Jubeh, T. T.; Haupt, S. M.; Rubinstein, A. *Crit Rev Ther Drug* **2000**, *17*, 425.
- (56) Rejman, J.; Bragonzi, A.; Conese, M. *Mol Ther* **2005**, *12*, 468.
- (57) Ruponen, M.; Honkakoski, P.; Tammi, M.; Urtti, A. *J Gene Med* **2004**, *6*, 405.
- (58) Perales, J. C.; Grossmann, G. A.; Molas, M.; Liu, G.; Ferkol, T.; Harpst, J.; Oda, H.; Hanson, R. W. *J Biol Chem* **1997**, *272*, 7398.
- (59) (a) Han, J.; Yeom, Y. I. *Int J Pharmaceut* **2000**, *202*, 151. (b) Hashida, M.; Takemura, S.; Nishikawa, M.; Takakura, Y. *J Control Release* **1998**, *53*, 301.
- (60) (a) Gosselin, M. A.; Lee, R. J. *Biotechnol Annu Rev* **2002**, *8*, 103. (b) Kakudo, T.; Chaki, S.; Futaki, S.; Nakase, I.; Akaji, K.; Kawakami, T.; Maruyama, K.; Kamiya, H.; Harashima, H. *Biochemistry-Us* **2004**, *43*, 5618. (c) Cho, K. C.; Kim, S. H.; Jeong, J. H.; Park, T. G. *Macromol Biosci* **2005**, *5*, 512.
- (61) Pathak, A.; Patnaik, S.; Gupta, K. C. *Biotechnol J* **2009**, *4*, 1559.
- (62) Pack, D. W.; Hoffman, A. S.; Pun, S.; Stayton, P. S. *Nat Rev Drug Discov* **2005**, *4*, 581.
- (63) (a) Gabrielson, N. P.; Pack, D. W. *Biomacromolecules* **2006**, *7*, 2427. (b) Schaffer, D. V.; Fidelman, N. A.; Dan, N.; Lauffenburger, D. A. *Biotechnol Bioeng* **2000**, *67*, 598. (c) Yadava, P.; Roura, D.; Hughes, J. A. *Oligonucleotides* **2007**, *17*, 213.
- (64) Kabanov, A. V.; Kabanov, V. A. *Bioconj Chem* **1995**, *6*, 7.
- (65) (a) Veron, L.; Ganee, A.; Ladaviere, C.; Delair, T. *Macromol Biosci* **2006**, *6*, 540. (b) Zhong, Z.; Song, Y.; Engbersen, J. F.; Lok, M. C.; Hennink, W. E.; Feijen, J. *J Control Release* **2005**, *109*, 317. (c) Lin, Y. L.; Jiang, G.; Birrell, L. K.; El-Sayed, M. E. *Biomaterials* **2010**, *31*, 7150.
- (66) Leung, R. K. M.; Whittaker, P. A. *Pharmacol Therapeut* **2005**, *107*, 222.
- (67) Dykxhoorn, D. M.; Lieberman, J. *Cell* **2006**, *126*, 231.
- (68) Scherr, M.; Morgan, M. A.; Eder, M. *Curr Med Chem* **2003**, *10*, 245.

Chapter 2.

Background

2.1 Challenge in Endosomal/lysosomal escape

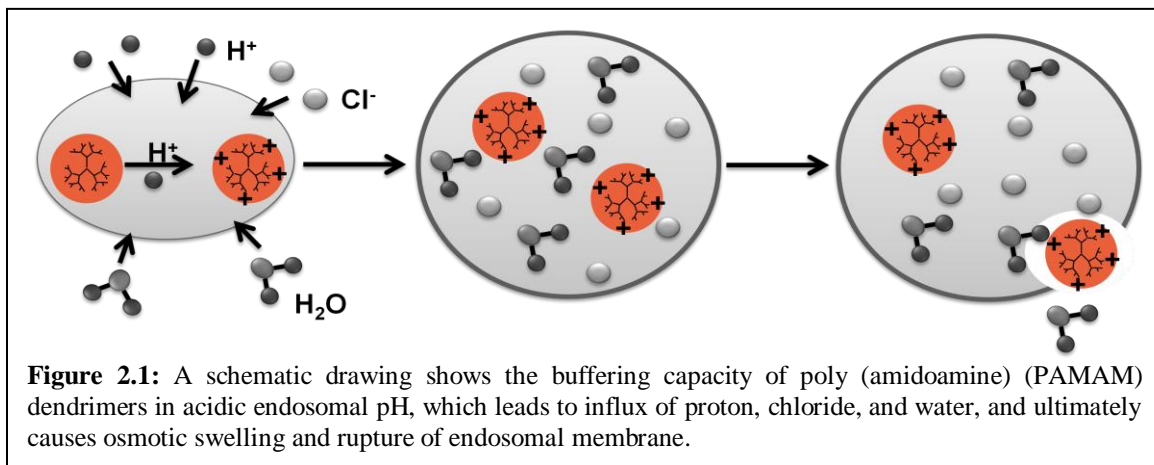
Endosomal entrapment is one of the major barriers, which limits the practical application of siRNA-based cancer therapy. In order to achieve effective gene silencing, many strategies have been developed to enhance the escape of nucleic acids from endosomal/lysosomal trafficking. Two mechanisms, including “proton sponge” effect and membrane-destabilizing effect, have been widely investigated to explain this escape and used in the development of non-viral vectors.¹

2.1.1 Mechanisms of endosomal escape

2.1.1.1 “Proton sponge” effect and carriers

The “proton sponge” effect was discovered in certain cationic polymers, which contain a large number of protonable secondary and tertiary amine groups with pKa close to endosomal/lysosomal pH (i.e. $5 < \text{pKa} < 7$).² In the endosome, polymers with the “proton sponge” effect become protonated, so the ATPase proton pumps on the endosomal membrane need to pump more protons from the cytosol into the endosomes to maintain the acidic pH environment. The transport of protons is accompanied by the influx of

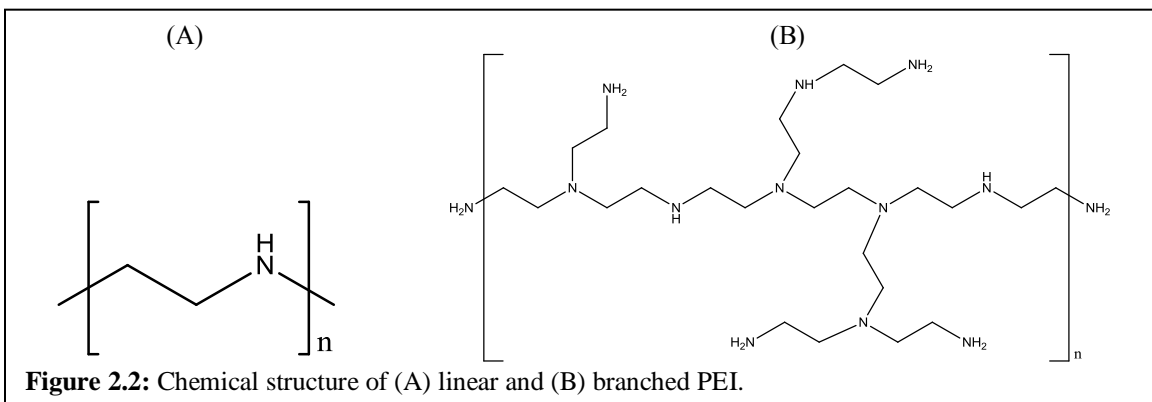
chloride counter ions and water, and ultimately causes osmotic swelling and rupture of endosomal membrane (**Figure 2.1**).^{1,3}



2.1.1.1.1 Polyethylenimine (PEI)

PEI is the most well-known cationic polymer which has been proved to be highly effective in gene delivery both *in vitro* and *in vivo*.^{3a} This could be attributed to the strong buffering capacity of PEI, due to their high density of protonable amine groups, resulting in rapid endosomal escape.⁴ A series of PEI have been synthesized in different molecular weights (MW) and structures (linear and branched) (**Figure 2.2**) to be used as transfection agents.⁵ Earlier researches showed that both the transfection efficiency and cytotoxicity of PEI-based vectors increases with increased molecular weight (600 Da-70 kDa),⁶ and the toxicity is due to the aggregation of PEI polyplexes on the cell membrane, which causes significant necrosis.⁷ In addition, higher-branched PEI showed stronger complexation with nucleic acids and better transfection efficiency than lower-branched one, but the cytotoxicity also increased with the degree of branching.⁸ In order to reduce the toxicity of PEI polyplexes while increase their stability and transfection efficiency, many efforts have been made to synthesize various degradable PEI derivatives. For

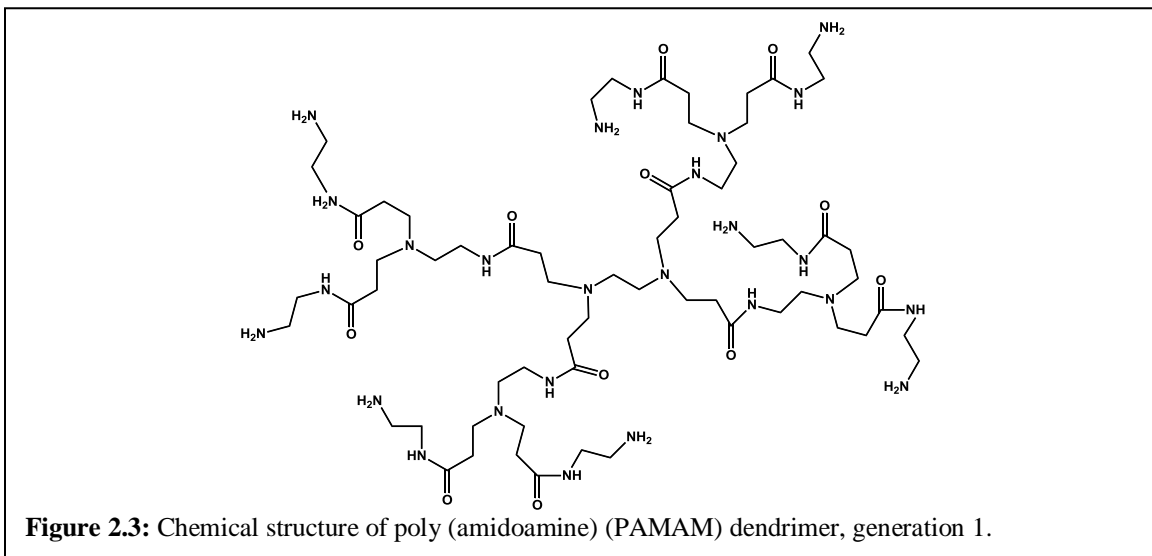
example, low MW PEI (2 kDa) was cross-linked via reducible disulfide linkage and conjugated to the hyaluronic acid (HA) to form (PEI-SS)-b-HA block copolymers, which encapsulated anti-vascular endothelial growth factor (VEGF) siRNA into serum-stable particles with negligible toxicity. The formed particles proved to suppress VEGF expression both *in vitro* and *in vivo*, and successfully inhibit tumor growth after intratumoral injection.⁹ Modification of branched PEI (25 kDa) by incorporation of negatively charged succinic acid groups to the backbone also obtained effective siRNA carriers with low toxicity.¹⁰ Further, branched PEI (25 kDa) was PEGylated with Arg-Gly-Asp (RGD) peptide ligands to achieve tumor-specific targeting and prolonged circulation *in vivo*.¹¹



2.1.1.1.2 Poly (amidoamine) (PAMAM) dendrimers

PAMAM dendrimers are a family of water-soluble polymers that is characterized by a unique tree-like branching architecture with a large number of primary, secondary, and tertiary amine groups (**Figure 2.3**).¹² The high density of protonable amine groups enables the rapid endosomal escape of PAMAM-based dendriplexes due to the “proton sponge” mechanism,¹³ but also leads to non-specific cytotoxicity. The toxicity of PAMAM dendrimers can be reduced by conjugation of hydrophilic polymers¹⁴ or by

partial neutralization of the cationic amine groups.¹⁵ However, their gene silencing capacity was also reduced due to the poor pH buffering capacity and endosomal escape.^{15a,16} Earlier researches also showed that heat-treated PAMAM dendrimers in water or butanol became partially degraded and more flexible which allowed them to better complex with DNA and exhibited better transfection efficiency with less toxicity compared to the intact PAMAM dendrimers.¹⁷



2.1.1.2 Amphiphilic membrane-destabilizing effect and carriers

Several viruses such as the influenza virus have evolved pH-responsive fusogenic proteins hemagglutinin to facilitate their infection in host cells. These fusogenic proteins are characterized by their unique ability to switch from an ionized and hydrophilic conformation at physiologic pH to a protonated and hydrophobic one in response to acidic endosomal pH gradients, which destabilizes the endosomal membrane leading to release of genetic cargos.¹⁸ Therefore, several synthetic peptides with similar pH-sensitive, membrane-destabilizing properties have been developed to enhance cytoplasmic gene delivery.¹⁹ However, the clinical application of these synthetic

fusogenic peptides are limited by their potential immunogenicity, low stability and high synthesis cost.²⁰

2.1.1.2.1 Amphiphilic carriers

To mimic the membrane-disruptive properties of viral fusogenic peptides, a family of pH-sensitive poly (alkylacrylic acid) polymers (

Figure 2.4) has been synthesized to enhance the cytoplasmic delivery of therapeutic DNA/RNA molecules.²¹

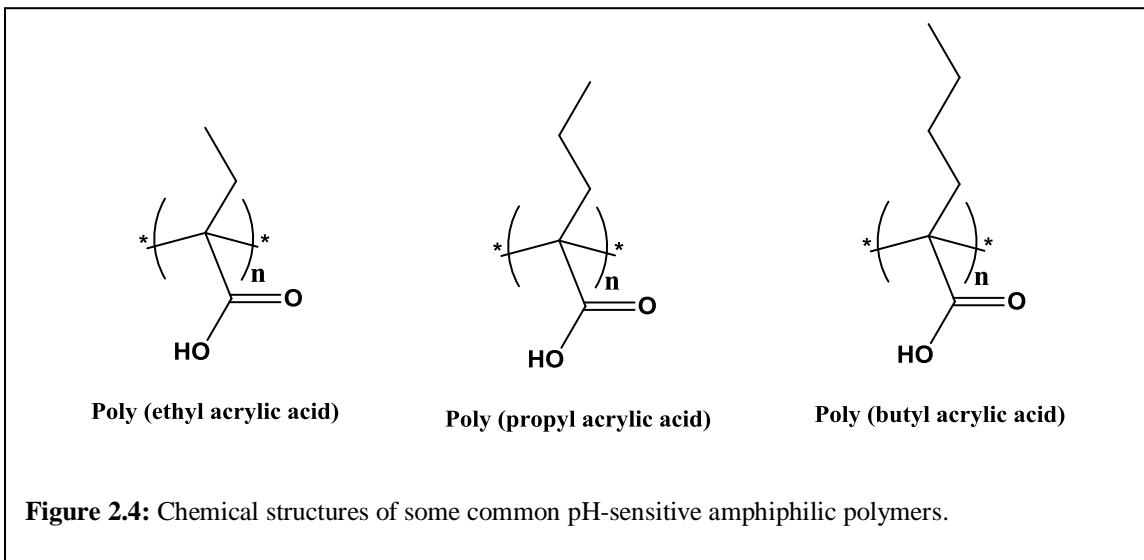
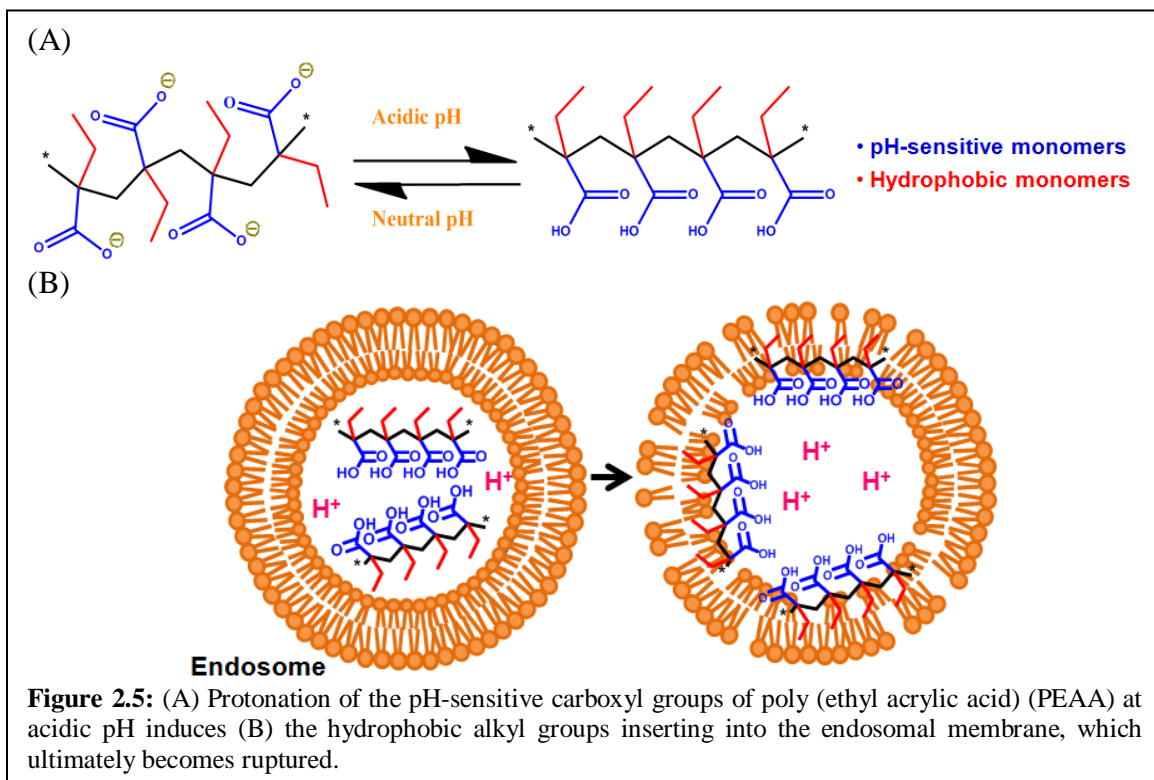


Figure 2.4: Chemical structures of some common pH-sensitive amphiphilic polymers.

The carboxyl groups can “sense” the changes in environmental pH and become protonated at acidic pH, while the hydrophobic alkyl groups can interact with the endosomal membrane, which collectively enable the rapid escape from endosomal/lysosomal trafficking (**Figure 2.5**).²² Poly (ethylacrylic acid) (PEAA) is the first polymer proved to cause membrane disruption of liposomes at acidic pH of 6.3 or lower.²³ Hoffman, Stayton, and coworkers then showed that the pH-responsive membrane-destabilizing activity can be modulated by changing the ratio of hydrophobic

alkyl groups in polymer composition. In addition, poly (propylacrylic acid) (PPAA) exhibited a pH-dependent membrane-destabilizing activity that is one order of magnitude higher than PEAA²² and proved to enhance the transfection efficiency of cationic lipid/pDNA complexes both *in vitro*²⁴ and *in vivo*.²⁵ Afterward, a functionalized monomer, pyridyl disulphide acrylate (PDSA), was incorporated to the backbone of pH-sensitive polymers through glutathione-sensitive disulfide linkages to allow direct conjugation of cationic peptides, which proved to complex with negatively charged therapeutic macromolecules.²⁶



2.1.2 Limitations of current siRNA carriers

Although both “proton sponge” effect and membrane-destabilizing effect proved efficient in enhancing cytoplasmic delivery of therapeutics nucleic acids, they both have some limitations. Cationic polymers with strong pH buffering capacity, such as PEI, usually

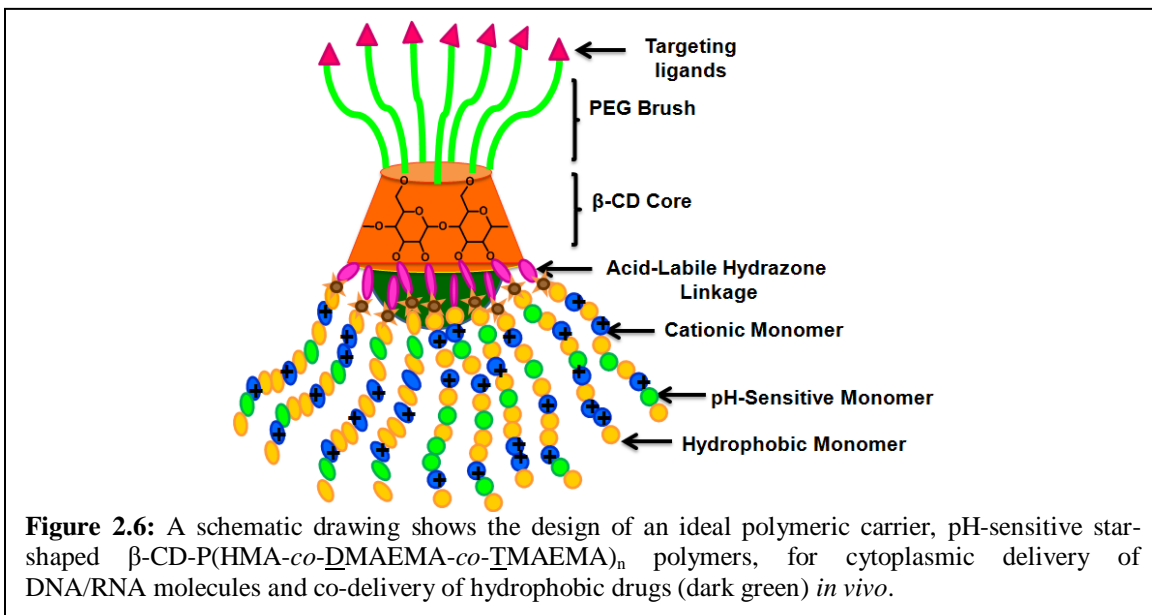
exhibit functional gene transfection when a large amount of polymer is used to carry sufficient DNA/RNA. This always leads to non-specific cytotoxicity due to the excess positive charge destabilizing cellular membrane.^{7,27} On the other hand, the membrane-destabilizing activity of pH-sensitive amphiphilic polymers is based on a delicate balance between the hydrophilic and hydrophobic monomers.^{22a,28} Excess positive charge abolishes their membrane-destabilizing activity, while excess amount hydrophobic groups makes them water-insoluble and ineffective.^{26a} Further, PEI and those pH-sensitive poly (alkylacrylic acid) polymers are non-biodegradable polymers. The ideal non-viral vectors need to be hydrolyzed and degraded into small fragments once they deliver their therapeutic cargos, so they can be eliminated from human body without causing accumulation and toxicity.^{26a,29} In addition, treatment of cancers usually requires systemic delivery, but incorporation of targeting ligands to these cationic polymers is not easy since it affects the proton buffering capacity and hydrophilic/hydrophobic balance. Finally, successful cancer therapy usually requires administration of anticancer drugs. Therefore, development of polymeric carriers that can deliver both therapeutic DNA/RNA and anticancer drugs at the same time has become a future target.

2.1.3 Structural requirements of an “ideal” polymeric carrier for *in vivo* siRNA delivery

Due to the limitations mentioned above, the ideal polymeric carrier should be (i) degradable, (ii) high drug loading, (iii) low toxicity, (iv) cell-specific, and (v) able to co-deliver other therapeutic drugs. We have designed and developed a new series of degradable, pH-sensitive, membrane-destabilizing, star-shaped polymers that proved to deliver therapeutic siRNA molecules into the cytoplasm of cancer cells and selectively

induce cellular apoptosis. These carriers have a β -cyclodextrin (β -CD) core, which is composed of 7 glucose units linked by α -1,4-linkages, forming a cone-shaped structure (**Figure 2.6**). The 7 hydroxyl groups on the primary face and 14 hydroxyl groups on the secondary face have different reactivity, which allow selectively conjugation of pH-sensitive/hydrophobic/cationic grafts on the secondary face while conjugation of hydrophilic PEG grafts displaying targeting motif on the primary face. The copolymer of pH-sensitive dimethyl aminoethyl methacrylate (DMAEMA), hydrophobic hexyl methacrylate (HMA) and cationic trimethyl aminoethyl methacrylate (TMAEMA) was grafted from the secondary face via acid-labile hydrazone linkages. Hydrazone linkages have previously been used to conjugate small molecular weight anticancer drugs (e.g. doxorubicin) to water-soluble hydroxypropyl methacrylate (HPMA) polymers and proved to hydrolyze and release the attached drug upon internalization into acidic intracellular vesicles.³⁰ Incorporation of the hydrazone linkages in these star-shaped polymers allows grafts of a large number of pH-sensitive/hydrophobic/cationic copolymers to achieve a high positive charge density that will allow the condensation of a large number of DNA/RNA molecules into pH-sensitive particles with high therapeutic loading.³¹ In addition, the acid-labile hydrazone linkages will be hydrolyzed in the endosome, which will result in fragmentation of the carriers into multiple grafts that can be easily eliminated from the body without inducing significant toxicity. Also, β -CD is a water-soluble polymer with a hydrophobic cavity, which allows the encapsulation of hydrophobic anticancer drugs inside and complexation of hydrophilic therapeutic DNA/RNA molecules outside.³² Overall, these degradable, pH-sensitive, membrane-

destabilizing, star-shaped polymers are believed to be a potential non-viral vector for intracellular delivery of therapeutic macromolecules.



2.1.4 Comparison between star-shaped polymers and other non-viral vectors

2.1.4.1 Polyethyleneimine-based carriers

PEI is one of the most effective non-viral vectors due to their buffering capacity, which causes endosomal swelling and rupture of endosomal membrane.^{3a,4} However, it usually requires a large excess of PEI to provide efficient buffering capacity, leading to non-specific toxicity both *in vitro* and *in vivo*.⁷ It has been proved that modification of PEI by covalently coupling PEG chains to form block or graft copolymers can decrease their cytotoxicity.³³ In addition, PEGylated PEI complexes displayed decreased interaction with serum proteins,³⁴ reduced activation of opsonization,³⁵ and prolonged plasma residence time *in vivo*.³⁶ Further, to prevent long-term accumulation of non-degradable PEI complexes in body, the incorporation of hydrolytically cleavable amide bonds or reductively cleavable disulfide bonds has been utilized to synthesize biodegradable

PEGylated PEI polymers for the delivery of DNA/RNA molecules.³⁷ An ideal gene delivery system also needs to provide cell-specific delivery to prevent adverse side effects. It has been proved that coupling of galactose to PEI can provide liver-specific delivery, due to the expression of asialoglycoprotein receptor on the surface of hepatocytes.³⁸ However, incorporation of targeting ligands in the PEGylated PEI carriers did not necessary enhance transfection efficiency, probably due to the low grafting ratio. Although various strategies have been proposed to address the limitations in the intracellular delivery of DNA/RNA using PEI-based complexes, the ideal carrier has not yet been established. The delivery efficiency relies on the molecular weight and architecture (linear and branched) of PEI.⁵ The incorporation of PEG grafts and targeting ligands has significant effects on the complexation of PEI and nucleic acids, their cellular uptake, and the transfection efficiency.⁵ Therefore, it requires systematical investigation on the parameters that affect therapeutic activity of PEI-based complexes. In addition, compare with our proposed star-shaped polymers, PEI carriers do not have the potential to co-deliver other therapeutic drugs, such as chemotherapeutic drugs and small molecule inhibitors, which may limit their clinical applications.

2.1.4.2 Cyclodextrin-based carriers

The first targeted delivery of siRNA in human was accomplished by using cyclodextrin-containing polymers in 2008. This siRNA delivery system includes a) a linear cyclodextrin-containing polymer to complex with siRNA through electrostatic interaction, b) an adamantane (AD)-PEG conjugate to provide steric stabilization and increase plasma residence time, c) the targeting component, transferrin (Tf)-PEG-AD, to allow selectively delivery to tumor cells, and d) imidazole groups to assist in endosomal escape.³⁹ This

polymer has been proved to successfully condense therapeutic siRNA into water-soluble nanoparticles, which reduced tumor growth by 50% *in vivo* without inducing immune responses.⁴⁰ However, earlier studies suggested that branched polymers provide better steric protection for loaded therapeutic cargo and longer plasma residence time compared to linear polymers, which collectively improve the transfection efficiency and biocompatibility of branched polymers.⁴¹ Our proposed star-shaped polymers may exhibit better gene delivery ability than this linear cyclodextrin-containing polymer. In addition, the star-shaped polymers have the potential to co-deliver other therapeutic drugs in the hydrophobic core of β -CD.

2.2 Objective and Hypothesis

The objective of this dissertation is to develop novel “smart” particles to enhance the cytoplasmic delivery of anti-Bcl-2 siRNA molecules to suppress anti-apoptotic Bcl-2 protein expression in head and neck cancer cells with subsequent induction of cancer cell death and inhibition of tumor growth. Specifically, we propose to synthesize degradable, pH-sensitive, membrane-destabilizing, comb- and star-shaped polymers. These polymers are characterized by their unique ability to switch from a hydrophilic, stealth-like conformation to a hydrophobic, membrane-destabilizing one in response to acidic endosomal pH gradients. We will utilize these pH-sensitive polymers to condense anti-Bcl-2 siRNA molecules into “smart” particles that will be taken up by head and neck cancer cells via endocytosis. These particles will “sense” the drop in endosomal pH, which will trigger the degradation of the polymeric carrier into small membrane-destabilizing fragments to destabilize the endosomal membrane and release the siRNA molecules into the cytoplasm. In addition, we propose to “switch of” anti-apoptotic Bcl-2

activity by using star-shaped polymers loaded with anti-Bcl-2 siRNA along with Bcl-2 small molecule inhibitor AT-101, to induce apoptotic head and neck cancer cell death and inhibit cancer cell growth.

We hypothesize that the degradable, pH-sensitive, membrane-destabilizing, comb-like polymers can complex a large dose of anti-Bcl-2 siRNA molecules into “smart” nanoparticles, which can functionally deliver their siRNA cargo into the cytoplasm of cancer cells to suppress Bcl-2 gene expression at both mRNA and protein levels. The star-shaped polymers can also condense anti-Bcl-2 siRNA into pH-sensitive particles that will be internalized in cancer cells via adsorptive endocytosis. In the endosome, the particles can destabilize endosomal membrane through both hydrophobic disruption and endosomal swelling mechanisms, releasing siRNA cargo into the cytoplasm of head and neck cancer cells to suppress Bcl-2 gene expression. We also hypothesize that combination treatment with AT-101 and star-shaped polymers encapsulating anti-Bcl-2 siRNA can synergistically induce head and neck cancer cell apoptosis and inhibit cancer cell growth.

2.3 Specific aims

The specific aims of this dissertation are:

1. Confirm the feasibility to design and synthesize a new family of degradable, pH-sensitive, membrane-destabilizing, comb-like polymers, which can complex siRNA molecules into “smart” particles. Prove the pH-dependent membrane-destabilizing activity of these particles can destabilize endosomal membrane without loss their therapeutic effect.

2. Design and synthesize a new family of degradable, pH-sensitive, membrane-destabilizing, star-shaped polymers. Engineer these star-shaped polymers to systematically evaluate the effect of graft's molecular weight, hydrophobic/hydrophilic balance, and degree of quaternization on their ability to deliver the RNA cargo past the endosomal membrane and into the cytoplasm of epithelial cancer cells.
3. Confirm both comb- and star-shaped polymers can achieve functional delivery of anti-Bcl-2 siRNA molecules in multiple cancer cells based on their ability to suppress Bcl-2 expression at the protein and mRNA levels.
4. Confirm the feasibility of combination treatment with Bcl-2 small molecule inhibitor AT-101 and “smart” particles encapsulating anti-Bcl-2 siRNA molecules based on the ability to a) induce apoptotic head and neck cancer cell death, and b) inhibit head and neck cancer cell growth.

References

- (1) Liang, W.; Lam, J. K. W. *Endosomal Escape Pathways for Non-Viral Nucleic Acid Delivery Systems*; InTech, 2012.
- (2) Wong, S. Y.; Pelet, J. M.; Putnam, D. *Prog Polym Sci* **2007**, *32*, 799.
- (3) (a) Boussif, O.; Lezoualch, F.; Zanta, M. A.; Mergny, M. D.; Scherman, D.; Demeneix, B.; Behr, J. P. *P Natl Acad Sci USA* **1995**, *92*, 7297. (b) Morille, M.; Passirani, C.; Vonarbourg, A.; Clavreul, A.; Benoit, J. P. *Biomaterials* **2008**, *29*, 3477.
- (4) Boussif, O.; Zanta, M. A.; Behr, J. P. *Gene Ther* **1996**, *3*, 1074.
- (5) Neu, M.; Fischer, D.; Kissel, T. *J Gene Med* **2005**, *7*, 992.
- (6) (a) Godbey, W. T.; Wu, K. K.; Mikos, A. G. *Biomaterials* **2001**, *22*, 471. (b) Godbey, W. T.; Wu, K. K.; Mikos, A. G. *J Biomed Mater Res* **1999**, *45*, 268.
- (7) (a) Fischer, D.; Li, Y. X.; Ahlemeyer, B.; Krieglstein, J.; Kissel, T. *Biomaterials* **2003**, *24*, 1121. (b) Fischer, D.; Bieber, T.; Li, Y. X.; Elsasser, H. P.; Kissel, T. *Pharmaceut Res* **1999**, *16*, 1273.
- (8) Fischer, D.; von Harpe, A.; Kunath, K.; Petersen, H.; Li, Y. X.; Kissel, T. *Bioconjugate Chem* **2002**, *13*, 1124.
- (9) Park, K.; Lee, M. Y.; Kim, K. S.; Hahn, S. K. *Biomaterials* **2010**, *31*, 5258.
- (10) Zintchenko, A.; Philipp, A.; Dehshahri, A.; Wagner, E. *Bioconjug Chem* **2008**, *19*, 1448.
- (11) Schiffelers, R. M.; Ansari, A.; Xu, J.; Zhou, Q.; Tang, Q. Q.; Storm, G.; Molema, G.; Lu, P. Y.; Scaria, P. V.; Woodle, M. C. *Nucleic Acids Res* **2004**, *32*.
- (12) (a) Frechet, J. M. J. *Science* **1994**, *263*, 1710. (b) Tomalia, D. A.; Frechet, J. M. J. *J Polym Sci Pol Chem* **2002**, *40*, 2719.
- (13) Sonawane, N. D.; Szoka, F. C.; Verkman, A. S. *J Biol Chem* **2003**, *278*, 44826.
- (14) (a) Kim, T. I.; Seo, H. J.; Choi, J. S.; Jang, H. S.; Baek, J. U.; Kim, K.; Park, J. S. *Biomacromolecules* **2004**, *5*, 2487. (b) Luo, D.; Haverstick, K.; Belcheva, N.; Han, E.; Saltzman, W. M. *Macromolecules* **2002**, *35*, 3456. (c) Jevprasesphant, R.; Penny, J.; Jalal, R.; Attwood, D.; McKeown, N. B.; D'Emanuele, A. *Int J Pharmaceut* **2003**, *252*, 263.
- (15) (a) Waite, C. L.; Sparks, S. M.; Uhrich, K. E.; Roth, C. M. *Bmc Biotechnol* **2009**, *9*. (b) Kolhatkar, R. B.; Kitchens, K. M.; Swaan, P. W.; Ghandehari, H. *Bioconjugate Chem* **2007**, *18*, 2054. (c) Patil, M. L.; Zhang, M.; Betigeri, S.; Taratula, O.; He, H.; Minko, T. *Bioconjugate Chem* **2008**, *19*, 1396.
- (16) Lee, J. H.; Lim, Y. B.; Choi, J. S.; Choi, M. U.; Yang, C. H.; Park, J. S. *B Kor Chem Soc* **2003**, *24*, 1637.
- (17) Tang, M. X.; Redemann, C. T.; Szoka, F. C. *Bioconjugate Chem* **1996**, *7*, 703.
- (18) (a) Cross, K. J.; Langley, W. A.; Russell, R. J.; Skehel, J. J.; Steinhauer, D. A. *Protein Pept Lett* **2009**, *16*, 766. (b) Skehel, J. J.; Wiley, D. C. *Annu Rev Biochem* **2000**, *69*, 531. (c) Wiley, D. C.; Skehel, J. J. *Annu Rev Biochem* **1987**, *56*, 365. (d) Hughson, F. M. *Curr Biol* **1995**, *5*, 265.
- (19) (a) Fattal, E.; Nir, S.; Parente, R. A.; Szoka, F. C., Jr. *Biochemistry-Us* **1994**, *33*, 6721. (b) Funhoff, A. M.; van Nostrum, C. F.; Lok, M. C.; Kruijtzter, J. A.; Crommelin, D. J.; Hennink, W. E. *J Control Release* **2005**, *101*, 233. (c) Li, W.; Nicol, F.; Szoka, F. C., Jr. *Adv Drug Deliv Rev* **2004**, *56*, 967.

- (20) Merdan, T.; Kopecek, J.; Kissel, T. *Adv Drug Deliver Rev* **2002**, *54*, 715.
- (21) (a) El-Sayed, M. E.; Hoffman, A. S.; Stayton, P. S. *Expert Opin Biol Ther* **2005**, *5*, 23. (b) Pack, D. W.; Hoffman, A. S.; Pun, S.; Stayton, P. S. *Nat Rev Drug Discov* **2005**, *4*, 581. (c) Yessine, M. A.; Leroux, J. C. *Adv Drug Deliv Rev* **2004**, *56*, 999.
- (22) (a) Murthy, N.; Chang, I.; Stayton, P. S.; Hoffman, A. S. *Macromolecular Symposia* **2001**, *172*, 49. (b) Murthy, N.; Robichaud, J. R.; Tirrell, D. A.; Stayton, P. S.; Hoffman, A. S. *J Control Release* **1999**, *61*, 137.
- (23) (a) Thomas, J. L.; Barton, S. W.; Tirrell, D. A. *Biophys J* **1994**, *67*, 1101. (b) Thomas, J. L.; Tirrell, D. A. *Accounts of Chemical Research* **1992**, *25*, 336.
- (24) (a) Cheung, C. Y.; Murthy, N.; Stayton, P. S.; Hoffman, A. S. *Bioconjug Chem* **2001**, *12*, 906. (b) Kiang, T.; Bright, C.; Cheung, C. Y.; Stayton, P. S.; Hoffman, A. S.; Leong, K. W. *J Biomater Sci Polym Ed* **2004**, *15*, 1405.
- (25) Kyriakides, T. R.; Cheung, C. Y.; Murthy, N.; Bornstein, P.; Stayton, P. S.; Hoffman, A. S. *J Control Release* **2002**, *78*, 295.
- (26) (a) El-Sayed, M. E.; Hoffman, A. S.; Stayton, P. S. *J Control Release* **2005**, *101*, 47. (b) Bulmus, V.; Woodward, M.; Lin, L.; Murthy, N.; Stayton, P.; Hoffman, A. *J Control Release* **2003**, *93*, 105.
- (27) Boeckle, S.; von Gersdorff, K.; van der Piepen, S.; Culmsee, C.; Wagner, E.; Ogris, M. *J Gene Med* **2004**, *6*, 1102.
- (28) (a) Kurisawa, M.; Yokoyama, M.; Okano, T. *J Control Release* **2000**, *68*, 1. (b) Oskuee, R. K.; Dehshahri, A.; Shier, W. T.; Ramezani, M. *J Gene Med* **2009**, *11*, 921. (c) Wadhwa, M. S.; Collard, W. T.; Adami, R. C.; McKenzie, D. L.; Rice, K. G. *Bioconjugate Chem* **1997**, *8*, 81. (d) Wen, Y. T.; Pan, S. R.; Luo, X.; Zhang, X.; Zhang, W.; Feng, M. *Bioconjugate Chem* **2009**, *20*, 322.
- (29) (a) Forrest, M. L.; Koerber, J. T.; Pack, D. W. *Bioconjugate Chem* **2003**, *14*, 934. (b) Thomas, M.; Ge, Q.; Lu, J. J.; Chen, J. Z.; Klibanov, A. M. *Pharmaceut Res* **2005**, *22*, 373.
- (30) (a) Etrych, T.; Chytil, P.; Jelinkova, M.; Rihova, B.; Ulbrich, K. *Macromol Biosci* **2002**, *2*, 43. (b) Etrych, T.; Strohalm, J.; Kovar, L.; Kabesova, M.; Rihova, B.; Ulbrich, K. *J Control Release* **2009**, *140*, 18. (c) Kovar, M.; Kovar, L.; Subr, V.; Etrych, T.; Ulbrich, K.; Mrkvan, T.; Loucka, J.; Rihova, B. *J Control Release* **2004**, *99*, 301.
- (31) Lin, Y. L.; Jiang, G.; Birrell, L. K.; El-Sayed, M. E. *Biomaterials* **2010**, *31*, 7150.
- (32) (a) Davis, M. E.; Brewster, M. E. *Nat Rev Drug Discov* **2004**, *3*, 1023. (b) Del Valle, E. M. M. *Process Biochem* **2004**, *39*, 1033. (c) Uekama, K.; Hirayama, F.; Irie, T. *Chem Rev* **1998**, *98*, 2045.
- (33) Kircheis, R.; Schuller, S.; Brunner, S.; Ogris, M.; Heider, K. H.; Zauner, W.; Wagner, E. *J Gene Med* **1999**, *1*, 111.
- (34) Tang, G. P.; Zeng, J. M.; Gao, S. J.; Ma, Y. X.; Shi, L.; Li, Y.; Too, H. P.; Wang, S. *Biomaterials* **2003**, *24*, 2351.
- (35) Finsinger, D.; Remy, J. S.; Erbacher, P.; Koch, C.; Plank, C. *Gene Ther* **2000**, *7*, 1183.
- (36) Ogris, M.; Brunner, S.; Schuller, S.; Kircheis, R.; Wagner, E. *Gene Ther* **1999**, *6*, 595.

- (37) (a) Lee, Y.; Koo, H.; Jin, G. W.; Mo, H.; Cho, M. Y.; Park, J. Y.; Choi, J. S.; Park, J. S. *Biomacromolecules* **2005**, *6*, 24. (b) Petersen, H.; Merdan, T.; Kunath, K.; Fischer, D.; Kissel, T. *Bioconjug Chem* **2002**, *13*, 812.
- (38) (a) Kunath, K.; von Harpe, A.; Fischer, D.; Kissel, T. *J Control Release* **2003**, *88*, 159. (b) Zanta, M. A.; Boussif, O.; Adib, A.; Behr, J. P. *Bioconjug Chem* **1997**, *8*, 839.
- (39) Davis, M. E. *Mol Pharm* **2009**, *6*, 659.
- (40) Bartlett, D. W.; Davis, M. E. *Biotechnol Bioeng* **2008**, *99*, 975.
- (41) (a) Gillies, E. R.; Frechet, J. M. J. *Journal of the American Chemical Society* **2002**, *124*, 14137. (b) Newland, B.; Tai, H. Y.; Zheng, Y.; Velasco, D.; Di Luca, A.; Howdle, S. M.; Alexander, C.; Wang, W. X.; Pandit, A. *Chemical Communications* **2010**, *46*, 4698. (c) Synatschke, C. V.; Schallon, A.; Jerome, V.; Freitag, R.; Muller, A. H. E. *Biomacromolecules* **2011**, *12*, 4247.

Chapter 3.

Degradable, pH-sensitive, membrane-destabilizing, comb-like polymers for intracellular delivery of nucleic acids

3.1 Introduction

Recent advances in drug design have led to the development of several classes of nucleic acid molecules such as plasmid DNA (pDNA), antisense oligodeoxynucleotides (ASODN), short interfering RNA (siRNA), and micro RNA (miRNA), which have the potential to treat cancer, viral infection, and cardiovascular and neurodegenerative diseases.¹ These nucleic acid therapies are typically internalized by endocytosis where they accumulate in the endosomal-lysosomal trafficking pathway, which results in their degradation and loss of therapeutic activity.² Transforming these nucleic acid molecules into therapeutic agents with defined dosing regimens and well-characterized activity requires the development of specialized carriers that can successfully condense and shield nucleic acid molecules into nano-sized particles that preferentially accumulate in the diseased tissue, selectively taken up by target cells, effectively escape the endosomal compartment, and deliver their therapeutic cargo into the cytoplasm to interact with defined intracellular targets and produce the desired therapeutic activity.³

Viral vectors proved to be highly efficient in delivering nucleic acids into the cytoplasm of infected cells.⁴ For example, the influenza virus utilizes the pH-sensitive membrane-

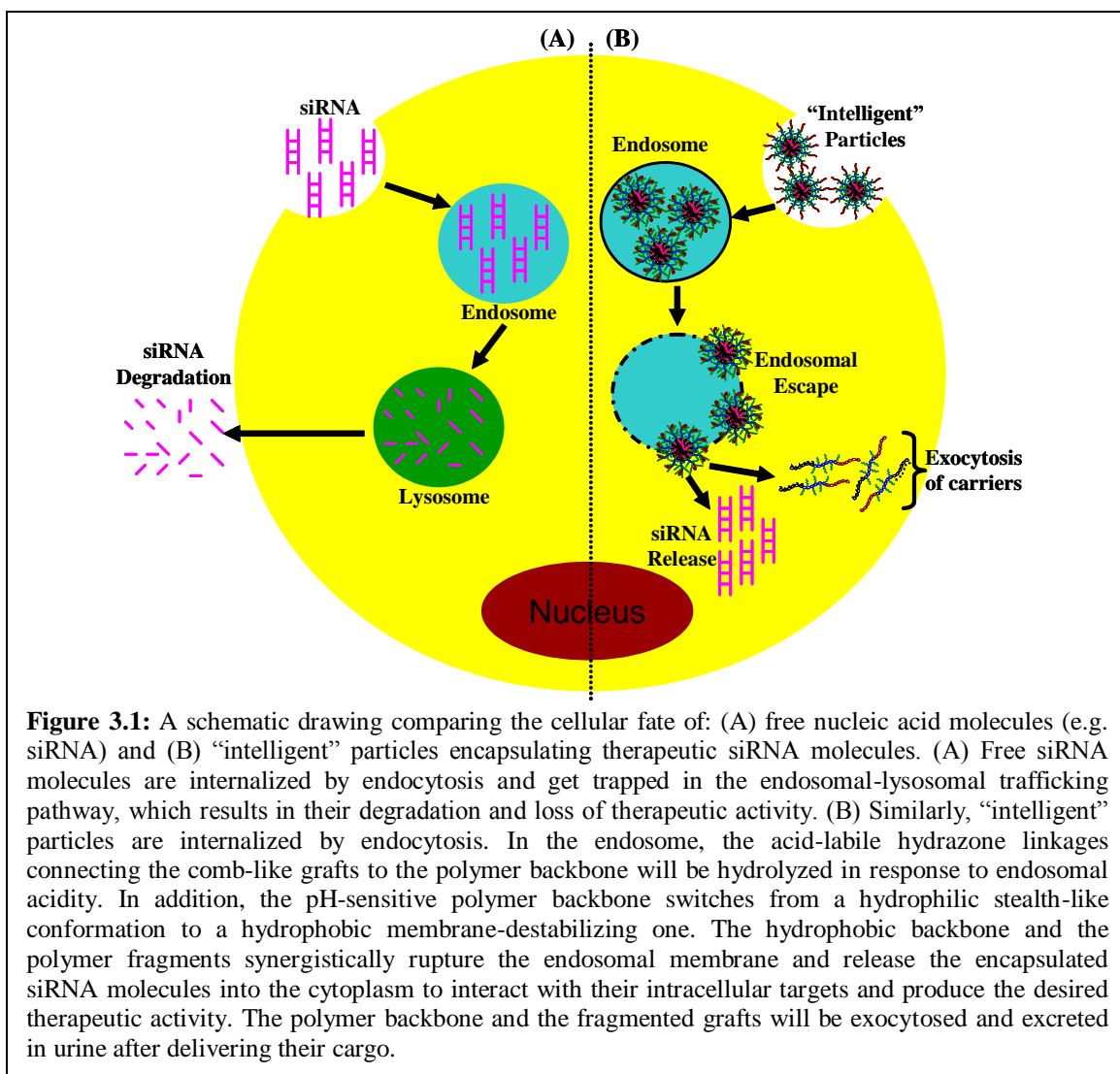
destabilizing Hemagglutinin protein displayed on the viral coat to disrupt the endosomal membrane and enter the cytoplasm.⁵ Hemagglutinin and other fusion proteins are characterized by their unique ability to switch from an ionized and hydrophilic conformation at physiologic pH to a hydrophobic and membrane-active one in response to acidic endosomal pH gradients, which destabilizes the endosomal membrane leading to leakage of endosomal contents into the cytoplasm.⁵ Szoka, Wagner, and others have used artificial, pH-sensitive, fusogenic peptides to enhance cytoplasmic gene delivery.⁶ Despite the endosomolytic activity of these fusogenic peptides, their potential immunogenicity and toxicity limit their clinical use.

Several groups have focused their efforts on the development of synthetic polymeric carriers that mimic the endosomolytic properties of fusogenic proteins and enhance the cytoplasmic delivery of therapeutic macromolecules.⁷ These polymers are characterized by their unique ability to “sense” the changes in environment pH where they undergo a change from a hydrophilic, stealth-like conformation at physiologic pH to a hydrophobic and membrane-destabilizing one in response to acidic endosomal pH gradients. Poly(ethylacrylic acid) (PEAA) is the first reported polymer to display a pH-dependent disruption of synthetic lipid vesicles at acidic pH of 6.3 or lower.⁸ Stayton, Hoffman, and coworkers expanded this family of synthetic polymers by synthesizing poly(propylacrylic acid) (PPAA) and copolymers of acrylic acid and alkyl acrylates, which showed a pH-dependent membrane-destabilizing activity that increased with the increase in the proportion of hydrophobic alkyl acrylates in polymer composition.⁹ PPAA exhibited a pH-dependent membrane-destabilizing activity that is one order of magnitude higher than PEAA⁹ and proved to enhance the transfection efficiency of cationic lipid/pDNA

complexes both *in vitro*¹⁰ and *in vivo*.¹¹ However, the number of anionic carboxylate groups of the PPAA polymer affects charge balance in cationic lipid and polymer/DNA complexes and the order of mixing of PPAA proved to affect the size, surface charge, stability, and transfection efficiency of these complexes.^{10a,12} Subsequent polymers incorporated a glutathione-sensitive monomer, pyridyl disulfide acrylate (PDSA), to allow direct coupling of cationic peptides to the pH-sensitive polymer backbone.¹³ These polymer-peptide conjugates proved to complex DNA nucleotides and retain their membrane-destabilizing activity in response to acidic pH gradients.¹³

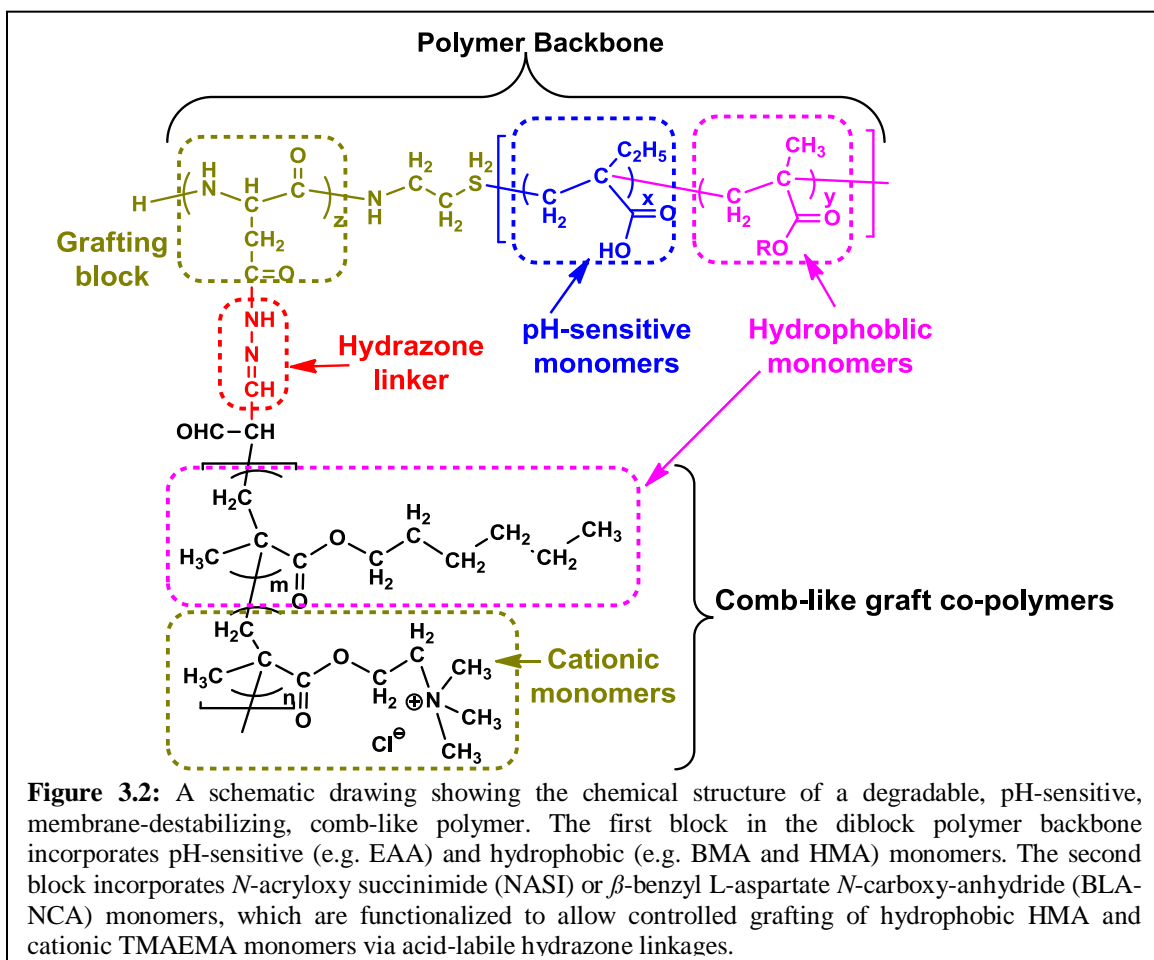
Earlier research showed that the membrane-destabilizing activity and the ability of these polymers to condense DNA/RNA molecules relies on a delicate balance between the content of pH-sensitive acrylic acid and hydrophobic alkyl acrylate monomers, the net positive charge of polymer-cationic peptide conjugates, and their overall molecular weight.^{13b} The optimum molar content of EAA and PAA monomers is typically more than 60% of the polymer backbone to maintain aqueous solubility and pH sensitivity of the polymer. However, this high content of anionic carboxylate groups causes electrostatic repulsion between the pH-sensitive polymer and the negatively charged phosphate groups of the loaded DNA/RNA molecules, which reduces the amount of nucleic acid incorporated in cationic lipid or polymer/DNA complexes.^{13b} Covalent conjugation of cationic peptides to PDSA-containing polymers significantly improved their aqueous solubility and allowed for effective complexation of DNA/RNA molecules.¹³ However, PDSA content in these polymers remains limited to avoid reducing the content of the hydrophobic alkyl acrylate monomers in the polymer backbone, which are essential to achieve the desired membrane-destabilizing activity.¹³

The membrane-destabilizing activity of these polymers increases with the increase in polymer's molecular weight. However, these are linear non-degradable polymers that rely on renal excretion to be eliminated from the body, which limits their molecular weight to a maximum of 45-50 KDa.^{13b}



This research focuses on the design and synthesis of polymeric carriers that can condense a large dose of therapeutic nucleic acids into particles that can “sense” the drop in environment pH after internalization into target cells via endocytosis, which will trigger particle degradation into small membrane-destabilizing polymer fragments that rupture

the endosomal membrane and release the encapsulated nucleic acid cargo into the cytoplasm to interact with their targets and produce the desired therapeutic activity (**Figure 3.1**). These comb-like polymers are constructed on diblock copolymers where the first block incorporates pH-sensitive EAA monomers and hydrophobic butyl methacrylate (BMA) or hexyl methacrylate (HMA) monomers at a 60/40 molar feed ratio. The second block is synthesized using *N*-acryloxy succinimide (NASI) or β -benzyl L-aspartate *N*-carboxy-anhydride (BLA-NCA) monomers, which are functionalized to allow for controlled grafting of hydrophobic HMA and cationic trimethyl aminoethyl methacrylate (TMAEMA) copolymers at a 50/50 molar feed ratio via acid-labile hydrazone linkages (**Figure 3.2**).



The polymer backbone is tailored to have a molecular weight below 45-50 KDa and to exhibit a high membrane-destabilizing activity in response to acidic stimuli. The comb-like grafts have an average molecular weight of 20 KDa per graft and incorporate cationic TMAEMA monomers for condensation of DNA/RNA molecules and hydrophobic HMA monomers to enhance their membrane-destabilizing activity. These comb-like polymers will complex nucleic acid molecules via electrostatic interaction forming pH-sensitive particles that will fragment upon exposure to acidic endosomal pH gradients due to hydrolysis of the hydrazone linkages connecting poly(HMA-*co*-TMAEMA) grafts to the polymers backbone (**Figure 3.3**). The membrane-destabilizing backbone and the hydrophobic monomers embedded in the comb-like grafts will synergistically disrupt the endosomal membrane and release the nucleic acid cargo into the cytoplasm to produce the desired therapeutic activity. These polymer fragments are engineered to be quickly eliminated *in vivo* by renal excretion.

This manuscript describes the synthesis, characterization, and membrane-destabilizing activity of a new family of degradable, pH-sensitive, comb-like polymers. It describes the ability of these comb-like polymers to condense siRNA molecules into particles and reports their size, zeta potential, and serum and nuclease stability. We also report the uptake of particles incorporating anti-GAPDH siRNA molecules into MCF-7 breast cancer cells and the associated knockdown of GAPDH gene expression as a function of particle composition.

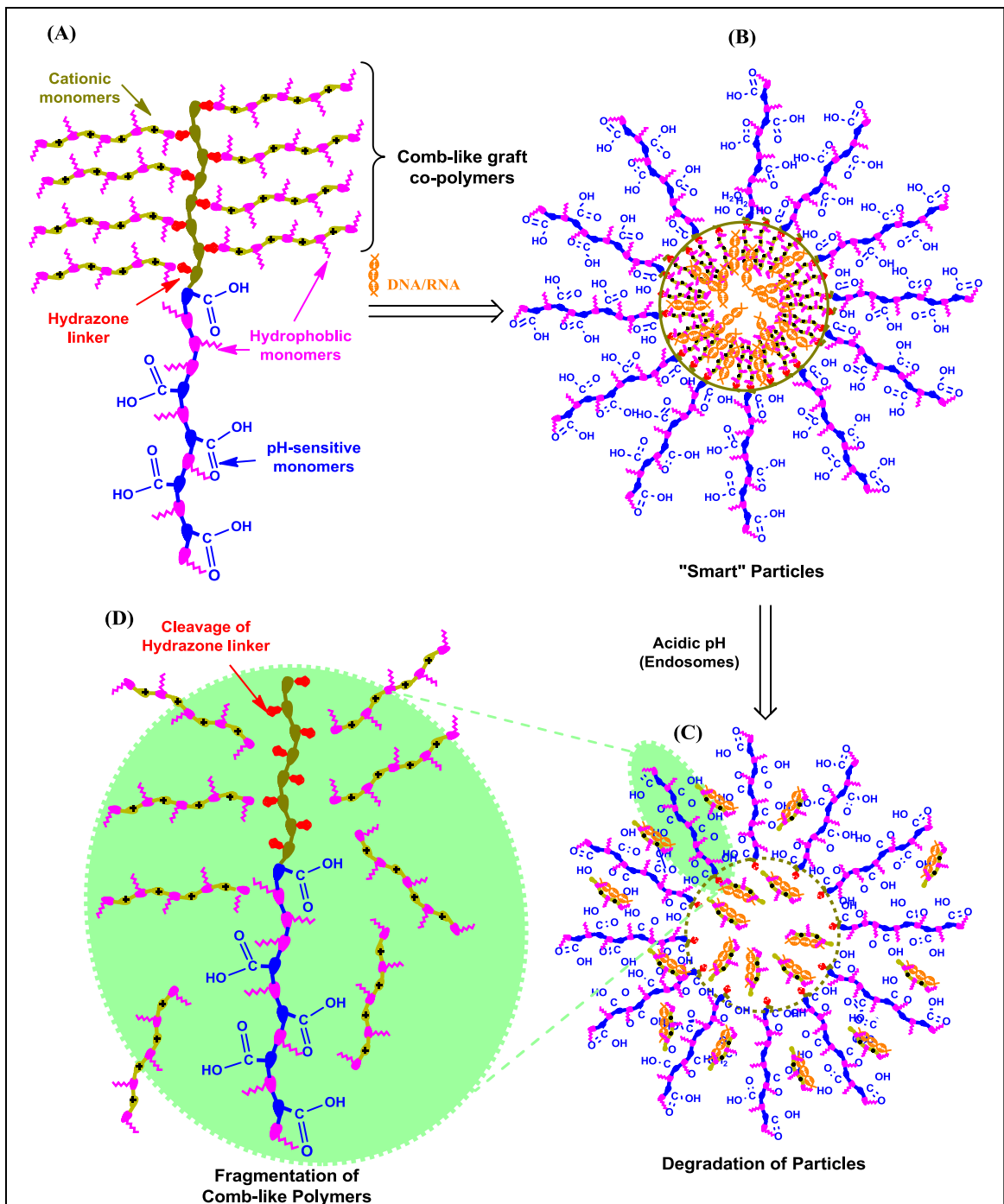


Figure 3.3: A schematic drawing showing the structure of a comb-like polymer, complexation of siRNA molecules into “smart” particles, their response to acidic pH, and fragmentation of the comb-like carrier. (A) is a schematic of a degradable, pH-sensitive, membrane-destabilizing, comb-like polymer at pH 7.4 with intact hydrazone linkages between the grafts and the polymer backbone. (B) This polymer condenses therapeutic nucleic acids into “smart” particles, which remain intact at neutral pH but degrade upon exposure to acidic endosomal pH gradients (C) due to hydrolysis of the acid-labile hydrazone linkage and fragmentation of the comb-like carrier (D).

3.2 Materials and methods

3.2.1 Materials

Copper (I) bromide (Cu(I)Br), 1,1,4,7,7-pentamethyldiethylenetriamine (PMDETA), 2,2'-Azo-bis(isobutyronitrile) (AIBN), BMA, HMA, NASI, TMAEMA, and all solvents were purchased from Sigma-Aldrich Chemical Co. (St. Louis, MO). All reagents were used as delivered without further purification except for AIBN, which was crystallized from methanol prior to use. EAA monomer and 2-dodecylsulfanylthiocarbonylsulfanyl-2-methyl propionic acid (DMP) chain transfer agent were synthesized following published procedures.¹⁴ The β -benzyl L-aspartate *N*-carboxy-anhydride (BLA-NCA) monomer was synthesized using triphosgene following the Fuchs-Farthing method.¹⁵ The human anti-GAPDH siRNA, FAM-labeled anti-GAPDH siRNA, negative siRNA sequence, KDaAlert GAPDH assay kit, RNase V1 enzyme, and siPORT-NH₂ transfection reagent were purchased from Ambion Inc. (Austin, TX). The RNeasy Mini Kit and Omniscript reverse transcriptase kit were purchased from Qiagen (Valencia, CA). The TaqMan universal PCR master mix and TaqMan gene expression assays for human GAPDH and β -actin genes were purchased from Applied Biosystems (Foster, CA). The PicoGreen assay was purchased from Molecular probes (Eugene, OR).

3.2.2 Synthesis of poly(ethyl acrylic acid-co-alkyl methyl acrylate) copolymers

The first block of the polymer backbone was synthesized by reversible addition-fragmentation chain transfer (RAFT) polymerization (**Figure 3.4A**) and random free radical polymerization (**Figure 3.5A**). For synthesis following RAFT polymerization techniques, we mixed EAA monomers (1.0 gm, 10×10^{-3} moles) with BMA monomers (3.3×10^{-3} moles), DMP (33 mg, 9.15×10^{-5} moles), and AIBN (3 mg, 1.83×10^{-5} moles) in

a 50 ml round bottom Schlenk tube. The reaction mixture was degassed by purging with nitrogen for 20 minutes and placed in an oil bath at 60 °C for 17 hours. The resulting crude polymer was dissolved in dimethyl formamide (DMF), precipitated in diethyl ether, and dried under vacuum to yield pure poly(EAA-*co*-BMA) polymer. For synthesis using random free radical polymerization, we replaced the DMP chain transfer agent with cysteamine (33 mg, 9.15×10^{-5} moles) and followed the same reaction protocol except for increasing the reaction time to 48 hours.

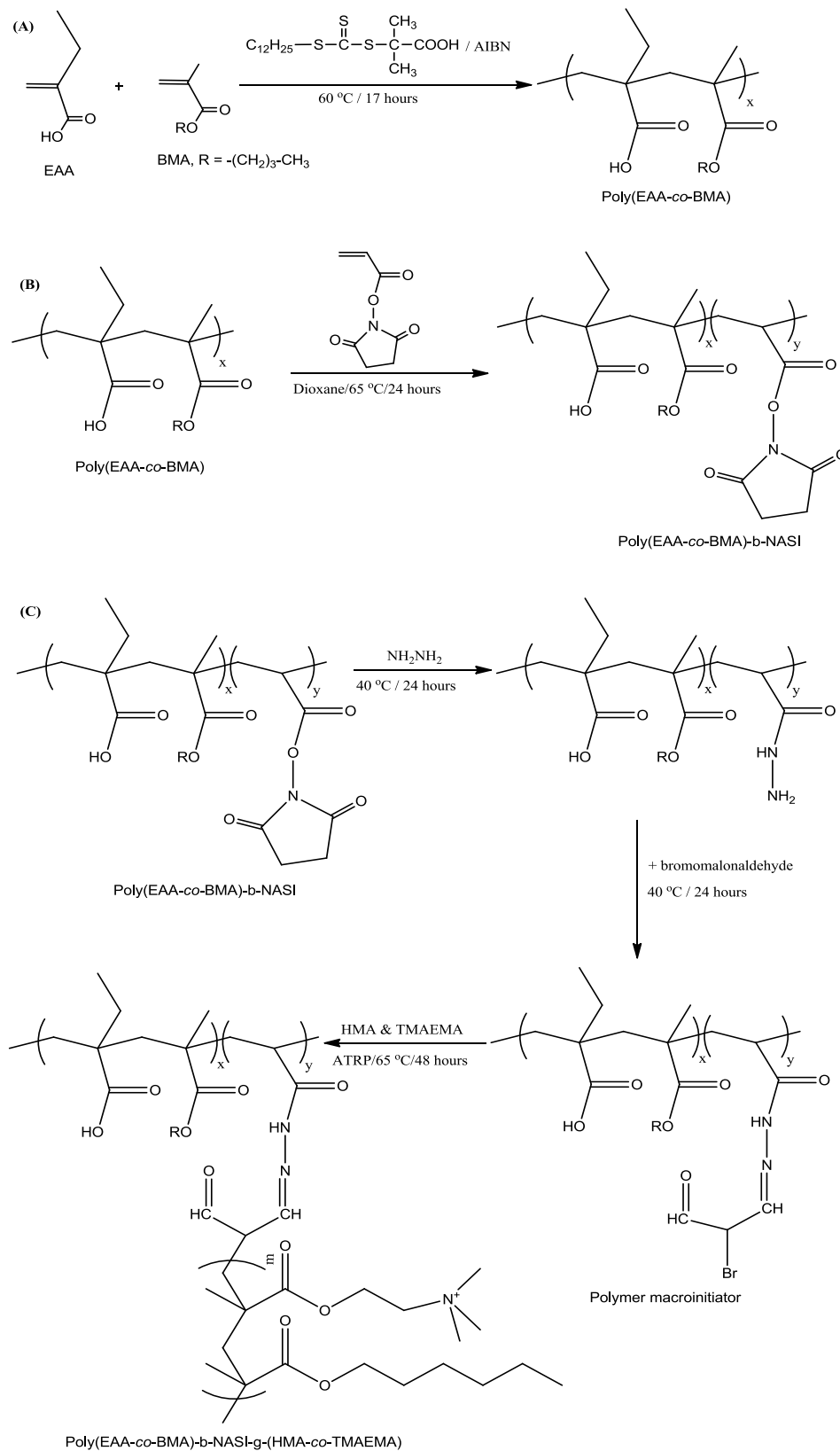
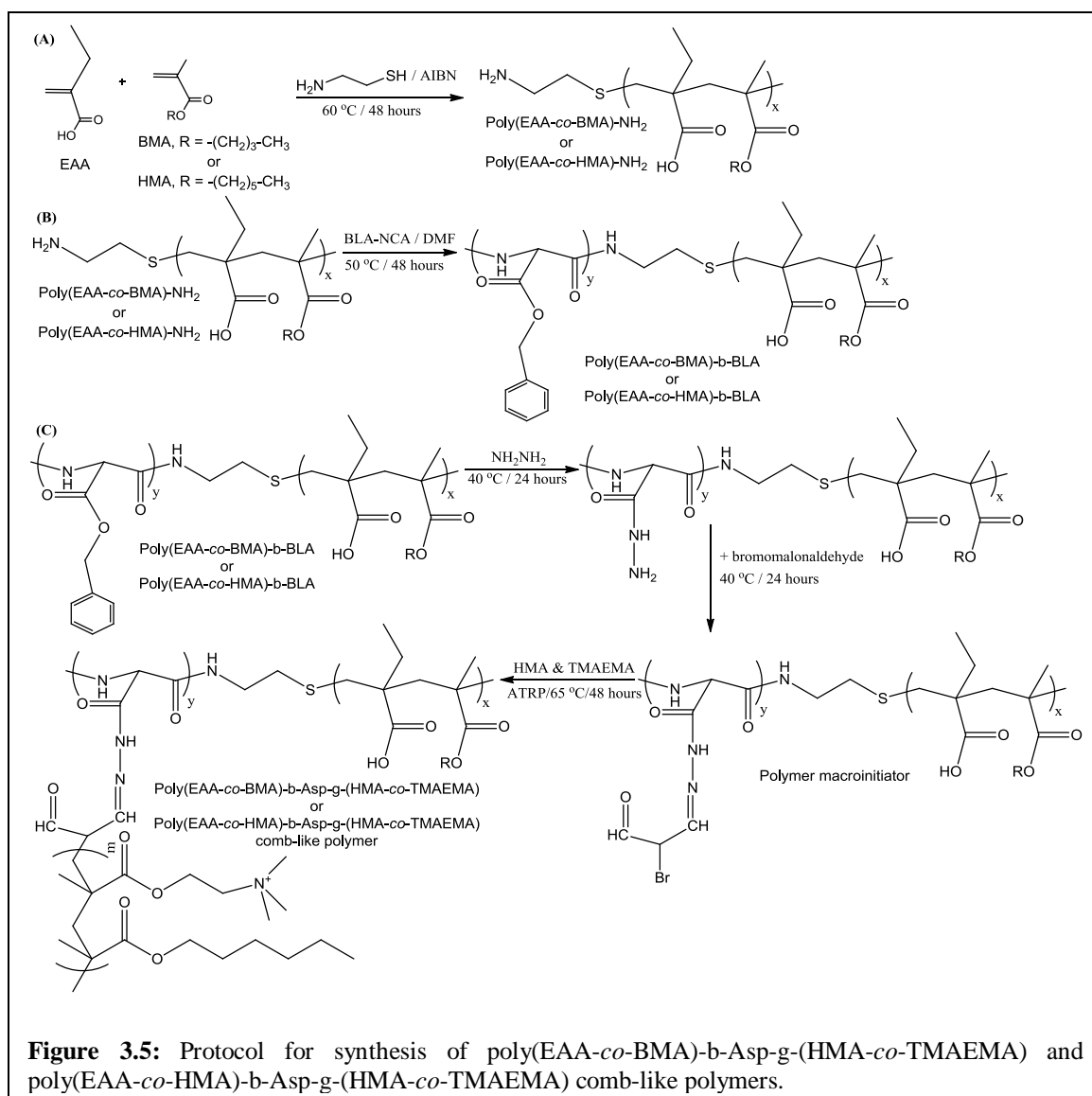


Figure 3.4: Protocol for synthesis of poly(EAA-co-BMA)-b-NASI-g-(HMA-co-TMAEMA) comb-like polymer.



3.2.3 Synthesis of poly(ethyl acrylic acid-co-butyl methacrylate)-b-N-acryloxy succinimide copolymers

The first block of this diblock copolymer, poly(EAA-co-BMA) polymer, was dissolved in dioxane and mixed with *N*-acryloxy succinimide (NASI) monomers at a 1:56 molar ratio in a round bottom Schlenk tube followed by purging with nitrogen for 15 minutes. The AIBN initiator (5 mg, 3.0×10^{-5} moles) was added to the reaction mixture before placing the tube in an oil bath at 65 °C for 24 hours (**Figure 3.4B**). The crude polymer

was dissolved in DMF, precipitated in diethyl ether, and dried under vacuum to yield pure poly(EAA-*co*-BMA)-*b*-NASI copolymer.

3.2.4 Synthesis of poly(ethyl acrylic acid-*co*-alkyl methyl acrylate)-*b*- β -benzyl L-aspartate copolymers

We dissolved poly(EAA-*co*-BMA)-NH₂ or poly(EAA-*co*-HMA)-NH₂ polymers synthesized by free radical polymerization in presence of cysteamine in DMF and mixed with β -benzyl L-aspartate *N*-carboxy anhydride (BLA-NCA) monomers at a 1:100 molar ratio in a round bottom Schlenk tube that was allowed to react at 50 °C for 48 hours (**Figure 3.5B**). BLA-NCA monomers reacted with the terminal NH₂ group of the first block through a ring-opening polymerization reaction forming the second poly(β -benzyl L-aspartate) block. The crude product was dissolved in DMF, precipitated in diethyl ether, and dried under vacuum to yield pure poly(EAA-*co*-BMA)-*b*-BLA and poly(EAA-*co*-HMA)-*b*-BLA polymers.

3.2.5 Graft polymerization of HMA and TMAEMA monomers via hydrazone linkages

The diblock polymer backbone with NASI and BLA blocks was used to synthesize macroinitiators for graft polymerization of HMA and TMAEMA monomers (**Figure 3.4C & Figure 3.5C**). The polymer backbone was dissolved in dimethyl sulfoxide (DMSO), mixed with anhydrous hydrazine in a Schlenk tube, and allowed to react at 40 °C for 24 hours. The crude product was dissolved in DMF, precipitated in diethyl ether, and dried under vacuum to yield pure polymer-hydrazine conjugates, which was dissolved in DMSO and allowed to react with bromomalonaldehyde at a hydrazine-to-bromomalonaldehyde molar ratio of 1:1.5 for 24 hours at room temperature. The pure

macroinitiator was precipitated in acetone, filtered, and dried overnight under vacuum. The selected macroinitiator was dissolved in DMF, mixed with equimolar concentrations of HMA and TMAEMA monomers, the [Cu(I)Br] catalyst, and HMTETA ligand at a 1:1 molar ratio followed by three freeze-vacuum-thaw cycles before placing the reaction mixture in an oil bath at 60 °C for 48 hours while stirring. The molar ratio of the macroinitiator, HMA, and TMAEMA were controlled to prepare poly(HMA-co-TMAEMA) grafts with a weight average molecular weight (M_w) of 20 KDa equally split between the HMA and TMAEMA units. The final comb-like polymers were precipitated in diethyl ether, dried under vacuum, and further purified by dialysis against a NaOH solution (pH = 10) for 24 hours followed by lyophilization for 48 hours.

3.2.6 Characterization of the diblock backbone and comb-like grafts

The purity and composition of the all the synthesized polymers were evaluated based on their $^1\text{H-NMR}$ spectra in DMSO- d_6 recorded using a 300 MHz Varian Mercury system (Palo Alto, CA) at ambient temperature. The weight average molecular weight and molecular weight distribution of each polymer were examined based on their elution volume on an Ultrahydrogel 500 column compared to a series of poly(ethylene glycol) standards (Polymer Laboratories Ltd, UK) using Tris-HCL buffer (pH = 8) as a mobile phase at a flow rate of 0.5 ml/min. Detection of the eluting polymers was done using a Waters 2414 refractive index detector under the control of Breeze software run by an external PC (Waters Corporation, Milford, MA). Fragmentation of comb-like polymers in response to acidic environment was evaluated by dissolving 5 mg of each of the comb-like polymers in phosphate-buffered saline (PBS) with pH 5.8 and incubating at 37 °C for 24 hours while stirring. A 100 μl sample was drawn from each of these polymer solutions

at 0.5, 1, 2, 6, 12, and 24 hours for analysis by gel permeation chromatography. The areas under the curve for the peaks corresponding to the parent comb-like polymer and poly(HMA-*co*-TMAEMA) fragments were used to quantify the amount of each polymer species present in solution at a given time point to determine the hydrolysis rate of the hydrazone linkages connecting the polymer grafts to the backbone.

3.2.7 Evaluation of the pH-dependent membrane-destabilizing activity of comb-like polymers

The membrane-destabilizing activity of the polymer backbone and comb-like polymers was assessed based on their ability to hemolyze red blood cells (RBCs) at different pH values. Briefly, human blood was collected in EDTA-containing vacutainers, which were centrifuged at 13,500xg to separate the RBCs. The plasma supernatant was discarded and the RBCs were washed three times using a 150 mM saline solution. After the third wash, the RBCs solution was equally divided into three vacutainers and suspended in 100 mM PBS solutions with pH 5.8, 6.6, or 7.4. The RBCs solutions were diluted 10-fold using PBS with the corresponding pH value to reach a concentration of 10^8 RBCs per 200 μ l solution. Stock polymer solutions were prepared by dissolving each polymer in PBS solution of pH 7.4. The hemolytic activity poly(EAA-*co*-BMA) and poly(EAA-*co*-HMA) copolymers and the comb-like polymers was evaluated as a function of polymer concentration (50, 100, and 200 μ g/ml). The appropriate volume of the polymer stock solution was added to 800 μ l of PBS solution and 200 μ l of RBCs solution with the appropriate pH to reach the desired polymer concentration. The RBCs solutions were gently inverted several times for mixing with the added polymer solution then incubated for 60 min at 37 °C. The membrane-destabilizing activity of a given polymer was

measured in terms of its ability to rupture the cell membrane of RBCs allowing the release of hemoglobin into the solution. At the end of the incubation time, RBCs solutions were centrifuged at 13,500xg for 5 min to pellet out intact and ruptured RBCs leaving the hemoglobin in the supernatant solution. Absorbance of hemoglobin in the supernatant was measured at its characteristic wavelength, 541 nm. The observed hemolysis of RBCs in PBS solutions with different pH values and in DI water was used as negative and positive controls, respectively. The observed hemolytic activity of a given polymer at a given concentration and pH value was normalized to that of the positive control, DI Water. All hemolysis experiments were carried out in triplicate.

3.2.8 Formulation and characterization of “smart” particles

The pH-sensitive comb-like polymers were dissolved in RNase free water and mixed with 0.5 µg of anti-GAPDH siRNA molecules dissolved in 1 µl of RNase free water at different nitrogen/phosphate (N/P) ratios. Each mixture was vortexed and allowed to stand at room temperature for 20 minutes before loading onto a 1% w/v agarose gel. The gel was immersed in a Tris acetate EDTA (TAE) buffer and run at 60 V for 1 hour before staining with SYBR Green II dye (Pierce, Rockford, IL) for 30 minutes and visualized under UV using a fluorescent green filter (Fotodyne Incorporated, Hartland, WI). Size and zeta potential of the particles prepared using different comb-like polymers at N/P ratio of 2.5/1 were measured using 90Plus particle size analyzer with ZetaPALS capability (Brookhaven Instruments Corporation, Holtsville, NY).

3.2.9 Culture of MCF-7 cells

MCF-7 breast cancer cells were purchased from ATCC (Manassas, VA) and cultured following established protocols. Briefly, MCF-7 cells were maintained in Eagle's

minimum essential medium (EMEM) supplemented with 10% fetal bovine serum, 0.01 mg/ml bovine insulin, 10,000 units/ml penicillin, 10,000 µg/ml streptomycin and regularly changing the growth medium every 2 days. MCF-7 cells were incubated at 37 °C, 5% CO₂, 95% relative humidity, and passaged upon reaching 70-90% confluency using 0.25% trypsin/EDTA mixture.

3.2.10 Cellular uptake of “smart” particles

Comb-like polymers and commercial siPORT-NH₂ were dissolved in OPTI-MEM solution and mixed with 0.57 µg of FAM-labeled anti-GAPDH siRNA molecules at N/P ratios of 1.5/1, 2.5/1, 4/1, 8/1, and 12/1 to prepare different particles that were incubated with MCF-7 cells for 6 hours at 37 °C, 5% CO₂, and 95% relative humidity. MCF-7 cells were washed with PBS, treated with 0.25% trypsin/EDTA solution for 10 minutes, harvested, and centrifuged to remove the supernatant and form a cell pellet. MCF-7 cell pellets were suspended in PBS and analyzed using Biosciences FACSCalibur (Becton Dickinson, Franklin Lakes, NJ) to determine the percentage of fluorescently-labeled MCF-7 cells for each treatment. MCF-7 cells were gated by forward/size scatter and 10,000 gated events were collected per sample to discriminate between live and dead cells and account for live cells only.

3.2.11 In vitro transfection of MCF-7 cells

MCF-7 cells were plated in 24-well plates at a seeding density of 40,000 cells/well and allowed to adhere for 24 hours. The particles and siPORT-NH₂ complexes incorporating 0.57 µg of anti-GAPDH siRNA or control siRNA molecules were incubated with MCF-7 cells at a final siRNA concentration of 100 nM for 6 hours followed by addition of 500 µl of fresh culture medium and incubation for a total of 48 hours. The effect of different

treatments on GAPDH expression was quantified based on mRNA and protein levels. For quantification of mRNA, total RNA was isolated from MCF-7 cells using the RNeasy Mini Kit and 0.25 μg of total RNA was reverse transcribed using Omniscript reverse transcriptase kit following manufacturer's protocols. Real time PCR was performed in a final volume of 20 μl containing 2 μl of cDNA (corresponding to 10 ng of total RNA for GAPDH and β -actin amplification), 1 μl of each primer, and 10 μl of the qPCR MasterMix in the 7500 Fast Real-Time PCR system. The amount of GAPDH protein expressed by MCF-7 cells was measured using the KDAlert assay following manufacturer's specifications. The level of GAPDH protein expression in response to different treatments was normalized to that of untreated control cells.

3.2.12 Effect of serum and nuclease enzymes on stability of “smart” particles

The particles were prepared by mixing pH-sensitive comb-like polymers with 0.57 μg of anti-GAPDH siRNA molecules at a N/P (+/-) ratio of 2.5/1 followed by addition of 10 or 25% FBS and incubation at 37 $^{\circ}\text{C}$ for 6 hours. The amount of siRNA released from different particles was measured by adding the PicoGreen dye and measuring the fluorescence intensity using a Fluoroskan microplate reader (Thermo Fisher Scientific Inc., Waltham, MA) at λ_{ex} of 485 nm and λ_{em} of 518 nm. The fluorescence intensity of each solution was normalized to that observed upon mixing the PicoGreen dye with 0.57 μg of anti-GAPDH siRNA to determine the amount of free siRNA present in solution.

The enzymatic stability of particle 1 was assayed using the gel retardation assay. Briefly, poly(EAA-*co*-BMA)-*b*-NASI-*g*-(HMA-*co*-TMAEMA) comb-like polymer was dissolved in RNase free water and mixed with 0.57 μg of anti-GAPDH siRNA molecules at N/P (+/-) ratios of 1/1, 2.5/1, 4/1, 8/1, and 12/1. Free siRNA and the complexes prepared at

different N/P ratios were incubated with RNase V1 enzyme at 37 °C for 30 minutes before loading onto a 1% w/v agarose gel, which was subjected to 60 mV electric current for 60 minutes and stained with SYBR Green II dye. UV was used to visualize siRNA shift. The fluorescence intensity of each band for the complexes treated with the RNase enzyme (+) was compared to that of complexes not treated (-) with the RNase enzyme using free siRNA as a control.

3.3 Results and Discussion

3.3.1 Synthesis of degradable, pH-sensitive, membrane-destabilizing, comb-like polymers

The focus of this work is the design and synthesis of pH-sensitive carriers that can successfully condense a large dose of DNA/RNA molecules into particles that will be internalized into target cells via endocytosis. In the endosome, these particles will “sense” the drop in pH, which triggers their degradation into small membrane-destabilizing fragments that disrupt the endosomal membrane and release the encapsulated nucleic acid into the cytoplasm to interact with specific intracellular targets to produce the desired therapeutic activity (**Figure 3.3**). These degradable, pH-sensitive, membrane-destabilizing, comb-like polymers are constructed on a diblock polymer backbone where the first block incorporates pH-sensitive EAA and hydrophobic BMA or HMA monomers at a 60/40 molar feed ratio. The second block in the backbone is either *N*-acryloxy succinimide (NASI) or β -benzyl L-aspartate *N*-carboxy-anhydride (BLA-NCA) monomers to allow controlled grafting of poly(HMA-*co*-TMAEMA) copolymers via acid-labile hydrazone linkages.

Results show that the first block in the polymer backbone, poly(EAA-*co*-BMA) and poly(EAA-*co*-HMA) copolymers, was successfully synthesized by RAFT and random free radical polymerization techniques with average yields of 97.2% and 91.7%, respectively. The molar ratio of EAA to BMA/HMA monomers in the synthesized polymers is approximately 55/45, which is similar to their feed ratio (**Table 3.1**). Controlled addition of the NASI monomers to poly(EAA-*co*-BMA) polymer yielded a diblock copolymer with an average polymerization yield of 90%. Similarly, poly(EAA-*co*-BMA)-NH₂ and poly(EAA-*co*-HMA)-NH₂ polymers reacted with BLA-NCA monomers via a ring-opening polymerization reaction to yield a diblock copolymer with an average yield of 92%. Both NASI- and BLA-containing polymers reacted with hydrazine and bromomalonolaldehyde to yield macroinitiators that incorporate an acid-labile hydrazone linkage. Atom transfer radical polymerization (ATRP)-controlled grafting of HMA and TMAEMA monomers to poly(EAA-*co*-BMA)-b-NASI backbone was efficient and produced 22 comb-like grafts, which account for 93% of the Br-activated NASI monomers present in the polymer backbone (**Table 3.1**). The molar ratio of HMA to TMAEMA monomers in the grafts closely followed their feed ratio (**Table 3.1**). Grafting of HMA and TMAEMA monomers to poly(EAA-*co*-BMA)-b-BLA and poly(EAA-*co*-HMA)-b-BLA polymers yielded 4 and 10 comb-like grafts, which account for grafting efficiencies of 37% and 38%, respectively (**Table 3.1**). It is important to note that NASI-containing polymers have a higher positive charge density compared to BLA-containing polymers due to the higher number of grafts attached per polymer backbone where poly(EAA-*co*-BMA)-b-NASI-g-(HMA-*co*-TMAEMA) comb-like polymer has the highest TMAEMA content per unit weight. The variation in TMAEMA content will vary

the amount of comb-like polymer necessary to complex a given dose of nucleic acid producing particles with different polymer content.

Table 3.1: Composition of new degradable, pH-sensitive, membrane-destabilizing, comb-like polymers

Polymer Name	Molecular Weight (g/mol)^a	Monomers Molar Ratio^b	Number of NASI or BLA Monomers^d	Number of Grafts/Grafting Efficiency^e	Number of TMAEMA Units per Graft/ Comb-like Polymer^f	Number of HMA Units per Graft/ Comb-like Polymer^g
Poly(EAA-co-BMA)	33,000	54.9 : 45.1	-	-	-	-
Poly(EAA-co-BMA)-b-NASI	37,000	51.3 : 36.2 : 12.5	24	-	-	-
Poly(EAA-co-BMA)-b-NASI-g-(HMA-co-TMAEMA)	481,000	48.3 : 51.7 ^c	24	22 / 93	60 / 1,330	57 / 1,250
Poly(EAA-co-BMA)-NH ₂	56,000	59.05 : 40.95	-	-	-	-
Poly(EAA-co-BMA)-b-BLA	58,000	54.6 : 29.2 : 16.1	11	-	-	-
Poly(EAA-co-BMA)-b-Asp-g-(HMA-co-TMAEMA)	135,000	54.5 : 45.5 ^c	11	4 / 37	53 / 205	64 / 247
Poly(EAA-co-HMA)-NH ₂	52,000	59.1 : 40.9	-	-	-	-
Poly(EAA-co-HMA)-b-BLA	57,000	40.9 : 41.6 : 17.4	26	-	-	-
Poly(EAA-co-HMA)-b-Asp-g-(HMA-co-TMAEMA)	256,000	41.2 : 58.8 ^c	26	10 / 38	69 / 684	49 / 482

^a The weight average molecular weight of each polymer is calculated based on its retention volume in relation to the elution volumes of a series of poly(ethylene glycol) standards run on an Ultrahydrogel 500 column using Tris-HCL buffer (pH = 8) as a mobile phase at a flow rate of 0.5 ml/min.

^b Monomer's molar ratio determined using the ¹H-NMR spectra of the pure polymer.

^c The molar ratio of the HMA and TMAEMA monomers incorporated in the comb-like grafts determined using the ¹H-NMR spectra of the pure polymer.

^d The number of NASI and BLA monomers incorporated in the second block of the polymer backbone calculated using the ¹H-NMR spectra of the pure polymer.

^e The number of poly(HMA-co-TMAEMA) grafts attached to the polymer backbone calculated based on the molecular weight of the comb-like polymer. Grafting efficiency is based on the ratio between the number of grafts to the number of NASI or BLA monomers incorporated in the polymer backbone.

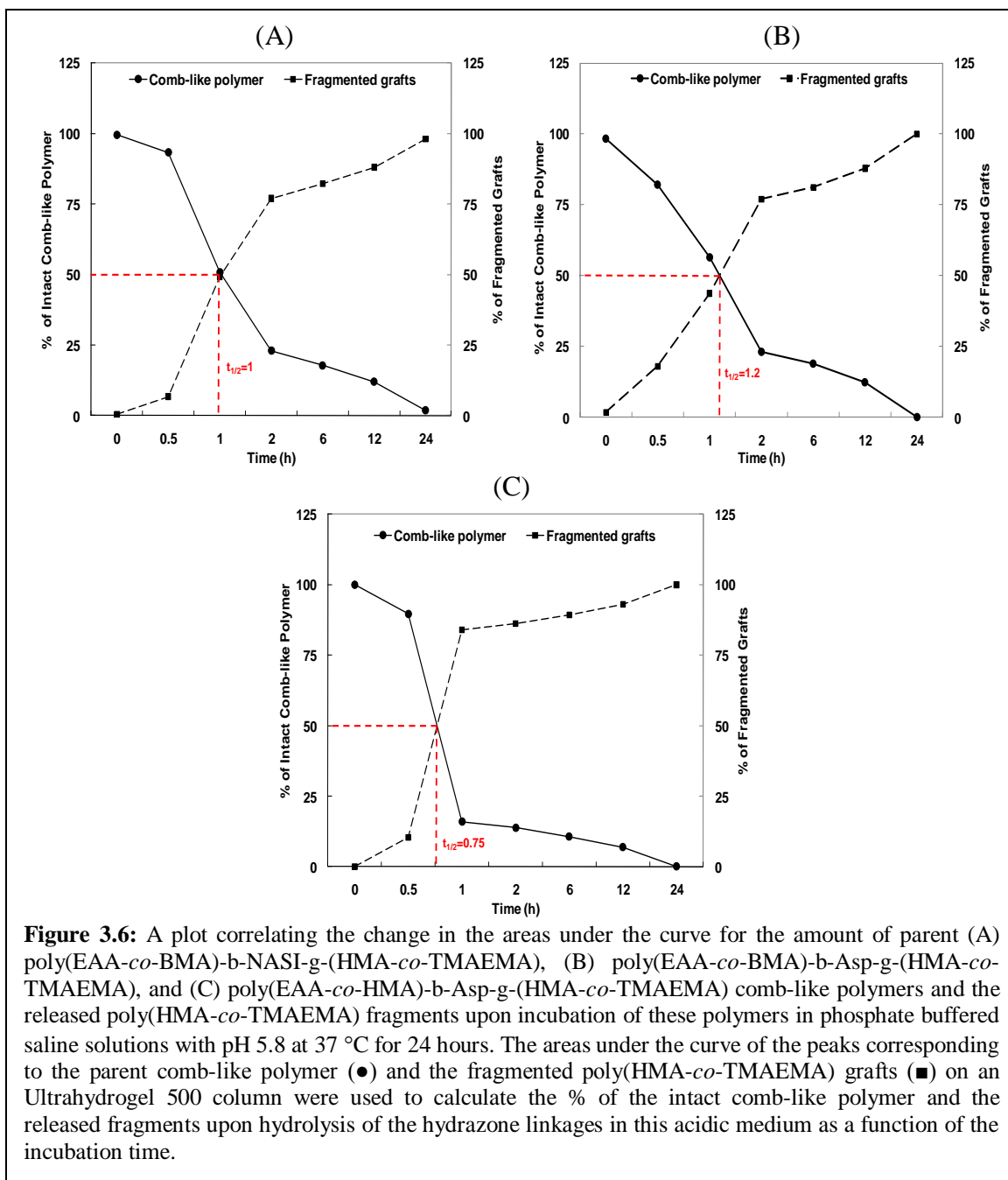
^f The number of cationic TMAEMA monomers is calculated based on its molar content in the grafts. The total number of TMAEMA monomers in the comb-like polymer accounts for the total number of the grafts.

^g The number of hydrophobic HMA monomers is calculated based on its molar content in the grafts. The total number of HMA monomers in the comb-like polymer accounts for the total number of the grafts.

The pH-responsiveness of these comb-like polymers is in part a result of using hydrazone linkages to connect the poly(HMA-*co*-TMAEMA) grafts to the polymer backbone. Hydrazone linkages have previously been used to conjugate small molecular weight anticancer drugs (e.g. doxorubicin) to water-soluble HPMA polymers and proved to hydrolyze and release the attached drug upon internalization into acidic intracellular vesicles.¹⁶ Torchilin and coworkers conjugated PEG chains to TAT-modified liposomes via hydrazone linkers to shield the liposomes from the reticular endothelial system, increase their plasma residence time, and enhance their accumulation into tumor and ischemic tissues. The hydrazone linkage connecting the PEG chains to the lipid shell is hydrolyzed in the acidic environment of tumor and ischemic tissues, which unmask the TAT peptide and trigger cell uptake.¹⁷ Hydrazone linkages have also been used to allow controlled degradation of temperature-sensitive hydrogels used for site-specific delivery of radioactive nuclides.¹⁸

The motivation to incorporate acid-labile hydrazone linkages in these comb-like polymers is to allow the grafting of a large number of cationic/hydrophobic polymer chains onto the polymer backbone to achieve a high positive charge density that will allow the condensation of a large number of DNA/RNA molecules into pH-sensitive particles with high therapeutic loading. The molecular weight of a cationic non-degradable polymer that can condense a similar dose of nucleic acids would exceed 250 KDa, which would result in non-specific cellular toxicity due to its poor degradation and elimination. On the other hand, the hydrzone linkages connecting poly(HMA-*co*-TMAEMA) grafts to the polymer backbone will hydrolyze in response to the acidity of the endosome, which will result in fragmenting the comb-like polymeric carrier into the

backbone and multiple grafts with average molecular weights of 40-45 and 20 KDa, respectively. These smaller fragments are hydrophilic and can be easily eliminated *in vivo* by renal excretion, which will significantly diminish their toxicity. Our results show that poly(EAA-*co*-BMA)-b-NASI-g-(HMA-*co*-TMAEMA), poly(EAA-*co*-BMA)-b-Asp-g-(HMA-*co*-TMAEMA), and poly(EAA-*co*-HMA)-b-Asp-g-(HMA-*co*-TMAEMA) comb-like polymers have similar degradation profiles with degradation half lives ($t_{1/2}$) of 1.0, 1.2, and 0.75 hour, respectively (**Figure 3.6**). Earlier research showed that acidification of endocytic vesicles loaded with cationic particles occurs within 15 minutes with drop in environment pH to 5.9¹⁹, which suggests that degradation of the particles prepared using these comb-like polymers will start shortly after their internalization and result in a rapid escape of the nucleic acid cargo into the cytoplasm. These comb-like polymers exhibited insignificant (< 5%) degradation at pH 7.4, which indicates that their membrane-destabilizing activity will be limited to the endosomal compartment, which enhances their overall biocompatibility.

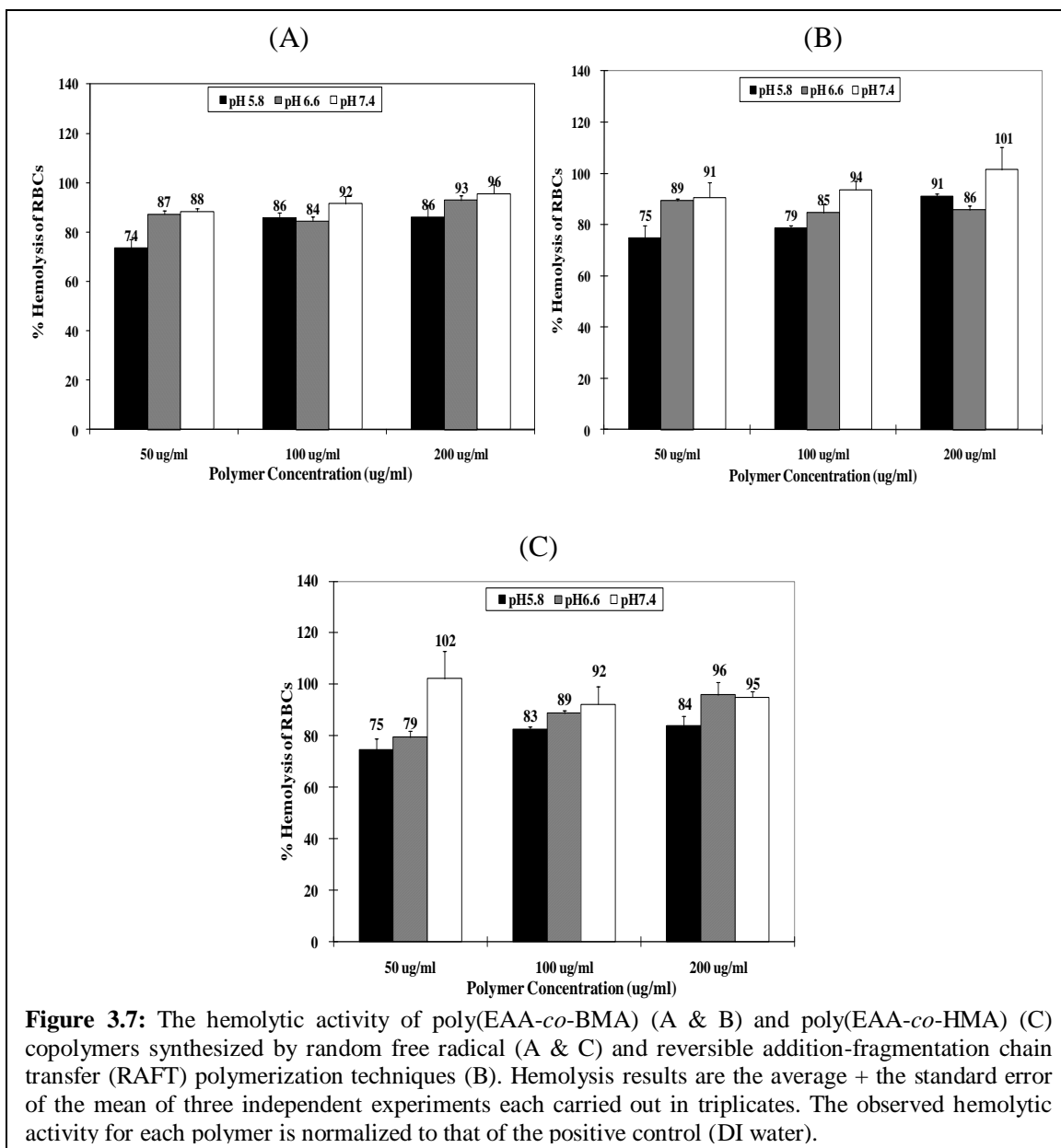


3.3.2 Membrane-destabilizing activity of comb-like polymers

The membrane-destabilizing activity of the polymer backbone and comb-like polymers was assessed based on their hemolytic activity as a function of polymer concentrations (50, 100, and 200 $\mu\text{g}/\text{ml}$) and solution pH (pH 5.8, 6.6, and 7.4). This hemolysis assay is

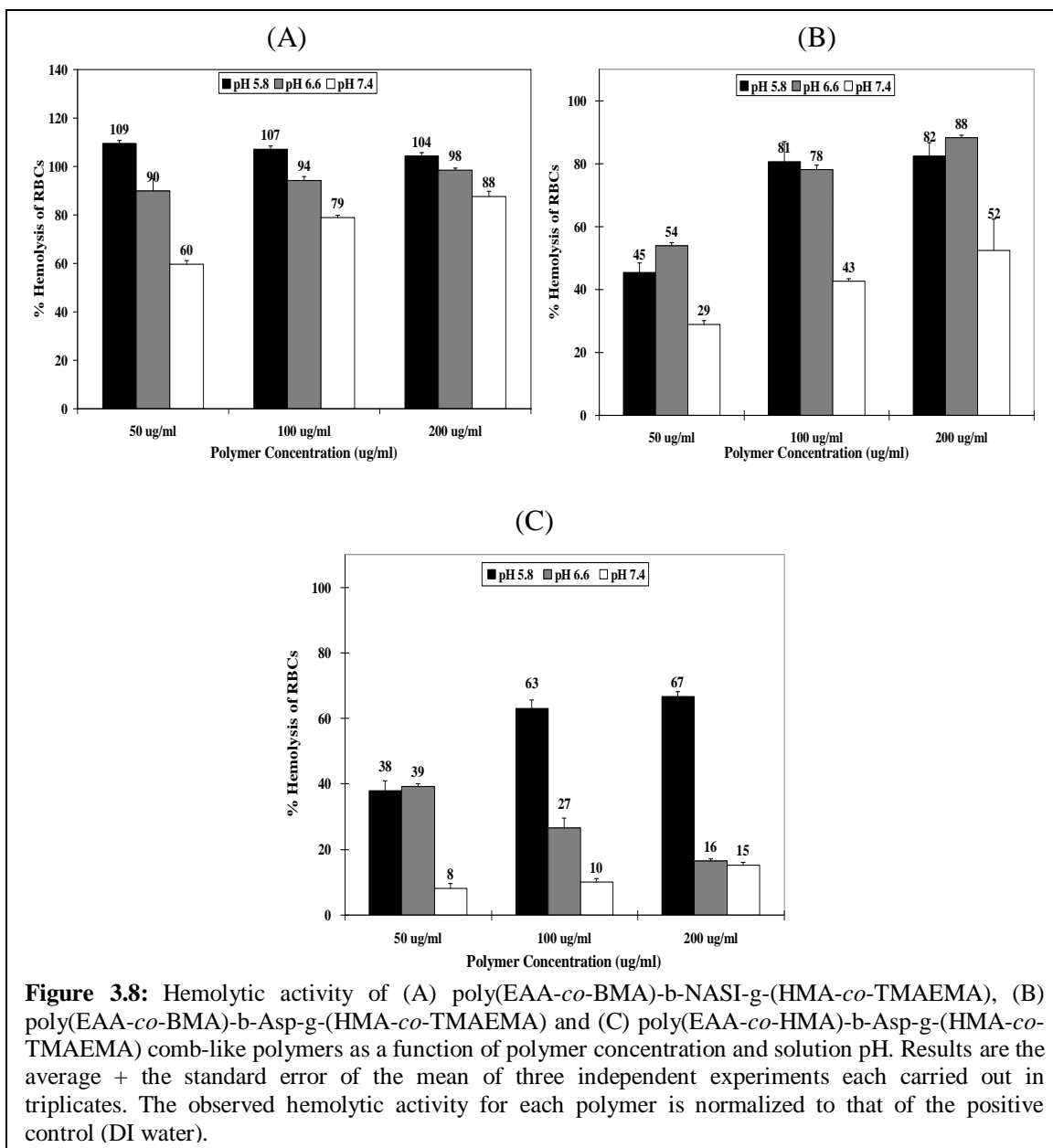
based on the established correlation between the observed hemolytic activity at acidic pH values and endosomal membrane disruption.^{6h,20} Polymers that exhibited a hemolytic activity $\geq 50\%$ of that observed with the positive control (DI water) at acidic pH values has the potential to function as endosomolytic carriers. The hemolytic activity of poly(EAA-co-BMA) and poly(EAA-co-HMA) copolymers prepared by random free radical and RAFT polymerization techniques caused $\geq 75\%$ hemolysis of the red blood cells at all concentrations and pH values (**Figure 3.7**).

This high hemolytic activity at all pH values is attributed to high BMA and HMA (45%) and low EAA (55%) content, which reduces the ability of these copolymers to sense the changes in environment pH compared to polymers with higher ($> 75\%$) acrylic acid content.¹³ Earlier results clearly showed that conjugation of cationic peptides and complexation with nucleic acids shift the polymer's hydrophilic/hydrophobic balance towards being more hydrophilic, which tunes its pH-responsiveness but can possibly reduce its membrane-destabilizing activity.^{13b} We hypothesized that these highly hemolytic polymers will retain their membrane-destabilizing activity upon grafting of cationic TMAEMA monomers and complexation with nucleic acids. Consequently, we utilized these poly(EAA-co-BMA) and poly(EAA-co-HMA) copolymers as the primary block in the backbone of the synthesized comb-like polymers.



Grafting of cationic poly(TMAEMA) polymers onto the polymer backbone via acid-labile hydrazone linkages significantly reduced the hemolytic activity of these polymers, which prompted us to incorporate an equal molar concentration of hydrophobic HMA monomers in the graft composition to enhance the membrane-destabilizing activity of the final comb-like polymer (data not shown). The hemolytic activity of poly(EAA-co-BMA)-b-NASI-g-(HMA-co-TMAEMA) comb-like polymer was $\geq 90\%$ at acidic pH

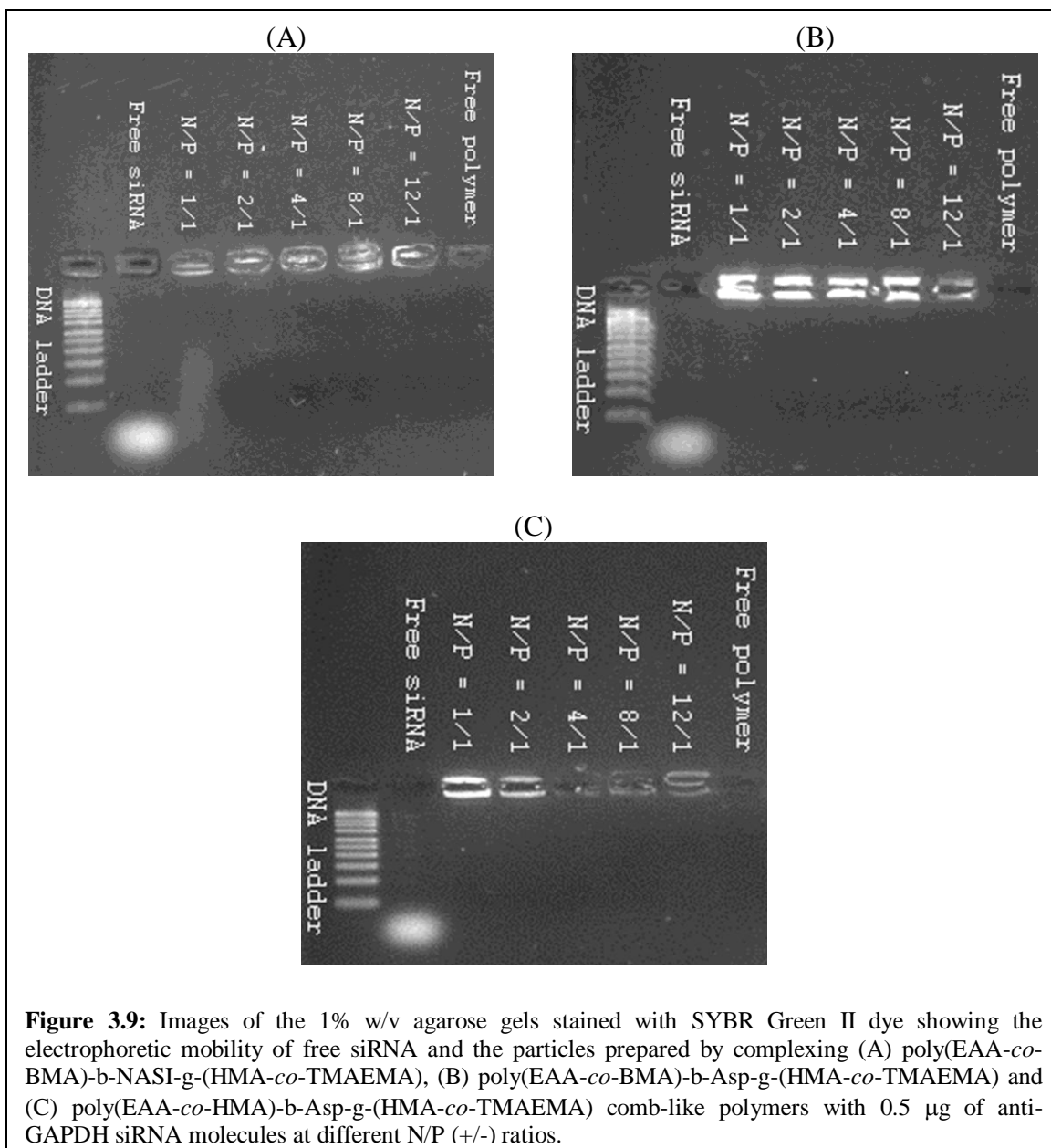
values of 6.6 and 5.8 at each of the studied concentrations (**Figure 3.8A**). At pH 7.4, the hemolytic activity of this polymer gradually increased from 60% to 88% with the increase in polymer concentration from 50 to 200 $\mu\text{g/ml}$, which can be a result of the high concentration of TMAEMA quaternary amine groups present in solution. Recent results showed that amphiphilic polymers incorporating quaternary amine groups cause pH-independent cell lysis.²¹ Poly(EAA-*co*-BMA)-b-Asp-g-(HMA-*co*-TMAEMA) comb-like polymer exhibited a clear pH- and concentration-dependant hemolytic profile (**Figure 3.8B**). At a concentration 50 $\mu\text{g/ml}$, the polymer produced a low hemolytic activity (29%) at pH 7.4 that increased to 54% and 45% at acidic pH of 6.6 and 5.8, respectively (**Figure 3.8B**). The hemolytic activity significantly increased with the increase in polymer's concentration reaching 80%-90% hemolysis at acidic pH values with a less pronounced increase at physiologic pH of 7.4 (**Figure 3.8B**). Similarly, poly(EAA-*co*-HMA)-b-Asp-g-(HMA-*co*-TMAEMA) comb-like polymer showed a low hemolytic activity at pH 7.4 compared to that observed at acidic pHs of 6.6 and 5.8, which increased with the increase in polymer's concentration (**Figure 3.8C**). The observed hemolytic activity of these polymers in acidic environment (pH 6.6 and 5.8) is attributed to the pH-sensitive poly(EAA-*co*-BMA) and poly(EAA-*co*-HMA) blocks in the polymer backbone aided with the hydrophobic HMA monomers embedded in the poly(HMA-*co*-TMAEMA) grafts, which get released into acidic solutions upon hydrolysis of the connecting hydrazone linkages. Hemolysis results indicate that all comb-like polymers exhibit a concentration-dependent membrane-destabilizing activity in response to acidic stimuli, which suggests their potential as carriers for intracellular delivery of therapeutic nucleic acids.



3.3.3 Formulation of “smart” particles

The ability of comb-like polymers to condense anti-GAPDH siRNA molecules into pH-sensitive particles was analysed using the standard gel retardation assay. Comb-like polymers were mixed with a fixed amount (0.5 μ g) of anti-GAPDH siRNA molecules at different N/P (+/-) ratios where the electrostatic interaction between the cationic quaternary amine groups of the TMAEMA monomers and the anionic phosphate groups

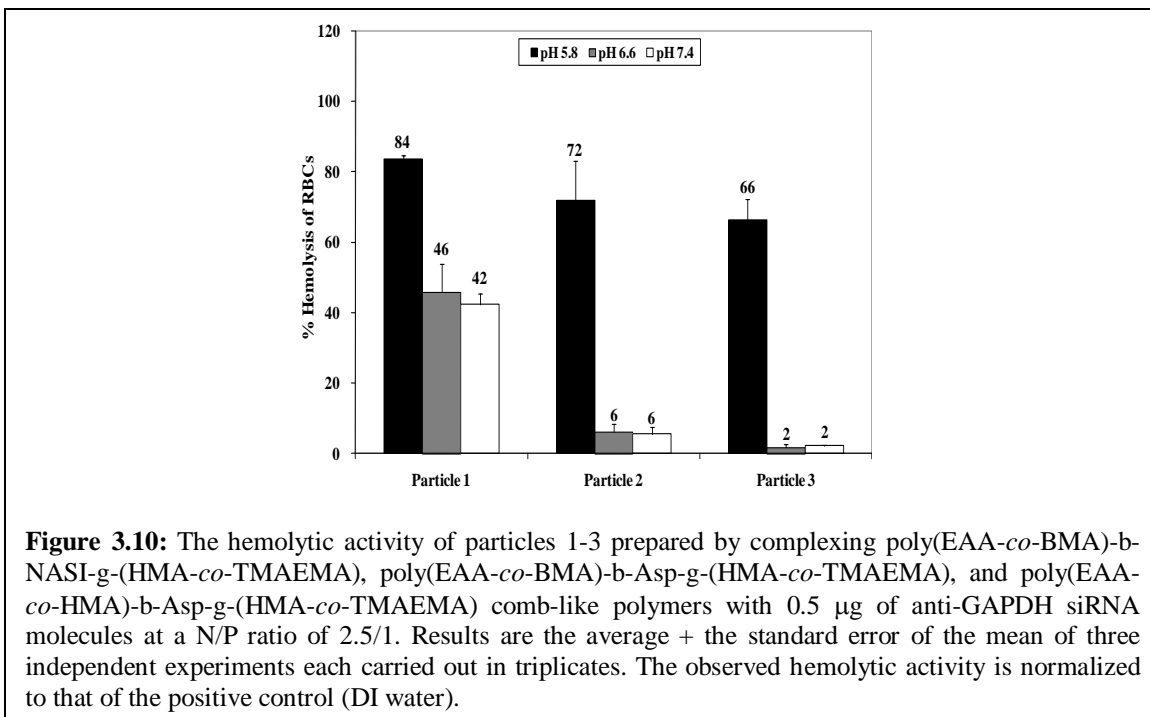
of the RNA molecules will lead to formation of particles that encapsulate the loaded RNA molecules. The amount of each comb-like polymer needed to complex the loaded siRNA molecules varied based on their TMAEMA content. Results show that all comb-like polymers successfully complexed the loaded siRNA molecules at all N/P ratios, which is indicated by their retention in the loading wells compared to the observed migration of free siRNA molecules (**Figure 3.9**). It is important to note that poly(EAA-*co*-BMA)-b-Asp-g-(HMA-*co*-TMAEMA) and poly(EAA-*co*-HMA)-b-Asp-g-(HMA-*co*-TMAEMA) polymers fully condensed the loaded siRNA molecules at a 1/1 N/P ratio whereas poly(EAA-*co*-BMA)-b-NASt-g-(HMA-*co*-TMAEMA) polymer partially condensed the same amount of siRNA molecules at a 1/1 N/P ratio and fully condensed the loaded siRNA molecules at 2/1 N/P ratio (**Figure 3.9**). This clearly shows that these new comb-like polymers can condense siRNA molecules at low N/P ratios compared to other acrylic acid-based polymers.¹³ This reduces the amount of comb-like polymers needed to complex a given dose of therapeutic nucleic acids and consequently minimizes the toxicity commonly associated with cationic carriers.



3.3.4 Membrane-destabilizing activity of “smart” particles

Comb-like polymers have to retain their membrane-destabilizing activity after their complexation with nucleic acid molecules in order to disrupt the endosomal membrane and release their therapeutic cargo into the cytoplasm in response to the acidic endosomal pH gradients. Conjugation of cationic peptides and complexation with DNA molecules have been shown to reduce the membrane-destabilizing activity of other pH-sensitive

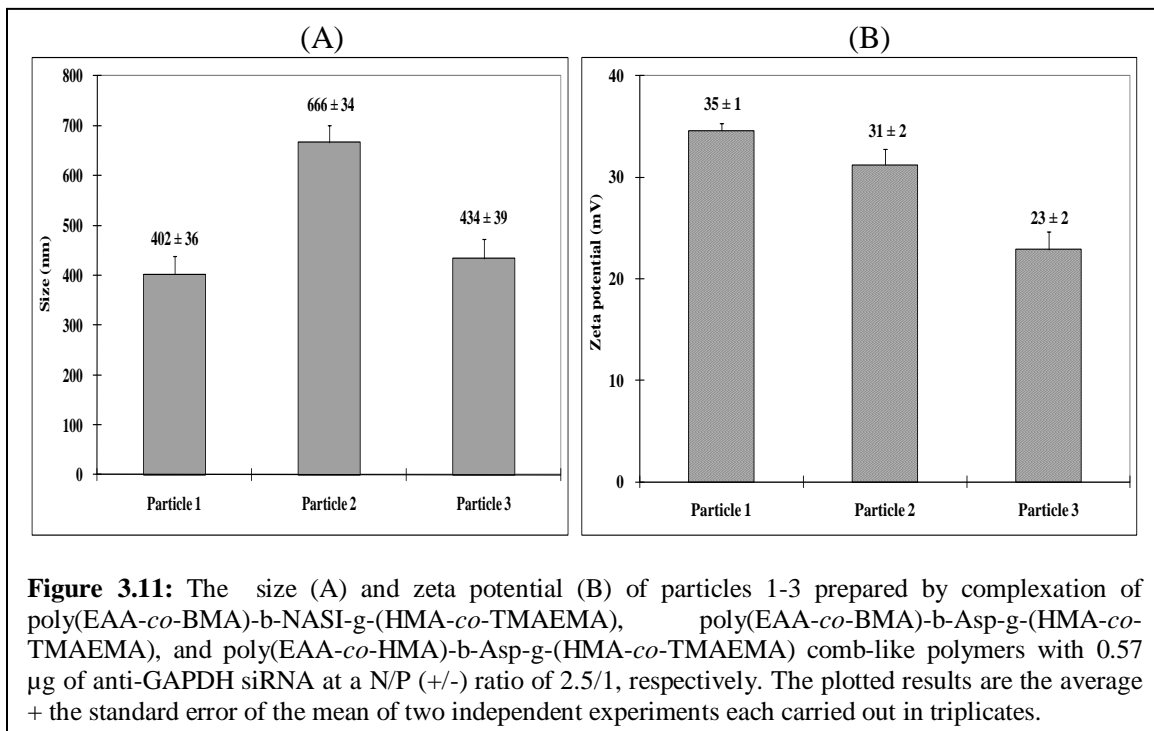
polymers due to a shift in the hydrophilic/hydrophobic balance in the formed complexes towards being more hydrophilic.¹³ Consequently, we evaluated the hemolytic activity of the particles prepared by complexation of comb-like polymers with 0.5 μg of anti-GAPDH siRNA molecules at N/P ratio of 2.5/1 as a function of solution pH. Results show that all particles exhibited a sharp membrane-destabilizing activity in acidic solutions (pH 5.8) compared to neutral ones (pH 7.4), which indicates their ability to “sense” the drop in environment pH (**Figure 3.10**). At pH 5.8, the particles formulated based on NASI-containing polymer displayed a high hemolytic activity (84%) compared to Asp-containing polymers, which displayed a lower hemolytic activity in the range of 66%-72%. All particles except those prepared using Poly(EAA-*co*-BMA)-b-NASI-g-(HMA-*co*-TMAEMA) comb-like polymers showed a low hemolytic activity at pHs 6.6 and 7.4, which clearly indicates the tuning of the membrane-destabilizing activity of these comb-like carriers upon complexation with nucleic acid molecules. This hemolysis profile clearly shows the membrane-disruptive activity of these particles in response to acidic endosomal pH gradients, which suggests their potential as carriers for enhancing the cytoplasmic delivery of nucleic acids.



3.3.5 Characterization of “smart” particles

Size and surface charge of these particles were measured using dynamic light scattering and zeta potential measurements, respectively. Results show that particles 1 and 3 have similar particle size in the range of 400 – 430 nm compared to particles 2, which have a larger size of 666 nm (**Figure 3.11A**). All particles display a cationic surface with an average zeta potential of 23 – 35 mV (**Figure 3.11B**). The combination of size and surface charge dictates the ability of these particles to escape recognition and scavenging by the reticular endothelial system, extravasate from the systemic circulation into tumor tissue, and become effectively internalized by target cells. Earlier research showed that the molecular size cut off for tumor vasculature is between 400 and 600 nm.²² Consequently, these particles particularly 1 and 3 are suited for delivery of nucleic acids into solid tumors. Additionally, the cationic nature of these particles will facilitate their

interaction and internalization into target cells via adsorptive endocytosis, which further emphasizes their potential as drug carriers.



3.3.6 Uptake of “smart” particles into MCF-7 breast cancer cells

We evaluated the internalization of fluorescently-labeled particles 1-3 prepared at different N/P ratios into MCF-7 breast cancer cells in comparison to complexes prepared using commercial siPORT amine transfection agent using flow cytometry. Results show that free siRNA molecules were not internalized and require a carrier to enhance their uptake by MCF-7 cancer cells (**Figure 3.12**). At low N/P ratios of 1.5/1 and 2.5/1, particles 3 showed higher uptake into MCF-7 cells compared to particles 2, which exhibited higher uptake than particles 1. However, at higher N/P ratios, all particles exhibited a similar uptake profile into MCF-7 cells, which can be attributed to their higher positive charge density due to the incorporation of excess comb-like polymers into

these particles. Similarly, siPORT amine-based complexes showed high internalization (95%) into MCF-7 cells. These results clearly show that all particles are efficiently internalized (> 75%) by MCF-7 cells regardless of the N/P ratio. Earlier research showed that increasing the particle's cationic nature is typically associated with toxicity²³ or low transfection efficiency due to poor decomplexation of the loaded DNA/RNA molecules.²⁴ Consequently, we decided to evaluate the transfection efficiency of the particles prepared at N/P ratio of 2.5/1, which will have the optimum number of cationic TMAEMA residues to complex the loaded siRNA molecules without inducing cellular toxicity or hindering the cytoplasmic decomplexation of the loaded siRNA.

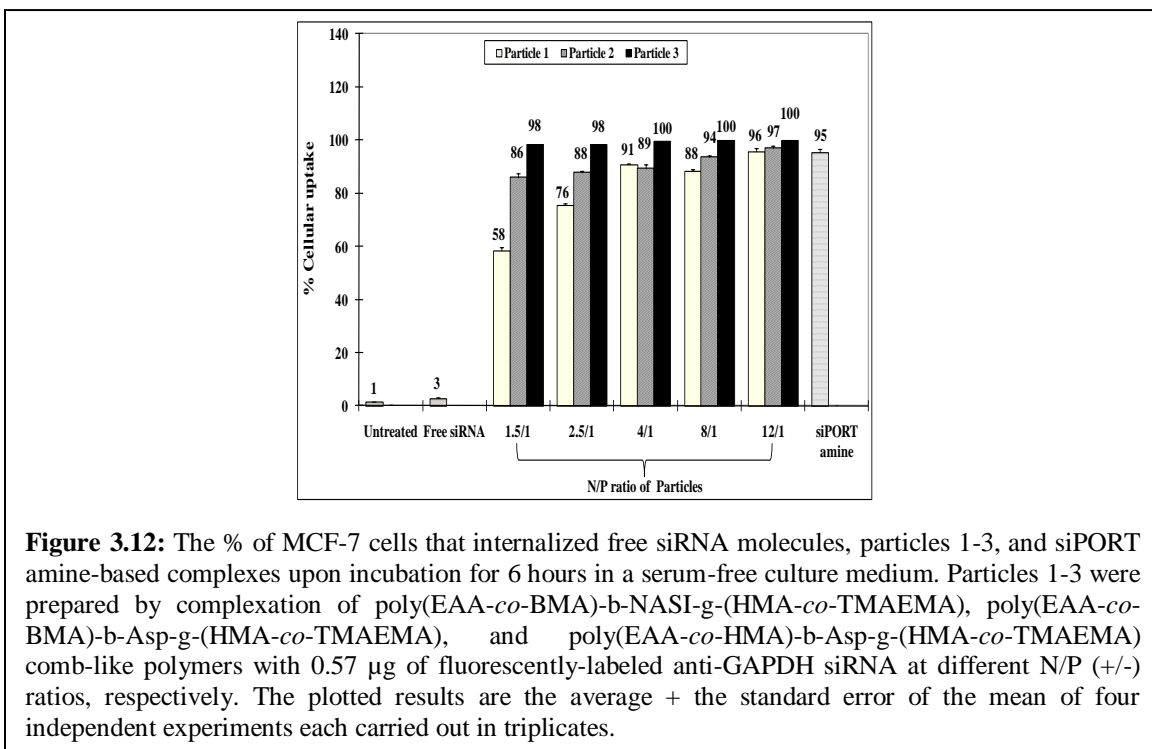
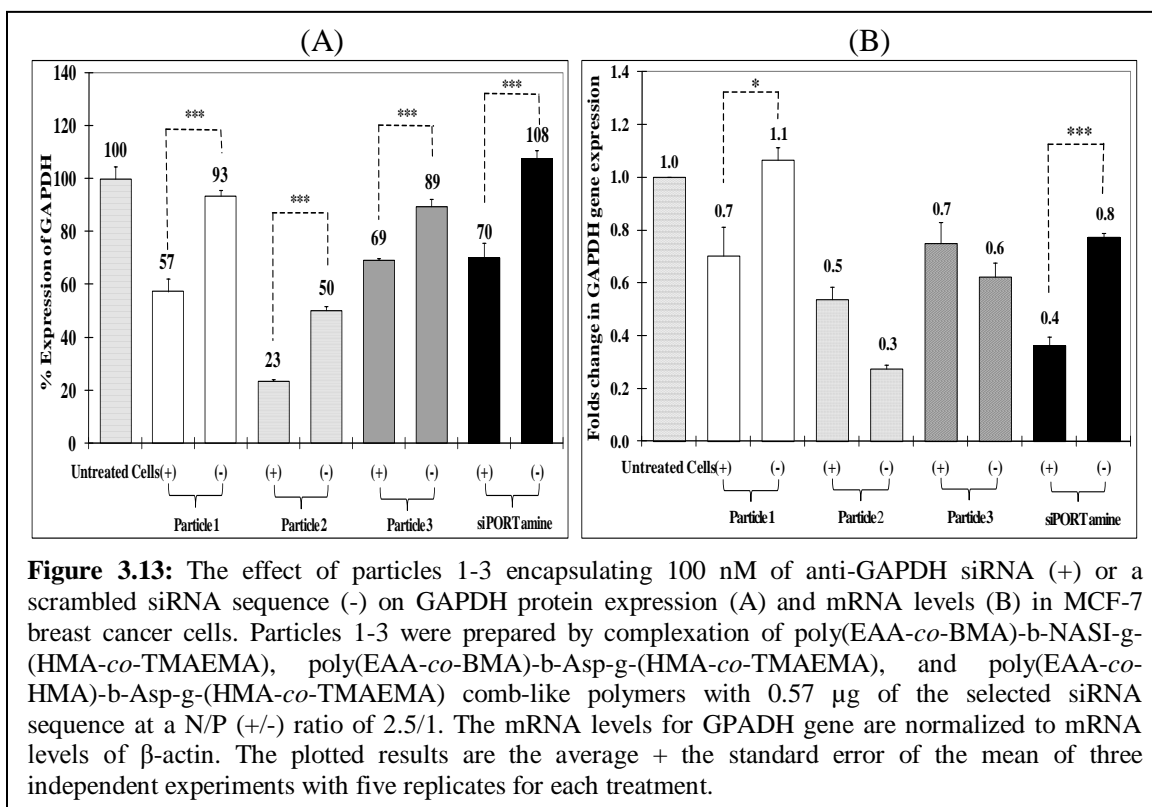


Figure 3.12: The % of MCF-7 cells that internalized free siRNA molecules, particles 1-3, and siPORT amine-based complexes upon incubation for 6 hours in a serum-free culture medium. Particles 1-3 were prepared by complexation of poly(EAA-co-BMA)-b-NASI-g-(HMA-co-TMAEMA), poly(EAA-co-BMA)-b-Asp-g-(HMA-co-TMAEMA), and poly(EAA-co-HMA)-b-Asp-g-(HMA-co-TMAEMA) comb-like polymers with 0.57 μ g of fluorescently-labeled anti-GAPDH siRNA at different N/P (+/-) ratios, respectively. The plotted results are the average + the standard error of the mean of four independent experiments each carried out in triplicates.

3.3.7 Effect of “smart” particles on GAPDH expression

The ability of particles 1-3 to deliver functional siRNA molecules into the cytoplasm of MCF-7 breast cancer cells was assayed based on their ability to selectively knockdown

GAPDH gene expression at the mRNA and protein levels. We utilized the KDAlert assay kit to measure the changes in GAPDH protein level upon incubation with particles that encapsulate the anti-GAPDH siRNA molecules compared to those encapsulating a scrambled siRNA sequence. We utilized siPORT amine-based complexes encapsulating an equal dose of anti-GAPDH siRNA molecules as a positive control to determine the maximum level of knockdown that can be achieved using robust commercial transfection reagents.

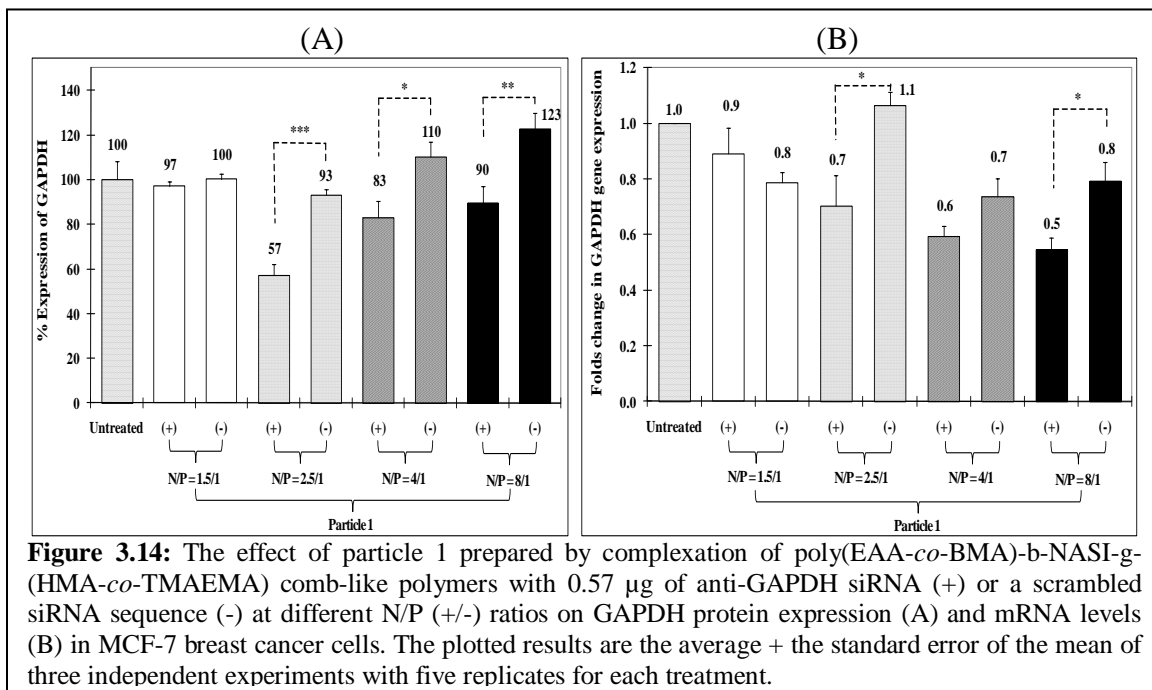


Results show that particles 1, 2, and 3 caused 36%, 27%, and 20% reduction in GAPDH protein expression, respectively (**Figure 3.13A**). Results also show that siPORT amine-based complexes produced 38% reduction in GAPDH protein expression. It is important to note that particle 2 caused non-specific reduction in GAPDH expression upon

incubation with the particles that encapsulate scrambled siRNA molecules, which may be a result of polymer's toxicity towards MCF-7 cells. By comparing the activity of particles 1 and 3, it is clear that particle 1 is more efficient in silencing the expression of the targeted gene (GAPDH) reaching the same level of knockdown achieved by commercial transfection reagents without inducing any toxicity. The observed reduction in GAPDH protein levels was also evident at the mRNA level with particle 1 and siPORT amine-based complexes inducing 40% knockdown in GAPDH mRNA levels (**Figure 3.13B**). The higher activity of particles 1 is a result of higher grafting efficiency (92.5%) and TMAEMA content per comb-like polymer compared to those used to prepare particles 2 and 3 (**Table 3.1**). These results collectively indicate that particle 1 is an effective carrier for intracellular delivery of therapeutic siRNA molecules.

We prepared a series of particle 1 by complexing poly(EAA-*co*-BMA)-*b*-NASI-*g*-(HMA-*co*-TMAEMA) comb-like polymers with siRNA molecules at different N/P ratios to determine the effect of particle composition on their ability to achieve functional knockdown of GAPDH expression in MCF-7 cells. Results show that particles prepared at N/P ratio of 1.5/1 failed to reduce GAPDH expression compared to those prepared at N/P ratio of 2.5/1, which reduced GAPDH expression by 36-40% at both the mRNA and protein levels (**Figure 3.14**). Particles prepared at 4/1 and 8/1 N/P ratios reduced GPADH expression by ~25%, however their effect was associated with reduction in cell viability indicated by the non-specific decline in mRNA levels observed upon treatment with particles encapsulating scrambled siRNA sequences (**Figure 3.14B**). These results are in agreement with earlier research clearly documenting the non-specific toxicity of particles with high content of cationic polymers^{23,25}. These results further confirmed the potential

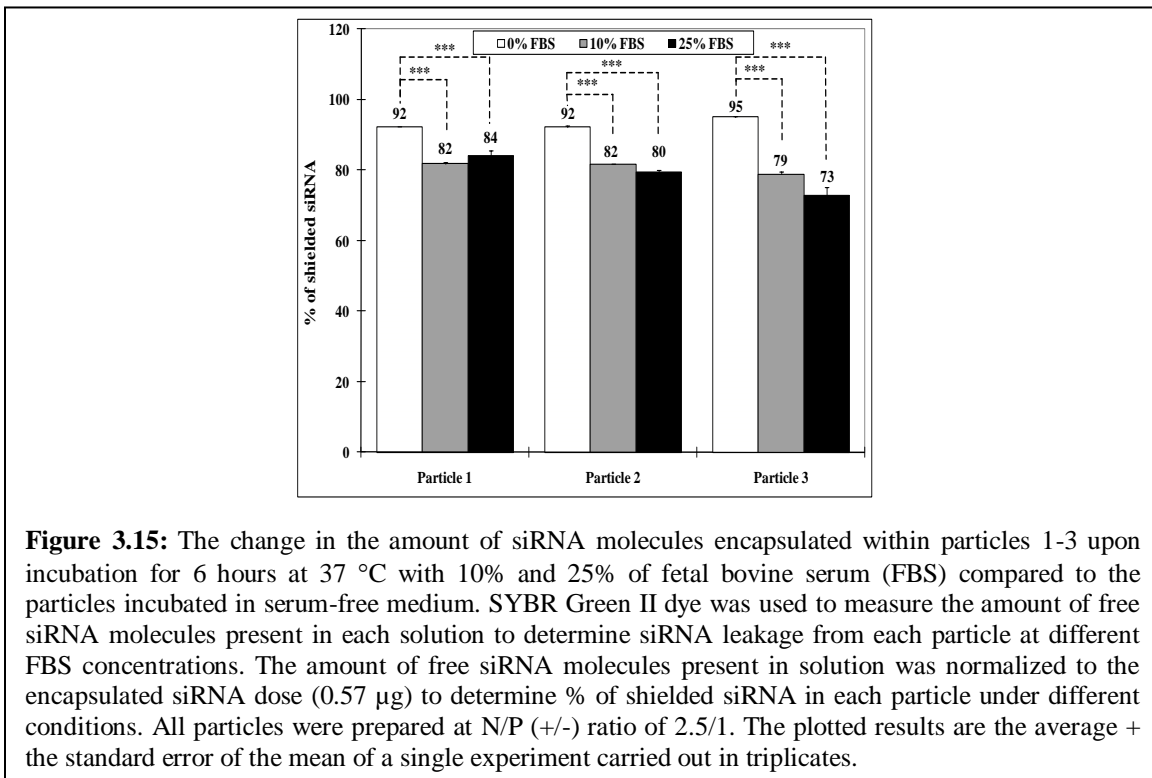
of the particles prepared by complexation of poly(EAA-co-BMA)-b-NASI-g-(HMA-co-TMAEMA) comb-like polymers with therapeutic siRNA molecules at N/P ratio of 2.5/1 as effective carriers for intracellular delivery of nucleic acid drugs.



3.3.8 Effect of serum and nuclease enzymes on “smart” particles

Particles have to shield and protect their therapeutic cargo from serum proteins and nuclease enzymes, which proved to degrade DNA/RNA molecules into small ineffective fragments^{23b,26} to become therapeutically effective *in vivo*. We examined the effect of serum proteins on particles 1-3 prepared at a N/P ratio of 2.5/1 by incubating these particles with 10% and 25% FBS for 6 hours at 37 °C and measuring the amount of siRNA released in solution using the PicoGreen dye. Results show that particles 1-3 retained 92-95% of the loaded siRNA molecules upon incubation in serum-free medium for 6 hours (**Figure 3.15**). However, incubation of these particles with 10-25% of FBS caused partial decomplexation of these particles and reduced the amount of shielded

siRNA molecules to 75-80% of the loaded siRNA molecules. Despite the partial release of 20-25% of the loaded siRNA molecules, these particles retained and shielded the bulk of the loaded dose at a low N/P ratio for a long incubation time.



We evaluated the stability of particle 1 prepared at different N/P ratios upon incubation with RNase V1 at 37 °C for 30 minutes using the standard gel retardation assay. By comparing the fluorescence intensity of the wells loaded with the particles treated with RNase enzyme (+) to those incubated with blank buffer (-) using Image J software, our results show that particle 1 prepared at N/P ratio of 2.5/1 and higher was able to retain and shield > 95% of the loaded siRNA molecules (**Figure 3.16**). The particles prepared at N/P ratio of 1/1 shielded the fraction of the siRNA molecules that is complexed with the polymeric carrier and entrapped into the loading well. The free fraction of siRNA molecules that appeared as a faint band with similar electrophoretic mobility to free

siRNA was digested by the RNase enzyme (**Figure 3.16**). These results collectively indicate that particles 1-3 retained and shielded > 75% of their siRNA cargo in presence of 25% (v/v) FBS and particle 1 protected > 95% of the loaded siRNA molecules in presence of nuclease enzymes at N/P ratio of 2.5/1 and higher, which indicate their potential as effective DNA/RNA carriers *in vivo*.

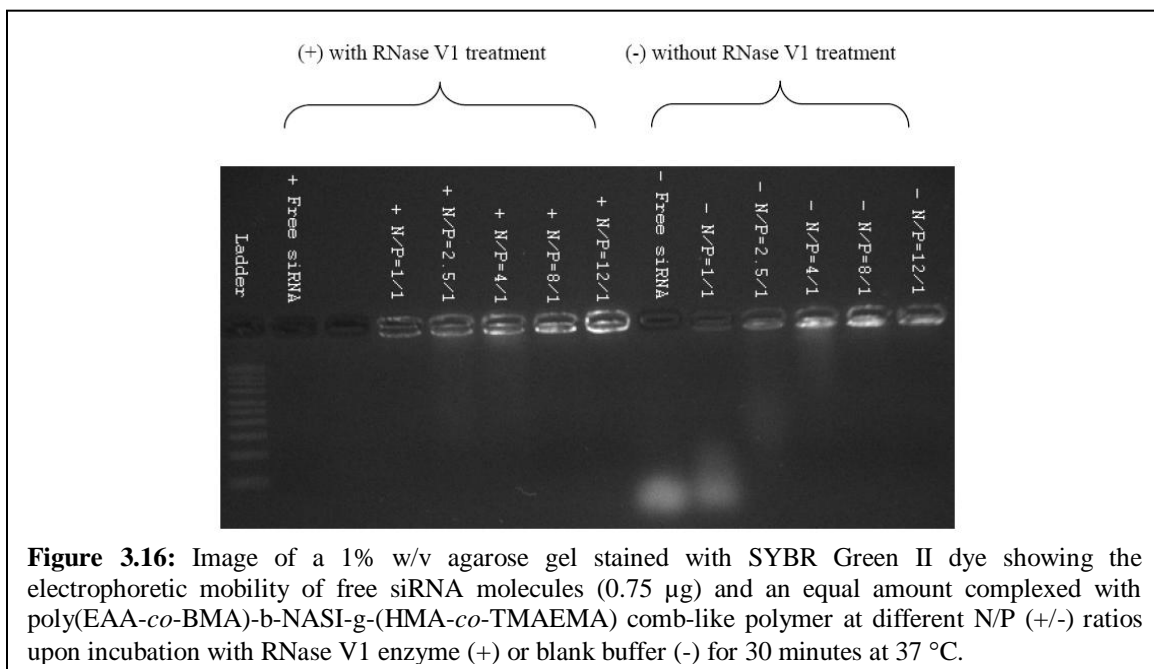


Figure 3.16: Image of a 1% w/v agarose gel stained with SYBR Green II dye showing the electrophoretic mobility of free siRNA molecules (0.75 μ g) and an equal amount complexed with poly(EAA-*co*-BMA)-b-NASI-g-(HMA-*co*-TMAEMA) comb-like polymer at different N/P (+/-) ratios upon incubation with RNase V1 enzyme (+) or blank buffer (-) for 30 minutes at 37 °C.

3.4 Conclusions

We have designed and synthesized a new series of degradable, pH-sensitive, membrane-destabilizing, comb-like polymers that exhibit a robust membrane-destabilizing activity in response to acidic pH gradients similar to those present in the endosome. These comb-like polymers proved to degrade into smaller fragments in acidic environment, which will minimize their toxicity and facilitate their *in vivo* elimination by renal excretion. These polymers successfully complexed model siRNA molecules into pH-sensitive, serum- and nuclease-stable particles at low N/P ratios, which indicate their ability to encapsulate

large doses of therapeutic nucleic acids. Particles 1-3 proved to successfully delivery functional siRNA molecules into the cytoplasm of MCF-7 breast cancer cells and achieve targeted gene knockdown at both mRNA and protein levels with particle 1 being the most effective formulation. These results collectively indicate the potential of these particles particularly particle 1 to serve as a carrier for enhancing the intracellular delivery of therapeutic nucleic acids.

Acknowledgments

This research was supported in part by the U.S. Department of Defence Breast Cancer Research Program (Award # W81XWH-05-1-0240 to M. El-Sayed). Lisa Birrell was supported by the Marian Sarah Parker Scholarship and Edmunson Summer Fund.

References

- (1) (a) deFougerolles, A.; Vornlocher, H.-P.; Maraganore, J.; Lieberman, J. *Nature Reviews Drug Discovery* **2007**, *6*, 443. (b) Hassan, A. *Recent Patents Cardiovascular Drug Discovery* **2006**, *1*, 141. (c) Koutsilieris, E.; Rethwilm, A.; Scheller, C. *Journal of Neural Transmission-Supplement* **2007**, *72*, 43. (d) Tili, E.; Michaille, J. J.; Gandhi, V.; Plunkett, W.; Sampath, D.; Calin, G. A. *Future Oncology* **2007**, *3*, 521. (e) Zhang, J.; Wu, Y. O.; Xiao, L.; Li, K.; Chen, L. L.; Sirois, P. *Molecular Biotechnology* **2007**, *37*, 225.
- (2) (a) Lechardeur, D.; Lukacs, G. L. *Current Gene Therapy* **2002**, *2*, 183. (b) Nielsen, P. E. *Quarterly Reviews of Biophysics* **2005**, *38*, 345.
- (3) (a) Jere, D.; Jiang, H. L.; Arote, R.; Kim, Y. K.; Choi, Y. J.; Cho, M. H.; Akaike, T.; Cho, C. S. *Expert Opinion on Drug Delivery* **2009**, *6*, 827. (b) Lai, W. F.; Lin, M. C. *Journal of Controlled Release* **2009**, *134*, 158. (c) Midoux, P.; Pichon, C.; Yaouanc, J. J.; Jaffrès, P. A. *British journal of pharmacology* **2009**, *157*, 166. (d) Pangburn, T. O.; Petersen, M. A.; Waybrant, B.; Adil, M. M.; Kokkoli, E. *Journal of Biomechanical Engineering* **2009**, *131*, 74005.
- (4) Grimm, D.; Kay, M. A. *Curr Gene Ther* **2003**, *3*, 281.
- (5) (a) Cross, K. J.; Langley, W. A.; Russell, R. J.; Skehel, J. J.; Steinhauer, D. A. *Protein and Peptide Letters* **2009**, *16*, 766. (b) Hughson, F. M. *Current Biology* **1995**, *5*, 265. (c) Ren, J.; Sharpe, J. C.; Collier, R. J.; London, E. *Biochemistry* **1999**, *38*, 976. (d) Skehel, J. J.; Wiley, D. C. *Annual Review of Biochemistry* **2000**, *69*, 531. (e) Wiley, D. C.; Skehel, J. J. *Annual Review of Biochemistry* **1987**, *56*, 365.
- (6) (a) Fattal, E.; Nir, S.; Parente, R. A.; Jr., F. C. S. *Biochemistry* **1994**, *33*, 6721. (b) Funhoff, A. M.; Nostrum, C. F. V.; Lok, M. C.; Kruijtzter, J. A.; Crommelin, D. J.; Hennink, W. E. *Journal of Controlled Release* **2005**, *101*, 233. (c) Lee, H.; Jeong, J. H.; Park, T. G. *Journal of Controlled Release* **2001**, *76*, 183. (d) Li, W.; Nicol, F.; Jr., F. C. S. *Advanced Drug Delivery Reviews* **2004**, *56*, 967. (e) Parente, R. A.; Nadasdi, L.; Subbarao, N. K.; Jr., F. C. S. *Biochemistry* **1990**, *29*, 8713. (f) Parente, R. A.; Nir, S.; Jr., F. C. S. *Journal of Biological Chemistry* **1988**, *263*, 4724. (g) Parente, R. A.; Nir, S.; Jr., F. C. S. *Biochemistry* **1990**, *29*, 8720. (h) Plank, C.; Oberhauser, B.; Mechtler, K.; Koch, C.; Wagner, E. *Journal of Biological Chemistry* **1994**, *269*, 12918. (i) Subbarao, N. K.; Parente, R. A.; Jr, F. C. S.; Nadasdi, L.; Pongracz, K. *Biochemistry* **1987**, *26*, 2964.
- (7) (a) El-Sayed, M. E. H.; Hoffman, A. S.; Stayton, P. S. *Expert Opinion on Biological Therapy* **2005**, *5*, 23. (b) Yessine, M. A.; Leroux, J. C. *Advanced Drug Delivery Reviews* **2004**, *56*, 999.
- (8) (a) Thomas, J. L.; Barton, S. W.; Tirrell, D. A. *Biophysical Journal* **1994**, *67*, 1101. (b) Thomas, J. L.; Tirrell, D. A. *Accounts of Chemical Research* **1992**, *25*, 336.
- (9) (a) Murthy, N.; Chang, I.; Stayton, P. S.; Hoffman, A. S. *Macromolecular Symposia* **2001**, *172*, 49. (b) Murthy, N.; Robichaud, J. R.; Tirrell, D. T.; Stayton, P. S.; Hoffman, A. S. *Journal of Controlled Release* **1999**, *61*, 137.
- (10) (a) Cheung, C. Y.; Murthy, N.; Stayton, P. S.; Hoffman, A. S. *Bioconjugate Chemistry* **2001**, *12*, 906. (b) Kiang, T.; Bright, C.; Cheung, C. Y.; Stayton, P. S.;

- Hoffman, A. S.; Leong, K. W. *Journal of Biomaterials Science, Polymer Edition* **2004**, *15*, 1405.
- (11) Kyriakides, T. R.; Cheung, C. Y.; Murthy, N.; Bornstein, P.; Stayton, P. S.; Hoffman, A. S. *Journal of Controlled Release* **2002**, *78*, 295.
- (12) Cheung, C. Y.; Stayton, P. S.; Hoffman, A. S. *Journal of Biomaterials Science, Polymer Edition* **2005**, *16*, 163.
- (13) (a) Bulmus, V.; Woodward, M.; Lin, L.; Murthy, N.; Stayton, P. S.; Hoffman, A. S. *Journal of Controlled Release* **2003**, *93*, 105. (b) El-Sayed, M. E. H.; Hoffman, A. S.; Stayton, P. S. *Journal of Controlled Release* **2005**, *101*, 47.
- (14) (a) Ferritto, M. S.; Tirrell, D. A. *Macromolecular Syntheses* **1992**, *11*, 59. (b) Lai, J. T.; Filla, D.; Shea, R. *Macromolecules* **2002**, *35*, 6754.
- (15) Yokoyama, M.; Okano, T.; Sakurai, Y.; Ekimoto, H.; Shibasaki, C.; Kataoka, K. *Cancer Research* **1991**, *51*, 3229.
- (16) (a) Etrych, T.; Chytil, P.; Jelínková, M.; Říhová, B.; Ulbrich, K. *Macromolecular Biosciences* **2002**, *2*, 43. (b) Etrych, T.; Strohalm, J.; Kovár, L.; Kabesová, M.; Říhová, B.; Ulbrich, K. *Journal of Controlled Release* **2009**, *140*, 18. (c) Kovár, M.; Kovár, L.; Subr, V.; Etrych, T.; Ulbrich, K.; Mrkvan, T.; Loucká, J.; Říhová, B. *Journal of Controlled Release* **2004**, *99*, 301. (d) Krakovicová, H.; Etrych, T.; Ulbrich, K. *European Journal of Pharmaceutical Sciences* **2009**, *37*, 405. (e) Kratz, F.; Beyer, U.; Schutte, M. T. *Critical Reviews on Therapeutic Drug Carrier Systems* **1999**, *16*, 245. (f) Říhová, B.; Etrych, T.; Pechar, M.; Jelínková, M.; Šťastný, M.; Hovorka, O.; Kovář, M.; Ulbrich, K. *Journal of Controlled Release* **2001**, *74*, 225. (g) Ulbrich, K.; Etrych, T.; Chytil, P.; Jelínková, M.; Říhová, B. *Journal of Drug Targeting* **2004**, *12*, 477.
- (17) (a) Kale, A. A.; Torchilin, V. P. *Bioconjugate Chemistry* **2007**, *18*, 363. (b) Kale, A. A.; Torchilin, V. P. *Journal of Drug Targeting* **2007**, *15*, 538. (c) Kale, A. A.; Torchilin, V. P. *J Liposome Res* **2007**, *17*, 197. (d) Sawant, R. M.; Hurley, J. P.; Salmaso, S.; Kale, A.; Tolcheva, E.; Levchenko, T. S.; Torchilin, V. P. *Bioconjugate Chemistry* **2006**, *17*, 943
- (18) Hruby, M.; Kucka, J.; Lebeda, O.; Mackova, H.; Babic, M.; Konak, C.; Studenovský, M.; Sikora, A.; Kozempel, J.; Ulbrich, K. *Journal of Controlled Release* **2007**, *119*, 25.
- (19) Sonawane, N. D.; Jr., F. C. S.; Verkman, A. S. *Journal of Biological Chemistry* **2003**, *278*, 44826.
- (20) (a) Murthy, N.; Campbell, J.; Fausto, N.; Hoffman, A. S.; Stayton, P. S. *Bioconjugate Chemistry* **2003**, *14*, 412. (b) Murthy, N.; Campbell, J.; Fausto, N.; Hoffman, A. S.; Stayton, P. S. *Journal of Controlled Release* **2003**, *89*, 365.
- (21) Palermo, E. F.; Kuroda, K. *Biomacromolecules* **2009**, *10*, 1416.
- (22) Yuan, F.; Dellian, M.; Fukumura, D.; Leunig, M.; Berk, D. A.; Torchilin, V. P.; Jain, R. K. *Cancer Research* **1995**, *55*, 3752.
- (23) (a) Oskuee, R. K.; Dehshahri, A.; Shier, W. T.; Ramezani, M. *Journal of Gene Medicine* **2009**, *11*, 921. (b) Wen, Y.; Pan, S.; Luo, X.; Zhang, X.; Zhang, W.; Feng, M. *Bioconjugate Chemistry* **2009**, *20*, 322.
- (24) (a) Gabrielson, N. P.; Pack, D. W. *Biomacromolecules* **2006**, *7*, 2427. (b) Kabanov, A. V.; Kabanov, V. A. *Bioconjugate Chemistry* **1995**, *6*, 7.

- (25) (a) Brownlie, A.; Uchegbu, I. F.; Schätzlein, A. G. *International Journal of Pharmaceutics* **2004**, *274*, 41. (b) Deng, R.; Yue, Y.; Jin, F.; Chen, Y.; Kung, H. F.; Lin, M. C.; Wu, C. *Journal of Controlled Release* **2009**, *140*, 40. (c) Gebhart, C. L.; Kabanov, A. V. *Journal of Controlled Release* **2001**, *73*, 401.
- (26) (a) Konopka, K.; Overlid, N.; Nagaraj, A. C.; Düzgüneş, N. *Cellular & Molecular Biology Letters* **2006**, *11*, 171. (b) Merdan, T.; Kunath, K.; Petersen, H.; Bakowsky, U.; Voigt, K. H.; Kopeček, J.; Kissel, T. *Bioconjugate Chemistry* **2005**, *16*, 785. (c) Liu, Y.; Reineke, T. M. *Bioconjugate Chemistry* **2006**, *17*, 101.

Chapter 4.

Smart, comb-like carriers for silencing Bcl-2 expression in epithelial cancer cells

4.1 Introduction

Recently, there are increased strategies of cancer treatment based on the selective down regulation of specific molecular targets involved in the process of cancer development and progression.¹ Nucleic acids, such as small interfering RNA (siRNA) and antisense oligonucleotides (ASODN), that complementary bind to specific mRNAs have been shown to be effective in regulating the expression of several mammalian genes.² In addition, many studies proved to support that decreased expression of genes which are directly involved in cancer development and progression could inhibit cancer cell growth.³

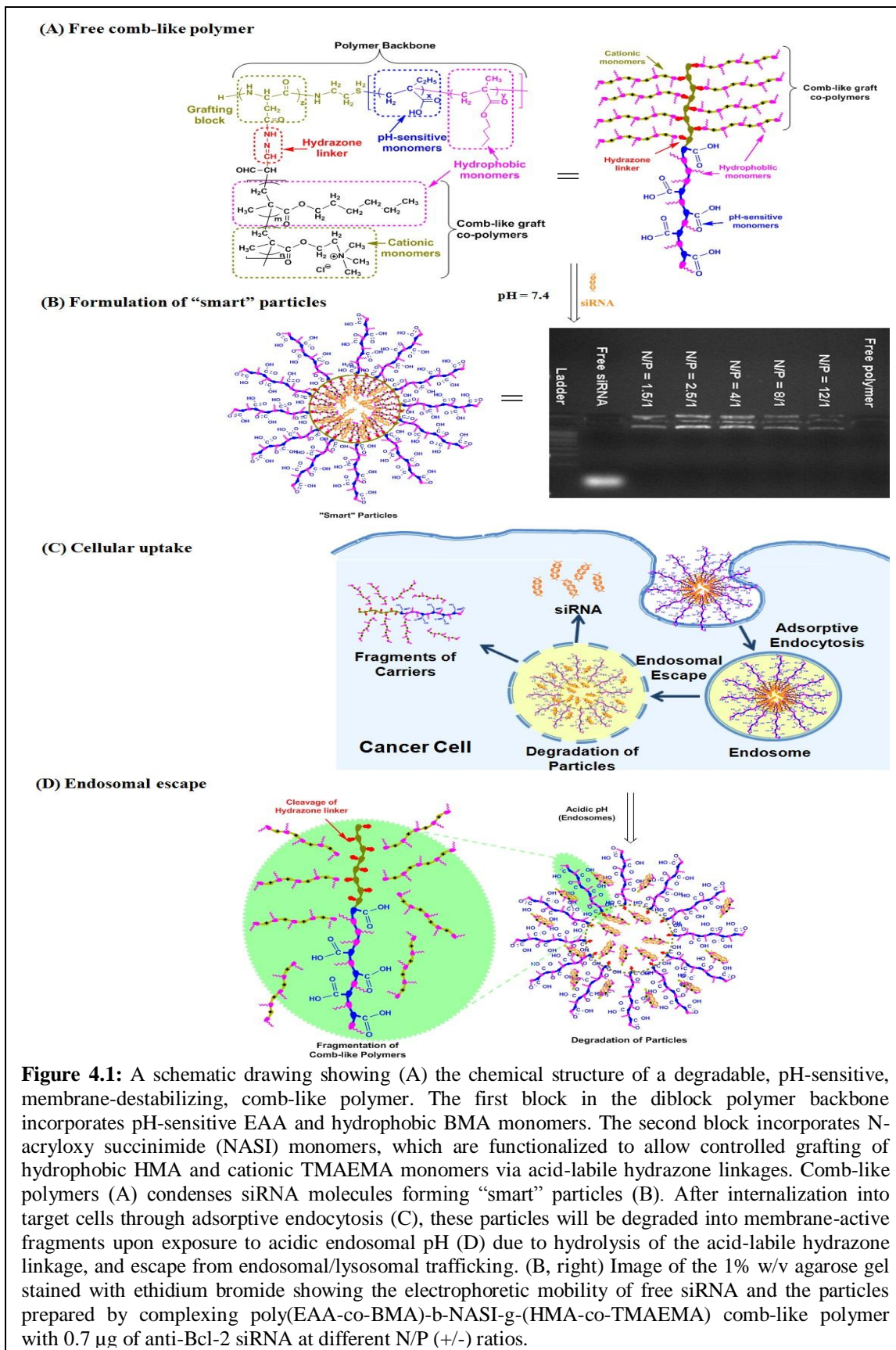
The B-cell lymphoma 2 (Bcl-2) family of proteins includes a number of apoptotic regulators with opposing functions.⁴ Among them, Bcl-2 is a pro-survival protein that is over expressed in various human cancer cells and responsible for dysregulation of apoptosis and prevention of death in cancer cells.⁵ Anti-apoptotic activity of Bcl-2 protein is attributed to its ability to stabilize the mitochondrial membrane and prevent the cytoplasmic release of cytochrome c, which inhibits the activation of caspases.^{5b,6} Over-expression of Bcl-2 has also been correlated with resistance to chemotherapy, radiotherapy, and development of hormone-resistant tumors.⁷ Earlier studies also showed

that Bcl-2 orchestrates the cross-talk between tumor cells and neovascular endothelial cells, which increases tumor angiogenesis and growth.⁸ In addition, targeting Bcl-2 expression in cancer cells using short hairpin RNA (shRNA) molecules proved to down regulate the expression of anti-apoptotic Bcl-2, and inhibit tumor growth in nude head and neck squamous cell carcinoma (HNSCC) tumor-bearing mice.^{8b} These studies suggest that reducing anti-apoptotic Bcl-2 expression using therapeutic nucleic acids is a viable strategy to suppress tumor growth and induce cancer cell death.

Although the significant advances in the design and synthesis of antisense oligonucleotides (ASODN) and small interfering RNA (siRNA) molecules, their selective delivery into the cytoplasm of diseased cells remains a significant challenge. The ideal carrier for delivery of therapeutic nucleic acids should successfully complex the DNA/RNA molecules into serum- and nuclease-stable particles that can preferentially accumulate into the diseased tissue and get selectively internalized into the targeted cells coupled with efficient escape from the endosomal/lysosomal trafficking pathway and delivery of the therapeutic cargo into the cytoplasm.⁹ Hoffman, Stayton, and coworkers have designed and developed a series of synthetic polymeric carriers that mimic the endosomolytic properties of fusogenic proteins and enhance the cytoplasmic delivery of therapeutic macromolecules.¹⁰ These polymers are characterized by their unique ability to “sense” the changes in environment pH where they undergo a change from a hydrophilic, stealth-like conformation at physiologic pH to a hydrophobic and membrane-destabilizing one in response to acidic endosomal pH gradients. We also designed and synthesized a series of “smart” pH-sensitive, membrane-destabilizing, comb-like polymers, which incorporating two blocks in their backbone.¹¹ The first block is

composed of pH-sensitive EAA monomers and hydrophobic butyl methacrylate (BMA) monomers whereas the second block incorporates N-acryloxy succinimide (NASI) monomers, which allows controlled grafting of hydrophobic and cationic copolymers via acid-labile hydrazone linkages (**Figure 4.1A**). At physiologic pH, these polymers retain their comb-like architecture and successfully complex siRNA molecules through electrostatic interactions with the cationic grafts forming “smart” pH-sensitive particles (**Figure 4.1B**) that are taken up into the cell by adsorptive endocytosis (**Figure 4.1C**). In the endosome, the comb-like polymer “senses” the drop in environment pH, which results in hydrolysis of the acid-labile hydrazone linkage and release of the hydrophobic/cationic grafts that rupture the endosomal membrane and release their siRNA cargo into the cytoplasm (**Figure 4.1D**). These polymers have been proved to successfully deliver functional siRNA molecules into the cytoplasm of MCF-7 breast cancer cells and achieve targeted gene knockdown at both mRNA and protein levels.¹¹

In this paper, we further evaluated the ability of these “smart” comb-like polymers to achieve functional delivery of anti-Bcl-2 siRNA molecules based on their ability to selectively knockdown Bcl-2 expression at the mRNA and protein levels in HeLa cervical carcinoma, and UM-SCC-17B head and neck squamous cell carcinoma. We also investigated the effect of incubation time on the suppression of Bcl-2 expression in head and neck cancer cells after treatment with these particles for 48, 72, and 96 hours.



4.2 Experimental Section

4.2.1 Materials

The human anti-GAPDH siRNA, FAM-labeled anti-GAPDH siRNA, negative siRNA sequence, KDAlert GAPDH assay kit, and siPORT-NH₂ transfection reagent were purchased from Ambion Inc. (Austin, TX). The anti-Bcl-2 siRNA sequence (5'-GCCUGAUUGUGUAUUAUUCA-3') was synthesized by Integrated DNA Technologies, Inc. (Coralville, Iowa). The RNeasy Mini Kit and Omniscript reverse transcriptase kit were purchased from Qiagen (Valencia, CA). The TaqMan universal PCR master mix and TaqMan gene expression assays for human GAPDH, human Bcl-2, β -actin, and 18S rRNA genes were purchased from Applied Biosystems (Foster, CA). The anti-human β -actin monoclonal antibody and anti-human Bcl-2 monoclonal antibody were purchased from Santa Cruz Biotechnology (Santa Cruz, CA) and BD Biosciences (San Jose, CA), respectively.

4.2.2 Formulation and characterization of “smart” particles

The pH-sensitive comb-like polymers were dissolved in RNase-free water and mixed with 0.7 μ g of anti-Bcl-2 siRNA molecules dissolved in 1 μ l of RNase-free water at different nitrogen/phosphate (N/P) ratios. Each mixture was vortexed and allowed to stand at room temperature for 20 minutes before loading onto a 1% w/v agarose gel containing ethidium bromide (EtBr). The gel was immersed in a Tris-acetate-EDTA (TAE) buffer and run at 60 V for 45 minutes and visualized under UV (Fotodyne Incorporated, Hartland, WI). Size and zeta potential of the particles prepared at N/P ratios of 2.5/1, 4/1, and 5/1 were measured using 90Plus particle size analyzer with ZetaPALS capability (Brookhaven Instruments Corporation, Holtsville, NY).

4.2.3 Culture of HeLa and UM-SCC-17B cells

HeLa cervical cancer and UM-SCC-17B head and neck cancer cells were generously provide by Dr. Nör and cultured following established protocols. Briefly, HeLa and UM-SCC-17B cells were maintained in DMEM supplemented with 10% fetal bovine serum, 10,000 units/ml penicillin, 10,000 µg/ml streptomycin and regularly changing the growth medium every 2 days. Cells were incubated at 37 °C, 5% CO₂, 95% relative humidity, and passaged upon reaching 70-90% confluency using 0.25% trypsin/EDTA mixture.

4.2.4 Cellular uptake of “smart” particles

Comb-like polymers and commercial siPORT-NH₂ were dissolved in OPTI-MEM solution and mixed with 0.57 µg of FAM-labeled anti-GAPDH siRNA molecules at N/P ratios of 1.5/1, 2.5/1, 4/1, 8/1, and 12/1 to prepare different particles that were incubated with HeLa and UM-SCC-17B cells for 6 hours at 37 °C, 5% CO₂, and 95% relative humidity. HeLa and UM-SCC-17B cells were washed with PBS, treated with 0.25% trypsin/EDTA solution for 10 minutes, harvested, and centrifuged to remove the supernatant and form a cell pellet. Cell pellets were suspended in PBS and analyzed using Biosciences FACSCalibur (Becton Dickinson, Franklin Lakes, NJ) to determine the percentage of fluorescently-labeled HeLa and UM-SCC-17B cells for each treatment. HeLa and UM-SCC-17B cells were gated by forward/size scatter and 10,000 gated events were collected per sample to discriminate between live and dead cells and account for live cells only.

4.2.5 In vitro evaluation of GAPDH knockdown in HeLa and UM-SCC-17B cells

HeLa and UM-SCC-17B cells were plated in 24-well plates at a seeding density of 20,000 cells/ well and allowed to adhere for 18 hours. The “smart” particles and siPORT-

NH₂ complexes incorporating 1.14 µg of anti-GAPDH siRNA or control siRNA molecules were incubated with HeLa and UM-SCC-17B cells at a final siRNA concentration of 200 nM for 6 hours followed by addition of 500 µl of fresh culture medium and incubation for a total of 48 hours. The effect of different treatments on GAPDH expression was quantified based on mRNA and protein levels. The amount of GAPDH protein expressed by HeLa and UM-SCC-17B cancer cells was measured using the KDalert GAPDH assay following manufacturer's specifications. The level of GAPDH protein expression in response to different treatments was normalized to that of untreated control cells. For quantification of GAPDH mRNA, total RNA was isolated from HeLa and UM-SCC-17B cells using the RNeasy Mini Kit and 0.25 µg of total RNA was reverse transcribed using Omniscript reverse transcriptase kit following manufacturer's protocols. Real-time PCR was performed in a final volume of 20 µl containing 2 µl of cDNA (corresponding to 10 ng of total RNA for GAPDH and β-actin amplification), 1 µl of each primer, and 10 µl of the qPCR MasterMix in the 7500 Fast Real-Time PCR system.

4.2.6 In vitro evaluation of Bcl-2 protein knockdown in HeLa and UM-SCC-17B cells

HeLa and UM-SCC-17B cells were plated in 6-well plates at a seeding density of 200,000 cells/ well and allowed to adhere for 18 hours. The “smart” particles and siPORT-NH₂ complexes incorporating 2.86 µg of anti-Bcl-2 siRNA or control siRNA molecules were incubated with HeLa and UM-SCC-17B cells at a final siRNA concentration of 200 nM for 6 hours followed by addition of 1250 µl of fresh culture medium and incubation for a total of 48, 72, or 96 hours. The amount of Bcl-2 protein expressed by HeLa and UM-SCC-17B cells was analyzed using the western blot

technique following established protocol.¹² Briefly, whole cell lysates were resolved by SDS-PAGE and membranes were probed overnight at 4°C with anti-human β -actin monoclonal antibody (1:1000000) and anti-human Bcl-2 monoclonal antibody (1:1000), and proteins were visualized with SuperSignal West Pico Chemiluminescent Substrate (Pierce, Rockford, IL). The knockdown of Bcl-2 protein expression in response to different treatments was quantified by Image J software (NIH, Bethesda, MD) and normalized to that of untreated cells.

4.2.7 In vitro evaluation of Bcl-2 mRNA knockdown in HeLa and UM-SCC-17B cells

HeLa and UM-SCC-17B cells were plated in 24-well plates at a seeding density of 20,000 cells/ well and allowed to adhere for 18 hours. The “smart” particles and siPORT-NH2 complexes incorporating 1.14 μ g of anti-Bcl-2 siRNA or control siRNA molecules were incubated with HeLa and UM-SCC-17B cells at a final siRNA concentration of 200 nM for 6 hours followed by addition of 500 μ l of fresh culture medium and incubation for a total of 48, 72, or 96 hours. For quantification of mRNA, total RNA was isolated from HeLa and UM-SCC-17B cells using the RNeasy Mini Kit and 0.25 μ g of total RNA was reverse transcribed using Omniscript reverse transcriptase kit following manufacturer’s protocols. Real-time PCR was performed in a final volume of 20 μ l containing 2 μ l of cDNA (corresponding to 10 ng of total RNA for Bcl-2 and 18S rRNA amplification), 1 μ l of each primer, and 10 μ l of the qPCR MasterMix in the 7500 Fast Real-Time PCR system.

4.3 Results

4.3.1 Formulation and characterization of “smart” particles

The ability of poly(EAA-*co*-BMA)-*b*-NASI-*g*-(HMA-*co*-TMAEMA) comb-like polymers to condense anti-Bcl-2 siRNA molecules into pH-sensitive particles was analysed using the standard gel retardation assay. Comb-like polymers were mixed with a fixed amount (0.7 μ g) of anti-Bcl-2 siRNA molecules at different N/P (+/-) ratios. The loaded RNA molecules were encapsulated into stable particles as a result of the electrostatic interaction between the cationic quaternary amine groups of the TMAEMA monomers and the anionic phosphate groups of the RNA molecules. Results show that poly(EAA-*co*-BMA)-*b*-NASI-*g*-(HMA-*co*-TMAEMA) comb-like polymers successfully complex the loaded siRNA molecules at all N/P ratios, which is indicated by their retention in the loading wells, while free siRNA molecules migrate towards the positive charge (**Figure 4.1B**). Size and surface

charge of particles prepared at N/P ratios of 2.5/1, 4/1, and 5/1 were measured using dynamic light scattering and zeta potential measurements, respectively. In **Figure 4.2**, results show that particles have 245, 373, and 313 nm in size at N/P ratios of 2.5/1, 4/1, and 5/1, respectively. These particles carry positive surface charges of 22.4, 24.9, and 32.3 mV, respectively.

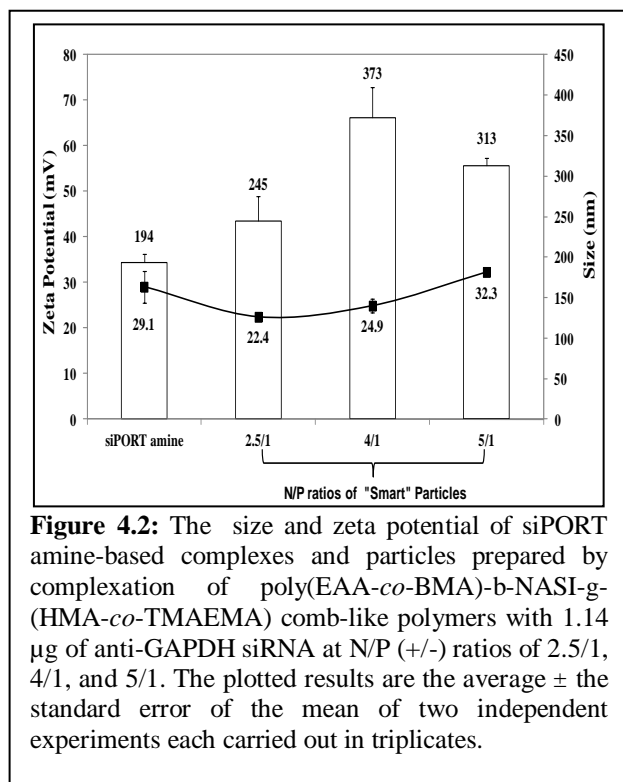


Figure 4.2: The size and zeta potential of siPORT amine-based complexes and particles prepared by complexation of poly(EAA-*co*-BMA)-*b*-NASI-*g*-(HMA-*co*-TMAEMA) comb-like polymers with 1.14 μ g of anti-GAPDH siRNA at N/P (+/-) ratios of 2.5/1, 4/1, and 5/1. The plotted results are the average \pm the standard error of the mean of two independent experiments each carried out in triplicates.

and 32.3 mV at N/P ratios of 2.5/1, 4/1, and 5/1, respectively. The sizes of “smart” particles are slightly larger than siPORT amine-based complexes, while the surface charges are relatively similar.

4.3.2 Uptake of “smart” particles into HeLa and UM-SCC-17B cells

We evaluated the internalization of fluorescently-labeled “smart” particles prepared at different N/P ratios into HeLa cervical carcinoma and UM-SCC-17B head and neck squamous cell carcinoma using flow cytometry. Complexes prepared using commercial siPORT amine transfection agents were used as positive controls. **Figure 4.3** shows that “smart” particles can be efficiently (> 97%) taken up into HeLa and UM-SCC-17B cells at N/P ratios higher than 2.5/1, and siPORT amine-based complexes also showed high internalization (~100%) into both cell types. These results indicate that our “smart” particles can be successfully

internalized by HeLa and UM-SCC-17B cancer cells through adsorptive endocytosis due to the positive surface charge of these particles. Earlier research showed that the increase of particle’s positive surface charge is typically associated with toxicity or low transfection efficiency due to poor decomplexation of the loaded DNA/RNA molecules.¹³ Consequently, we decided to evaluate the transfection

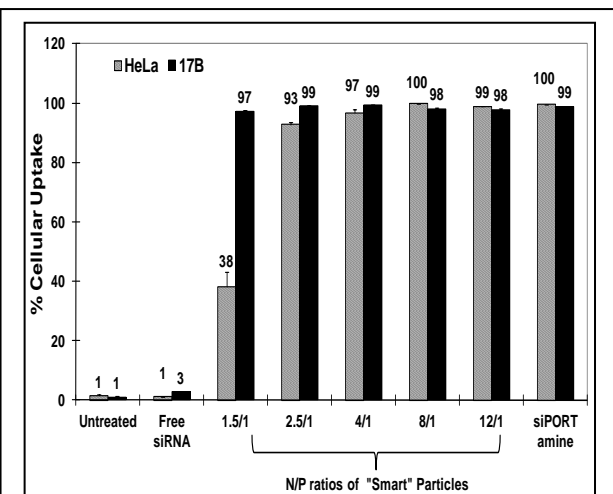


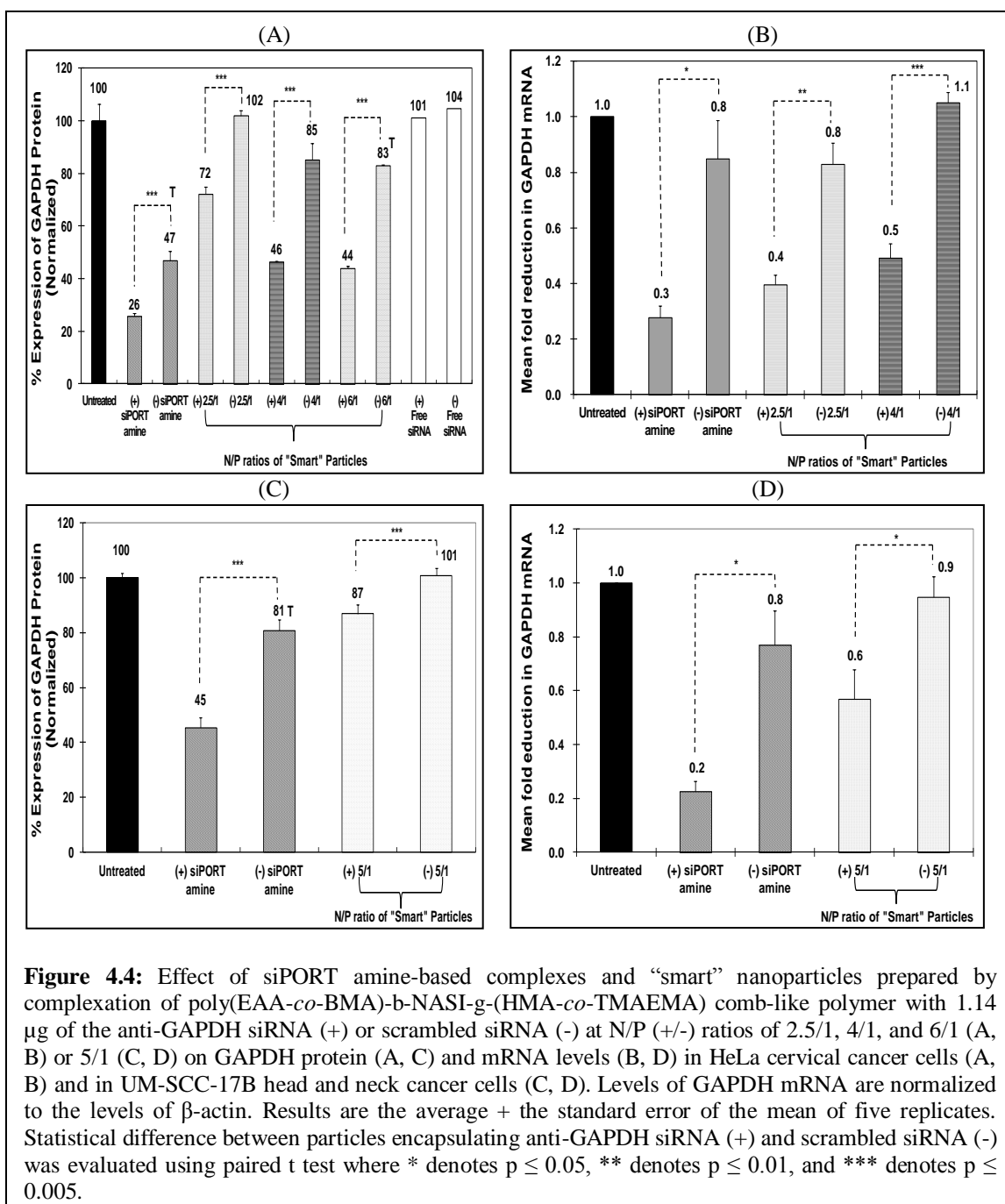
Figure 4.3: Percentage of HeLa cervical cancer and UM-SCC-17B head and neck cancer cells that internalize siPORT amine-based complexes and “smart” nanoparticles prepared by complexation of poly(EAA-*co*-BMA)-*b*-NASI-*g*-(HMA-*co*-TMAEMA) comb-like polymers with 1.14 μg of fluorescently-labeled anti-GAPDH siRNA at different N/P (+/-) ratios upon incubation for 6 hours in a serum-free culture medium. Results are the average + the standard error of the mean of three replicates.

efficiency of the particles prepared at N/P ratios of 2.5/1, 4/1 and 6/1, which will have a sufficient number of cationic TMAEMA residues to complex the loaded siRNA molecules, while eliminating cellular toxicity without preventing cytoplasmic decomplexation of the loaded siRNA molecules.

4.3.3 Effect of “smart” particles on GAPDH expression

The ability of “smart” particles to deliver siRNA molecules into the cytoplasm of HeLa and UM-SCC-17B cancer cells and perform their function was evaluated based on their ability to selectively knockdown GAPDH gene expression at the protein and mRNA levels. We utilized the KDAlert GAPDH assay kit to measure the changes in GAPDH protein level upon incubation with particles that encapsulate the anti-GAPDH siRNA molecules. These particles were compared to those encapsulating a scrambled siRNA sequence. We utilized siPORT amine-based complexes encapsulating an equal dose of anti-GAPDH siRNA molecules as a positive control to determine the maximum level of knockdown that can be achieved using robust commercial transfection agents. As shown in **Figure 4.4A**, particles prepared at N/P ratios of 2.5/1 and 4/1 induced 30 and 39% knockdown in GAPDH protein expression in HeLa cells, respectively. This knockdown is better than siPORT amine-based complexes, which inhibited GAPDH protein expression by only 21% with toxicity, since scrambled siRNA molecules also induced 53% GAPDH reduction compared to untreated cells. “Smart” particles prepared at an N/P ratio of 6/1 also induced 39% knockdown in GAPDH protein expression, which was associated with non-specific toxicity possibility due to the use of excess cationic carriers. To prevent their toxicity, we decided to use particles prepared at 2.5/1 and 4/1 ratios for the rest of the experiments in HeLa cells. The particles prepared at N/P ratios of 2.5/1 and

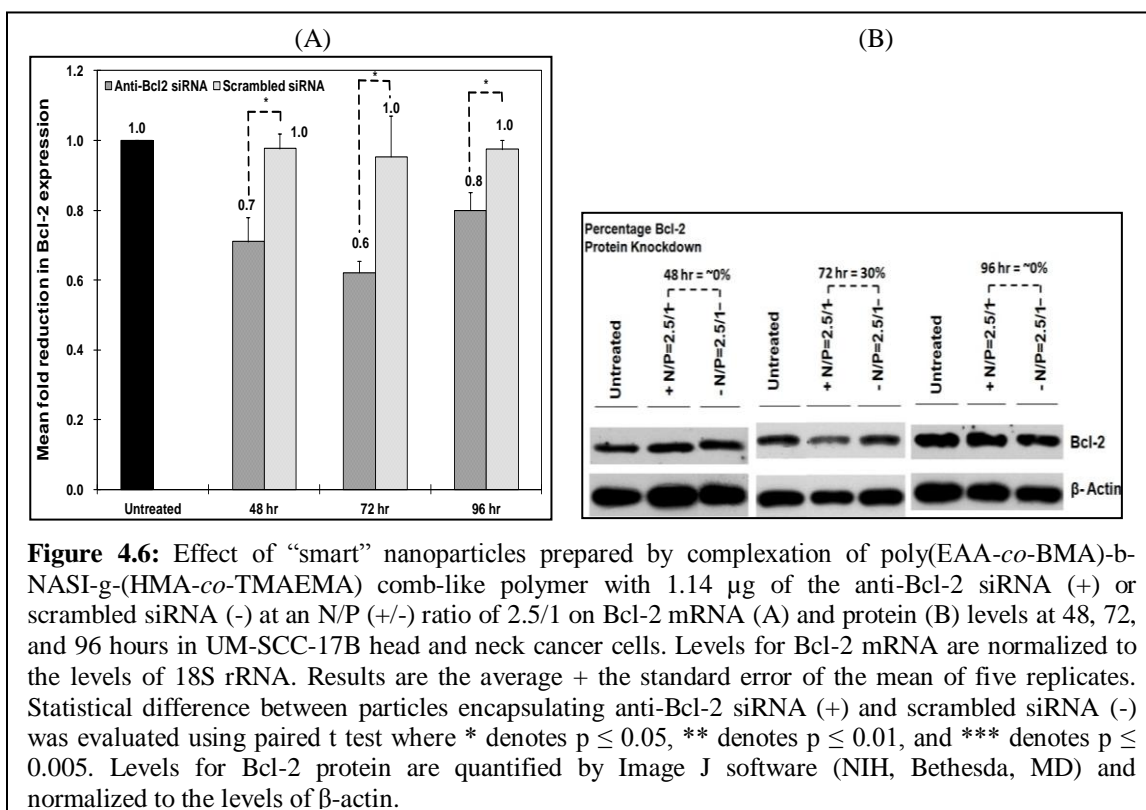
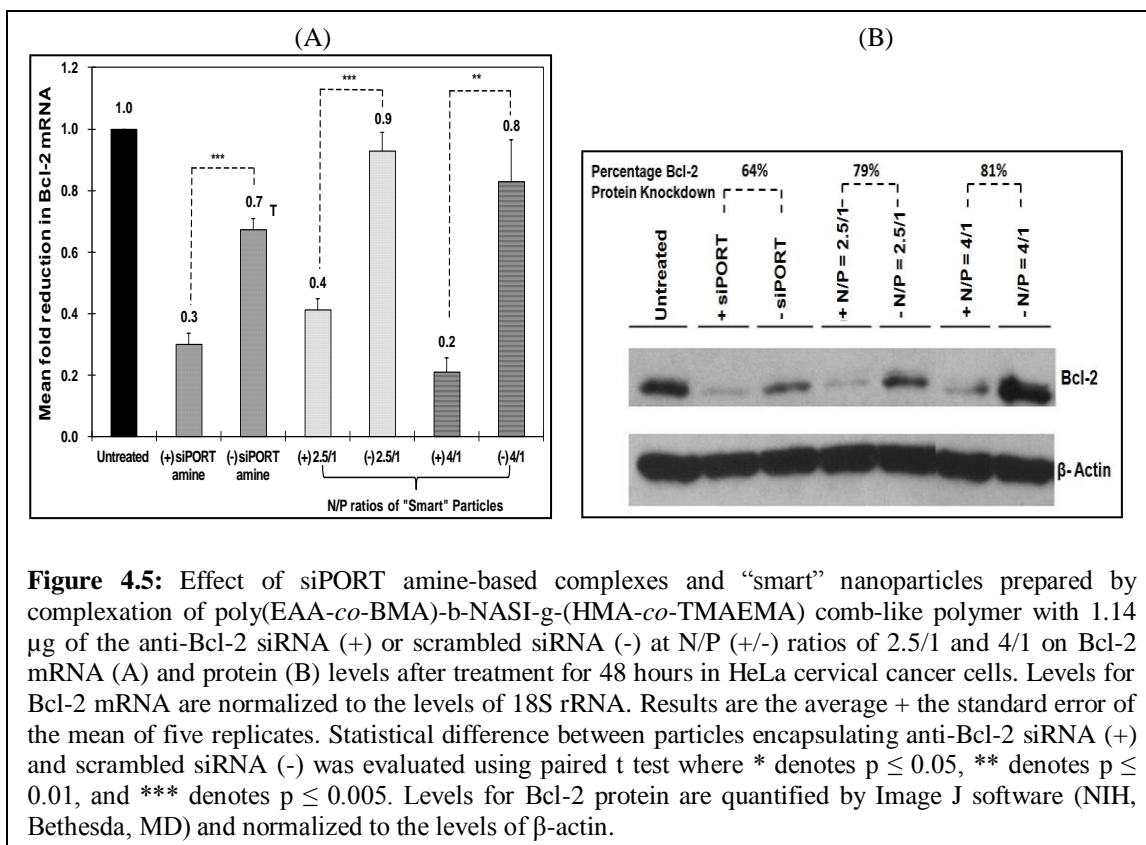
4/1 did not induce significant knockdown in GAPDH protein expression in UM-SCC-17B (data not shown), and this may be caused by the delayed decrease in endosomal pH and thus inefficient cytoplasmic release of siRNA molecules in head and neck cells.¹⁴ So in **Figure 4.4C**, the particles were prepared at an N/P ratio of 5/1, which induced 14% knockdown in GAPDH protein expression in UM-SCC-17B cells without toxicity, while siPORT amine-based complexes induce 36% GAPDH protein knockdown with toxicity. The low transfection efficiency of “smart” particles in UM-SCC-17B cells was perhaps due to the poor decomplexation of siRNA from particles after endosomal escape since a higher amount of polymer was used at an N/P ratio of 5/1 than 2.5/1 and 4/1. We further utilized qRT-PCR to evaluate the changes in GAPDH mRNA level upon incubation with particles that encapsulated the anti-GAPDH siRNA molecules. As can be seen in **Figure 4.4B**, particles prepared at N/P ratios of 2.5/1 and 4/1 induced 40 and 60% knockdown in GAPDH mRNA expression in HeLa cells, respectively, while siPORT amine-based complexes induced 50% knockdown. **Figure 4.4D** shows that particles prepared at 5/1 ratio induced 38% knockdown in GAPDH mRNA expression in UM-SCC-17B cells, compared to siPORT amine-based complexes that induced 54% knockdown. These particles proved to transfect HeLa and UM-SCC-17B cells more effectively than the commercial transfection agent without toxicity. Overall, the results suggest our “smart” combe-like polymers can function as an effective carrier for intracellular delivery of therapeutic siRNA molecules.



4.3.4 Effect of “smart” particles on Bcl-2 expression

The therapeutic activity of “smart” particles was evaluated based on their ability to selectively knockdown Bcl-2 gene expression at both the mRNA and protein levels. We utilized the qRT-PCR to measure the changes in Bcl-2 mRNA level upon incubation with

particles that encapsulate the anti-Bcl-2 siRNA molecules, and compare to those encapsulating a scrambled siRNA sequence. We utilized siPORT amine-based complexes encapsulating an equal dose of anti-Bcl-2 siRNA molecules as a positive control to determine the maximum level of knockdown that can be achieved using robust commercial transfection agents. As shown in **Figure 4.5A**, particles prepared at N/P ratios of 2.5/1 and 4/1 selectively induced 50 and 60% knockdown in Bcl-2 mRNA expression in HeLa cells, respectively. This knockdown is better than siPORT amine-based complexes which only inhibited Bcl-2 mRNA expression by 40% accompanied with toxicity. In **Figure 4.5B**, particles prepared at N/P ratios of 2.5/1 and 4/1 induced 79 and 81% knockdown in Bcl-2 protein expression in HeLa cells, respectively, while siPORT amine-based complexes induced only 64% knockdown. For UM-SCC-17B cells, in order to exclude the issue of poor decomplexation of particles prepared at an N/P ratio of 5/1, we decreased the N/P ratio to 2.5/1 but increased the incubation time to solve the possible problem of delayed endosomal pH drop. As shown in **Figure 4.6A**, Bcl-2 mRNA expression was inhibited by 30, 40, and 20% after treatment with particles for 48, 72, and 96 hours, respectively. Inhibition of Bcl-2 protein expression was only shown after treatment for 72 hours by 30% knockdown (**Figure 4.6B**). The results suggested that the therapeutic effects of anti-Bcl-2 siRNA delivered by using comb-like polymers is most effective after treatment for 72 hours in UM-SCC-17B cancer cells. In summary, these results prove our “smart” comb-like polymers can be utilized as effective carriers for the delivery of therapeutic siRNA molecules into various mammalian epithelial cells.



4.4 Discussions

The regulation of Bcl-2 expression using therapeutic nucleic acids has recently caused increasing interests due to the role of Bcl-2 in tumor development and angiogenesis. However, development of an efficient approach to deliver therapeutic anti-Bcl-2 nucleic acids to its target site is still a challenge. Therefore, it is important to develop an effective nucleic acid carrier to selectively inhibit Bcl-2 expression in cancer cells.

In this paper, we evaluated the possibility of using our “smart” pH-sensitive, membrane-destabilizing, comb-like poly(EAA-*co*-BMA)-*b*-NASI-*g*-(HMA-*co*-TMAEMA) polymer to knockdown Bcl-2 expression in HeLa cervical cancer and UM-SCC-17B head and neck cancer cells. The gel retardation result clearly shows that the polymers can condense siRNA molecules at lower N/P ratios compared to those of other acrylic acid-based polymers,¹⁵ thus reducing the amount of comb-like polymers needed to complex a given dose of therapeutic nucleic acids and consequently minimizing the toxicity commonly associated with cationic carriers.¹⁶ The size of these “smart” particles proved to fall below the molecular cut off size of 400-600 nm for tumor vasculature,¹⁷ and that the cationic nature of these particles will facilitate their interaction and internalization into target cells via adsorptive endocytosis, which is proved by the high cellular uptake into HaLa and UM-SCC-17B cancer cells. Most importantly, results show that the transfection efficiency of “smart” comb-like polymers, which is determined based on the inhibition of GAPDH and Bcl-2 expression at both protein and mRNA levels, is overall better than commercial transfection agent, siPORT amine. Transfection efficiency differs among tumor cell types probably due to their differences in the endosomal pH, resulting in ineffective endosomal escape in UM-SCC-17B cells. It has been proved that various

combinations of Na⁺, K⁺-ATPases and chloride channels, which regulate endosomal pH, could lead to two types of cancer cells. One type of cancer cells have an early endosomal pH of 6.1-6.2 and a late endosomal pH of 5.4-5.6, while the other type have similar early and late endosomal pH of 5.4-5.6.^{14,18} In addition, when we increased the incubation time from 48 to 72, and 96 hours, results showed that the most significant inhibition of Bcl-2 expression was induced after treatment for 72 hours, which matches earlier studies¹⁹ and suggests the transfection condition should be optimized in different cell types. Overall, the results suggest that the poly(EAA-*co*-BMA)-*b*-NASI-*g*-(HMA-*co*-TMAEMA) comb-like polymers are potential carriers for cytoplasmic delivery of therapeutic siRNA molecules.

4.5 Conclusions

In summary, we proved that our “smart” pH-sensitive, membrane-destabilizing, comb-like polymers can successfully complex model siRNA molecules into stable nano-sized particles at low N/P ratios, which indicate their ability to encapsulate large doses of therapeutic nucleic acids with minimum toxicity. These particles proved to be efficiently internalized into cancer cells, and achieve selectively knockdown in GAPDH and Bcl-2 expression at both the protein and mRNA levels. The results collectively indicate the potential of these particles to serve as a carrier for silencing Bcl-2 expression in cancer cells, and inducing cancer cell apoptosis.

References

- (1) Elsayed, Y. A.; Sausville, E. A. *Oncologist* **2001**, *6*, 517.
- (2) (a) Galderisi, U.; Cascino, A.; Giordano, A. *Journal of Cellular Physiology* **1999**, *181*, 251. (b) Santos, A. O.; Pereira, J. P.; de Lima, M. C. P.; Simoes, S.; Moreira, J. N. *Brazilian Journal of Medical and Biological Research* **2010**, *43*, 1001.
- (3) (a) Cho-Chung, Y. S. *Pharmacology & Therapeutics* **1999**, *82*, 437. (b) Futami, T.; Miyagishi, M.; Seki, M.; Taira, K. *Nucleic Acids Res Suppl* **2002**, 251. (c) Sonoke, S.; Ueda, T.; Fujiwara, K.; Sato, Y.; Takagaki, K.; Hirabayashi, K.; Ohgi, T.; Yano, J. *Cancer Research* **2008**, *68*, 8843.
- (4) Adams, J. M.; Cory, S. *Science* **1998**, *281*, 1322.
- (5) (a) Reed, J. C. *Curr Opin Oncol* **1999**, *11*, 68. (b) Reed, J. C. *J Clin Oncol* **1999**, *17*, 2941.
- (6) Kaufmann, S. H.; Gores, G. J. *Bioessays* **2000**, *22*, 1007.
- (7) (a) Jansen, B.; Schlagbauer-Wadl, H.; Brown, B. D.; Bryan, R. N.; van Elsas, A.; Muller, M.; Wolff, K.; Eichler, H. G.; Pehamberger, H. *Nature Medicine* **1998**, *4*, 232. (b) Kymionis, G. D.; Dimitrakakis, C. E.; Konstadoulakis, M. M.; Arzimanoglou, I.; Leandros, E.; Chalkiadakis, G.; Keramopoulos, A.; Michalas, S. *Journal of Surgical Research* **2001**, *99*, 161.
- (8) (a) Biroccio, A.; Candiloro, A.; Mottolese, M.; Saporà, O.; Albinì, A.; Zupi, G.; Del Bufalo, D. *Faseb Journal* **2000**, *14*, 652. (b) Kaneko, T.; Zhang, Z. C.; Mantellini, M. G.; Karl, E.; Zeitlin, B.; Verhaegen, M.; Soengas, M. S.; Lingem, M.; Strieter, R. M.; Nunez, G.; Nor, J. E. *Cancer Research* **2007**, *67*, 9685.
- (9) (a) Jere, D.; Jiang, H. L.; Arote, R.; Kim, Y. K.; Choi, Y. J.; Cho, M. H.; Akaike, T.; Cho, C. S. *Expert Opinion on Drug Delivery* **2009**, *6*, 827. (b) Lai, W. F.; Lin, M. C. *Journal of Controlled Release* **2009**, *134*, 158. (c) Midoux, P.; Pichon, C.; Yaouanc, J. J.; Jaffrès, P. A. *British journal of pharmacology* **2009**, *157*, 166.
- (10) (a) El-Sayed, M. E. H.; Hoffman, A. S.; Stayton, P. S. *Expert Opinion on Biological Therapy* **2005**, *5*, 23. (b) Yessine, M. A.; Leroux, J. C. *Advanced Drug Delivery Reviews* **2004**, *56*, 999.
- (11) Lin, Y. L.; Jiang, G. H.; Birrell, L. K.; El-Sayed, M. E. H. *Biomaterials* **2010**, *31*, 7150.
- (12) Neiva, K. G.; Zhang, Z.; Miyazawa, M.; Warner, K. A.; Karl, E.; Nor, J. E. *Neoplasia* **2009**, *11*, 583.
- (13) (a) Brownlie, A.; Uchegbu, I. F.; Schätzlein, A. G. *Int J Pharm* **2004**, *274*, 41. (b) Deng, R.; Yue, Y.; Jin, F.; Chen, Y.; Kung, H. F.; Lin, M. C.; Wu, C. *Journal of Controlled Release* **2009**, *140*, 40. (c) Gebhart, C. L.; Kabanov, A. V. *Journal of Controlled Release* **2001**, *73*, 401.
- (14) Rybak, S. L.; Lanni, F.; Murphy, R. F. *Biophys J* **1997**, *73*, 674.
- (15) (a) Bulmus, V.; Woodward, M.; Lin, L.; Murthy, N.; Stayton, P. S.; Hoffman, A. S. *Journal of Controlled Release* **2003**, *93*, 105. (b) El-Sayed, M. E. H.; Hoffman, A. S.; Stayton, P. S. *Journal of Controlled Release* **2005**, *101*, 47.
- (16) Boeckle, S.; von Gersdorff, K.; van der Piepen, S.; Culmsee, C.; Wagner, E.; Ogris, M. *J Gene Med* **2004**, *6*, 1102.
- (17) Yuan, F.; Dellian, M.; Fukumura, D.; Leunig, M.; Berk, D. A.; Torchilin, V. P.; Jain, R. K. *Cancer Research* **1995**, *55*, 3752.

- (18) Cain, C. C.; Sipe, D. M.; Murphy, R. F. *P Natl Acad Sci USA* **1989**, *86*, 544.
- (19) Buck, A. C.; Shen, C. X.; Schirrmeister, H.; Schmid-Kotsas, A.; Munzert, G.; Guhlmann, A.; Mehrke, G.; Klug, N.; Gross, H. J.; Bachem, M.; Reske, S. N. *Cancer Biother Radio* **2002**, *17*, 281.

Chapter 5.

Development of degradable, pH-sensitive, star vectors for cytoplasmic delivery of nucleic acids

5.1 Introduction

Small interfering RNA (siRNA) molecules are double stranded RNA molecules that can selectively hybridize with the target mRNA sequence in the cytoplasm and trigger its degradation by RNase H enzyme, which reduces the expression of the encoded gene.¹ Several preclinical investigations showed the potential of siRNA in inhibiting pathological gene expression, which proved effective in treatment of AIDS,² cardiovascular,³ and neurodegenerative diseases.⁴ However, transforming siRNA drug candidates into actual therapies with a defined dosing regimen remains a significant challenge due to the lack of an efficient biocompatible carrier that can deliver the necessary dose selectively into the cytoplasm of the diseased cells while sparing neighboring healthy ones.⁵ Cationic lipids,⁶ polymers,⁷ and peptides^{5d} have been used to condense siRNA via electrostatic interaction forming ionic complexes that are internalized by endocytosis. However, these complexes are often trapped in the endosomal/lysosomal trafficking pathway where the loaded siRNA cargo is degraded, which diminishes their therapeutic activity.⁸

Amphiphilic pH-sensitive polymers have been used to complex siRNA forming “smart” particles that bypass the endosomal/lysosomal trafficking pathway and deliver their cargo into the cytoplasm.⁹ These polymers utilize their unique ability to switch from a hydrophilic stealth-like conformation at physiologic pH to a hydrophobic membrane-destabilizing one in response to acidic endosomal pH gradients to rupture the endosomal membrane and release the entrapped RNA cargo into the cytoplasm to produce the desired effect.¹⁰ pH-sensitive membrane-destabilizing polymers proved effective in delivering plasmid DNA,¹¹ antisense oligodeoxynucleotides,¹² siRNA,¹³ and proteins¹⁴ into the cytoplasm of multiple cells both *in vitro*¹²⁻¹³ and *in vivo*.¹⁵ These amphiphilic polymers typically incorporate ionizable acidic moieties, hydrophobic motifs, and cationic groups for sensing the change in environment pH, disruption of the endosomal membrane, and complexation of the loaded DNA/RNA, respectively.¹⁶ Earlier research showed that the membrane-destabilizing activity increases with the increase in polymer’s molecular weight.¹⁷ However, given their non-degradable composition, these polymers are poorly eliminated by urinary excretion *in vivo*, which increases the risk of their long term accumulation leading to non-specific toxicity.^{17b} In addition, increasing the number of hydrophobic motifs to enhance the membrane-disruptive activity dramatically reduced polymer’s aqueous solubility and therapeutic utility.^{17b} Further, increasing the molar fraction of the cationic group to increase DNA/RNA loading and incorporation of targeting ligands (e.g. sugars, antibody fragments) has been shown to diminish the membrane-destabilizing activity of the formed particles and reduce the associated transfection capacity.¹⁸

Polyethyleneimine (PEI) and polyamidoamine (PAMAM) dendrimers represent another class of cationic polymers that resist the drop in endosomal pH through the buffering effect of their secondary and tertiary amine groups, which causes endosomal swelling and rupture resulting in leakage of its contents into the cytoplasm.^{7,19} Many targeting ligands have been covalently conjugated to PEI- and PAMAM-based complexes and proved effective in achieving selective internalization by diseased cells.²⁰ However, formulation of stable and efficient ionic complexes requires 10- to 20-fold N/P (+/-) ratio resulting in the use of excess polymer, which leads to significant toxicity both *in vitro* and *in vivo*.²¹

To address the limitations of both amphiphilic pH-sensitive membrane-destabilizing and endosomal buffering polymers, we report the synthesis of degradable, pH-sensitive, membrane-destabilizing, star-shaped polymers that proved efficient in delivering siRNA past the endosomal membrane and into the cytoplasm of multiple cell lines achieving the desired gene knockdown at the mRNA and protein levels. Specifically, we utilize β -cyclodextrin (β -CD), which is a FDA-approved, water-soluble, cone-shaped oligosaccharide composed of seven glucose units linked by α -1,4-glycosidic linkages as the core for the star-shaped vectors.²² We recognize that the β -CD core has seven primary hydroxyl groups at the C-6 position and fourteen secondary hydroxyl groups at the C-2 and C-3 positions providing two rims of hydroxyl groups with different chemical reactivity, which can be asymmetrically functionalized to display different motifs.²³ Therefore, we grafted amphiphilic membrane-destabilizing polymers from the secondary face of the β -CD core via acid-labile hydrazone linkages while leaving the primary face for subsequent modification aimed at achieving cell specific targeting (**Figure 5.1A**). We

grafted a random copolymer of hydrophobic hexyl methacrylate (HMA) and pH-sensitive dimethyl aminoethyl methacrylate (DMAEMA) monomers from the secondary face of the β -CD core via acid-labile hydrazone linkages forming star-shaped polymer where DMAEMA monomers were partially (50%) or fully (100%) quaternized into cationic trimethyl aminoethyl methacrylate (TMAEMA) for complexation of siRNA molecules. We hypothesized that star-shaped β -CD-P(HMA-*co*-DMAEMA-*co*-TMAEMA)_n polymers will condense siRNA into pH-sensitive particles that will be internalized via adsorptive-mediated endocytosis. In the endosome, the acid-labile hydrazone linkages will hydrolyze releasing the membrane-active P(HMA-*co*-DMAEMA-*co*-TMAEMA) grafts from the β -CD core to destabilize the endosomal membrane and release the siRNA cargo into the cytoplasm (**Figure 5.1B**).

We used atom transfer radical polymerization (ATRP) technique to control the number, molecular weight (25 and 40 kDa), and molar ratio of HMA/DMAEMA monomers (50/50 and 75/25) in the grafted P(HMA-*co*-DMAEMA) polymers to investigate the effect of the molecular weight and the hydrophobic/hydrophilic balance of these membrane-active fragments on the endosomal escape capacity indicated by the effect of the siRNA cargo. It is important to note that DMAEMA monomers have been shown to exhibit gradual protonation with the drop in environment pH producing an appreciable endosomal buffering capacity.²⁴ Comparing the transfection capacity of “smart” pH-sensitive particles that incorporate the same star-shaped β -CD carrier with identical graft composition but differ in the % of residual DMAEMA monomers that were not converted to cationic TMAEMA (i.e. retained their buffering capacity) allowed us to investigate the possibility of combining hydrophobic membrane disruption with endosomal burst to

achieve enhanced cytoplasmic delivery and the relative contribution of each mechanism to carrier activity.

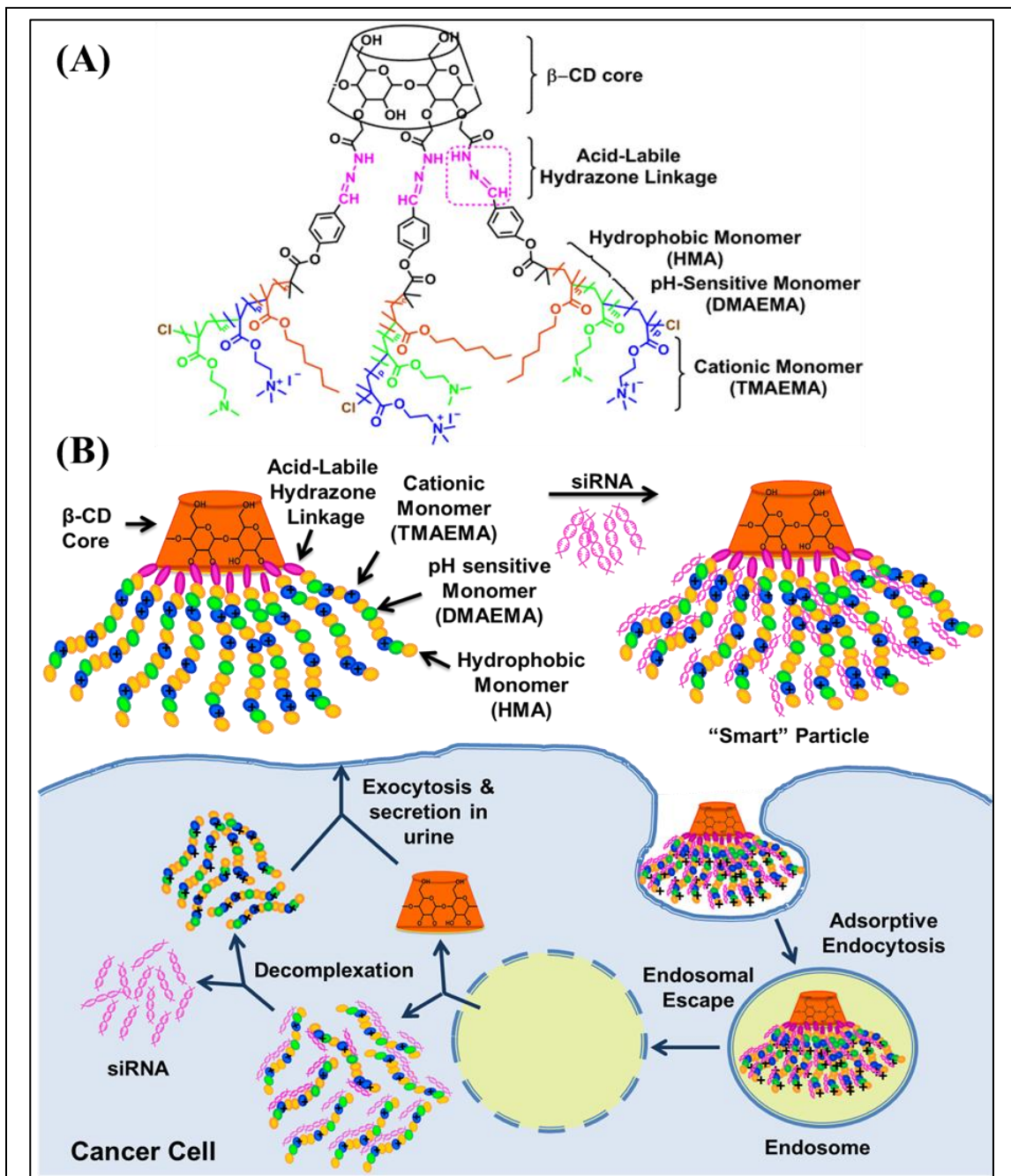


Figure 5.1: (A) Structure of pH-sensitive star-shaped β -CD-P(HMA-co-DMAEMA-co-TMAEMA)_n polymers. (B) A schematic drawing showing condensation of siRNA molecules by star-shaped pH-sensitive polymers forming "smart" particles, which are internalized by endocytosis. In the endosome, acid-labile hydrazone linkages are hydrolyzed by the acidic pH and release the P(HMA-co-TMAEMA-co-DMAEMA) grafts, which rupture the endosomal membrane and release the loaded siRNA cargo into the cytoplasm.

5.2 Experimental Section

5.2.1 Synthesis and characterization of degradable, pH-sensitive, star-shaped polymers

We synthesized a series of degradable, pH-sensitive, star-shaped β -CD-P(HMA-*co*-**D**MAEMA-*co*-**T**MAEMA)_{4,8} polymers where we varied the molecular weight (25 or 40 kDa) of the P(HMA-*co*-**D**MAEMA-*co*-**T**MAEMA) grafts, the molar ratio of HMA/DMAEMA monomers (50/50 or 75/25), and the degree of quaternization (50% or 100%) of DMAEMA monomers to cationic TMAEMA to systematically investigate the effect of these parameters on their ability to deliver siRNA molecules into the cytoplasm of epithelial cells. Detailed description of the experimental procedures for the synthesis and characterization of these polymers along with the supporting spectra are provided in the attached **Supplementary Information**.

5.2.2 Formulation and characterization of “smart” particles

All star-shaped pH-sensitive polymers were dissolved in RNase-free water except (β -CD-5 and β -CD-7 polymers, which were dissolved in 100% DMSO before mixing with 0.7 μ g of anti-GAPDH siRNA at different N/P ratios. Each mixture was vortexed and allowed to stand at room temperature for 20 minutes before loading onto a 1% w/v agarose gel containing ethidium bromide (EtBr). The gel was immersed in a Tris-acetate-EDTA (TAE) buffer and run at 60 V for 45 minutes before visualizing under UV using a fluorescent green filter (Fotodyne Incorporated, Hartland, WI). Size and zeta potential of the particles prepared at N/P ratios of 2.5/1 and 4/1 using β -CD 1-8 star polymers were measured by 90Plus particle size analyzer with ZetaPALS capability (Brookhaven Instruments Corporation, Holtsville, NY).

5.2.3 Cell culture

UM-SCC-17B head and neck squamous cell carcinoma and HeLa cervical cancer cells were generously provided by Dr. Jacques Nör (University of Michigan, School of Dentistry) and cultured following established protocols.²⁵ Briefly, HeLa and UM-SCC-17B cells were maintained in DMEM (Life Technologies, Grand Island, NY) supplemented with 10% fetal bovine serum (Life Technologies, Grand Island, NY), penicillin (10,000 Uml⁻¹), and streptomycin (10,000 µgml⁻¹) while regularly changing the growth medium every 2 days. MCF-10A mammary epithelial cells were generously provided by Dr. Sofia Merajver (University of Michigan, Department of Internal Medicine) and cultured in DMEM/F-12 (1:1) medium supplemented with 5% horse serum, EGF, cholera toxin, bovine insulin, and hydrocortisone. HeLa, UM-SCC-17B, and MCF-10A cells were incubated at 37 °C, 5% CO₂, 95% relative humidity, and passaged upon reaching 70-90% confluency using 0.25% trypsin/EDTA mixture.

5.2.4 Cellular uptake of “smart” particles

Star-shaped polymers and commercial siPORT-NH₂ were dissolved in OPTI-MEM solution (Life Technologies, Grand Island, NY) before mixing with 1.14 µg of FAM-labeled anti-GAPDH siRNA (Ambion Inc, Austin, TX) at N/P ratios of 1.5/1, 2.5/1, and 4/1 to prepare different complexes, which were incubated 6 hours at 37 °C, 5% CO₂, and 95% relative humidity with HeLa, UM-SCC-17B, or MCF-10A cells seeded at a seeding density of 4x10⁴ cells per well. Cells were then washed with PBS, treated with 0.25% trypsin/EDTA solution for 10 minutes, harvested, and centrifuged to form a cell pellet and remove the supernatant medium with free particles. Cell pellets were suspended in PBS

and analyzed using Biosciences FACSCalibur Flow Cytometer (Becton Dickinson, Franklin Lakes, NJ) to determine the percentage of fluorescently-labeled cells for each treatment. Cells were gated by forward/size scatter and 10,000 gated events were collected per sample to discriminate between live and dead cells and account for live cells only.

5.2.5 In vitro evaluation of “smart” particles

HeLa, UM-SCC-17B, and MCF-10A cells were plated in 24-well plates at a seeding density of 2×10^4 cells per well and allowed to adhere for 18 hours. Different “smart” particles and siPORT-NH₂ complexes incorporating anti-GAPDH siRNA (Ambion Inc, Austin, TX) or the scrambled siRNA sequence condensed at a N/P ratio of 2.5/1 were incubated with the cells for 6 hours at a final siRNA concentration of 100-200 nM before the addition of fresh culture medium (500 μ l) and incubating for a total of 48 hours. The effect of different treatments on GAPDH expression was quantified based on mRNA and protein levels. Briefly, total RNA was isolated from the cells using the RNeasy Mini Kit (Qiagen Inc, Valencia, CA) and a total of 0.25 μ g RNA was reverse transcribed using Omniscript reverse transcriptase kit (Qiagen Inc, Valencia, CA) following manufacturer’s protocols. Real-time PCR was performed in a final volume of 20 μ l containing 2 μ l of cDNA (corresponding to 10 ng of total RNA for GAPDH and β -actin amplification), 1 μ l of each primer, and 10 μ l of the qPCR MasterMix in the 7500 Fast Real-Time PCR system (Life Technologies, Grand Island, NY). The amount of GAPDH protein expressed by cells was measured using the KDAlert GAPDH assay (Ambion Inc, Austin, TX) following manufacturer’s specifications. The level of GAPDH protein expression in response to different treatments was normalized to that of untreated control cells.

5.3 Results and Discussion

5.3.1 Synthesis of degradable, pH-sensitive, star-shaped polymers

As described in the associated **Supplementary Information**, we successfully utilized the asymmetric distribution of primary and secondary hydroxyl groups on opposite faces of the β -CD core to graft amphiphilic P(HMA-*co*-DMAEMA) polymers from the secondary face via acid-labile hydrazone linkages using ATRP. We engineered these star-shaped polymers to systematically evaluate the effect of graft's molecular weight (25 and 40 kDa), hydrophobic/hydrophilic balance defined by the ratio of HMA/DMAEMA monomers (50/50 and 75/25), and degree of quaternization of DMAEMA monomers (50% and 100%) on the complexation of siRNA molecules into "smart" particles and their ability to deliver the RNA cargo past the endosomal membrane and into the cytoplasm of epithelial cancer cells. Specifically, we controlled the molecular weight of the P(HMA-*co*-DMAEMA) grafts in β -CD-1, -2, -5, and -6 polymers to be ~25 kDa compared to ~40 kDa in β -CD-3, -4, -7, and -8 polymers (**Table 5.1**). Earlier research showed the significant contribution of hydrophobic monomers (e.g. HMA) to the endosomal escape of ionic complexes.^{17b,18a,b} Therefore, we increased the ratio of HMA/DMAEMA monomers from 50/50 in β -CD-1, -2, -3, and -4 polymer to 75/25 in β -CD-5, -6, -7, and -8 polymers (**Table 5.1**) to examine the effect of HMA ratio on polymer's aqueous solubility and transfection efficiency of the formed complexes. Earlier research also showed that poly(dimethyl aminoethyl methacrylate) (**P**DMAEMA) polymers exhibit higher transfection efficiency compared to poly(trimethyl aminoethyl methacrylate) (**P**TMAEMA) polymers with similar molecular weight,²⁶ which is attributed to the endosomal buffering capacity of **P**DMAEMA polymers ($pK_a = 7.5$)

resulting in efficient destabilization of the endosomal membrane and release of the loaded nucleic acid cargo into the cytoplasm.²⁴ Therefore, we compared the transfection capacity of β -CD-1, -3, -5, and -7 polymers that have 50% of DMAEMA monomers converted to cationic TMAEMA to the transfection efficiency of β -CD-2, -4, -6, and -8 polymers with 100% of DMAEMA monomers converted to TMAEMA (Table 5.1).

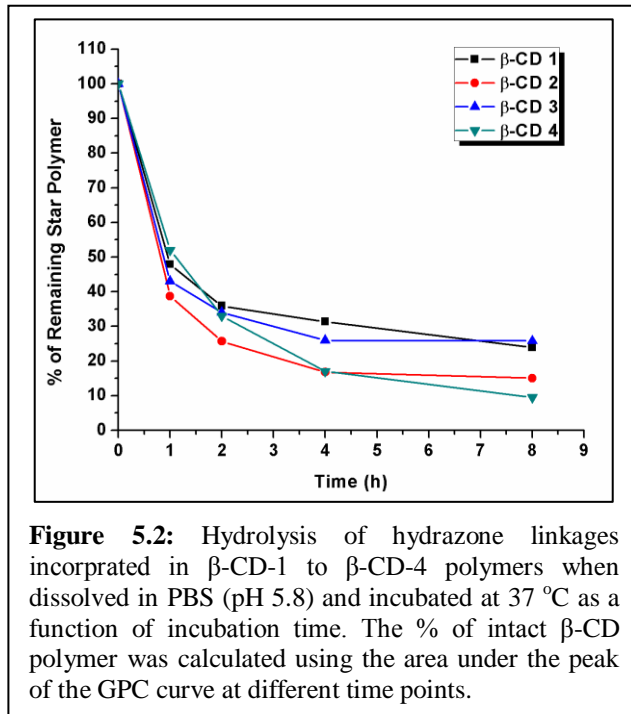
Table 5.1: Composition of the degradable, pH-sensitive, star-shaped β -CD-based vectors

Polymer Code	M_n of each arm^a (g/mol)	Copolymer Composition (% HMA/DMAEMA)^a	# of HMA units^a	# of DMAEMA units^a	# of TMAEMA units^a	% of Quaternization^a
β -CD-1	25580	47:53	73	26	58	69
β -CD-2	25580	47:53	73	0	84	100
β -CD-3	40750	49:51	122	57	70	55
β -CD-4	40750	49:51	122	0	127	100
β -CD-5	25050	76:24	113	20	19	46
β -CD-6	24930	74:26	110	0	39	100
β -CD-7	41200	76:24	186	31	29	49
β -CD-8	41200	76:24	186	0	60	100

^aCalculated from the ¹H NMR spectra

The motivation to incorporate acid-labile hydrazone linkages in polymer composition is to engineer a carrier with a large number of cationic and hydrophobic groups necessary for complexation of a large dose of siRNA molecules and endosomal escape of the formed particles, which will degrade into small membrane-active fragments that can be eliminated by urinary excretion, which will address the long-term accumulation of linear non-degradable polymers and the associated *in vivo* toxicity.²⁷ Our results show that the

average degradation half life ($t_{1/2}$) of the acid-labile hydrazone linkages in star-shaped β -CD polymers incubated in an acidic buffer solution (pH 5.8) at 37 °C is 60 ± 2 min (**Figure 5.2**), which is consistent with previously published results.¹³ We used the β -CD core to develop new star-shaped carriers for delivery of siRNA based on the established advantages of the



star architecture compared to the linear counterpart.²⁸ For example, 3- and 5-arms star PDMAEMA polymers exhibit higher transfection efficiency and lower toxicity compared to the corresponding linear polymers with the transfection efficiency and biocompatibility increasing with the increase in degree of polymer branching.²⁹ This is further supported by the reported high transfection efficiency of particles prepared using dendrimers³⁰ and hyper-branched cationic polymers³¹ that provide steric protection for loaded cargo, long retention in the systemic circulation, and high accumulation in the tumor tissue. Therefore, distributing the number of cationic TMAEMA groups necessary for condensation of siRNA molecules over multiple polymer grafts in a star-like conformation will eliminate the significant cytotoxicity observed with the linear conformation particularly at high molecular weights.^{28b,32}

ATRP³³ and reversible addition fragmentation chain transfer (RAFT)³⁴ polymerization techniques are the two most efficient methods to synthesize well-defined block,³⁵ graft,³⁶

and star-shaped^{28b,32c,37} polymeric carriers. We utilized ATRP to control the number, molecular weight, molecular weight distribution, composition, architecture, and site-specific functionality of the formed star-shaped polymers (**Table 5.1**). It is important to note that the asymmetric grafting of P(HMA-*co*-DMAEMA) polymers from the secondary face of the β -CD core is engineered to allow selective coupling of hydrophilic poly(ethylene glycol) (PEG) chains to the primary hydroxyl groups via non-degradable linkages, which will confer resistance to the formed “smart” particles against the adsorption of serum proteins, increase their residence time in the systemic circulation, and allow passive accumulation in tumor tissue when administered *in vivo*. These PEG chains can be further functionalized to display an array of targeting ligands to allow cell-specific internalization and delivery of the loaded cargo.

5.3.2 Formulation of “smart” particles

We evaluated the ability of different star polymers (β -CD-1 to β -CD-8) to complex 0.7 μ g of anti-GAPDH (glyceraldehyde 3-phosphate dehydrogenase) siRNA at different (+/-) nitrogen (N)/phosphate (P) ratios using the standard gel retardation assay. The amount of β -CD polymer mixed with the anti-GAPDH siRNA was calculated based on the cationic TMAEMA content to take into account the difference in the % of quaternized DMAEMA monomers in each polymer composition. Results show that all β -CD polymers successfully condensed the loaded siRNA into particles that were retained into the loading wells at low N/P ratios (**Figure 5.3**). Comparing between β -CD-1 and β -CD-3, which have a similar number of P(HMA-*co*-DMAEMA-*co*-TMAEMA) grafts, similar HMA/DMAEMA ratio, and ~50% of DMAEMA monomers quaternized into TMAEMA units but differ in the molecular weight of the grafts shows that β -CD-3 polymer fully

condenses the loaded siRNA at N/P ratio of 1.5/1 whereas full RNA condensation with β -CD-1 occurs at N/P ratio of 2.5/1 (**Figure 5.3A & C**). This shows that higher molecular weight of the P(HMA-*co*-DMAEMA-*co*-TMAEMA) graft (40 kDa) in β -CD-3 compared to β -CD-1 (25 kDa) results in a more efficient condensation of the loaded siRNA molecules while using a smaller (2 μ g) amount of β -CD-3 polymer compared to 3 μ g of β -CD-1. Similarly, β -CD-1 and β -CD-2 have identical number of polymeric grafts with the same molecular weight (25 kDa) and the same number of HMA and DMAEMA monomers attached to the β -CD core but differ in the % of DMAEMA monomers transformed to cationic TMAEMA complex the loaded siRNA molecules at N/P ratios of 2.5/1 and 1.5/1, respectively (**Figure 5.3A & B**). This is not surprising given that 100% of DMAEMA monomers were transformed to cationic TMAEMA in β -CD-2, which allows tighter binding to siRNA phosphate groups compared to partially quaternized β -CD-1 polymer. This led to the use of only 1 μ g of β -CD-2 compared to 3 μ g of β -CD-1 to complex the same amount of anti-GAPDH siRNA molecules.

Increasing the molar ratio of HMA/DMAEMA monomers from 50/50 (e.g β -CD-2) to 75/25 (e.g β -CD-6) increased the N/P ratio and amount of polymer needed to complex the loaded siRNA molecules. Specifically, β -CD-2 and β -CD-6 polymers complex equal amounts of anti-GAPDH siRNA at N/P ratios of 1.5/1 and 4/1, respectively (**Figure 5.3B & F**). This increase in the amount (6 μ g) of β -CD-6 polymer and the N/P ratio where full condensation of the loaded siRNA is observed is a result of the reduction in the number of cationic TMAEMA monomers/graft available for complexation with the anionic phosphate groups. Further, increasing the fraction of hydrophobic HMA monomers in graft composition reduced the aqueous solubility of the formed star polymer particularly

the partially (50%) quaternized β -CD-5 and β -CD-7 polymers. It is important to note that all the synthesized β -CD-based carriers successfully complexed the loaded siRNA molecules at N/P ratios that are much lower than established transfection reagents like PEI and cationic PAMAM dendrimers, which are routinely used at N/P ratios $> 15/1$.³⁸ This is a significant improvement over existing carriers as it allows the use of small amounts of β -CD-based vectors for condensation and delivery of a high dose of siRNA molecules, which will eliminate the need for excess cationic carrier and reduce the associated side effects.

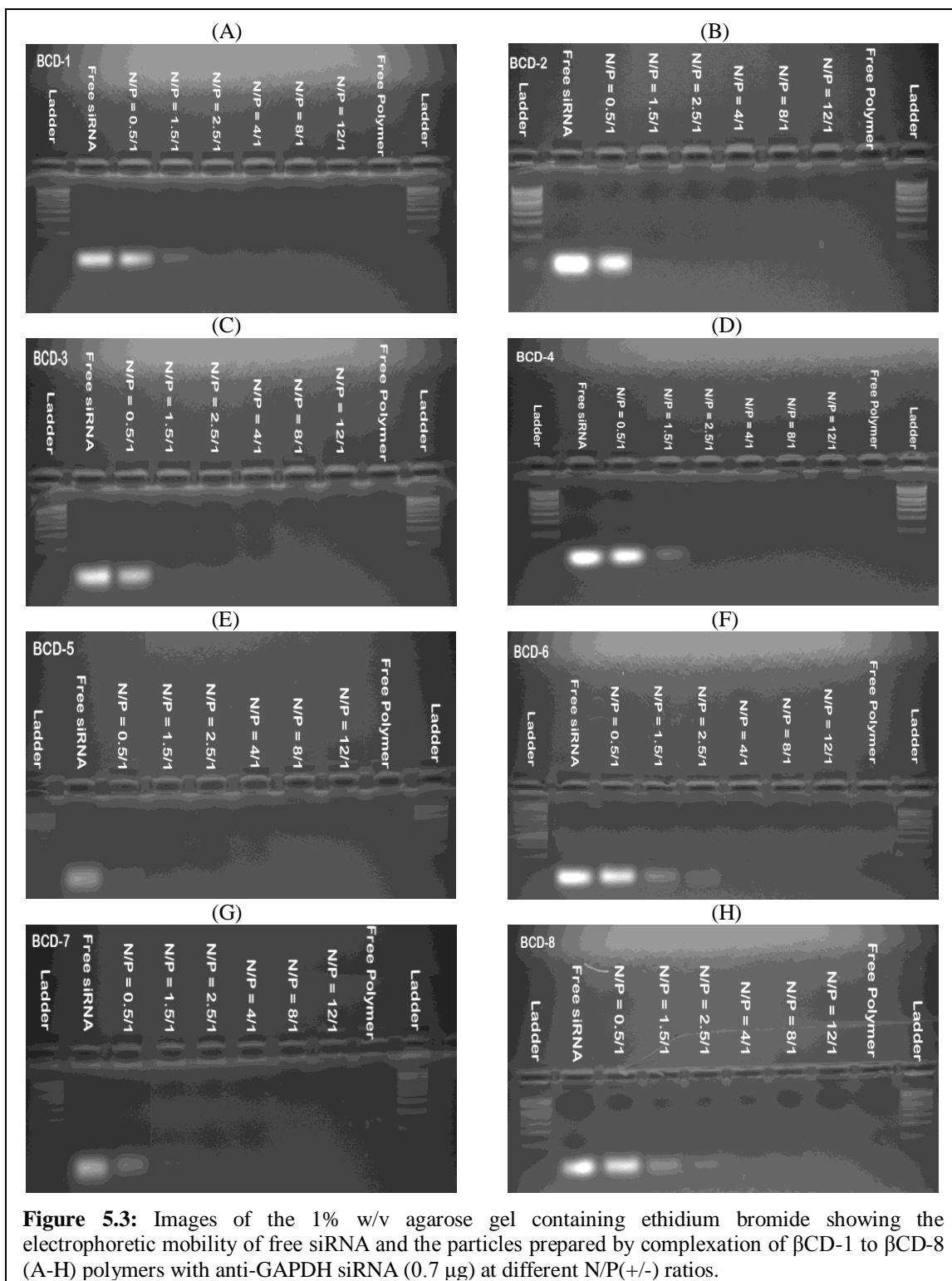
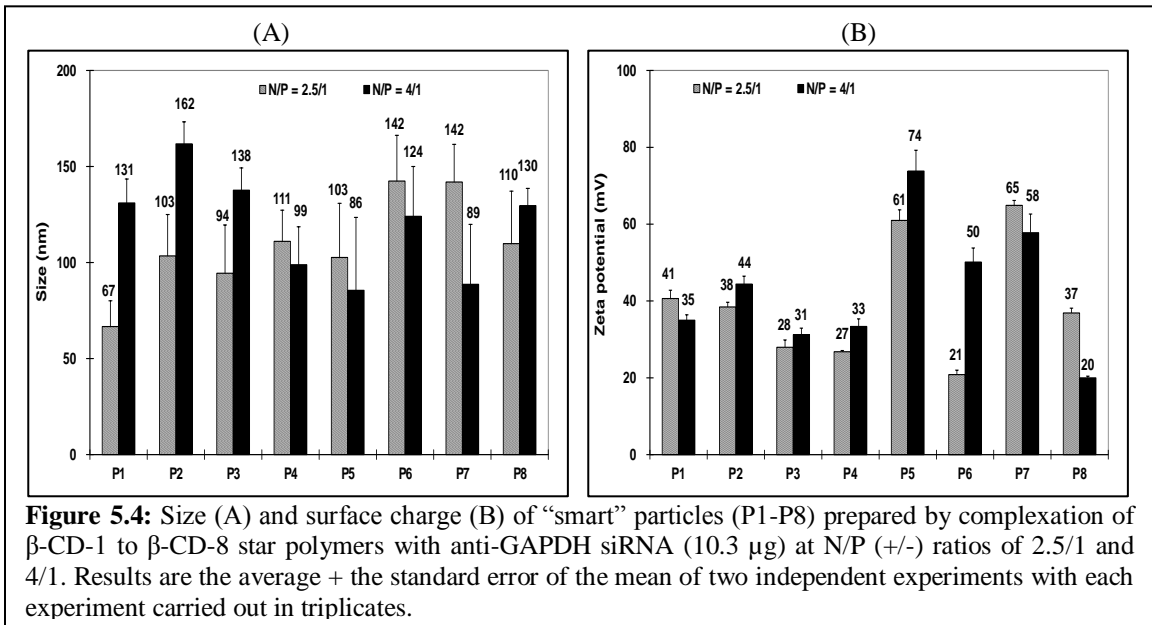


Figure 5.3: Images of the 1% w/v agarose gel containing ethidium bromide showing the electrophoretic mobility of free siRNA and the particles prepared by complexation of β CD-1 to β CD-8 (A-H) polymers with anti-GAPDH siRNA (0.7 μ g) at different N/P(+/-) ratios.

5.3.3 Characterization of “smart” particles

All star polymers (β -CD-1 to β -CD-8) were mixed with 10.3 μ g of anti-GAPDH siRNA at N/P ratios of 2.5/1 and 4/1 to prepare “smart” particles (P1-P8) that were characterized in terms of size and surface charge using dynamic light scattering and zeta potential measurements, respectively. Results show that particle size ranged between 67 - 142 nm for those prepared at N/P ratio of 2.5/1, which increased to 86 – 162 nm for particles prepared at N/P ratio of 4/1 (**Figure 5.4A**). Given that the molecular size cut off for tumor vasculature is between 400 and 600 nm,³⁹ these “smart” particles (P1-P8) are suited for delivery of siRNA into solid tumors. Zeta potential measurements show that P1-P8 prepared at N/P ratio of 2.5/1 have a net positive charge of 21-65 mV, which increased to 20-74 mV for particles prepared at N/P ratio of 4/1 (**Figure 5.4B**). The cationic surface of these “smart particles (P1-P8) will trigger efficient internalization by epithelial cancer cells via adsorptive endocytosis.^{13,40}



5.3.4 Uptake of “smart” particles into HeLa cervical cancer cells

We prepared fluorescently-labeled particles (P1-P8) by complexation of β -CD-1 to β -CD-8 polymers with FAM-labeled anti-GAPDH siRNA at N/P ratios of 1.5/1, 2.5/1, and 4/1 and evaluated their uptake into HeLa cervical cancer cells in comparison to free siRNA and siPORT amine-based complexes using flow cytometry. Results show that free siRNA molecules were not internalized and require a carrier to enhance their

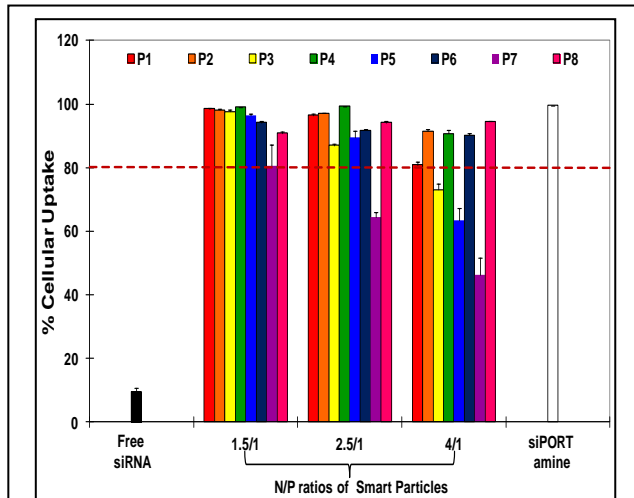


Figure 5.5: Percentage of fluorescently-labeled HeLa cancer cells after incubating for 6 hours in a serum-free culture medium with free siRNA, siPORT amine-based complexes, and “smart” P1-P8 particles prepared by complexation of β -CD-1 to β -CD-8 polymers with FAM-labeled anti-GAPDH siRNA (1.14 μ g) at N/P ratios of 1.5/1, 2.5/1, and 4/1. Results are the average + the standard error of the mean of four independent experiments with each experiment carried out in triplicates.

uptake by HeLa cells (**Figure 5.5**). All the particles (P1-P8) formulated at N/P ratios of 1.5/1 and 2.5/1 were internalized by $\geq 80\%$ of HeLa cancer cells except for P7. Further, P5 and P7 particles prepared at a N/P ratio of 4/1 were poorly internalized by HeLa cells (**Figure 5.5**). The observed drop in number of fluorescently-labeled HeLa cells upon incubation with P5 and P7 particles can be attributed to higher positive surface charge density (**Figure 5.4B**), which could lead to cell death as shown with other cationic particles.^{18c,d} Consequently, we limited our study to “smart” particles (P1-P8) prepared at N/P ratio of 2.5/1 and investigated their ability to deliver anti-GAPDH siRNA into the cytoplasm of HeLa cancer cells indicated by knockdown of GAPDH expression at the mRNA and protein levels.

5.3.5 Effect of “smart” particles on GAPDH expression

The ability of “smart” particles (P1-P8) to deliver functional anti-GAPDH siRNA molecules past the endosomal membrane and into the cytoplasm of HeLa cells was assayed based on their ability to selectively knockdown GAPDH gene expression at the mRNA and protein levels. We utilized the kDAlert assay kit to measure the changes in GAPDH protein level upon incubation with particles that encapsulate (+) the anti-GAPDH siRNA compared to those encapsulating (-) a scrambled siRNA sequence. We utilized siPORT amine-based complexes encapsulating an equal dose of (+) anti-GAPDH siRNA molecules as a positive control to determine the maximum level of knockdown that can be achieved using a robust commercial transfection reagent (**Figure 5.6**). Results show that P1-P4 were more efficient in knocking down GAPDH protein expression compared to P5-P8 indicating that star-shaped β -CD-based carriers that incorporated equal ratios (50/50) of HMA and DMAEMA monomers were more effective in delivering the RNA cargo into HeLa cells compared to those with higher HMA content. The lack of GAPDH knockdown observed with P6 and P8 particles can be a result of poor particle solubility in culture medium whereas the non-specific GAPDH knockdown exhibited by P5 and P7 is a result of the high positive surface charge density resulting in cell death. Results show that P1 is the most efficient formulation indicated by the $73 \pm 1.4\%$ reduction in GAPDH protein expression observed upon incubation with P1 particles loaded with (+) anti-GAPDH siRNA compared to those loaded with (-) the scrambled siRNA sequence (**Figure 5.6**). Comparing GAPDH knockdown observed upon incubation of HeLa cells with P1 particles to that observed with P3 particles shows the effect of increasing the molecular weight of P(HMA-*co*-**D**MAEMA-*co*-**T**MAEMA)

grafts from 25 kDa (P1) to 40 kDa (P3). Results show that P3 particles were partially toxic to HeLa cells indicated by the reduction in GAPDH protein expression upon treatment with (-) the scrambled siRNA sequence. Specifically, P3 particles loaded with (+) anti-GAPDH siRNA produced $30 \pm 2.5\%$ knockdown in GAPDH expression compared to the $73 \pm 1.4\%$ reduction observed with P1 particles. These results clearly show that β -CD polymers

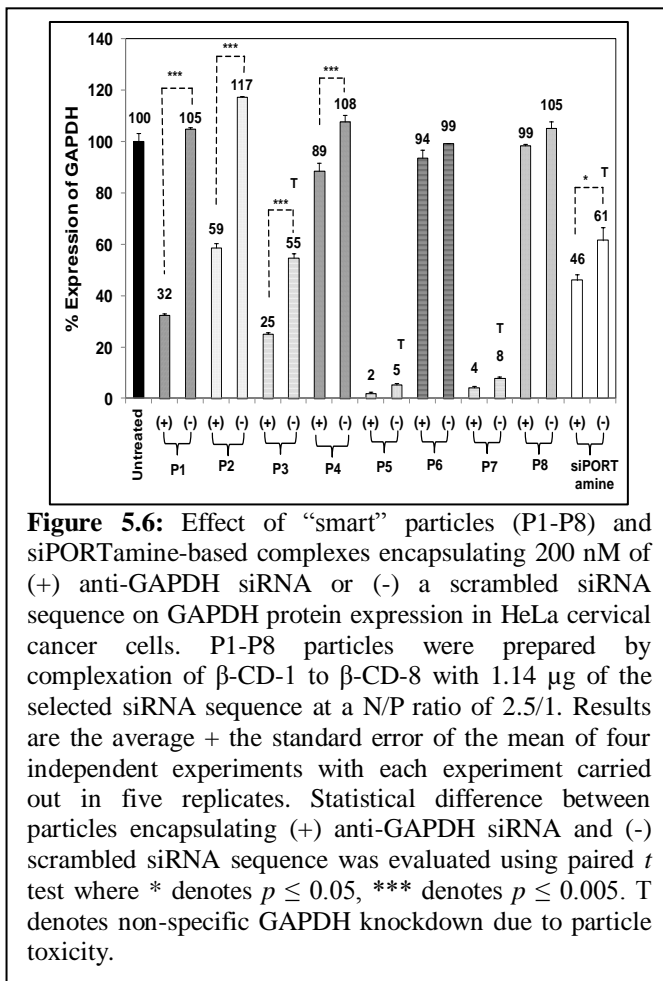


Figure 5.6: Effect of “smart” particles (P1-P8) and siPORTamine-based complexes encapsulating 200 nM of (+) anti-GAPDH siRNA or (-) a scrambled siRNA sequence on GAPDH protein expression in HeLa cervical cancer cells. P1-P8 particles were prepared by complexation of β -CD-1 to β -CD-8 with 1.14 μ g of the selected siRNA sequence at a N/P ratio of 2.5/1. Results are the average \pm the standard error of the mean of four independent experiments with each experiment carried out in five replicates. Statistical difference between particles encapsulating (+) anti-GAPDH siRNA and (-) scrambled siRNA sequence was evaluated using paired *t* test where * denotes $p \leq 0.05$, *** denotes $p \leq 0.005$. T denotes non-specific GAPDH knockdown due to particle toxicity.

incorporating P(HMA-*co*-DMAEMA-*co*-TMAEMA) grafts with an average molecular weight of ~ 25 kDa are more efficient than longer grafts in delivery of functional siRNA into HeLa cancer cells (**Figure 5.6**). These findings are supported by recently published results showing that 3- and 5-arm branched PDMAEMA polymers exhibit measurable transfection of CHO-K1 cells at an average molecular weight ≥ 20 kDa.⁴¹ However, PDMAEMA carriers with much higher molecular weight exhibited high cellular toxicity that diminished their transfection efficiency.⁴¹

Comparing between GAPDH knockdown observed upon incubation of HeLa cells with P1 and P2 particles shows the contribution of the buffering capacity of DMAEMA

monomers to the endosomal escape and transfection efficiency of P1 particles. Specifically, P1 particles are formulated using β -CD-1 polymer with 69% of the DMAEMA monomers converted to cationic TMAEMA, which leaves 31% of the DMAEMA monomers ($pK_a = 7.5$) to exhibit their buffering capacity at acidic endosomal pH. Whereas, P2 particles are formulated using β -CD-2 polymer with 100% of DMAEMA monomers transformed to cationic TMAEMA (i.e. no endosomal buffering capacity). Results show that P2 particles loaded with (+) anti-GAPDH siRNA produce $58 \pm 2.3\%$ knockdown in GAPDH protein expression compared to $73 \pm 1.4\%$ GAPDH knockdown observed with P1 particles (**Figure 5.6**). Similarly, P4 particles (100% of DMAEMA monomers transformed to cationic TMAEMA) loaded with anti-GAPDH siRNA caused $19 \pm 5.6\%$ reduction in GAPDH expression compared to $30 \pm 2.5\%$ observed with P3 particles (only 55% of DMAEMA monomers transformed to cationic TMAEMA leaving 45% of DMAEMA monomers with endosomal buffering capacity) (**Figure 5.6**). Given that P1, P2, P3, and P4 particles exhibit similar uptake by HeLa cancer cells (**Figure 5.5**), higher GAPDH knockdown observed with P1 and P3 particles compared to P2 and P4 particles can be attributed to the endosomal buffering capacity of DMAEMA monomers, which results in endosomal burst and enhanced release of the loaded siRNA into the cytoplasm. These results are supported by earlier reports showing the enhanced endosomal escape of PDMAEMA through their endosomal buffering capacity.²⁴ It is important to note that siPORT amine-based complexes produced only $15 \pm 7.2\%$ reduction in GAPDH protein expression and it was associated with significant toxicity indicated by GAPDH knockdown upon incubation with siPORT amine-based complexes loaded with the scrambled siRNA sequence (**Figure 5.6**).

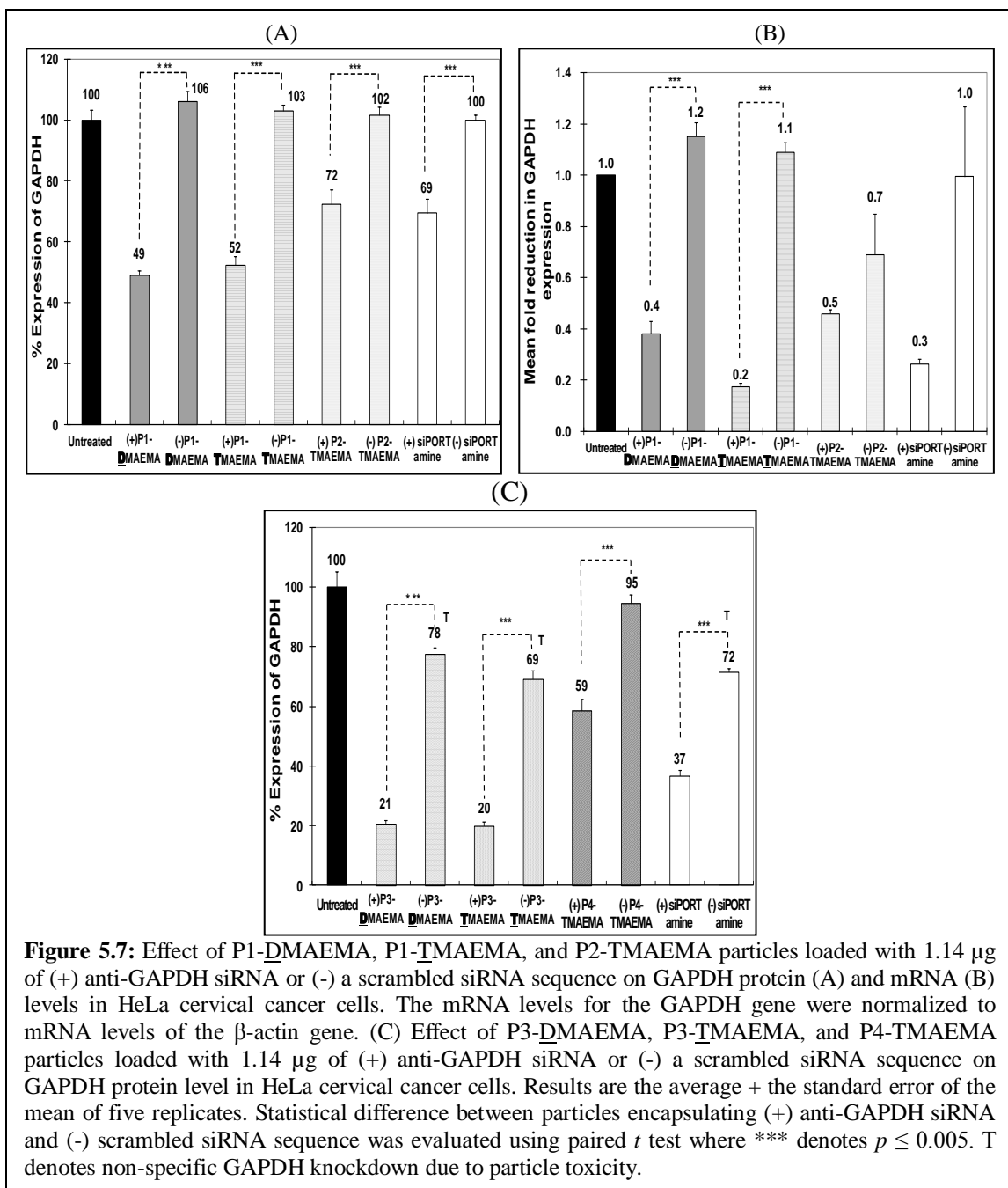
5.3.6 Contribution of DMAEMA monomers to carrier's transfection capacity

The amount of cationic quaternary amine groups (TMAEMA) needed to complex 1.14 μg of anti-GAPDH siRNA at N/P ratio of 2.5/1 is 4.62×10^{-8} moles. We used the number of TMAEMA monomers present in each β -CD polymer to calculate the amount of polymer needed to complex the same dose (1.14 μg) of anti-GAPDH siRNA at N/P ratio of 2.5/1. Given that β -CD-1 polymer has only 58 TMAEMA units/graft compared to 84 TMAEMA units/graft in β -CD-2 polymer (**Table 5.1**), we used a higher amount of β -CD-1 (27 μg) than β -CD-2 (21 μg) to complex the same amount (1.14 μg) of anti-GAPDH siRNA at N/P ratio of 2.5/1. We investigated whether the observed higher activity of P1 particles in reducing GAPDH protein expression compared to P2 particles is a result of the higher amount of β -CD-1 polymer used to complex the anti-GAPDH siRNA or the higher number of DMAEMA monomers/graft, which enhances the endosomal escape of the formed particles through their established endosomal buffering capacity. Specifically, we mixed 27 μg of β -CD-1 and 21 μg of β -CD-2 polymers with 1.14 μg of (+) anti-GAPDH siRNA or (-) the scrambled sequence to prepare P1-TMAEMA and P2-TMAEMA particles at N/P ratio of 2.5/1 based on the number of cationic TMAEMA monomers present in each carrier. We also mixed 21 μg of β -CD-1 polymer with 1.14 μg of (+) anti-GAPDH siRNA or (-) the scrambled sequence to prepare P1-DMAEMA particles based on the number of DMAEMA monomers present in the β -CD-1 carrier. We evaluated the effect of P1-DMAEMA, P1-TMAEMA, and P2-TMAEMA particles on GAPDH expression in HeLa cervical cancer cells compared to commercial siPORT amine-based complexes (**Figure 5.7**).

Results show that P1-TMAEMA and P1-DMAEMA particles produce a similar knockdown in GAPDH protein expression by $57 \pm 4.6\%$ and $51 \pm 4.7\%$, respectively (**Figure 5.7A**). Similarly, P1-TMAEMA and P1-DMAEMA particles reduced the levels of GAPDH mRNA by $80 \pm 10.0\%$ and $90 \pm 5.0\%$, respectively (Figure 5.7B). The fact that P1-TMAEMA particles with higher carrier content (27 μg of $\beta\text{-CD-1}$) did not show higher activity compared to P1-DMAEMA particles (21 μg of $\beta\text{-CD-1}$) indicates that the amount of $\beta\text{-CD-1}$ polymer does not play a significant role in the observed activity of P1 particles. In comparison, P2-TMAEMA particles reduced the levels of GAPDH protein and mRNA by only $30 \pm 7.0\%$ and $23 \pm 17.7\%$, respectively (**Figure 5.7A & B**). Therefore, the observed low GAPDH knockdown by P2-TMAEMA particles compared to P1-DMAEMA and P1-TMAEMA particles is due to the residual DMAEMA monomers (26 monomers/graft) present in the $\beta\text{-CD-1}$ carrier that exhibit an appreciable endosomal buffering capacity²⁴ leading to endosomal swelling and burst, which further enhances the cytoplasmic delivery of the loaded anti-GAPDH siRNA molecules.

We confirmed the contribution of DMAEMA monomers to the enhanced endosomal escape of P3 particles by comparing GAPDH knockdown by P3-DMAEMA and P3-TMAEMA particles to GAPDH knockdown observed with P4-TMAEMA particles (**Figure 5.7C**). Results show that P3-DMAEMA and P3-TMAEMA particles caused a similar knockdown of GAPDH protein expression by $49 \pm 4.3\%$ and $57 \pm 3.2\%$, respectively, which further confirms that the amount of $\beta\text{-CD-3}$ polymer used to prepare different particles at N/P ratio of 2.5/1 does not contribute to the observed activity. In comparison, P4-TMAEMA particles reduced GAPDH protein expression by $36 \pm 6.7\%$, which is less than the observed knockdown with both P3-DMAEMA and P3-TMAEMA

particles. These results collectively show that β -CD-1 and β -CD-3 polymers with partially quaternized (50%) DMAEMA monomers exhibit more efficient cytoplasmic delivery of the complexed siRNA molecules compared to their fully quaternized counterparts (β -CD-2 and β -CD-4 polymers), which is a result of the synergistic combination of DMAEMA endosomal buffering capacity with HMA membrane-destabilizing effect on the same membrane-active P(HMA-*co*-DMAEMA-*co*-TMAEMA) grafts.



5.3.7 Cellular uptake and activity of P1/P2 particles in MCF-10A and UM-SCC-17B cells

Results show that P1 and P2 particles prepared by complexation of β -CD-1 and β -CD-2 polymers with anti-GAPDH siRNA at N/P ratio of 2.5/1 are efficiently internalized by

HeLa cervical cancer cells (**Figure 5.5**) and achieve robust knockdown of GAPDH expression at the mRNA and protein levels (**Figure 5.7**). We investigated the uptake of P1 and P2 particles loaded with anti-GAPDH siRNA into normal human mammary epithelial cells (MCF-10A) and head and neck squamous cell carcinoma (UMSCC-17B) and the associated knockdown in GAPDH expression to confirm the utility of these “smart” particles in multiple cell lines. Results show that “smart” P1 and P2 particles are internalized by 98-100% of MCF-10A cells at N/P ratios of 1.5/1 and 2.5/1, which drops to 76-83% of the cells upon incubation with the particles prepared at higher 4/1 N/P ratio (**Figure 5.8A**). In comparison, 93-100% of UM-SCC-17B cells internalized P1 and P2 particles prepared at N/P ratios of 1.5/1, 2.5/1, and 4/1 (**Figure 5.8B**).

We investigated the effect of “smart” P1 and P2 particles prepared by complexation of β -CD-1 and β -CD-2 polymers with (+) anti-GAPDH siRNA and (-) scrambled siRNA sequence at N/P ratio of 2.5/1 using the same polymer amounts listed in section 2.5 on GAPDH expression in MCF-10A and UM-SCC-17B cells. In MCF-10A cell, P1 and P2 particles reduced GAPDH protein levels by $31 \pm 4.6\%$ and $25 \pm 11.2\%$, respectively (**Figure 5.8C**). P1 and P2 particles loaded with anti-GAPDH siRNA reduced GAPDH mRNA levels by $50 \pm 18\%$, and $50 \pm 38\%$, respectively (**Figure 5.8E**). In UM-SCC-17B cancer cells, P1 and P2 particles loaded with anti-GAPDH siRNA caused a similar reduction in GAPDH protein expression by $21 \pm 4.3\%$ and $30 \pm 6.9\%$, respectively (**Figure 5.8D**). However, qRT-PCR results show that only P1 particles reduced GAPDH mRNA levels by $40 \pm 14\%$ while P2 particles did not affect GAPDH mRNA level (**Figure 5.8F**).

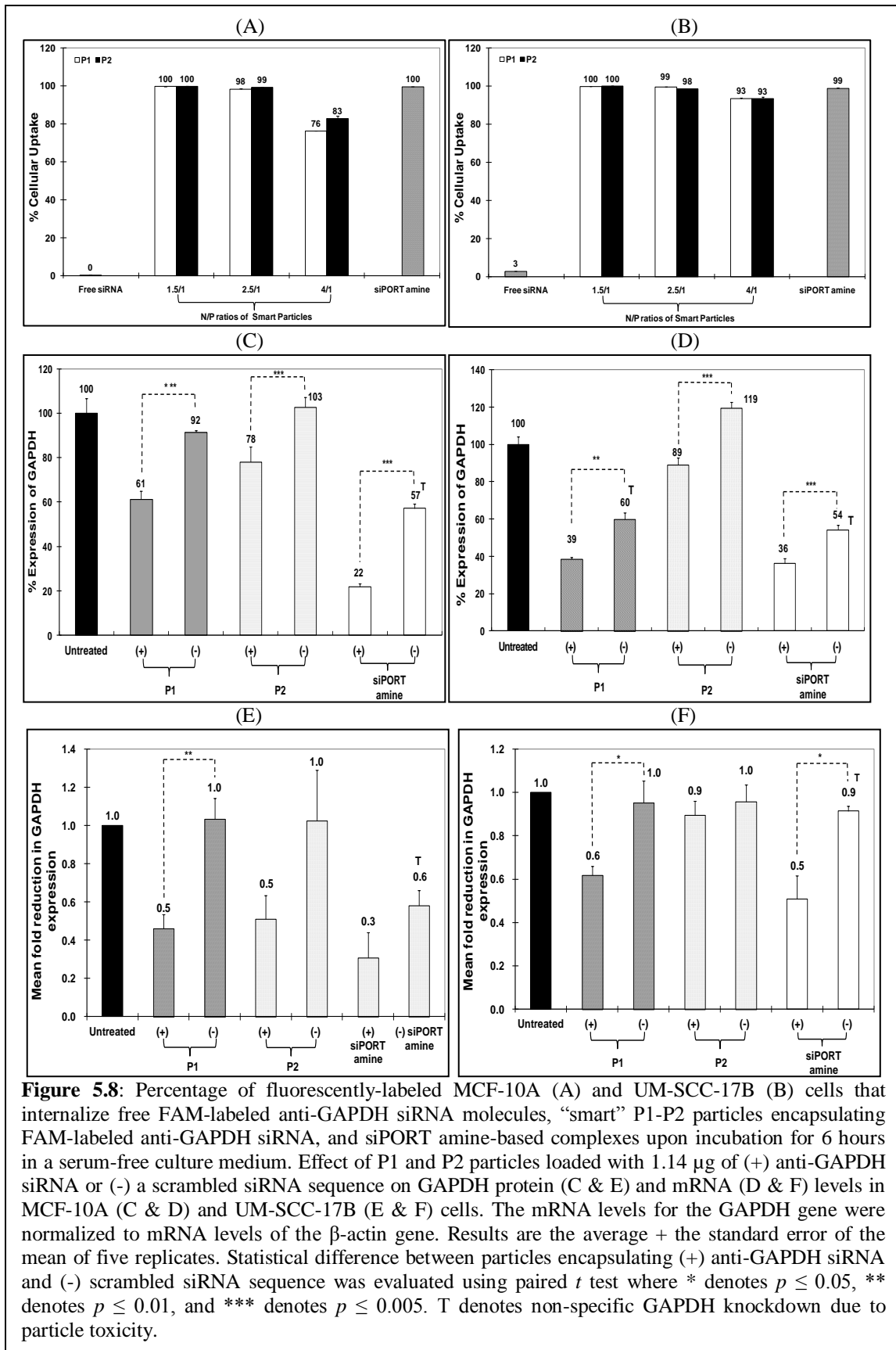


Figure 5.8: Percentage of fluorescently-labeled MCF-10A (A) and UM-SCC-17B (B) cells that internalize free FAM-labeled anti-GAPDH siRNA molecules, “smart” P1-P2 particles encapsulating FAM-labeled anti-GAPDH siRNA, and siPORT amine-based complexes upon incubation for 6 hours in a serum-free culture medium. Effect of P1 and P2 particles loaded with 1.14 μg of (+) anti-GAPDH siRNA or (-) a scrambled siRNA sequence on GAPDH protein (C & E) and mRNA (D & F) levels in MCF-10A (C & D) and UM-SCC-17B (E & F) cells. The mRNA levels for the GAPDH gene were normalized to mRNA levels of the β -actin gene. Results are the average + the standard error of the mean of five replicates. Statistical difference between particles encapsulating (+) anti-GAPDH siRNA and (-) scrambled siRNA sequence was evaluated using paired *t* test where * denotes $p \leq 0.05$, ** denotes $p \leq 0.01$, and *** denotes $p \leq 0.005$. T denotes non-specific GAPDH knockdown due to particle toxicity.

The observed difference in GAPDH knockdown induced by P1 and P2 particles loaded with anti-GAPDH siRNA in HeLa, MCF-10, and UM-SCC-17B cells can be explained by the difference in intracellular pH between these cells lines. The literature shows that normal cells generally have neutral cytosolic pH (7.2) and acidic endosomal (pH 6.0) and lysosomal (pH 5.0) environment.⁴² Whereas, many tumor cells have an acidified cytosol and more alkaline endosomes/lysosomes with both pH values is around 6.7.⁴² Although the reason for alkalization of the endosomal and lysosomal compartments remains elusive, the elevated organelle pH in tumor cells has been confirmed in many reports^{42b,43} and proved to dramatically reduce the transfection efficiency of non-viral vectors in tumor cells.⁴⁴ Similarly, low GAPDH knockdown in UM-SCC-17B cancer cells can be attributed to endosomal alkalization, which will reduce the hydrolysis of the hydrazone linkages connecting the membrane-active P(HMA-*co*-DMAEMA-*co*-TMAEMA) grafts to the β -CD core. Incomplete release of P(HMA-*co*-DMAEMA-*co*-TMAEMA) grafts will reduce the net disruption of the endosomal membrane, which will limit the delivery of the loaded anti-GAPDH siRNA into the cytoplasm and diminish the associated GAPDH knockdown. This explains lower GAPDH knockdown observed with P1 ($21 \pm 4.3\%$) in UM-SCC-17B cancer cells compared to that observed ($31 \pm 4.6\%$) with normal MCF-10A mammary epithelial cells. These results show that type of targeted cells can influence the transfection efficiency of “smart” star-shaped β -CD carriers. Nevertheless, our results collectively show the ability of β -CD-1 polymers to complex siRNA at low N/P ratio and achieve efficient functional delivery of the loaded cargo into the cytoplasm of different cells.

5.4 Conclusions

In summary, we used FDA-approved, water-soluble, cone-shaped β -CD to prepare a series (β -CD-1 to β -CD-8) of degradable, pH-sensitive, star-shaped polymers and evaluated their ability to deliver anti-GAPDH siRNA past the endosomal membrane and into the cytoplasm of multiple epithelial cell lines. Using ATRP, we grafted P(HMA-*co*-DMAEMA) copolymers from the secondary face of the β -CD core via acid-labile hydrazone linkages. We varied the molecular weight (25 and 40 kDa), molar ratio of HMA/DMAEMA monomers (50/50 and 75/25), and degree of quaternization (50% and 100%) of DMAEMA monomers into cationic TMAEMA to systematically investigate the effect of these parameters on siRNA condensation into “smart” particles and the associated transfection efficiency. Results show that β -CD polymers incorporating 50% DMAEMA monomers/graft complex the loaded siRNA at low N/P (+/-) ratios of 1.5/1 and 2.5/1 whereas the β -CD polymers with lower DMAEMA content form their complexes at a 4/1 N/P ratio. The average sizes of “smart” P1-P8 particles was < 200 nm and have a net positive surface charge, which suggest their ability to diffuse from the systemic circulation into tumor’s interstitial space followed by efficient cell uptake via endocytosis when administered *in vivo*. Results show that β -CD polymers with 25 kDa P(HMA-*co*-DMAEMA) grafts are more efficient in delivering the siRNA cargo compared to those with longer (40 kDa) grafts while exhibiting no cytotoxicity. Increasing the mole fraction of hydrophobic HMA monomers to 75% of the graft reduced aqueous solubility and transfection efficiency of the β -CD carriers compared to those with lower HMA content (50%/graft). Transforming 100% of DMAEMA monomers to cationic TMAEMA enhanced the condensation of the loading siRNA molecules.

However, combining the endosomal buffering capacity of DMAEMA monomers with the hydrophobic disruptive effect of HMA units in a single membrane-active P(HMA-*co*-DMAEMA-*co*-TMAEMA) graft proved to increase the efficiency of “smart” P1 and P3 particles by enhancing their endosomal escape. These results provide a clear description of key structural features necessary for development of efficient β -CD star-shaped carriers for siRNA delivery. Further, it establishes β -CD-1 polymer as a robust vector for enhanced cytoplasmic delivery of siRNA.

Acknowledgements

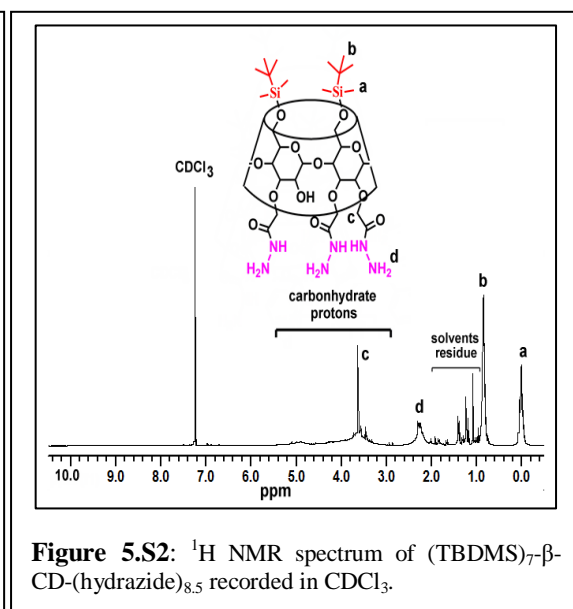
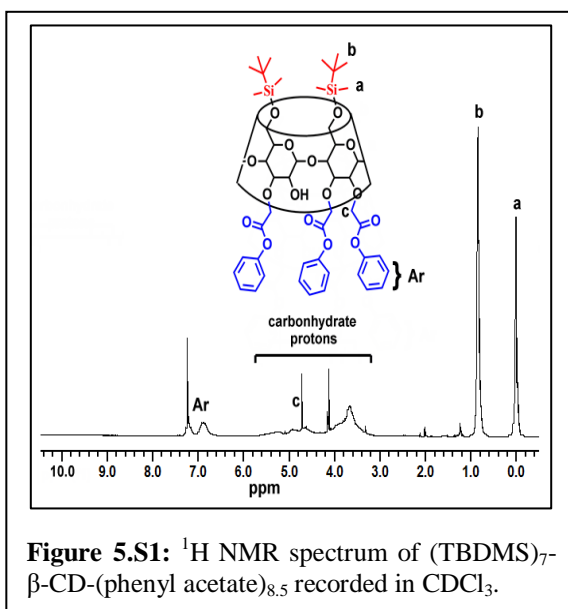
This research is partially funded by Susan G. Komen Breast Cancer Foundation.

Supplementary Information

S1. Synthesis of “Smart” β -CD-Based Vectors

We successfully utilized the asymmetric distribution of primary hydroxyl groups on the primary face and secondary hydroxyl groups on the secondary face of the β -CD core to graft amphiphilic P(HMA-*co*-DMAEMA) polymers from the secondary face via acid-labile hydrazone linkages using ATRP. As shown in **Scheme 5.S1**, we used *tert*-butyldimethylsilyl chloride (TBDMSCl) to cap 96% of the primary hydroxyl groups forming (TBDMS)₇- β -CD (compound **2**), which allowed us to selectively modify the secondary hydroxyl groups in subsequent reactions. The average number of secondary hydroxyl groups that reacted with phenyl acetate was 8.5 yielding (TBDMS)₇- β -CD-(phenyl acetate)_{8.5} (compound **3**), which was completely (100%) transformed to the corresponding acyl hydrazide (TBDMS)₇- β -CD-(hydrazide)_{8.5} (compound **4**). We utilized the aromatic protons of the phenyl groups to quantitatively confirm the formation of the phenyl acetate ester and subsequent transformation to the acyl hydrazide based on

the ^1H NMR spectra (**Figures 5.S1 and 5.S2**). We reacted $(\text{TBDMS})_7\text{-}\beta\text{-CD-}(\text{hydrazide})_{8,5}$ (compound **4**) with 2-bromo-2-methyl-propionic acid-4-formyl-phenyl ester (compound **5**) to introduce the initiation sites for ATRP conjugated via acid-labile hydrazone linkages to the $\beta\text{-CD}$ secondary face following published protocols^{13,45}. By comparing the ratio between TBDMS and the aromatic protons in the $(\text{TBDMS})_7\text{-}\beta\text{-CD-}(\text{hydrazone-Br})_{4,8}$ (compound **6**), we confirmed the conjugation of 4.8 ATRP initiation sites (**Figure 5.S3**), which is sufficient for grafting the desired number of cationic groups for condensation of a large dose of siRNA molecules without causing undesirable gelation of the formed star polymers at higher grafting densities.



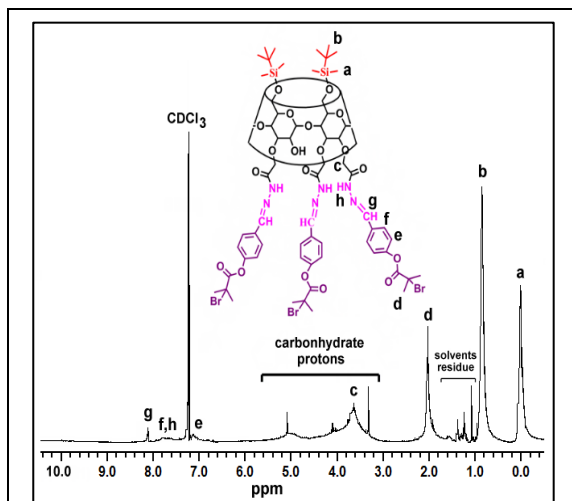
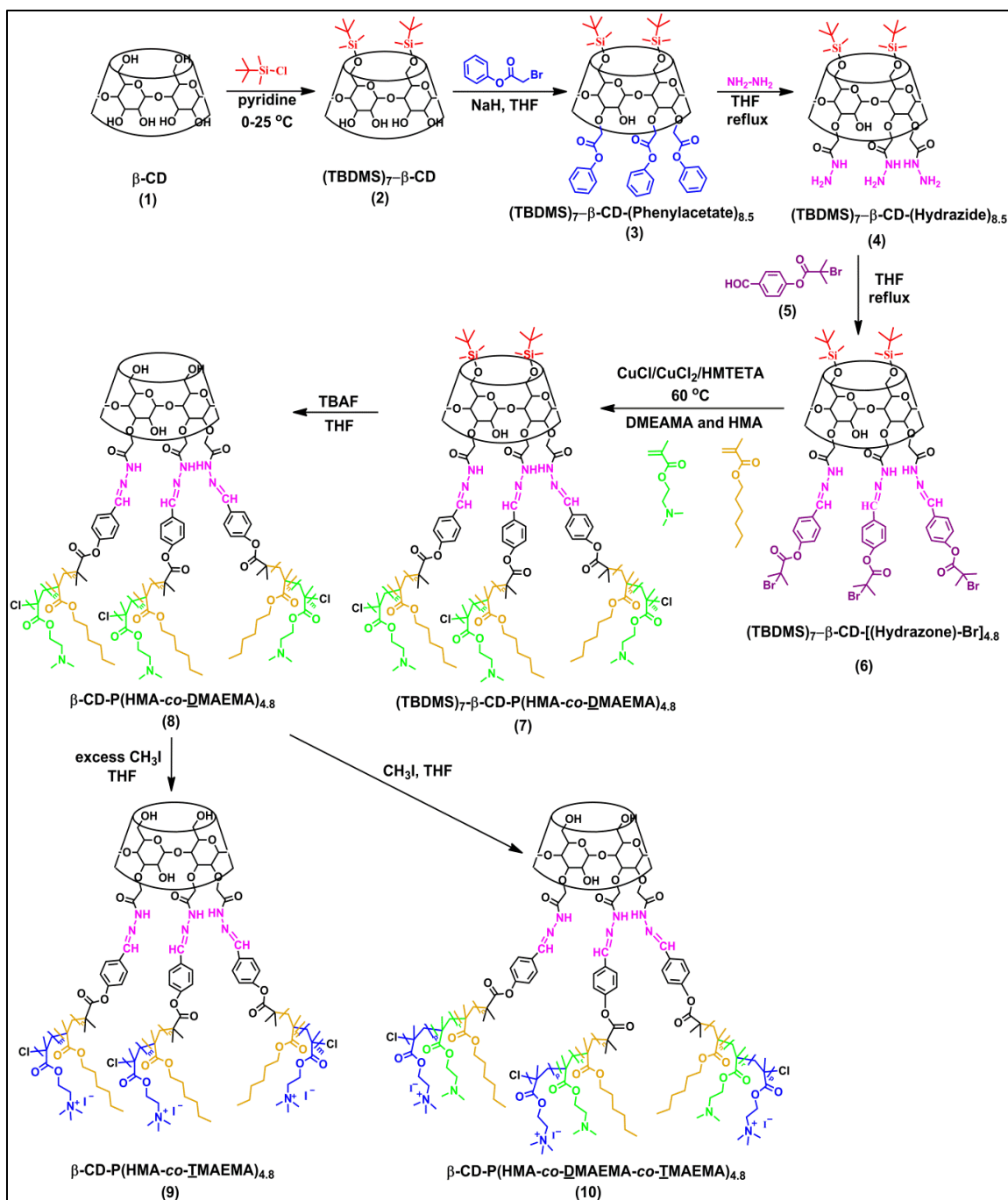


Figure 5.S3: ¹H NMR spectrum of (TBDMS)₇-β-CD-(hydrazone-Br)_{4,8} recorded in CDCl₃.



Scheme 5.S1: Protocol for synthesis of β -CD-P(HMA-co-IMAEMA)_{4.8} and β -CD-P(HMA-co-DMAEMA-co-IMAEMA)_{4.8} polymers.

We used (TBDMS)₇-β-CD-(hydrazone-Br)_{4,8} (Compound **6**) as a macroinitiator for copolymerization of HMA and DMAEMA monomers using the CuCl/CuCl₂/HMATETA catalytic system in anisole or tetrahydrofuran at 60 °C, which yielded (TBDMS)₇-β-CD-P(HMA-*co*-DMAEMA)_{4,8} (compound **7**) star polymers with two different graft compositions (HMA/DMAEMA ratio of 50/50 or 75/25) and degree of polymerization (molecular weight of 25 kDa or 40 kDa) (**Table 5.S1**). Details of the polymerization reactions are listed in **Table 5.S1** and graft composition was confirmed based on the corresponding ¹H NMR spectrum (**Figure 5.S4A**). The number average molecular weight and the number of HMA and DMAEMA units in the each graft were calculated based on the ratio between the aromatic protons inserted in the initiating group and the methylene protons of each monomer located next the ester and amine groups of the HMA and DMAEMA monomers, respectively (**Table 5.1**). We analyzed the molecular weight and molecular weight distribution for all star polymers using gel permeation chromatograph. Results show that all the synthesized star polymers exhibit narrow molecular weight distribution (**Figure 5.S5 & Table 5.S1**). However, given the established interaction between DMAEMA monomers and the packing material of GPC columns ²⁹ and difference in topography between star-shaped and the linear polymers, we used the number average molecular weight obtained from the ¹H NMR spectra in all subsequent calculations in this research.

Table 5.S1: Copolymerization of HMA and DMAEMA monomers from β -Cyclodextrin macroinitiator using ATRP

Polymer Code	[M]/[I][CuCl]₂/[CuCl₂]/[HMTETA]^a	Time (h)	Copolymer Composition,% (HMA/DMAEMA)^d	Conversion (%)^a	<i>M</i>_{ntheo} of each arm^e (g/mol)	<i>M</i>_{nNMR} of each arm^d (g/mol)	<i>M</i>_w/<i>M</i>_n^f
β-CD-1&2	200/1/0.8/0.2/1 ^a	47	47:53	70	23170	25580	1.45
β-CD-3&4	600/1/0.8/0.2/1 ^c	45	49:51	39	38310	40750	1.75
β-CD-5	200/1/0.8/0.2/1 ^a	48	76:24	44	14670	25050	1.13
β-CD-6	200/1/0.8/0.2/1 ^b	48	74:26	53	17800	24930	1.17
β-CD-7&8	600/1/0.8/0.2/1 ^c	50	76:24	25	25850	41200	1.25

^a1,1,4,7,10,10-Hexamethyltriethylenetetramine and (TBDMS)₇- β -CD-(hydrazone-Br)_{4,8} were used as ligand and initiator, respectively.

^bPolymerization was performed in THF.

^cPolymerization was performed in Anisole.

^dCalculated by using ¹H NMR spectra.

^eDetermined gravimetrically.

^fDetermined from GPC measurements based on methyl methacrylate standard. *M*_n is the number average molecular weight and *M*_w is the weight average molecular weight.

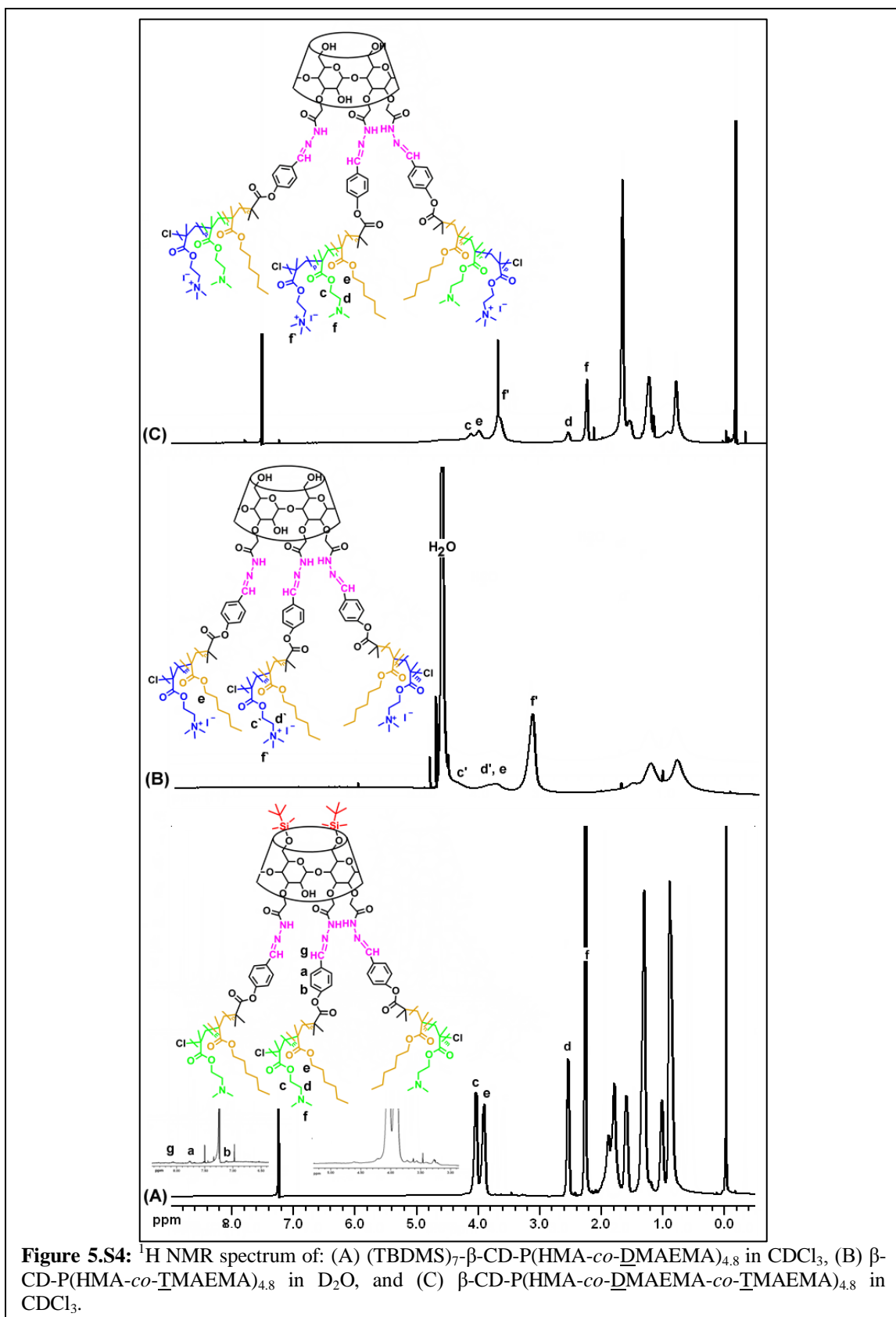
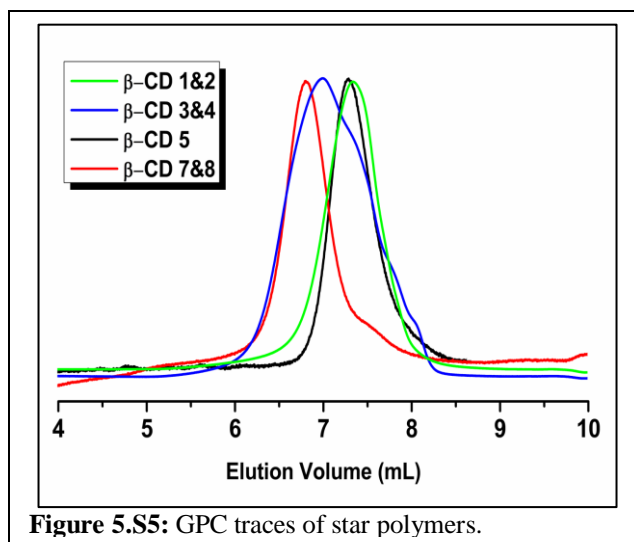


Figure 5.S4: ^1H NMR spectrum of: (A) $(\text{TBDMS})_7\text{-}\beta\text{-CD-P(HMA-co-DMAEMA)}_{4.8}$ in CDCl_3 , (B) $\beta\text{-CD-P(HMA-co-TMAEMA)}_{4.8}$ in D_2O , and (C) $\beta\text{-CD-P(HMA-co-DMAEMA-co-TMAEMA)}_{4.8}$ in CDCl_3 .



The TBDMS protecting groups were removed to yield β -CD-P(HMA-*co*-DMAEMA)_{4,8} (compound **8**) star polymers before partial (50%) or complete (100%) quaternization of the DMAEMA monomers into trimethyl aminoethyl methacrylate (TMAEMA) monomers using methylene iodide to obtain β -CD-P(HMA-*co*-TMAEMA)_{4,8} (compound **9**) and β -CD-P(HMA-*co*-DMAEMA-*co*-TMAEMA)_{4,8} (compound **10**) polymers. As shown in **Figure 5. S4B and S4C**, we used the ratio between the methyl protons of the DMAEMA monomers at 2.26 ppm and those of the TMAEMA monomers at 3.61 ppm to calculate the % of DMAEMA quaternization in different star polymers (**Table 5.1**).

S1.1 Materials

β -Cyclodextrin (β -CD) (Aldrich, 98 %) was freeze-dried before use. Dimethylamino ethyl methacrylate (DMAEMA) (Aldrich, 98 %) and hexyl methacrylate (HMA) (Aldrich, 98 %) were passed through basic alumina column to remove the associated inhibitor before use. 1,1,4,7,10,10-Hexamethyltriethylenetetramine (HMTETA) ligand (Aldrich, 97 %) was distilled before use. 2-Bromo-2-methyl-propionic acid 4-formyl-phenyl ester (Ald-Br) was synthesized following a published protocol ⁴⁶. Copper (I) chloride (CuCl)

(Aldrich, 99.9 %), copper (II) chloride (CuCl_2) (Aldrich, 99.9%), *tert*-butyldimethylsilyl chloride (TBDMS) (Aldrich, 97%), bromophenyl acetate (Aldrich, 98%), sodium hydride (NaH) (Aldrich, 60% dispersion in mineral oil), hydrazine anhydrous (Aldrich, 98%), pyridine anhydrous (Aldrich, 98%), 2-bromoisobutyryl bromide (Fluka, > 97%), tetrabutylammonium fluoride 1.0 M solution in tetrahydrofuran (TBAF) (Aldrich), iodomethane (Aldrich, 99%), anisole anhydrous (Aldrich, 99.7 %), tetrahydrofuran anhydrous (THF) (Aldrich, > 99.9 %) were used as received.

S1.2 Characterization

^1H NMR and ^{13}C NMR spectra of 5–10 % (w/w) solutions in CDCl_3 or D_2O with $\text{Si}(\text{CH}_3)_4$ as an internal standard were recorded using 400 MHz and 500 MHz Varian Mercury system (Palo Alto, CA) at room temperature, respectively. Gel permeation chromatography (GPC) analyses were done using a Viscotek GPCmax Autosampler system equipped with a Water 2414 refractive index (RI) detector. The molecular weight and molecular weight distribution of final polymers were determined based on their elution volume on an Styragel HR 4E column compared to a series of poly(methyl methacrylate) standards (PolyAnalytik Inc, Canada) using THF containing 5 % TEA as a mobile phase at a flow rate of 1 mL/min at 35 °C. Data were analyzed using Viscotek OmniSEC Omni-01 software. Fragmentation of star polymers in acidic solution was evaluated by dissolving 2 mg of each star polymer in 1 mL phosphate-buffered saline (PBS) with pH 5.8 and incubating at 37 °C for 8 hours while shaking. A 100 μL sample was drawn by the autosampler from polymer solution at 1, 2, 4, and 8 hours for GPC analysis using a Styragel HR 3, 4 and 5 DMF column system connected in series. DMF was used as an eluent at flow rate of 0.8 mL min^{-1} at 50°C for this fragmentation study.

The areas under the curve for the peaks corresponding to the star polymer were used to quantify the amount of degraded polymer at a given time point to determine the hydrolysis rate of the hydrazone linkages connecting the polymer grafts to the secondary face of the β -CD core. FT-IR spectra were recorded on a Jasco FT-IR Spectrum 4100 type A.

S1.3 Synthesis of (TBDMS)₇- β -CD-(hydrazone-Br)_{4,8} Macroinitiator

S1.3.1 Synthesis of (TBDMS)₇- β -CD

The primary OH groups of β -CD (**1**) were capped using *tert*-butyldimethylsilyl groups to yield compound (TBDMS)₇- β -CD (**2**) following published protocols⁴⁷. Briefly, β -CD (2.8 g, 2.46 mmol) was dissolved by vigorous stirring in dry pyridine (30 mL) followed by cooling the solution on an ice bath to produce a thick gel. Dry *tert*-butyldimethylsilyl chloride (TBDMSCl) (3.0 g, 20 mmol) was dissolved in dry pyridine (20 mL) and added dropwise by a syringe to the cooled reaction vessel containing β -CD over 30 minutes, which liquefied the β -CD gel. The reaction vessel was kept in an ice bath for 3 hours before allowing it to warm up to room temperature while stirring overnight (18 h). The reaction mixture was poured into ice-cold water (500 mL) and stirred vigorously for 10 minutes to precipitate the crude product, which was filtered off, washed with ice-cold water, and dissolved in ethyl acetate (70 mL). The ethyl acetate solution was washed with 5% aqueous HCl solution (3 times x 50 mL), saturated aqueous NaHCO₃ solution (50 mL), and saturated brine (50 mL) before drying the solution using anhydrous Na₂SO₄, filtering, and concentrating to get a white solid. The solid product was purified by flash chromatography on silica gel using a gradient mobile phase composed of 9/1 ethyl acetate/hexane followed by 18/1.9/0.1 dichloromethane/methanol/water to yield 3 g of

compound (**2**) with 96 % of the primary OH capped with TBDMS group. ^1H NMR (400 MHz, CDCl_3): $\delta_{\text{H}}=$ 0.02 (s, 21H, Si- CH_3), 0.03 (s, 21H, Si- CH_3), 0.86 (s, 63H, C-(CH_3) $_3$), 3.55 (dd, $J=8.8, 9.2$, 7H, H-6a), 3.60 (bs, 7H, H-2), 3.64 (dd, $J=4, 9.6$, 7H, H-5), 3.71 (bd, $J=10.8$, 7H, H-3), 3.90 (dd, $J=2.8, 11.2$, 7H, H-6b), 4.00-4.05 (dd, $J=8.8, 9.6$, 7H, H-4), 4.88 (d, $J=3.6$ 7H, H-1), 5.26 (s, 7H, OH), 6.73 (s, 7H, OH). ^{13}C NMR (125 MHz, CDCl_3): $\delta_{\text{C}}=$ -5.2, - 5.1, 18.2, 25.9, 61.6, 72.5, 73.4, 73.6, 81.8, 102.0. FT-IR (cm^{-1}): 3323, 2951-2855, 1565, 1465, 1367, 1251, 1151, 1032, 961, 829, 771. EIMS m/z $[\text{M}+\text{H}]^+$ calculated for $\text{C}_{84}\text{H}_{168}\text{O}_{35}\text{Si}_7$ is 1934.8, found 1935.7.

S1.3.2 Etherification of Secondary Hydroxyl Groups

(TBDMS) $_7$ - β -CD (**2**) (3.0 g, 1.55 mmol) was dissolved in dry THF (60 mL) and added to sodium hydride (NaH) (2.16 g washed with hexane, 54.24 mmol) while cooling the reaction flask in an ice bath. Once the evolution of H_2 subsided, phenyl bromoacetate (12.30 g, 48.48 mmol) was added to the reaction mixture in an ice bath under N_2 atmosphere and the reaction mixture was kept 1 more hour in an ice bath. After 16 h, the reaction mixture was cooled on an ice bath followed by dropwise addition of methanol to inactivate excess NaH followed by removal of solvents under reduced pressure to yield a solid residue. The residue was suspended in CH_2Cl_2 and washed with H_2O followed by saturated aqueous NaCl solution. The CH_2Cl_2 layer was recovered and evaporated to dryness to yield brown oil, which was purified by column chromatography starting with 1/4 ethyl acetate/hexane solvent mixture followed by 18/2 dichloromethane/methanol mixture to yield 1.96 g of (TBDMS) $_7$ - β -CD-(phenyl acetate) $_{8.5}$ (compound **3**) (54% conversion). ^1H NMR (400 MHz, CDCl_3): $\delta_{\text{H}}=$ -0.04 (s, 42H, Si- CH_3), 0.89 (s, 63H, C-(CH_3) $_3$), 3.57-4.06 (bm, 42H, H-2, H-3, H-4, H-5, H-6a, H-6b), 4.73 (s, 17H, OCH_2CO),

4.45-4.90 (b, 7H, H-1), 5.33 (s, OH), 6.83-7.40 (b, 42.5H, aromatic protons). ^{13}C NMR (125 MHz, CDCl_3): $\delta_{\text{C}}=-5.01, 18.1, 25.9, 57.3, 61.6, 72.2, 72.9, 73.0, 75.6, 97.5, 114.5, 121.7, 129.5, 151.2, 157.7$. FT-IR (cm^{-1}): 2997, 2980, 2926, 2851, 1745, 1590, 1492, 1251, 1158, 1079, 1032, 833, 750.

S1.3.3 Incorporation of Acid-Labile Hydrazine Groups

(TBDMS) $_7$ - β -CD-(phenyl acetate) $_{8.5}$ (**3**) (1.96 g, 7.75×10^{-4} mol containing 6.59×10^{-3} moles of ester unit) was dissolved in THF (80 mL). Hydrazine (2.06 mL, 6.59×10^{-2} mol) was added to reaction mixture and refluxed at 65 °C for 36 h before removing the THF. The residual solid was dissolved in CH_2Cl_2 and extracted with 2.5% NaOH solution and the organic layer was dried to separate (TBDMS) $_7$ - β -CD-(hydrazide) $_{8.5}$ (**4**) as a light brown solid (0.75 g, conversion ~ 99%). ^1H NMR (400 MHz, CDCl_3): $\delta_{\text{H}}=-0.01$ (s, 42H, Si- CH_3), 0.85 (s, 63H, C-(CH_3) $_3$), 2.25 (bs, NH- NH_2), 3.10-4.40 (bm, 59H, H-2, H-3, H-4, H-5, H-6a, H-6b and OCH_2CO), 4.45-5.33 (b, 7H, H-1 overlapped with OH), 7.69 (CO-NH- NH_2). ^{13}C NMR (125 MHz, CDCl_3): $\delta_{\text{C}}=-5.02, 18.2, 25.9, 59.5, 61.8, 72.5, 73.2, 73.5, 79.2, 101.8, 208.1$. FT-IR (cm^{-1}): 3309, 2930-2855, 1673, 1598, 1462, 1362, 1251, 1143, 1082, 1036, 961, 829, 775.

(TBDMS) $_7$ - β -CD-(hydrazide) $_{8.5}$ (**4**) (0.7 g, 3.5×10^{-4} mol containing 2.97×10^{-3} moles of NH_2 units) was dissolved in THF (20 mL) followed by addition of 2-bromo-2-methylpropionic acid-4-formyl-phenyl ester (**5**) (8.06 g, 2.97×10^{-2} mol) to the reaction flask and refluxing the mixture at 65 °C for 24 h before evaporating the THF and isolating the crude product, which was purified by flash chromatography on silica gel using a gradient mobile phase composed of 9/1 ethyl acetate/hexane mixture followed by 18/2

dichloromethane/methanol mixture containing 1% w/v TEA to yield 0.15 g of (TBDMS)₇-β-CD-(hydrazone-Br)_{4.8} (**6**) (80% conversion). ¹H NMR (400 MHz, CDCl₃): δ_H= 0.03 (s, 42H, Si-CH₃), 0.87 (s, 63H, C-(CH₃)₃), 2.09 (s, 28H, C(CH₃)₂-Br), 3.38-4.53 (bm, 59H, H-2, H-3, H-4, H-5, H-6a, H-6b and OCH₂CO), 4.88-5.13 (b, 7H, H-1 and s, OH), 6.82-7.21 (b, 9.6H, aromatic protons) 7.30-7.95 (b, 14.5H aromatic protons and NH-N). 8.15 (s, CH). ¹³C NMR (125 MHz, CDCl₃): δ_C=- 5.1, 19.2, 25.9, 29.7, 29.9, 55.9, 59.6, 61.9, 71.8, 72.05, 74.10, 81.8, 99.3, 121.2, 127, 131.7, 145.5, 150.8, 164.7, 170.9. FT-IR (cm⁻¹): 3294, 3069-2855, 1749, 1684, 1652 1602, 1555 1458, 1387, 1251, 1158, 1082, 1032, 957, 829, 775.

S1.4 Grafting of HMA/DMAEMA Monomers from the Secondary Face of β-CD

Compound **6** (13.5 mg, 3.48 x 10⁻⁶ mol containing 1.77 x 10⁻⁵ Br unit) and HMTETA (4.83 μL, 1.77 x 10⁻⁵ mol) were mixed with 1 mL of anisole or THF in Schlenk tube and degassed by three freeze–pump–thaw cycles. CuCl (1.4 mg, 1.42 x 10⁻⁵ mol), CuCl₂ (0.47 mg, 3.55 x 10⁻⁶ mol), DMAEMA (0.88 mL, 5.33 x 10⁻³ mol), HMA (1.05 mL, 5.33 x 10⁻³ mol) and 2 mL of anisole or THF were mixed in a second Schlenk tube followed by degassing the reaction mixture by three freeze–pump–thaw cycles. The initiator solution was transferred to the reaction vessel by a syringe and the reaction mixture was heated in an oil bath at 60 °C. The reaction product was dissolved in THF, passed through a basic alumina column to remove the catalyst, rotary evaporated to remove the solvent, and added to cold heptane to precipitate (TBDMS)₇-β-CD-P(HMA-*co*-DMAEMA)_{4.8} (**7**). ¹H NMR (400 MHz, CDCl₃): δ_H= 0.03 (s, 42H, Si-CH₃), 0.86-2.03 (C-(CH₃)₃, CH₂-C(CH₃), CH₂-C(CH₃), O-CH₂-(CH₂)₂-CH₃, O-CH₂-(CH₂)₂-CH₃), 2.26 (bs, N(CH₃)₂), 2.54 (CH₂-N(CH₃)₂), 3.56 (7H, H-6a), 3.62-3.72 (21H, H-2, H-3, H-5), 3.92 (COOCH₂(CH₂)₄-CH₃

overlap with H-6b, H-4), 4.04 (COOCH₂-CH₂-N(CH₃)₂), 4.90-5.11 (7H, H-1 and OH residue), 6.78-7.05 (Aromatic protons), 7.61-7.99 (Aromatic protons and NH-N=CH), 8.08 (NH-N=CH). FT-IR (cm⁻¹): 2951-2725, 1726, 1458, 1376, 1266, 1143, 1061, 965, 746.

S1.5 Deprotection of (TBDMS)₇-β-CD-P(HMA-co-DMAEMA)_{4.8} Polymer

(TBDMS)₇-β-CD-P(HMA-co-DMAEMA)_{4.8} polymer (**7**) (100 mg, 3.44 x 10⁻⁷ mol with 2.40 x 10⁻⁶ mol of TBDMS units) was dissolved in anhydrous THF (3 mL), mixed with tetrabutylammonium fluoride (TBAF) (24 μL, 2.40 x 10⁻⁵ mol) under argon atmosphere, and stirred for 8 h at room temperature followed by removing the solvent and precipitating the polymer in cold heptane. ¹H NMR (400 MHz, CDCl₃): δ_H=0.86-2.03 (CH₂-C(CH₃), CH₂-C(CH₃), O-CH₂-(CH₂)₂-CH₃, O-CH₂-(CH₂)₂-CH₃), 2.26 (s, N(CH₃)₂), 2.54 (CH₂-N(CH₃)₂), 3.56 (7H, H-6a), 3.62-3.72 (21H, H-2, H-3, H-5), 3.92 (COOCH₂(CH₂)₄-CH₃ overlap with H-6b, H-4), 4.04 (COOCH₂-CH₂- N(CH₃)₂), 4.90-5.26 (7H, H-1 and OH residue), 6.78-7.05 (Aromatic protons), 7.61-7.92 (Aromatic protons and CO-NH-N), 8.08 (CO-NH-N=CH). FT-IR (cm⁻¹): 3423, 2958-2768, 1723, 1650, 1573, 1458, 1383, 1269, 1147, 1061, 961, 882, 746.

S1.6 Quaternization of DMAEMA Monomers into Cationic TMAEMA Monomers

β-CD-P(HMA-co-DMAEMA)_{4.8} (**8**) (90 mg, 3.1 x 10⁻⁷ mol with 2.88 x 10⁻⁴ mol of tert-amine groups) was dissolved in anhydrous THF (5 mL) followed by addition of methyl iodide (36 μL, 5.76 x 10⁻⁴ mol) to the reaction vessel and allowing the reaction mixture to stand overnight at room temperature under an argon atmosphere. Pure β-CD-P(HMA-co-TMAEMA)_{4.8} (**9**) was isolated by removing the THF solvent by rotary evaporation, dissolving the reaction product in water and dialyzing it against deionized water for 3

days followed by lyophilization. To prepare partially (50%) quaternized polymers, methyl iodide was used at 1/2 equivalent of the concentration of *tert*-amine groups of polymer (**8**) to yield β -CD-P(HMA-*co*-DMAEMA-*co*-TMAEMA)_{4.8}, (**10**), which was purified the same way as β -CD-P(HMA-*co*-TMAEMA)_{4.8}. ¹H NMR (400 MHz, D₂O): δ_{H} =0.84-2.05 (*CH*₂-C(CH₃), *CH*₂-C(*CH*₃), O-*CH*₂-(*CH*₂)₄-CH₃, O-*CH*₂-(*CH*₂)₂-*CH*₃), 3.16 (bs, N(*CH*₃)₂), 3.75 (O-*CH*₂-(*CH*₂)₄-CH₃ overlap with *CH*₂-N(*CH*₃)₂), 4.35 (COO*CH*₂-*CH*₂-N(*CH*₃)₂). FT-IR (cm⁻¹): 3334, 2951-2851, 1720, 1648, 1477, 1387, 1237, 1140, 982, 961, 879.

References

- (1) (a) Elbashir, S. M.; Harborth, J.; Lendeckel, W.; Yalcin, A.; Weber, K.; Tuschl, T. *Nature* **2001**, *411*, 494. (b) McManus, M. T.; Sharp, P. A. *Nat Rev Genet* **2002**, *3*, 737. (c) Scherr, M.; Morgan, M. A.; Eder, M. *Curr Med Chem* **2003**, *10*, 245. (d) Timmons, L.; Fire, A. *Nature* **1998**, *395*, 854.
- (2) Zhang, J.; Wu, Y. O.; Xiao, L.; Li, K.; Chen, L. L.; Sirois, P. *Mol Biotechnol* **2007**, *37*, 225.
- (3) Hassan, A. *Recent Pat Cardiovasc Drug Discov* **2006**, *1*, 141.
- (4) (a) de Fougerolles, A.; Vornlocher, H. P.; Maraganore, J.; Lieberman, J. *Nat Rev Drug Discov* **2007**, *6*, 443. (b) Koutsilieris, E.; Rethwilm, A.; Scheller, C. *J Neural Transm Suppl* **2007**, 43.
- (5) (a) Jere, D.; Jiang, H. L.; Arote, R.; Kim, Y. K.; Choi, Y. J.; Cho, M. H.; Akaike, T.; Cho, C. S. *Expert Opin Drug Deliv* **2009**, *6*, 827. (b) Lai, W. F.; Lin, M. C. *J Control Release* **2009**, *134*, 158. (c) Midoux, P.; Pichon, C.; Yaouanc, J. J.; Jaffres, P. A. *Br J Pharmacol* **2009**, *157*, 166. (d) Pangburn, T. O.; Petersen, M. A.; Waybrant, B.; Adil, M. M.; Kokkoli, E. *J Biomech Eng* **2009**, *131*, 074005.
- (6) (a) Martin, B.; Sainlos, M.; Aissaoui, A.; Oudrhiri, N.; Hauchecorne, M.; Vigneron, J. P.; Lehn, J. M.; Lehn, P. *Curr. Pharm. Des.* **2005**, *11*, 375. (b) Medvedeva, D. A.; Maslov, M. A.; Serikov, R. N.; Morozova, N. G.; Serebrennikova, G. A.; Sheglov, D. V.; Latyshev, A. V.; Vlassov, V. V.; Zenkova, M. A. *J. Med. Chem.* **2009**, *52*, 6558.
- (7) Boussif, O.; Lezoualc'h, F.; Zanta, M. A.; Mergny, M. D.; Scherman, D.; Demeneix, B.; Behr, J. P. *Proc Natl Acad Sci U S A* **1995**, *92*, 7297.
- (8) Medina-Kauwe, L. K.; Xie, J.; Hamm-Alvarez, S. *Gene Therapy* **2005**, *12*, 1734.
- (9) (a) Hoffman, A. S.; Stayton, P. S.; Press, O.; Murthy, N.; Lackey, C. A.; Cheung, C.; Black, F.; Campbell, J.; Fausto, N.; Kyriakides, T. R.; Bornstein, P. *Polym. Adv. Technol.* **2002**, *13*, 992. (b) Stayton, P. S.; El-Sayed, M. E.; Murthy, N.; Bulmus, V.; Lackey, C.; Cheung, C.; Hoffman, A. S. *Orthod Craniofac Res* **2005**, *8*, 219.
- (10) (a) El-Sayed, M. E.; Hoffman, A. S.; Stayton, P. S. *Expert Opin Biol Ther* **2005**, *5*, 23. (b) Henry, S. M.; El-Sayed, M. E. H.; Pirie, C. M.; Hoffman, A. S.; Stayton, P. S. *Biomacromolecules* **2006**, *7*, 2407. (c) Stayton, P. S.; Hoffman, A. S.; El-Sayed, M.; Kulkarni, S.; Shimoboji, T.; Murthy, N.; Bulmus, V.; Lackey, C. *P Ieee* **2005**, *93*, 726.
- (11) Schoen, P.; Chonn, A.; Cullis, P. R.; Wilschut, J.; Scherrer, P. *Gene Therapy* **1999**, *6*, 823.
- (12) Johns, R. E.; El-Sayed, M. E. H.; Bulmus, V.; Cuschieri, J.; Maier, R.; Hoffman, A. S.; Stayton, P. S. *J Biomat Sci-Polym E* **2008**, *19*, 1333.
- (13) Lin, Y. L.; Jiang, G. H.; Birrell, L. K.; El-Sayed, M. E. H. *Biomaterials* **2010**, *31*, 7150.
- (14) Lackey, C. A.; Press, O. W.; Hoffman, A. S.; Stayton, P. S. *Bioconjugate Chem.* **2002**, *13*, 996.
- (15) Kyriakides, T. R.; Cheung, C. Y.; Murthy, N.; Bornstein, P.; Stayton, P. S.; Hoffman, A. S. *J. Controlled Release* **2002**, *78*, 295.

- (16) El-Sayed, M. E. H.; Hoffman, A. S.; Stayton, P. S. *J. Controlled Release* **2005**, *104*, 415.
- (17) (a) Bulmus, V.; Woodward, M.; Lin, L.; Murthy, N.; Stayton, P.; Hoffman, A. *J. Controlled Release* **2003**, *93*, 105. (b) El-Sayed, M. E. H.; Hoffman, A. S.; Stayton, P. S. *J. Controlled Release* **2005**, *101*, 47.
- (18) (a) Kurisawa, M.; Yokoyama, M.; Okano, T. *J. Controlled Release* **2000**, *68*, 1. (b) Murthy, N.; Chang, I.; Stayton, P.; Hoffman, A. *Macromol. Symp.* **2001**, *172*, 49. (c) Oskuee, R. K.; Dehshahri, A.; Shier, W. T.; Ramezani, M. *Journal of Gene Medicine* **2009**, *11*, 921. (d) Wen, Y. T.; Pan, S. R.; Luo, X.; Zhang, X.; Zhang, W.; Feng, M. *Bioconjugate Chem.* **2009**, *20*, 322.
- (19) (a) Boussif, O.; Zanta, M. A.; Behr, J. P. *Gene Ther* **1996**, *3*, 1074. (b) Merdan, T.; Kunath, K.; Petersen, H.; Bakowsky, U.; Voigt, K. H.; Kopecek, J.; Kissel, T. *Bioconjugate Chem.* **2005**, *16*, 785.
- (20) Schiffelers, R. M.; Ansari, A.; Xu, J.; Zhou, Q.; Tang, Q. Q.; Storm, G.; Molema, G.; Lu, P. Y.; Scaria, P. V.; Woodle, M. C. *Nucleic Acids Res* **2004**, *32*.
- (21) (a) Boeckle, S.; von Gersdorff, K.; van der Piepen, S.; Culmsee, C.; Wagner, E.; Ogris, M. *Journal of Gene Medicine* **2004**, *6*, 1102. (b) Forrest, M. L.; Koerber, J. T.; Pack, D. W. *Bioconjugate Chem.* **2003**, *14*, 934. (c) Thomas, M.; Ge, Q.; Lu, J. J.; Chen, J. Z.; Klibanov, A. M. *Pharm. Res.* **2005**, *22*, 373.
- (22) (a) Davis, M. E.; Brewster, M. E. *Nat. Rev. Drug Discovery* **2004**, *3*, 1023. (b) Del Valle, E. M. M. *Process Biochem.* **2004**, *39*, 1033. (c) Uekama, K.; Hirayama, F.; Irie, T. *Chem. Rev.* **1998**, *98*, 2045.
- (23) (a) Fulton, D. A.; Stoddart, J. F. *Org. Lett.* **2000**, *2*, 1113. (b) Ortega-Caballero, F.; Mellet, C. O.; Le Gourrierec, L.; Guilloteau, N.; Di Giorgio, C.; Vierling, P.; Defaye, J.; Fernandez, J. M. G. *Org. Lett.* **2008**, *10*, 5143. (c) Srinivasachari, S.; Fichter, K. M.; Reineke, T. M. *J. Am. Chem. Soc.* **2008**, *130*, 4618.
- (24) van de Wetering, P.; Moret, E. E.; Schuurmans-Nieuwenbroek, N. M. E.; van Steenbergen, M. J.; Hennink, W. E. *Bioconjugate Chem.* **1999**, *10*, 589.
- (25) Imai, A.; Zeitlin, B. D.; Visioli, F.; Dong, Z. H.; Zhang, Z. C.; Krishnamurthy, S.; Light, E.; Worden, F.; Wang, S. M.; Nor, J. E. *Cancer Res* **2012**, *72*, 716.
- (26) Zuidam, N. J.; Posthuma, G.; de Vries, E. T. J.; Crommelin, D. J. A.; Hennink, W. E.; Storm, G. *J. Drug Targeting* **2000**, *8*, 51.
- (27) Neu, M.; Fischer, D.; Kissel, T. *J Gene Med* **2005**, *7*, 992.
- (28) (a) Pafiti, K. S.; Mastroiannopoulos, N. P.; Phylactou, L. A.; Patrickios, C. S. *Biomacromolecules* **2011**, *12*, 1468. (b) Xu, F. J.; Zhang, Z. X.; Ping, Y.; Li, J.; Kang, E. T.; Neoh, K. G. *Biomacromolecules* **2009**, *10*, 285. (c) Dai, F. Y.; Sun, P.; Liu, Y. J.; Liu, W. G. *Biomaterials* **2010**, *31*, 559.
- (29) Synatschke, C. V.; Schallon, A.; Jerome, V.; Freitag, R.; Muller, A. H. E. *Biomacromolecules* **2011**, *12*, 4247.
- (30) Gillies, E. R.; Frechet, J. M. J. *J. Am. Chem. Soc.* **2002**, *124*, 14137.
- (31) Newland, B.; Tai, H. Y.; Zheng, Y.; Velasco, D.; Di Luca, A.; Howdle, S. M.; Alexander, C.; Wang, W. X.; Pandit, A. *Chem. Commun.* **2010**, *46*, 4698.
- (32) (a) vandeWetering, P.; Cherng, J. Y.; Talsma, H.; Hennink, W. E. *J. Controlled Release* **1997**, *49*, 59. (b) Layman, J. M.; Ramirez, S. M.; Green, M. D.; Long, T. E. *Biomacromolecules* **2009**, *10*, 1244. (c) Georgiou, T. K.; Vamvakaki, M.;

- Patrickios, C. S.; Yamasaki, E. N.; Phylactou, L. A. *Biomacromolecules* **2004**, *5*, 2221.
- (33) (a) Wang, J. S.; Matyjaszewski, K. *J. Am. Chem. Soc.* **1995**, *117*, 5614. (b) Kato, M.; Kamigaito, M.; Sawamoto, M.; Higashimura, T. *Macromolecules* **1995**, *28*, 1721.
- (34) (a) Ganachaud, F.; Monteiro, M. J.; Gilbert, R. G.; Dourges, M. A.; Thang, S. H.; Rizzardo, E. *Macromolecules* **2000**, *33*, 6738. (b) Chiefari, J.; Chong, Y. K.; Ercole, F.; Krstina, J.; Jeffery, J.; Le, T. P. T.; Mayadunne, R. T. A.; Meijs, G. F.; Moad, C. L.; Moad, G.; Rizzardo, E.; Thang, S. H. *Macromolecules* **1998**, *31*, 5559.
- (35) (a) Liu, H.; Jiang, X. Z.; Fan, J.; Wang, G. H.; Liu, S. Y. *Macromolecules* **2007**, *40*, 9074. (b) Xu, F. J.; Li, H. Z.; Li, J.; Zhang, Z. X.; Kang, E. T.; Neoh, K. G. *Biomaterials* **2008**, *29*, 3023. (c) York, A. W.; Kirkland, S. E.; McCormick, C. L. *Adv. Drug Delivery Rev.* **2008**, *60*, 1018.
- (36) Ping, Y. A.; Liu, C. D.; Tang, G. P.; Li, J. S.; Li, J.; Yang, W. T.; Xu, F. J. *Adv. Funct. Mater.* **2010**, *20*, 3106.
- (37) Georgiou, T. K.; Vamvakaki, M.; Phylactou, L. A.; Patrickios, C. S. *Biomacromolecules* **2005**, *6*, 2990.
- (38) (a) Park, M. R.; Han, K. O.; Han, I. K.; Cho, M. H.; Nah, J. W.; Choi, Y. J.; Cho, C. S. *J Control Release* **2005**, *105*, 367. (b) Qi, R.; Gao, Y.; Tang, Y.; He, R. R.; Liu, T. L.; He, Y.; Sun, S.; Li, B. Y.; Li, Y. B.; Liu, G. *Aaps J* **2009**, *11*, 395.
- (39) (a) Yuan, F.; Dellian, M.; Fukumura, D.; Leunig, M.; Berk, D. A.; Torchilin, V. P.; Jain, R. K. *Cancer Research* **1995**, *55*, 3752. (b) Yuan, F.; Dellian, M.; Fukumura, D.; Leunig, M.; Berk, D. A.; Torchilin, V. P.; Jain, R. K. *Cancer Res* **1995**, *55*, 3752.
- (40) Neu, M.; Fischer, D.; Kissel, T. *Journal of Gene Medicine* **2005**, *7*, 992.
- (41) Synatschke, C. V.; Schallon, A.; Jérôme, V.; Freitag, R.; Müller, A. H. E. *Biomacromolecules* **2011**, *12*, 4247.
- (42) (a) Simon, S. M. *Drug Discovery Today* **1999**, *4*, 32. (b) Rybak, S. L.; Lanni, F.; Murphy, R. F. *Biophys J* **1997**, *73*, 674. (c) Cain, C. C.; Sipe, D. M.; Murphy, R. F. *Proc. Natl. Acad. Sci. U.S.A.* **1989**, *86*, 544.
- (43) (a) Weisz, O. A. *Traffic* **2003**, *4*, 57. (b) Duvvuri, M.; Konkar, S.; Hong, K. H.; Blagg, B. S. J.; Krise, J. P. *ACS Chem Biol* **2006**, *1*, 309. (c) Simon, S.; Roy, D.; Schindler, M. *Proc. Natl. Acad. Sci. U.S.A.* **1994**, *91*, 1128.
- (44) Zhang, B.; Mallapragada, S. *Acta Biomaterialia* **2011**, *7*, 1580.
- (45) (a) Etrych, T.; Chytil, P.; Jelinkova, M.; Rihova, B.; Ulbrich, K. *Macromol. Biosci.* **2002**, *2*, 43. (b) Masek, V.; Anzenbacherova, E.; Etrych, T.; Strohalm, J.; Ulbrich, K.; Anzenbacher, P. *Drug Metab. Dispos.* **2011**, *39*, 1704. (c) Ulbrich, K.; Etrych, T.; Chytil, P.; Jelinkova, M.; Rihova, B. *J. Controlled Release* **2003**, *87*, 33.
- (46) Haddleton, D. M.; Waterson, C. *Macromolecules* **1999**, *32*, 8732.
- (47) Ashton, P. R.; Koniger, R.; Stoddart, J. F.; Alker, D.; Harding, V. D. *J. Org. Chem.* **1996**, *61*, 903.

Chapter 6.

Synergistic inhibition of anti-apoptotic Bcl-2 activity by smart, star-shaped vector and small molecule inhibitor in head & neck cancer cells

6.1 Introduction

Head and neck cancer is one of the most commonly diagnosed cancers, which accounts for approximately 650,000 new cases and 350,000 cancer-related deaths in the world every year.¹ The five-year survival of head and neck cancer at all stages is 50-60%, which is one of the lowest five-year survival rates among all cancers.² Although treatment of head and neck cancer with both chemotherapy and radiation has been shown to improve the outcome of patients compared with radiation alone,³ the efficacy is highly limited by the emergence of resistant cancer cells.⁴ Therefore, it is important to develop an effective strategy to restore the sensitivity of head and neck cancer cells to radio- and chemo-therapy.

Bcl-2 is a pro-survival protein that is over-expressed in various human cancer cells and responsible for dysregulation of apoptosis and prevention of death in cancer cells.⁵ Anti-apoptotic activity of Bcl-2 protein is attributed to its ability to stabilize the mitochondrial membrane and inhibit the cytoplasmic release of cytochrome c, which prevents the activation of caspases and incidence of cellular apoptosis.^{5b,6} In addition, over-expression

of Bcl-2 has been shown to increase the resistance of cancer cells to chemotherapeutic drugs and radiotherapy.⁷ Application of nucleic acid macromolecules, such as antisense oligodeoxynucleotide (ASODN) and short hairpin RNA (shRNA), to suppress Bcl-2 expression in cancer cells proved to successfully induce head and neck cancer cell death and sensitize cancer cells to chemotherapy both *in vitro* and *in vivo*.⁸ Therefore, these studies suggest that it is applicable to target Bcl-2 expression by therapeutic nucleic acids to inhibit tumor growth and restore the sensitivity of tumor cells to chemotherapeutic drugs.

However, successfully deliver therapeutic DNA/RNA molecules into the cytoplasm of cancer cells to perform functional gene silencing requires an ideal carrier that can complex the nucleic acids into nano-sized particles, which preferentially accumulate in tumor tissues and be selectively taken up by target cells coupled with efficient escape from the endosomal/lysosomal trafficking pathway and release the therapeutic cargo into the cytoplasm.⁹ We have designed and synthesized a series of degradable, pH-sensitive, membrane-destabilizing, star-shaped polymers that can shuttle a large dose of model siRNA molecules past the endosomal membrane and into the cytoplasm of multiple cell types, including HeLa cervical cancer cells, UM-SCC-17B head and neck cancer cells, and MCF-10A normal mammary epithelial cells.¹⁰ To be specific, we grafted a random copolymer of hydrophobic hexyl methacrylate (HMA) and pH-sensitive dimethyl aminoethyl methacrylate (DMAEMA) monomers from the secondary face of the β -cyclodextrin (β -CD) core via acid-labile hydrazone linkages forming star-shaped polymer where DMAEMA monomers were partially (50%) quaternized into cationic trimethyl aminoethyl methacrylate (TMAEMA) for complexation of siRNA molecules into “smart”

particles via electrostatic interaction. These cationic particles remain stable at physiologic pH and be internalized into cells through adsorptive endocytosis, but hydrolyze into membrane-active fragments that disrupt the endosomal membrane and release the nucleic acid cargo into the cytoplasm when exposed to acidic endosomal pH gradients (**Figure 6.1**).¹⁰ These polymers have been proved to exhibit enhanced gene suppression at protein and mRNA levels probably due to the combined endosomal escape mechanisms of hydrophobic membrane disruption and endosomal burst.¹⁰

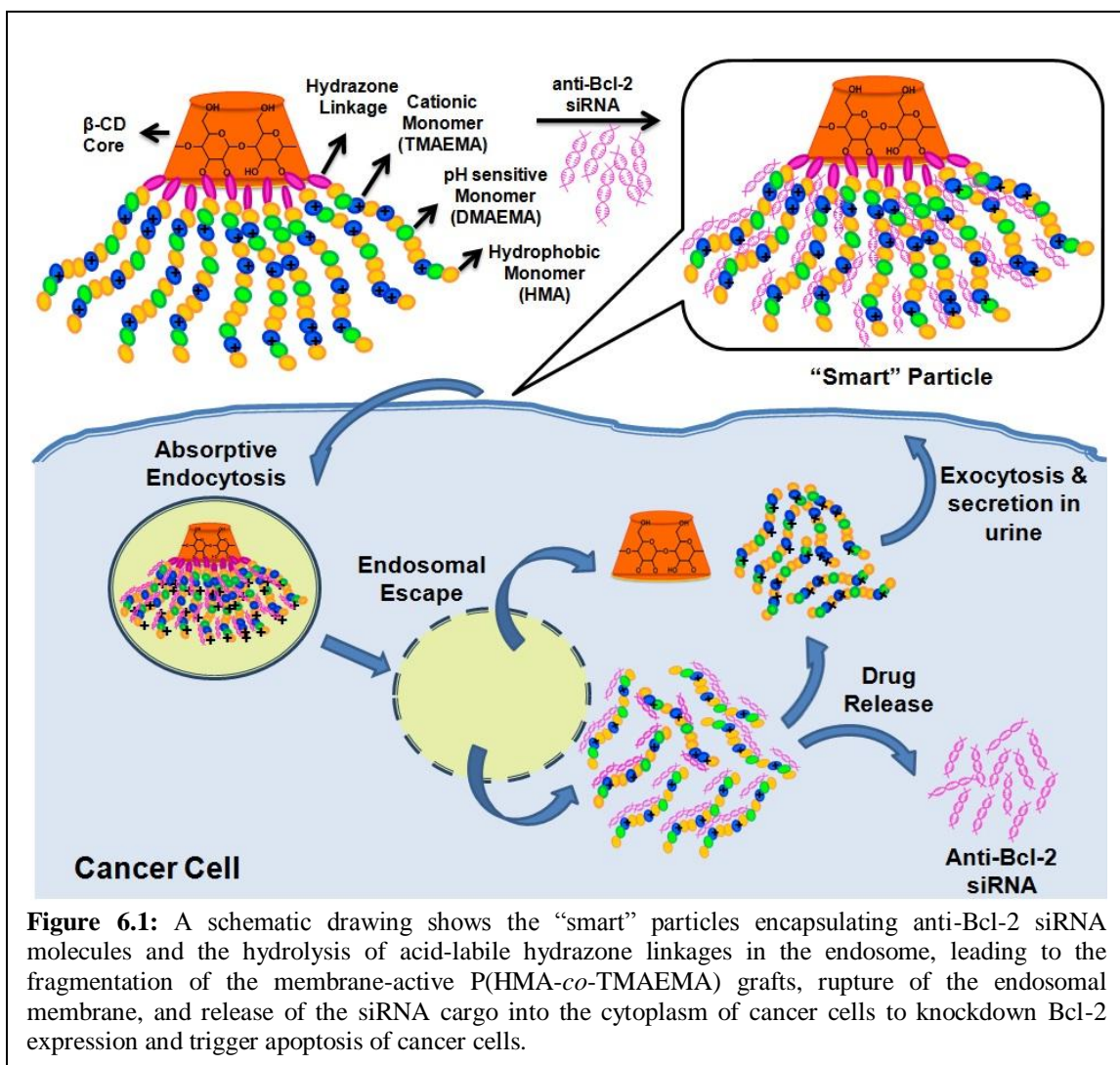


Figure 6.1: A schematic drawing shows the “smart” particles encapsulating anti-Bcl-2 siRNA molecules and the hydrolysis of acid-labile hydrazone linkages in the endosome, leading to the fragmentation of the membrane-active P(HMA-co-TMAEMA) grafts, rupture of the endosomal membrane, and release of the siRNA cargo into the cytoplasm of cancer cells to knockdown Bcl-2 expression and trigger apoptosis of cancer cells.

In this study, we evaluated the therapeutic activity of these pH-sensitive, star-shaped polymers to achieve functional delivery of anti-Bcl-2 siRNA molecules based on their ability to selectively inhibit Bcl-2 expression at the mRNA and protein levels in UM-SCC-17B head and neck cancer cells. In addition, we explored the possibility to inhibit the anti-apoptotic function of residual Bcl-2 proteins by simultaneously treat cancer cells with BH3-mimetic compounds, AT-101, which is a small molecule inhibitor, verified to restore the anti-apoptotic pathway and sensitize head and neck cancer cells to chemotherapeutic drugs by blocking the heterodimerization of Bcl-2 proteins with pro-apoptotic proteins.¹¹ In this way, the Bcl-2 protein can be largely inhibited by both gene silencing mechanism and Bcl-2 antagonist to achieve better inhibition compared to single treatment, which triggers apoptotic cell death in response to therapeutic treatments.

6.2 Materials and Methods

6.2.1 Materials

The anti-Bcl-2 siRNA sequence (5'-GCCUGAUUGUGUAUUAUCA-3') was synthesized by Integrated DNA Technologies, Inc. (Coralville, Iowa). Scrambled siRNA molecules were purchased from Ambion Inc. (Austin, TX). The RNeasy Mini Kit and Omniscript reverse transcriptase kit were purchased from Qiagen (Valencia, CA). The TaqMan universal PCR master mix and TaqMan gene expression assays for human Bcl-2 and 18S rRNA genes were purchased from Applied Biosystems (Foster, CA). The anti-human β -actin monoclonal antibody and anti-human Bcl-2 monoclonal antibody were purchased from Santa Cruz Biotechnology (Santa Cruz, CA) and BD Biosciences (San Jose, CA), respectively. The AT-101 was purchased from Tocris Bioscience (Minneapolis, MN). Trichloroacetic acid, trizma base, and sulforhodamine B solium salt

were purchased from Sigma-Aldrich (St. Louis, MO). Propidium iodide was purchased from MP Biomedicals (Santa Ana, CA).

6.2.2 Culture of UM-SCC-17B cells

UM-SCC-17B head and neck cancer cells were generously provided by Dr. Nör and cultured following established protocols.¹¹ Briefly, UM-SCC-17B cells were maintained in DMEM supplemented with 10% fetal bovine serum, 10,000 units/ml penicillin, 10,000 µg/ml streptomycin and regularly changing the growth medium every 2 days. Cells were incubated at 37 °C, 5% CO₂, 95% relative humidity, and passaged upon reaching 70-90% confluency using 0.25% trypsin/EDTA mixture.

6.2.3 *In vitro* evaluation of Bcl-2 protein knockdown in UM-SCC-17B cells

UM-SCC-17B cells were plated in 6-well plates at a seeding density of 200,000 cells/well and allowed to adhere for 18 hours. The “smart” particles incorporating 1.43 µg of anti-Bcl-2 siRNA or scrambled siRNA molecules were incubated with UM-SCC-17B cells at a final siRNA concentration of 100 nM for 6 hours followed by addition of 1250 µl of fresh culture medium and incubation for a total of 48 and 72 hours. The amount of Bcl-2 protein expressed by UM-SCC-17B cells was analyzed using the western blot technique following established protocol.¹² Briefly, whole cell lysates were resolved by SDS-PAGE and membranes were probed overnight at 4°C with anti-human β-actin monoclonal antibody (1:1000000) and anti-human Bcl-2 monoclonal antibody (1:1000), and then proteins were visualized with SuperSignal West Pico Chemiluminescent Substrate (Pierce, Rockford, IL). The knockdown of Bcl-2 protein expression in response to different treatments was quantified by Image J software (NIH, Bethesda, MD) and normalized to that of negative control cells.

6.2.4 *In vitro* evaluation of Bcl-2 mRNA knockdown in UM-SCC-17B cells

UM-SCC-17B cells were plated in 24-well plates at a seeding density of 20,000 cells/well and allowed to adhere for 18 hours. The “smart” particles incorporating 0.57 µg of anti-Bcl-2 siRNA or scrambled siRNA molecules were incubated with UM-SCC-17B cells at a final siRNA concentration of 100 nM for 6 hours followed by addition of 500 µl of fresh culture medium and incubation for a total of 48 and 72 hours. For quantification of mRNA, total RNA was isolated from UM-SCC-17B cells using the RNeasy Mini Kit and 0.25 µg of total RNA was reverse transcribed using Omniscript reverse transcriptase kit following manufacturer’s protocols. Real-time PCR was performed in a final volume of 20 µl containing 2 µl of cDNA (corresponding to 10 ng of total RNA for Bcl-2 and 18S rRNA amplification), 1 µl of each primer, and 10 µl of the qPCR MasterMix in the 7500 Fast Real-Time PCR system.

6.2.5 Determination of IC₂₅, IC₅₀, and IC₇₅ of AT-101

UM-SCC-17B cells were plated in 24-well plates at a seeding density of 10,000 cells/well and allowed to adhere for 18 hours, and then treated with 0, 0.1, 0.5, 1, 2, 4, 8, and 10 µM AT-101 for 48 and 72 hours. Cell survival was determined by the Sulforhodamine B (SRB) assay following the established protocol.¹¹ Briefly cells were fixed onto the plates by addition of 10% trichloroacetic acid (final concentration) for 1 hour at 4°C. Cellular protein was stained by 0.4% SRB in 1% acetic acid for 30 minutes at room temperature. Unbound SRB was removed by washing with 1% acetic acid and plates were allowed to air dry. Bound SRB was resolubilized in 10 mM Tris base and absorbance was determined by a Fluoroskan plate reader (Thermo scientific, Asheville,

NC) at 565 nm. The cell survival in response to different treatments was normalized against initial plating density and drug-free controls.

6.2.6 Cell growth after combination treatment

UM-SCC-17B cells were plated in 24-well plates at a seeding density of 10,000 cells/well and allowed to adhere for 18 hours. AT-101 (IC₂₅) alone or with the “smart” particles incorporating 0.57 µg of anti-Bcl-2 siRNA or scrambled siRNA molecules were incubated with UM-SCC-17B cells at a final siRNA concentration of 100 nM for 6 hours followed by addition of 500 µl of fresh culture medium with AT-101 (IC₂₅) and incubation for a total of 72 hours. Cell survival was determined by the Sulforhodamine B (SRB) assay. The synergism or additivity was calculated by CalcuSyn ver. 2.0 software (Biosoft, Cambridge, UK) using the combinatorial index (CI), a mathematical and quantitative evaluation of a two-drug pharmacologic interaction. A synergistic effect is represented by $CI < 0.9$; an additive effect by $0.9 \leq CI \leq 1.1$; and absence of combinatorial effect $CI > 1.1$.

6.2.7 Cellular apoptosis after combination treatment

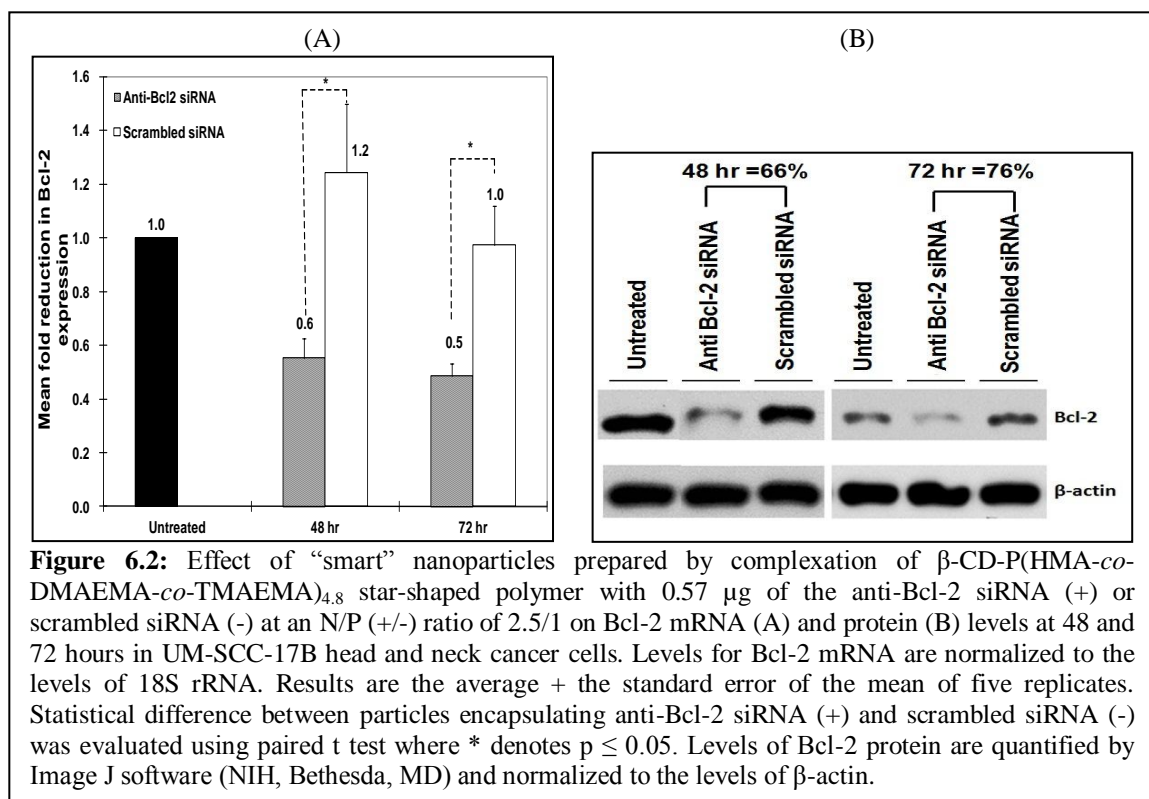
UM-SCC-17B cells were plated in 12-well plates at a seeding density of 20,000 cells/well and allowed to adhere for 18 hours. AT-101 (IC₂₅) alone or with the “smart” particles incorporating 1.14 µg of anti-Bcl-2 siRNA or scrambled siRNA molecules were incubated with UM-SCC-17B cells at a final siRNA concentration of 100 nM for 6 hours followed by addition of 1000 µl of fresh culture medium with AT-101 (IC₂₅) and incubation for a total of 72 hours. Cells were treated with 0.25% trypsin/EDTA solution, harvested, and centrifuged to remove the supernatant and form a cell pellet. Cell pellets were suspended in PBS and stained with propidium iodide (PI) for 20 minutes. Apoptotic

cells and cell cycle were determined by Biosciences FACSCalibur (Becton Dickinson, Franklin Lakes, NJ).

6.3 Results

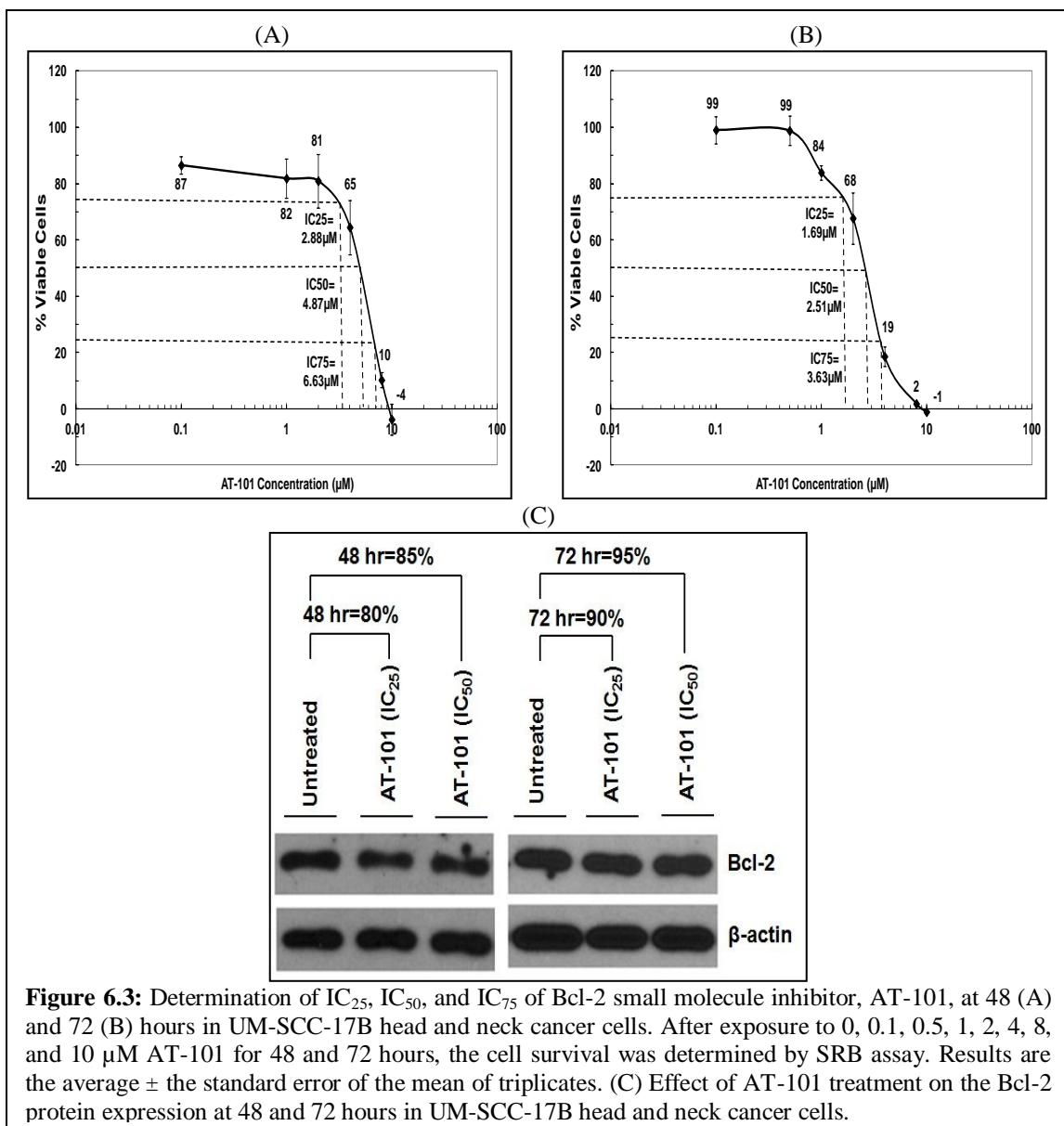
6.3.1 Effect of “smart” particles on Bcl-2 expression

The therapeutic activity of “smart” particles to deliver functional anti-Bcl-2 siRNA molecules past the endosomal membrane and into the cytoplasm of UM-SCC-17B head and neck cells was evaluated based on their ability to selectively knockdown Bcl-2 gene expression at both the mRNA and protein levels. We utilized the qRT-PCR to measure the changes in Bcl-2 mRNA level upon incubation with particles that encapsulate the anti-Bcl-2 siRNA molecules, and compare to those encapsulating a scrambled siRNA sequence. Results show that particles selectively induced 60 and 50% knockdown in Bcl-2 mRNA expression in UM-SCC-17B cells at 48 and 72 hours, respectively (**Figure 6.2A**). The particles also induced 66 and 76% Bcl-2 protein suppression in UM-SCC-17B cells at 48 and 72 hours, respectively (**Figure 6.2B**). These results suggest that these particles can induce gene silencing for at least 72 hours.



6.3.2 Determination of IC₂₅, IC₅₀, and IC₇₅ of AT-101

The IC₂₅, IC₅₀, and IC₇₅ of AT-101 in UM-SCC-17B cancer cells were determined based on percentage of cell survival after treatment with 0, 0.1, 0.5, 1, 2, 4, 8, and 10 μ M AT-101 for 48 and 72 hours, and then analyzed by SRB cytotoxic assay. As shown in **Figure 6.3A&B**, IC₂₅, IC₅₀, and IC₇₅ of AT-101 at 48 hours is 2.88, 4.87, and 6.63 μ M, respectively, while IC₂₅, IC₅₀, and IC₇₅ of AT-101 at 72 hours is 1.69, 2.51, and 3.63 μ M, respectively. This indicates that less AT-101 is required to cause cell death at longer incubation time. The effect of AT-101 on Bcl-2 expression in UM-SCC-17B was also evaluated after treatment with AT-101 at IC₂₅ and IC₅₀ for 48 and 72 hours by using western blot. Results show that AT-101 induced 15-20 and 5-10% reduction in Bcl-2 protein expression at 48 and 72 hours, respectively (**Figure 6.3C**).



6.3.3 Effect of AT-101 on cellular apoptosis and cell cycle

Cellular apoptosis in UM-SCC-17B cancer cells was determined after 48 and 72 hour treatment with AT-101 at IC_{25} , IC_{50} , and IC_{75} by PI staining followed by flow cytometry analysis. As shown in **Figure 6.4A**, percentage of apoptotic cells increased from 4, 8, to 21% at 48 hours and increased from 5, 30, to 47% at 72 hours with the concentration of AT-101 increased from IC_{25} , IC_{50} , and IC_{75} . In addition, analysis of cell cycle shows that

treatment with AT-101 also induced cell arrest in G₁ phase and inhibition of cell growth as indicated by decreased cellular mitosis (**Figure 6.4B&C, Table 6.1**). These results suggest that AT-101 inhibited cell survival through both enhanced cellular apoptosis and reduced cell growth.

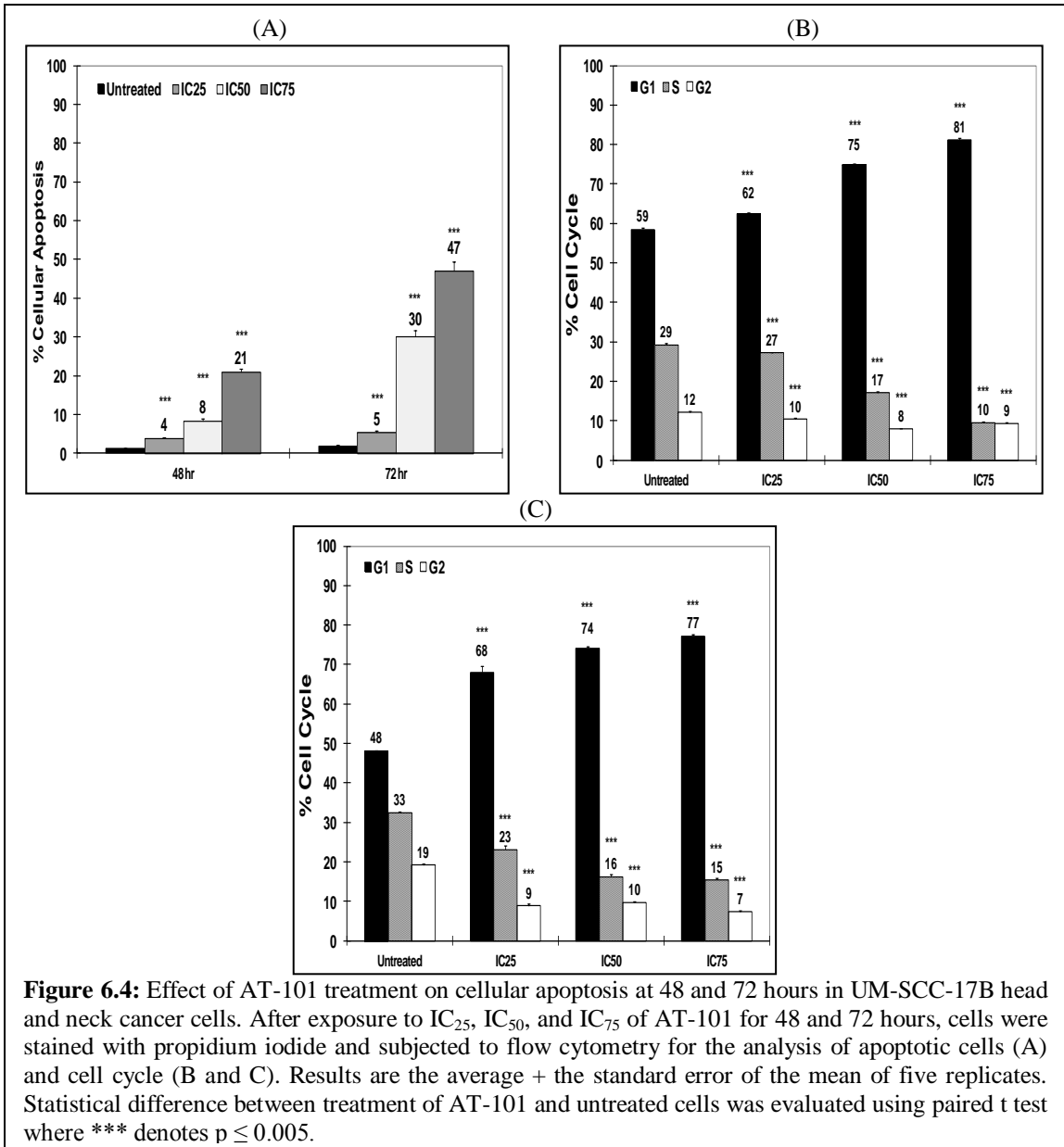


Table 6.1: Cell cycle distribution and mitotic index of UM-SCC-17B cells after treatment with AT-101

AT-101	Cell cycle phases (% of cells)			Mitotic index (S+G ₂ /G ₁)	AT-101	Cell cycle phases (% of cells)			Mitotic index (S+G ₂ /G ₁)
	G ₁	S	G ₂			G ₁	S	G ₂	
	48 hr					72 hr			
Untreated	59	29	12	0.69	Untreated	48	33	19	1.08
AT-101_IC₂₅	62	27	10	0.60	AT-101_IC₂₅	68	23	9	0.47
AT-101_IC₅₀	75	17	8	0.33	AT-101_IC₅₀	74	16	10	0.35
AT-101_IC₇₅	81	10	9	0.23	AT-101_IC₇₅	77	15	7	0.29

6.3.4 Effect of combination treatment on cell growth

After incubation of UM-SCC-17B cancer cells with AT-101 at IC₂₅ alone or with AT-101 and “smart” particles that encapsulate anti-Bcl-2 siRNA molecules for 48 and 72 hours, the percentage of live cells was evaluated by SRB assay and normalized to untreated cells. As shown in **Figure 6.5**, AT-101 alone induced 23 and 21% cell death at 48 and 72 hours, respectively. Combination treatment with AT-101 and “smart” particles encapsulating anti-Bcl-2 siRNA molecules induced 63 and 75% cell death at 48 and 72 hours, respectively, while treatment with AT-101 and “smart” particles encapsulating a scrambled siRNA sequence did not further increase cell death compared to AT-101 treatment alone. Synergistic effects were observed when UM-SCC-17B cancer cells were treated with both AT-101 and anti Bcl-2 siRNA molecules. These results proved that knockdown of Bcl-2 expression using siRNA coupled with AT-101 treatment could inhibit cancer cell growth.

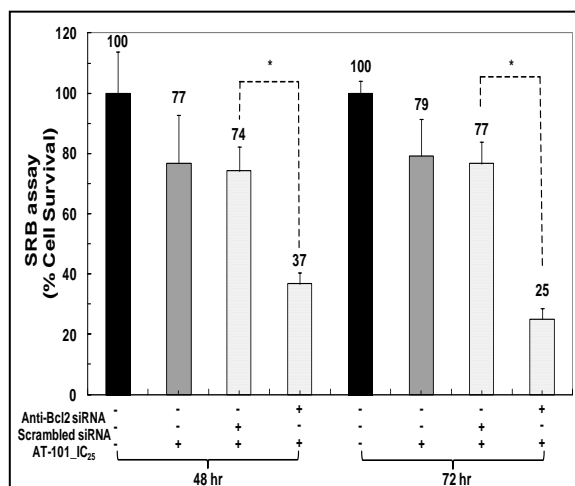


Figure 6.5: Effect of AT-101 and “smart” nanoparticles prepared by complexation of β -CD-P(HMA-co-DMAEMA-co-TMAEMA)_{4,8} star-shaped polymer with 0.57 μ g of the anti-Bcl-2 siRNA (+) or scrambled siRNA (-) at an N/P (+/-) ratio of 2.5/1 on cell survival at 48 and 72 hours in UM-SCC-17B head and neck cancer cells. The cell survival was determined by SRB assay, and the results are the average + the standard error of the mean of triplicates. Statistical difference between particles encapsulating anti-Bcl-2 siRNA (+) and scrambled siRNA (-) was evaluated using paired t test where * denotes $p \leq 0.05$. Combinatorial index (CI) was calculated for each experimental condition. Pound sign (#) depicts synergistic effect (CI<0.9).

6.3.5 Effect of combination treatment on cellular apoptosis

We evaluated the cellular apoptosis and cell cycle of UM-SCC-17B cells after treatment with “smart” particles loaded with anti-Bcl-2 siRNA and AT-101 (IC₂₅) for 48 and 72 hours using PI staining followed by flow cytometry analysis. Results show that AT-101 alone induced only 4 and 3% cellular apoptosis at 48 and 72 hours, respectively (**Figure 6.6A**). Treatment with AT-101 and “smart” particles loaded with anti-Bcl-2 siRNA molecules further increased apoptotic cells to 12 and 14% at 48 and 72 hours, respectively, which is significantly higher than treatment with AT-101 and “smart” particles loaded with a scrambled siRNA sequence. In addition, combination treatment with both AT-101 and “smart” particles encapsulating anti-Bcl-2 siRNA molecules caused cell arrest in G₁ phase of 76 and 75% at 48 and 72 hours, respectively (**Figure 6.6B**). This population is significantly higher than the cells treated with AT-101 alone (62

and 65%) or treated with AT-101 and “smart” particles encapsulating scrambled siRNA molecules (68%). Calculation of mitotic index also shows that the proliferation of UM-SCC-17B cancer cells decreased after combination treatment AT-101 and Bcl-2 knockdown (**Table 6.2**). The results indicated that Bcl-2 gene suppression using siRNA coupled with AT-101 treatment could enhance cellular apoptosis and decrease cell mitosis, which collectively inhibit cancer cell growth.

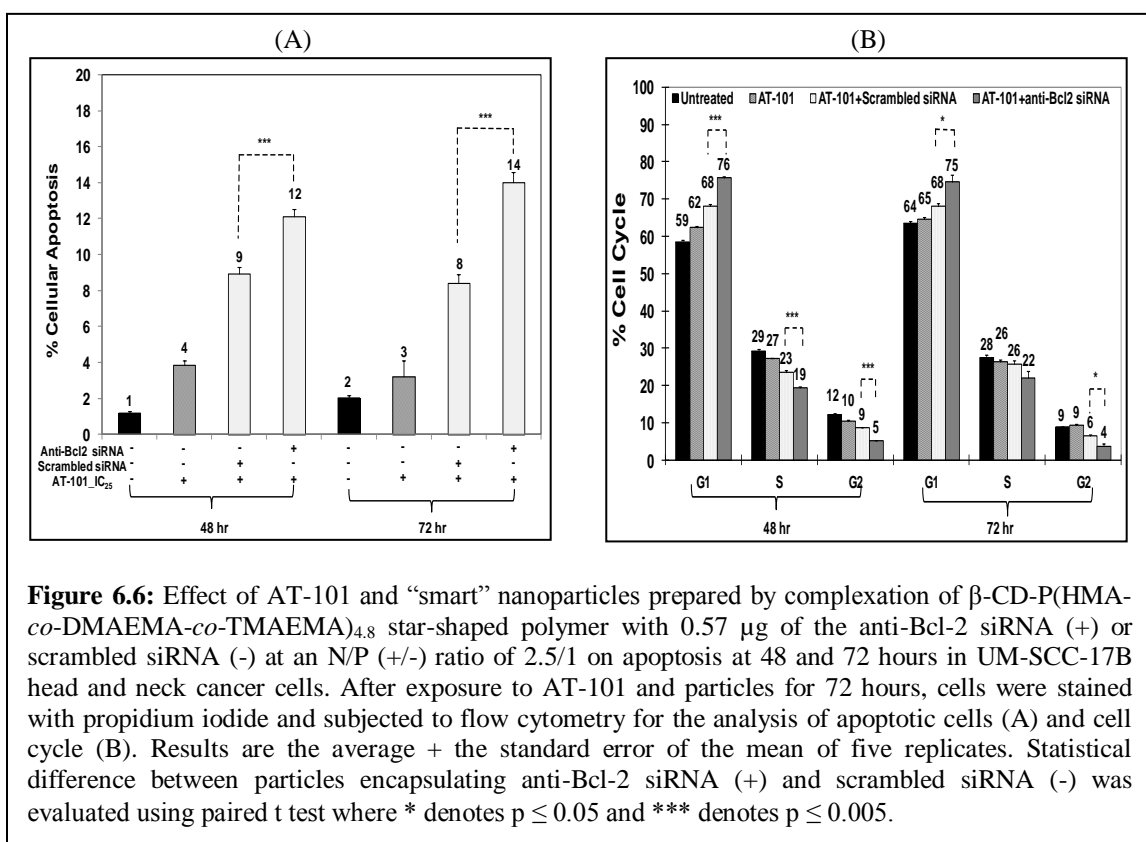


Table 6.2: Cell cycle distribution and mitotic index of UM-SCC-17B cells after combination treatment with AT-101 and “smart” particles encapsulating anti-Bcl2 (+) or scrambled (-) siRNA molecules

	Cell cycle phases (% of cells)				Mitotic index (S+G ₂ /G ₁)		Cell cycle phases (% of cells)				Mitotic index (S+G ₂ /G ₁)
	G ₁ S G ₂			G ₁ S G ₂							
	48 hr						72 hr				
Untreated	59	29	12	0.69	Untreated	64	28	9	0.58		
AT-101_IC ₂₅	62	27	10	0.60	AT-101_IC ₂₅	65	26	9	0.54		
Scrambled siRNA + AT-101_IC ₂₅	68	23	9	0.47	Scrambled siRNA + AT-101_IC ₂₅	68	26	6	0.47		
Bcl-2 siRNA + AT-101_IC ₂₅	76	19	5	0.32	Bcl-2 siRNA + AT-101_IC ₂₅	75	22	4	0.35		

6.4 Discussion

Previous studies have shown that we successfully designed and synthesized a series of degradable, pH-sensitive, membrane-destabilizing, star-shaped polymers.¹⁰ These polymers can shuttle a large dose of model siRNA molecules past the endosomal membrane and into the cytoplasm of multiple cell types, including HeLa cervical cancer cells, UM-SCC-17B head and neck cancer cells, and MCF-10A normal mammary epithelial cells. In this study, we wanted to see if these pH-sensitive “smart” polymers can deliver therapeutic anti-Bcl-2 siRNA molecules into UM-SCC-17B cancer cells to selectively suppress Bcl-2 gene expression. In addition, we evaluated the potential of combining Bcl-2 knockdown using “smart” particles loaded with anti-Bcl-2 siRNA molecules with a BH3-mimetic drug (AT-101) to induce apoptotic cell death.

6.4.1 Effect of “smart” particles on Bcl-2 expression

Results show that the gene silencing effect of “smart” star-shaped particles loaded with anti-Bcl-2 siRNA molecules, which is determined based on the inhibition of Bcl-2 expression at protein and mRNA levels in UM-SCC-17B cancer cells, can last for at least 72 hours *in vitro*. This result matches earlier studies showing that Bcl-2 expression was

largely inhibited after 48-72 hour treatment with antisense oligodeoxynucleotide (ASODN), but gradually recovered after 96 hour.¹³ Therefore, we chose to evaluate the effect of Bcl-2 suppression on cell growth and cellular apoptosis after treatment with Bcl-2 “smart” particles for 48 and 72 hours.

6.4.2 Effect of AT-101 on cellular apoptosis and cell cycle

The IC₅₀ of AT-101 was 2.88 and 1.69 μ M in UM-SCC-17B at 48 and 72 hours, respectively, which is similar to earlier studies.¹¹ Treatment of head and neck cancer cells with AT-101 alone with the increased concentration of IC₂₅, IC₅₀, and IC₇₅ caused increased apoptotic cell death based on the analysis of PI staining. This is due to the binding of AT-101, a BH3-mimetic small molecule inhibitor, to the BH3 binding groove of anti-apoptotic Bcl-2 proteins, which prevents the heterodimerization between Bcl-2 and other pro-apoptotic proteins (such as Bad, Bim, Bax), therefore allowing the cells go apoptosis.^{4,14} In addition, results show that AT-101 can also increase the G₁-phase cell cycle arrest to prevent cell growth, probably through regulating the expression of cell cycle regulatory proteins retinoblastoma (Rb) and cyclin D1.¹⁵ This suggests that treatment of AT-101 can inhibit cell growth by both increase of cellular apoptosis and inhibition of cell proliferation.

6.4.3 Effect of combination treatment on cell growth, cellular apoptosis, and cell cycle

Investigating the effect of treatment with both AT-101 and “smart” particles loaded with anti-Bcl-2 siRNA molecules, UM-SCC-17B cell growth was inhibited 2-3 folds more comparing to treatment with AT-101 alone. The synergistic effect of Bcl-2 knockdown using siRNA molecules and AT-101 suggests that Bcl-2 gene silencing can sensitize

cancer cells to BH-3 mimetic drugs, which decreases the dose of AT-101 and the associated toxicity. In addition, simultaneously treatment with AT-101 and “smart” particles encapsulating anti-Bcl-2 siRNA molecules in UM-SCC-17B enhanced cellular apoptosis and G₁-phase cell cycle arrest, which collectively leads to reduced cancer cell growth. Overall, UM-SCC-17B cell survival was significantly decreased to 25% after combination treatment for 72 hours, which proves the potential of combining both Bcl-2-targeted strategies, including Bcl-2 gene silencing and BH3- mimetic drugs, to treat head and neck cancer with less adverse side effects.

6.5 Conclusions

In summary, we proved the degradable, pH-sensitive, star-shaped polymers can successfully deliver anti-Bcl-2 siRNA molecules into the cytoplasm of head and neck cancer cells and inhibit Bcl-2 expression at both protein and mRNA levels. In addition, simultaneously inhibit Bcl-2 function by using siRNA molecules and AT-101 was shown to synergistically inhibit cancer cell growth due to induction of cellular apoptosis and G₁ phase cell cycle arrest. These results collectively suggest the potential of combining two Bcl-2 targeted therapeutic strategies to inhibit tumor cell growth and restore their radio- and chemo-sensitivity for effective head and neck cancer therapy.

References

- (1) Argiris, A.; Karamouzis, M. V.; Raben, D.; Ferris, R. L. *Lancet* **2008**, *371*, 1695.
- (2) Jemal, A.; Siegel, R.; Xu, J. Q.; Ward, E. *Ca-Cancer J Clin* **2010**, *60*, 277.
- (3) (a) Adelstein, D. J.; Li, Y.; Adams, G. L.; Wagner, H., Jr.; Kish, J. A.; Ensley, J. F.; Schuller, D. E.; Forastiere, A. A. *J Clin Oncol* **2003**, *21*, 92. (b) Cooper, J. S.; Pajak, T. F.; Forastiere, A. A.; Jacobs, J.; Campbell, B. H.; Saxman, S. B.; Kish, J. A.; Kim, H. E.; Cmelak, A. J.; Rotman, M.; Machtay, M.; Ensley, J. F.; Chao, K. S.; Schultz, C. J.; Lee, N.; Fu, K. K. *N Engl J Med* **2004**, *350*, 1937.
- (4) Oliver, C. L.; Bauer, J. A.; Wolter, K. G.; Ubell, M. L.; Narayan, A.; O'Connell, K. M.; Fisher, S. G.; Wang, S.; Wu, X.; Ji, M.; Carey, T. E.; Bradford, C. R. *Clin Cancer Res* **2004**, *10*, 7757.
- (5) (a) Reed, J. C. *Curr Opin Oncol* **1999**, *11*, 68. (b) Reed, J. C. *J Clin Oncol* **1999**, *17*, 2941.
- (6) Kaufmann, S. H.; Gores, G. J. *Bioessays* **2000**, *22*, 1007.
- (7) (a) Jansen, B.; Schlagbauer-Wadl, H.; Brown, B. D.; Bryan, R. N.; van Elsas, A.; Muller, M.; Wolff, K.; Eichler, H. G.; Pehamberger, H. *Nat Med* **1998**, *4*, 232. (b) Kymionis, G. D.; Dimitrakakis, C. E.; Konstadoulakis, M. M.; Arzimanoglou, I.; Leandros, E.; Chalkiadakis, G.; Keramopoulos, A.; Michalas, S. *J Surg Res* **2001**, *99*, 161.
- (8) (a) Kaneko, T.; Zhang, Z.; Mantellini, M. G.; Karl, E.; Zeitlin, B.; Verhaegen, M.; Soengas, M. S.; Lingen, M.; Strieter, R. M.; Nunez, G.; Nor, J. E. *Cancer Res* **2007**, *67*, 9685. (b) Sharma, H.; Sen, S.; Lo Muzio, L.; Mariggio, A.; Singh, N. *Cancer Biol Ther* **2005**, *4*, 720.
- (9) (a) Jere, D.; Jiang, H. L.; Arote, R.; Kim, Y. K.; Choi, Y. J.; Cho, M. H.; Akaike, T.; Cho, C. S. *Expert Opin Drug Deliv* **2009**, *6*, 827. (b) Lai, W. F.; Lin, M. C. *J Control Release* **2009**, *134*, 158. (c) Midoux, P.; Pichon, C.; Yaouanc, J. J.; Jaffres, P. A. *Br J Pharmacol* **2009**, *157*, 166.
- (10) Yasemin Yuksel Durmaz, Y.-L. L., and Mohamed E. H. ElSayed *Advanced Functional Materials* (submitted).
- (11) Imai, A.; Zeitlin, B. D.; Visioli, F.; Dong, Z. H.; Zhang, Z. C.; Krishnamurthy, S.; Light, E.; Worden, F.; Wang, S. M.; Nor, J. E. *Cancer Res* **2012**, *72*, 716.
- (12) Neiva, K. G.; Zhang, Z.; Miyazawa, M.; Warner, K. A.; Karl, E.; Nor, J. E. *Neoplasia* **2009**, *11*, 583.
- (13) Buck, A. C.; Shen, C. X.; Schirrmeister, H.; Schmid-Kotsas, A.; Munzert, G.; Guhlmann, A.; Mehrke, G.; Klug, N.; Gross, H. J.; Bachem, M.; Reske, S. N. *Cancer Biother Radio* **2002**, *17*, 281.
- (14) Ashimori, N.; Zeitlin, B. D.; Zhang, Z.; Warner, K.; Turkienicz, I. M.; Spalding, A. C.; Teknos, T. N.; Wang, S.; Nor, J. E. *Mol Cancer Ther* **2009**, *8*, 893.
- (15) Ligueros, M.; Jeoung, D.; Tang, B.; Hochhauser, D.; Reidenberg, M. M.; Sonenberg, M. *Br J Cancer* **1997**, *76*, 21.

Chapter 7.

Conclusions & future direction

7.1 Conclusions

7.1.1 “Smart” pH-sensitive, comb-like polymers

In the studies of the development of degradable, pH-sensitive, membrane-stabilizing, comb-like polymers, we successfully synthesized a series of “smart” comb-like polymers that can encapsulate siRNA molecules into nuclease- and serum-stable particles at physiological pH, and be internalized into cells through adsorptive endocytosis. These particles hydrolyze into membrane-active fragments upon exposure to acidic endosomal gradients, leading to cytoplasmic release of siRNA molecules and functional gene knockdown. In these polymers, we incorporated acid-labile hydrazone linkages to allow controlled grafting a large number of hydrophobic hexyl methacrylate (HMA) and cationic trimethyl aminoethyl methacrylate (TMAEMA) polymer chains to the backbone of copolymers of pH-sensitive ethyl acrylic acid (EAA) and hydrophobic butyl methacrylate (BMA). This design enabled the comb-like polymers to carry a large dose of DNA/RNA molecules with high therapeutic loading, but degrade into small fragments, which can be easily eliminated *in vivo* by renal excretion, after escape from endosomal/lysosomal trafficking. Overall, the cytotoxicity of comb-like polymers can be largely decreased due to their high drug loading preventing the use of excess cationic

carriers, and non-specific accumulation in human body. However, there are some limitations in these comb-like polymers for *in vivo* application. First, they cannot selectively deliver therapeutic cargo into diseased cells. Second, they will be rapidly recognized by macrophage and cleared from blood circulation by reticuloendothelial system due to their positive surface charge. Third, they cannot co-deliver other drugs, such as chemotherapeutic drugs, at the same time to promote cancer cell death. Therefore, we tried to solve the above limitations by design and synthesis of another series of degradable, pH-sensitive, membrane-destabilizing, star-shaped polymeric carriers.

7.1.2 “Smart” pH-sensitive, star-shaped polymers

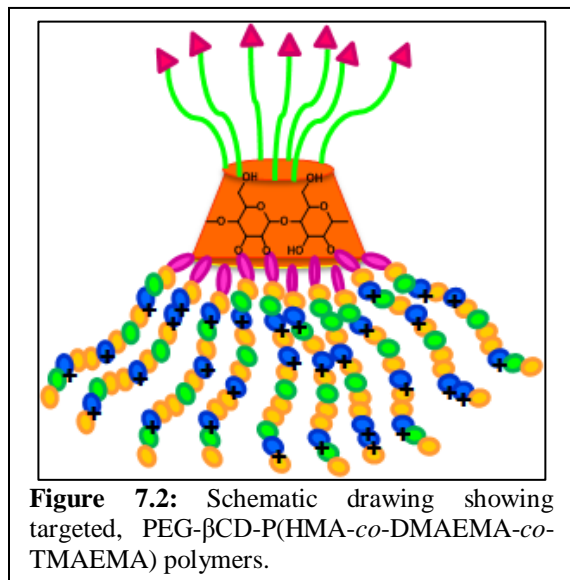
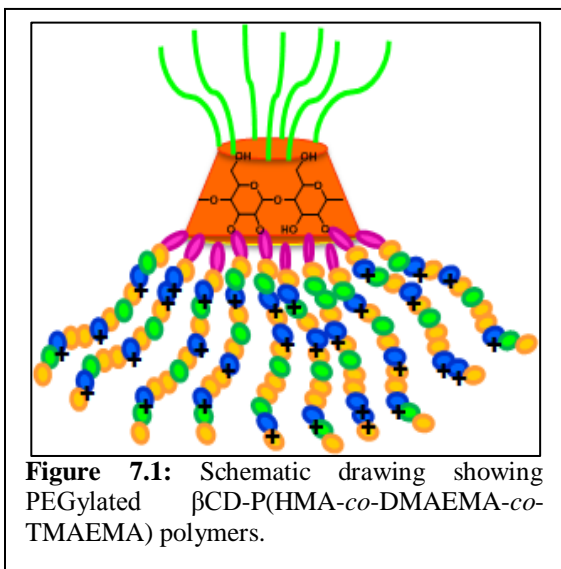
We utilize β -cyclodextrin (β -CD), which is a FDA-approved, cone-shaped oligosaccharide composed of seven glucose units as the core for the star-shaped vectors. The seven primary hydroxyl groups on the primary face of the core of β -CD and the fourteen secondary hydroxyl groups on the secondary face have different chemical reactivity; therefore, allow us to graft amphiphilic membrane-destabilizing polymers from the secondary face of the β -CD core via acid-labile hydrazone linkages while leaving the primary face for further modification. We controlled the molecule weight (25 and 40 kDa) and hydrophobic/hydrophilic ratio (50/50 and 75/25) of the grafted polymers to investigate the effect of the molecular weight and the hydrophobic/hydrophilic balance of these membrane-active fragments on the endosomal escape capacity. In addition, we explored the possibility of combining two endosomal escape mechanism, including hydrophobic membrane disruption with endosomal burst, to enhance cytoplasmic release of siRNA molecules by modulation of the ratio of DMAEMA/TMAEMA in the grafts. For the first time, we systemically identified the key parameters for the design of an ideal

star-shaped vector and proved the combination of two endosomal escape effects based on the gene knockdown efficiency. Further, we showed that successful Bcl-2 inhibition by star-shaped polymers encapsulating siRNA molecules can sensitize head and neck cancer cells to the treatment of small molecule inhibitor, which synergistically inhibits cancer cell growth and induces cancer cell apoptosis. Bcl-2-targeted therapy by both gene silencing and BH3-mimetic compound, therefore, is an applicable strategy to treat head and neck cancer. It is important to mention that these degradable, pH-sensitive, membrane-destabilizing, star-shaped vectors remain the potential to incorporate hydrophilic polyethylene glycol (PEG) grafts on their primary face, which prolongs their plasma residence time and prevents non-specific distribution into tissues, such as liver, spleen, and lung. In addition, the incorporated hydrophilic PEG grafts allows the conjugation of targeting ligands, so the vectors can selectively deliver therapeutic DNA/RNA molecules into diseased cells without causing potential adverse side effects to normal cells. Further, water-soluble β -CD-based vectors have a relatively hydrophobic interior, which enables the inclusion of a large variety of hydrophobic drugs, such as chemotherapeutic drugs and small molecule inhibitors.¹ Therefore, these star-shaped carriers can be utilized to simultaneously deliver therapeutic nucleic acids and therapeutic drugs to targeted cells for enhanced cancer treatment.

7.2 Future directions

In order to translate the degradable, pH-sensitive, membrane-destabilizing, star-shaped vectors into clinic application for head and neck cancer therapy, we will develop a new family of targeted, degradable, biocompatible, and star-shaped vectors to deliver therapeutic anti-Bcl-2 siRNA molecules into the cytoplasm of tumor cells. To be specific,

we will conjugate hydrophilic PEG to the primary face of β -CD via non-degradable linkages to prepare an asymmetric, star-shaped, pH-sensitive polymer (**Figure 7.1**). We will conjugate the synthetic GE11 peptide (YHWYGYTPQNVI) to the free ends of PEG chains to function as a targeting ligand for the epidermal growth factor receptor (EGFR) (**Figure 7.2**),² which is over-expressed on the surface of > 80% of head and neck cancer cells.³ We hypothesize that the proposed asymmetric, pH-sensitive, membrane-destabilizing polymers can complex a large dose of anti-Bcl-2 siRNA into serum- and nuclease-stable “smart” particles that: i) escape recognition and entrapment by the reticular endothelial system (liver, lungs, spleen) and exhibit long residence time in the systemic circulation, ii) preferentially accumulate in the tumor tissues, iii) selectively internalized by head and neck cancer cells, iv) successfully shuttle their RNA cargo into the cytoplasm to knockdown Bcl-2 gene expression and sensitize head and neck cancer cells to BH3-mimetic drugs, v) encapsulate hydrophobic therapeutic drugs into the cavity of β -CD core and release drugs in the tumor cells.



7.2.1 Development of EGFR-targeted, PEG- β CD-P(HMA-*co*-DMAEMA-*co*-TMAEMA) polymers

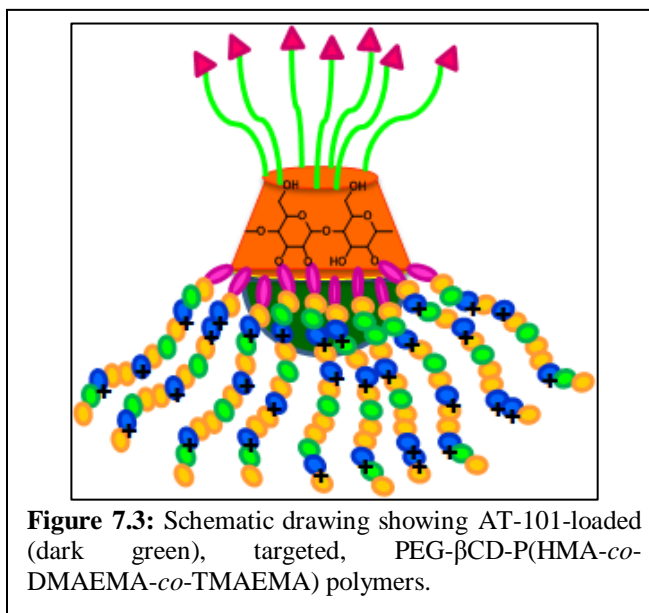
Incorporation of hydrophilic PEG monomers in the design of nucleic acid carriers has been proved to prevent the cationic vectors be recognized by macrophages and be rapidly cleared through the reticular endothelial systems.⁴ The PEG brush displayed on the surface of carriers can also protect the therapeutic cargo from enzymatic degradation, decrease the non-specific cytotoxicity of carriers, and prevent their non-specific distribution in human body.⁵ However, the incorporated PEG grafts has been shown to affect the complexation between vectors and DNA/RNA molecules.⁵ The hydrophilic PEG brush also decreases the endocytosis of particles into target cells.⁵ Therefore, it is important to determine the optimum number and length of PEG grafts that are conjugated from the primary surface of our well-established star-shaped polymers. The number of targeting peptides conjugated on the PEG also needs to be controlled to enhance cellular uptake through receptor-mediated endocytosis without affecting particle's *in vivo* stability. We will synthesize a series of EGFR-targeted and non-targeted PEG- β CD-P(HMA-*co*-DMAEMA-*co*-TMAEMA) polymers with different PEG molecular weight (2, and 5 kDa), different numbers of conjugated PEG chains (3-6) per β -CD, and different numbers of GE11 peptides attached per β -CD carriers. We will compare the complexation of β CD-P(HMA-*co*-DMAEMA-*co*-TMAEMA), PEG- β CD-P(HMA-*co*-DMAEMA-*co*-TMAEMA), and GE11-PEG- β CD-P(HMA-*co*-DMAEMA-*co*-TMAEMA) polymers with anti-Bcl-2 siRNA as a function of the N/P (+/-) ratio. We will also investigate the physicochemical properties of the formed “smart” particles in terms of size, surface charge, and stability upon incubation with serum proteins and nuclease

enzymes to identify key parameters that reduce particle size and surface charge and increase their stability. We will evaluate the uptake of GE11-targeted and non-targeted “smart” particles into UM-SCC-17B head and neck cancer cells compared to commercial transfection agent, siPORT amine-based particles to identify the critical parameters (e.g. length and number of PEG grafts, number of GE11 peptides, etc.) required for efficient particle internalization by cancer cells. We will also compare the anticancer activity of GE11-targeted and non-targeted “smart” particles and siPORT amine-based particles based on their ability to: a) knockdown Bcl-2 expression, and b) induce apoptosis of head and neck cancer cells.

7.2.2 Development of GE-11-targeted, PEG- β CD-P(HMA-*co*-DMAEMA-*co*-TMAEMA) polymers with Bcl-2 small molecule inhibitor inclusion

Bcl-2 small molecule inhibitors have been proved induce cell apoptosis by occupying the hydrophobic groove of anti-apoptotic proteins to prevent their binding to pro-apoptotic proteins.⁶ For example, AT-101 is a BH3-mimetic compound, which shows high affinity to the anti-apoptotic Bcl-2 proteins, and therefore sensitizes head and neck cancer cells to chemotherapeutic drugs and enhances apoptotic cell death.⁷ However, the low aqueous solubility and non-specific toxicity of hydrophobic small molecule inhibitors makes it difficult to be developed as drug.¹ In order to overcome the limitations, we plan to use the EGFR-targeted, PEG- β CD-P(HMA-*co*-DMAEMA-*co*-TMAEMA) polymers to encapsulate AT-101 in the cavity to improve their solubility and prevent non-specific distribution (**Figure 7.3**). β -CD is a water-soluble molecule, which has been widely used to produce inclusion complexes with various hydrophobic drugs.⁸ We will evaluate the ability of GE-11-targeted, PEG- β CD-P(HMA-*co*-DMAEMA-*co*-TMAEMA) polymers to

encapsulate AT-101 and deliver them into subcellular targets without affecting their therapeutic effects. We will compare the complexation with anti-Bcl-2 siRNA molecules and the size, zeta potential, and cellular uptake of formed particles before and after the encapsulation of AT-101. We will also investigate the anticancer activity of co-delivery of anti-Bcl-2 siRNA molecules and AT-101 using GE-11-targeted, PEG- β CD-P(HMA-co-DMAEMA-co-TMAEMA) polymers based on their ability to: a) knockdown Bcl-2 expression, and b) induce apoptosis of head and neck cancer cells.



7.2.3 *In vivo* evaluation of “smart” particles

For clinical application, we need to prove that targeted, PEG- β CD-P(HMA-co-DMAEMA-co-TMAEMA) polymers can escape recognition and entrapment by the reticular endothelial system (liver, lungs, spleen) and exhibit long residence time in the systemic circulation, preferentially accumulate in the tumor tissues, and selectively internalized by head and neck cancer cells. We will investigate the biodistribution of GE-11-targeted, and non-targeted “smart” particles loaded with anti-Bcl-2 siRNA in nude

tumor-bearing mice to a) examine the relationship between the number of GE-11 peptides/particle on its distribution, accumulation, and retention in tumor tissue, and b) identify the particle(s) that exhibit highest accumulation and retention in tumor tissue. The “smart” particles that deliver > 25% of the loaded siRNA dose into tumor tissues will be used in the subsequent *in vivo* experiment. We will also investigate the anti-tumor activity of the particles identified in the biodistribution experiments based on their ability to a) suppress Bcl-2 expression and b) decrease tumor size. Particles that produce > 50% knockdown in Bcl-2 expression in head and neck cancer cells, and achieve > 50% reduction in tumor size will be considered effective.

References

- (1) Zhang, Z.; Wu, G.; Gao, J.; Song, T. *Mol Pharm* **2010**, *7*, 1348.
- (2) (a) Li, Z.; Zhao, R.; Wu, X.; Sun, Y.; Yao, M.; Li, J.; Xu, Y.; Gu, J. *Faseb J* **2005**, *19*, 1978. (b) Milane, L.; Duan, Z.; Amiji, M. *Mol Pharm* **2011**, *8*, 185.
- (3) (a) Goerner, M.; Seiwert, T. Y.; Sudhoff, H. *Head Neck Oncol* **2010**, *2*, 8. (b) Kundu, S. K.; Nestor, M. *Tumour Biol* **2012**, *33*, 707.
- (4) van Vlerken, L. E.; Vyas, T. K.; Amiji, M. M. *Pharm Res* **2007**, *24*, 1405.
- (5) Jokerst, J. V.; Lobovkina, T.; Zare, R. N.; Gambhir, S. S. *Nanomedicine (Lond)* **2011**, *6*, 715.
- (6) Paoluzzi, L.; Gonen, M.; Gardner, J. R.; Mastrella, J.; Yang, D.; Holmlund, J.; Sorensen, M.; Leopold, L.; Manova, K.; Marcucci, G.; Heaney, M. L.; O'Connor, O. A. *Blood* **2008**, *111*, 5350.
- (7) Imai, A.; Zeitlin, B. D.; Visioli, F.; Dong, Z. H.; Zhang, Z. C.; Krishnamurthy, S.; Light, E.; Worden, F.; Wang, S. M.; Nor, J. E. *Cancer Research* **2012**, *72*, 716.
- (8) Carrier, R. L.; Miller, L. A.; Ahmed, I. *J Control Release* **2007**, *123*, 78.

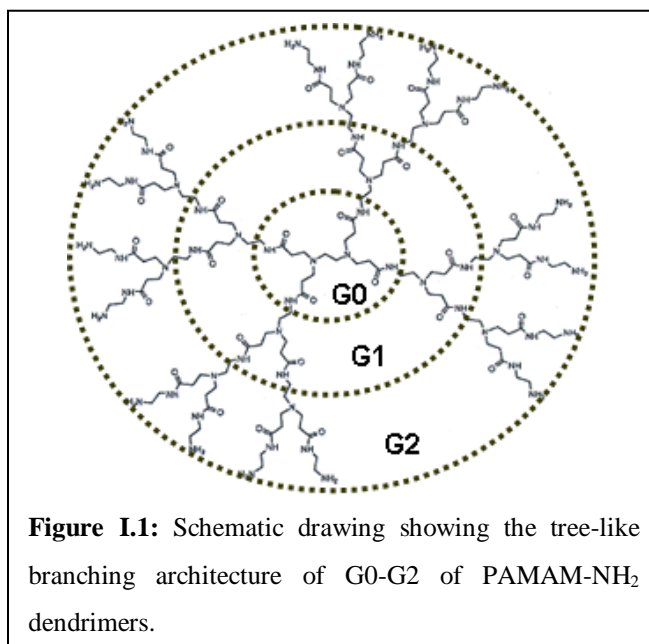
Appendix I.

Quantitative evaluation of the effect of poly (amidoamine) dendrimers on the porosity of Caco-2 cell monolayers

I.1 Introduction

Oral delivery is the most desirable route for drug administration due to lower healthcare cost and higher patient compliance compared to other routes.¹ However, oral absorption of polymeric drug delivery systems such as polymeric particles and polymer-drug conjugates remains a significant challenge.² Currently, oral drug delivery using polymeric carriers is limited to mucosal vaccination where natural or synthetic polymers encapsulate different antigens forming stable micro- or nano-particles, which are recognized, internalized, and processed by Peyer's patches in the lower ileum to induce a systemic and/or mucosal immune response.³ To date, there are no polymeric drug delivery systems that are effectively absorbed from the gastrointestinal tract. This can be

attributed to the large size and molecular weight of the polymeric carriers, which hinder their diffusion across the intestinal epithelium into the systemic blood circulation⁴.



Poly (amidoamine) (PAMAM) dendrimers are a family of water-soluble polymers that is characterized by a unique tree-like branching architecture and a compact spherical geometry in solution (**Table I.1 & Figure I.1**).⁵

The potential of PAMAM dendrimers in controlled drug delivery stems from their large number of surface groups, which can be utilized to immobilize drugs, enzymes, antibodies or other bioactive agents providing a high density of biological agents in a compact therapeutic system.⁶ For example, phospholipids were conjugated to the NH₂ surface groups of generation 4 (G4) to prepare a hydrophilic-hydrophobic core-shell

structure that successfully entrapped the 5-fluorouracil anticancer drug.⁷ This formulation showed a sustained release of the encapsulated drug *in vitro* and enhanced its oral absorption via the lymphatic system *in vivo*.⁷ PAMAM dendrimers have also been used to enhance the oral absorption of drug molecules that are substrates of the P-glycoprotein (P-gp) efflux pump.⁸ Several PAMAM-drug conjugates proved to enhance the aqueous solubility and oral absorption of the incorporated drugs both *in vitro* and *in vivo* by escaping the P-gp efflux pump.⁹ Similarly, physical mixtures of doxorubicin with the cationic PAMAM-NH₂ (G3) dendrimers showed enhanced uptake by Caco-2 cell monolayers and increased oral bioavailability *in vivo*.¹⁰

Table I.1: The physicochemical properties of mannitol and PAMAM dendrimers.

Probe	Molecular Weight ^a (Da)	Radius ^a (Å)	Number of Surface Groups ^a	Surface Functionality ^a	Valency ^b	Diffusion Coefficient ^c ($\times 10^6$ cm ² /s at 37 °C)
Mannitol	182	4.1	-	-	-	6.20
G0-NH ₂	517	15	4	NH ₂	1	1.70
G1-NH ₂	1430	22	8	NH ₂	2	1.15
G2-NH ₂	3256	29	16	NH ₂	4	0.88
G3-NH ₂	6909	36	32	NH ₂	7	0.71
G4-NH ₂	14,215	45	64	NH ₂	14	0.56
G2-OH	3272	29	16	OH	-	0.88
G3-OH	6941	36	32	OH	-	0.71
G4-OH	14,279	45	64	OH	-	0.56
G-0.5-COOH	436	-	4	COOH	1	-
G0.5-COOH	1269	9.2	8	COOH	2	2.76
G1.5-COOH	2935	12.8	16	COOH	4	1.98
G2.5-COOH	6267	14.7	32	COOH	7	1.73
G3.5-COOH	12,931	24.5	64	COOH	14	1.04
G4.5-COOH	26,258	31.0	128	COOH	28	0.82

^a Reported by Tomalia et al.⁵ and Dubin et al.¹¹

^b Number of ionized surface groups calculated using the Henderson-Hasselbalch equation.¹²

^c The diffusion coefficient is calculated based on Stokes-Einstein equation.¹³

Earlier studies by El-Sayed and coworkers established a clear relationship between the size, molecular weight, surface chemistry, and net charge of PAMAM dendrimers and their transport across Caco-2 cell monolayers.¹⁴ These studies showed that small cationic PAMAM-NH₂ dendrimers (G0-G2) exhibit moderate to high permeability across Caco-2 cell monolayers, which increased with the increase in dendrimers concentration, incubation time, and generation number.^{14a} The decline in the transepithelial electrical resistance (TEER) coupled with the increase in mannitol's paracellular permeability across Caco-2 cell monolayers indicated the effect of cationic G0-G2 on the integrity of the epithelial tight junctions.^{14a,b} Anionic G2.5 and G3.5 PAMAM-COOH dendrimers caused an increase in mannitol permeability and a decrease in TEER values across Caco-2 cell monolayers compared to neutral PAMAM-OH dendrimers, which exhibited no effect of the integrity of Caco-2 cells.^{14b} These results indicated that cationic G0-G2 and anionic G2.5 and G3.5 dendrimers can be utilized as polymeric carriers for oral drug delivery. Subsequent studies focused on elucidating the mechanism(s) of transport of PAMAM dendrimers across the intestinal epithelium. Microscopic studies revealed that fluorescently-labeled cationic (G2 and G4) and anionic (G1.5 and G3.5) dendrimers permeate across Caco-2 cell monolayers by a combination of paracellular transport that is associated with reorganization of tight junction proteins^{14c,15} and transcellular transport

via endocytosis.¹⁵⁻¹⁶ Earlier studies have established the relationship between paracellular permeability and the changes in pore size of intercellular tight junctions using small molecular weight molecules.^{13,17} In this manuscript, we use a similar approach to mathematically calculate the changes in porosity of Caco-2 cell monolayers as a function of concentration, incubation time, generation number, surface chemistry, and net charge of PAMAM dendrimers to quantitatively delineate the effect of PAMAM dendrimers on paracellular diffusion across intestinal epithelial barriers.

I.2 Methods

I.2.1 The relationship between porosity and the paracellular permeability across Caco-2 cell monolayers

Electron micrographs of the paracellular space in Caco-2 monolayers show the presence of two barriers in series; the tight junctions (length < 0.1 μm) followed by a relatively long and tortuous lateral space ($\sim 20 \mu\text{m}$ cell height and $\sim 75 \text{ \AA}$ gap width with a tortuosity factor of 2.0-2.5).¹⁸ Since the radius of the tight junction is 12 \AA and the gap width of the tortuous lateral space is approximately 75 \AA , the tight junction is considered the rate-limiting barrier for diffusion of different molecules across the paracellular space.¹⁹ We hypothesize that the observed increase in mannitol paracellular permeability

across Caco-2 cell monolayers upon incubation with selected cationic and anionic PAMAM dendrimers is due to changes in the conformation of the tight junctions associated with an increase in the size of tight junctional pores. We are using the Renkin function for cylindrical channels (equation 1),¹⁹ which compares the molecular radius (r) of the diffusing probe to the radius of the paracellular pores (R) to mathematically calculate the changes in tight junctional pore size in response to PAMAM dendrimers.

$$F\left(\frac{r}{R}\right) = \left[1 - \left(\frac{r}{R}\right)\right]^2 \left[1 - 2.104\left(\frac{r}{R}\right) + 2.09\left(\frac{r}{R}\right)^3 - 0.95\left(\frac{r}{R}\right)^5\right] \quad (1)$$

Using the Renkin function equation, we calculated the changes in porosity of Caco-2 cell monolayers upon incubation with cationic G0-G4, neutral G2-G4, and anionic G-0.5 - G4.5 PAMAM dendrimers reflected by the observed changes in mannitol paracellular permeability.^{14a,b}

I.2.2 Calculation of porosity and Renkin function of Caco-2 cell monolayers

The paracellular permeability coefficient (P_p) of the diffusing mannitol molecules is given by the following equation:¹³

$$P_p = \frac{\varepsilon DF(r/R)}{\delta} \quad (2)$$

Where ε is the porosity or volume fraction of pores, $\delta = \tau \times L$ is the tortuosity (τ) times the path length across the Caco-2 cell monolayer (L , μm), D (cm^2/sec) is solutes diffusion coefficient in water at 37 °C, and $F\left(\frac{r}{R}\right)$ is the Renkin function. Equation 2 was reorganized to calculate porosity and Renkin function (Equation 3).

$$\frac{\varepsilon}{\delta} F\left(\frac{r}{R}\right) = \frac{P}{D} \quad (3)$$

We calculated the aqueous diffusion coefficient (D) of mannitol using the Stokes-Einstein relationship (equation 4).¹³

$$D = \frac{KT}{6\pi\eta r} \quad (4)$$

Where K is the Boltzmann's constant ($1.38 \times 10^{-23} \frac{\text{kg} \times \text{m}^2}{\text{s}^2 \times \text{K}}$), T is the absolute temperature used for permeability measurements and matches physiological temperature (310 K), η is the viscosity of water at 37 °C ($8.9 \times 10^{-4} \frac{\text{kg}}{\text{m} \times \text{s}}$), which is the main constituent of the HBSS buffer used in the transport experiments, and r is the radius of diffusing mannitol molecules ($4.1 \times 10^{-10} \text{m}$). We used our published mannitol permeability data to calculate the changes in porosity and Renkin function of Caco-2 cell monolayers as a function of PAMAM concentration, incubation time, generation number, and net surface charge.^{14a,b}

I.2.3 Calculation of porosity and Renkin function of Caco-2 cell monolayers based on PAMAM-NH₂ permeability

The permeability coefficient (P_p^+) of cationic molecules such as PAMAM-NH₂ is given by the following equation:

$$P_p^+ = \frac{\varepsilon DF(r/R)}{\delta} \left(\frac{\kappa}{1-e^{-\kappa}} \right) \quad (5)$$

By reorganizing Equation 5 to calculate porosity and Renkin function (Equation 6):

$$\frac{\varepsilon}{\delta} F\left(\frac{r}{R}\right) = \frac{P}{D\left(\frac{\kappa}{1-e^{-\kappa}}\right)} \quad (6)$$

We used equation 7 to calculate κ , which is a dimensionless electrochemical energy function across the tight junction pores.

$$\kappa = \frac{ez|\Delta\psi|}{KT} \quad (7)$$

Where e is the unit charge of an ion (1.602×10^{-19} Coulombs), z is the valence of the diffusing ions, $|\Delta\psi|$ is the net electrical potential across the tight junction, K is the Boltzmann's constant ($1.38 \times 10^{-23} \frac{\text{kg} \times \text{m}^2}{\text{s}^2 \times \text{K}}$), and T is the absolute temperature used for permeability measurements and matches physiological temperature (310 K).

To solve for z , we calculated the valence of different PAMAM-NH₂ generations using the Henderson-Hasselbalch equation (Equation 8).¹²

$$pH = pK_a + \log \left[\frac{base}{salt} \right] \quad (8)$$

We used the TEER values collected experimentally to calculate $|\Delta\psi|$ using equation 9:

$$|\Delta\psi| = V = IR = I \times (TEER \times A) \quad (9)$$

Where V is the voltage (volts), I is the current (Amp), R is the resistance (Ω), $TEER$ is the transepithelial electrical resistance ($\Omega \cdot \text{cm}^2$), and A is the surface area of Caco-2 cell monolayers (cm^2).

I.3 Results and Discussion

I.3.1 Calculation of effective porosity of Caco-2 cell monolayers based on mannitol permeability

Our data shows that the effective porosity of Caco-2 cell monolayers, which is the product of Renkin function $F\left(\frac{r}{R}\right)$ and the volume fraction of the paracellular pores $\frac{\varepsilon}{\delta}$ remained constant for unperturbed monolayers (**Figure I.2**). In comparison, the incubation of Caco-2 cell monolayers with 0.1 and 1.0 mM G0-NH₂ caused an increase in monolayer's effective porosity at an incubation time of 210 minutes, whereas 10 mM G0-

NH₂ caused an increase in effective porosity at all incubation time points ($p < 0.005$) (**Figure I.2A**). The incubation of Caco-2 cell monolayers with 0.1, 1.0, and 10.0 mM G1-NH₂ caused an increase in monolayer's effective porosity at all incubation time points compared to baseline porosity values ($p < 0.005$) (**Figure I.2B**). Similarly, the incubation of Caco-2 cell monolayers with 1.0 and 10.0 mM G2-NH₂ resulted in a significant increase ($p < 0.005$) in monolayer's effective porosity at 150, 180, and 210 minutes incubation times (**Figure I.2C**). G3-NH₂ produced a significant increase in the effective porosity of Caco-2 cell monolayers at all concentrations and incubation time points (**Figure I.2D**). However, the observed increase in effective porosity at an incubation time point of 210 minutes may be a result of polymer's toxicity. G4-NH₂ produced a significant increase in monolayer's effective porosity at all concentrations and incubation time points, which can be a result of the associated polymer's toxicity (**Figure I.2E**). These results collectively indicate that cationic PAMAM-NH₂ dendrimers (G0-G4) increase the effective porosity of Caco-2 cell monolayers in a concentration-, incubation time-, and generation-dependent fashion.

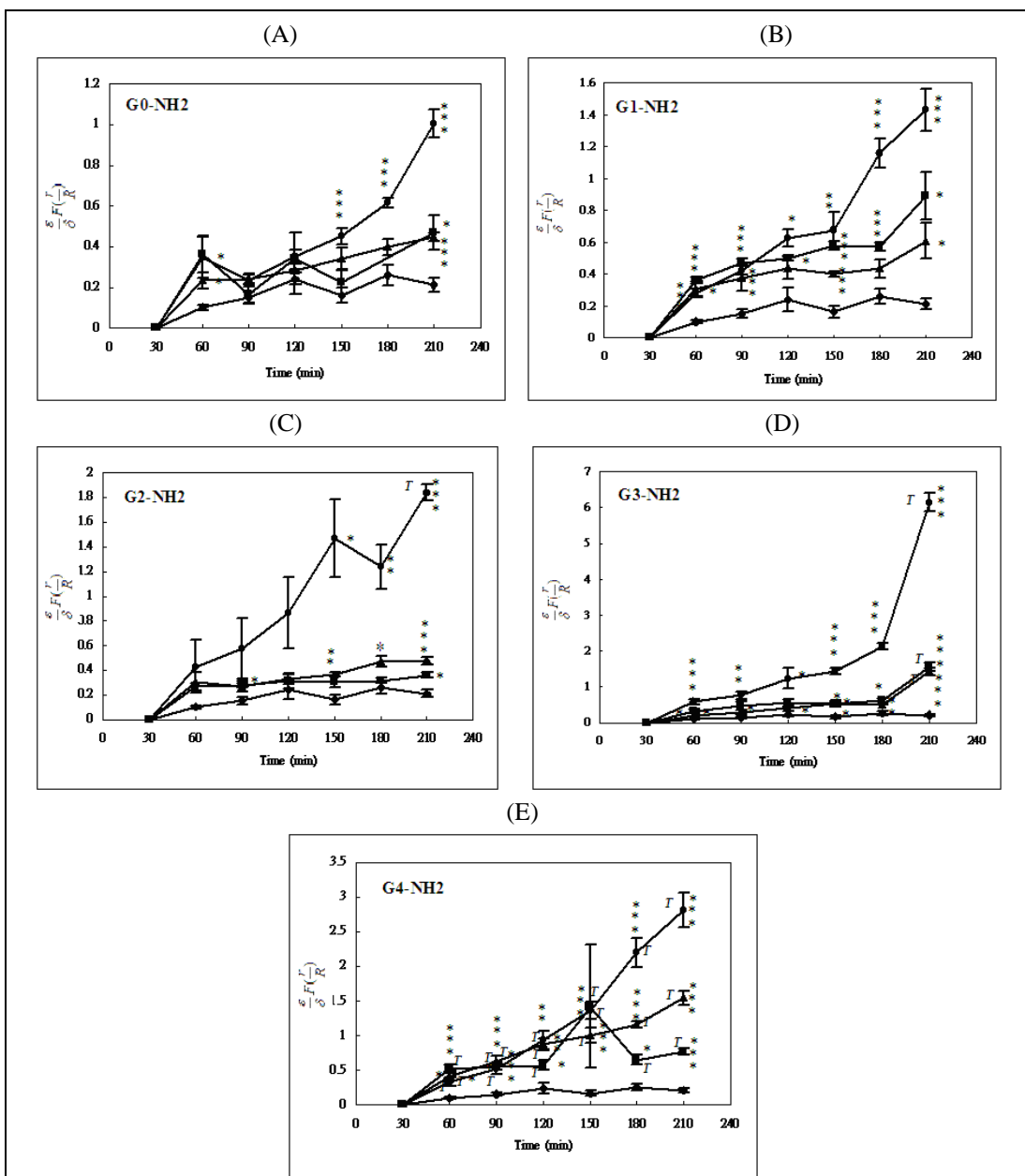


Figure I.2: Relationship between the porosity $\frac{\epsilon}{\delta} F(\frac{r}{R})$ of unperturbed Caco-2 cell monolayers (\diamond) and those incubated with 0.1 mM (\blacksquare), 1.0 mM (\blacktriangle) and 10 mM (\bullet) of PAMAM-NH₂ (G0-G4) dendrimers and the incubation time. Each data point represents the average \pm standard error of the mean of three independent measurements. Γ denotes the toxicity of PAMAM dendrimers at a specific concentration and incubation time point. The porosity of Caco-2 cell monolayers upon incubation with different concentrations of PAMAM-NH₂ dendrimers is compared to that of the unperturbed monolayer at the same incubation time point using student t -test where *, **, and *** denote $p \leq 0.05$, 0.01, and 0.005, respectively.

Anionic PAMAM-COOH dendrimers increased the effective porosity of Caco-2 cell monolayers in a concentration- and generation number-dependent fashion (**Figure I.3**). The smallest PAMAM-COOH dendrimers (G-0.5) caused no change in monolayer's porosity, whereas larger G0.5 and G1.5 caused a statistically significant increase in effective porosity at a concentration 10.0 mM and incubation times 150, 180, and 210 minutes, which can be attributed to their observed toxicity at this concentration and incubation times (**Figure I.3A-C**). G2.5 and G3.5 caused an increase in monolayer's effective porosity at short non-toxic incubation times (60, 90, and 120 minutes) and to a greater extent at longer incubation times, which proved to be toxic to Caco-2 cells (**Figure I.3D & E**). In comparison, G4.5 increased the effective porosity of Caco-2 cell monolayers only at toxic concentrations and incubation time points (**Figure I.3F**). The observed increase in effective porosity with anionic G2.5 and G3.5 PAMAM-COOH dendrimers at non-toxic concentrations and incubation time points can be attributed to their negative charge, which allows them to act as efficient Ca^{+2} ion chelators thus reducing the integrity of the tight junctions.

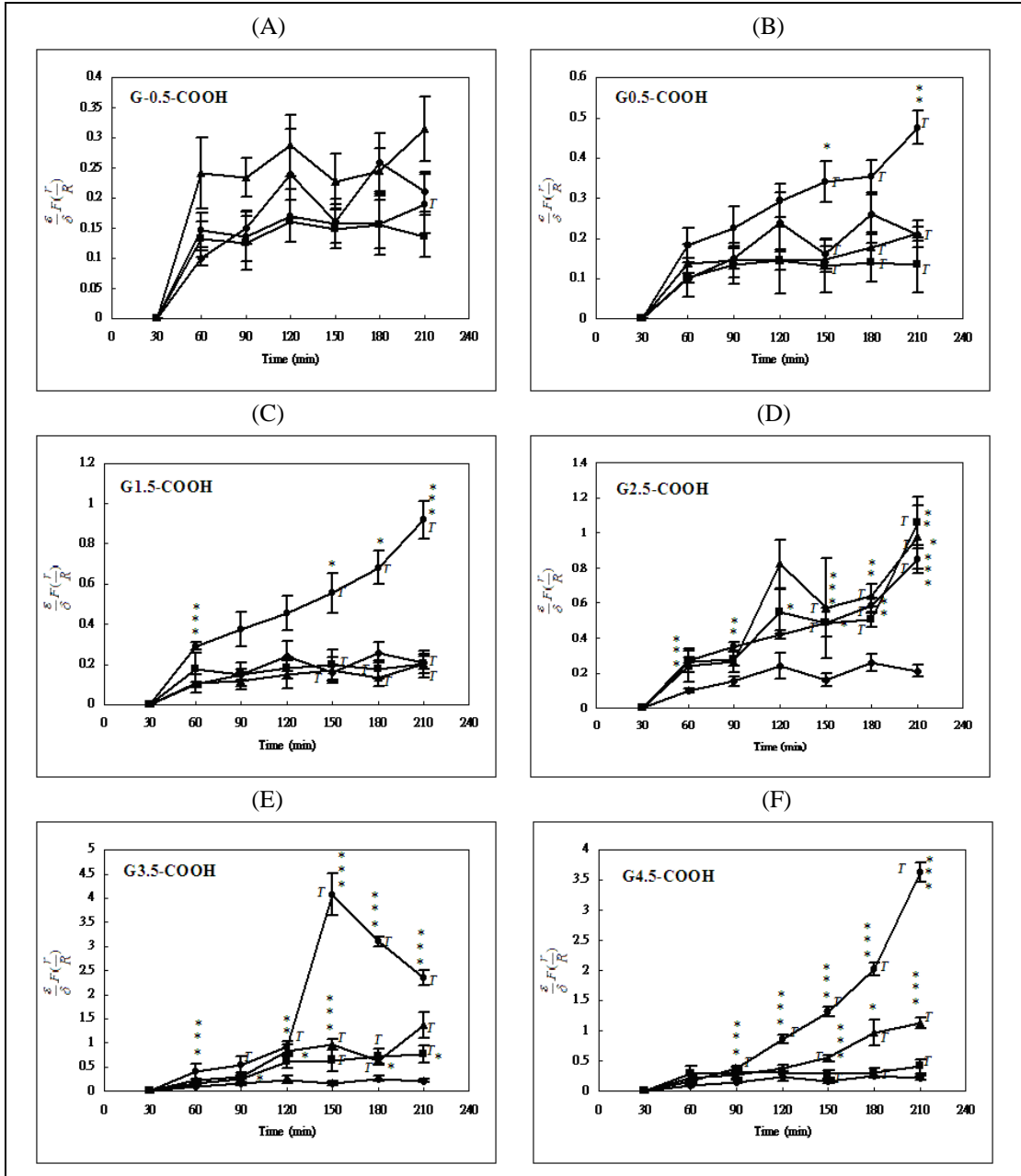
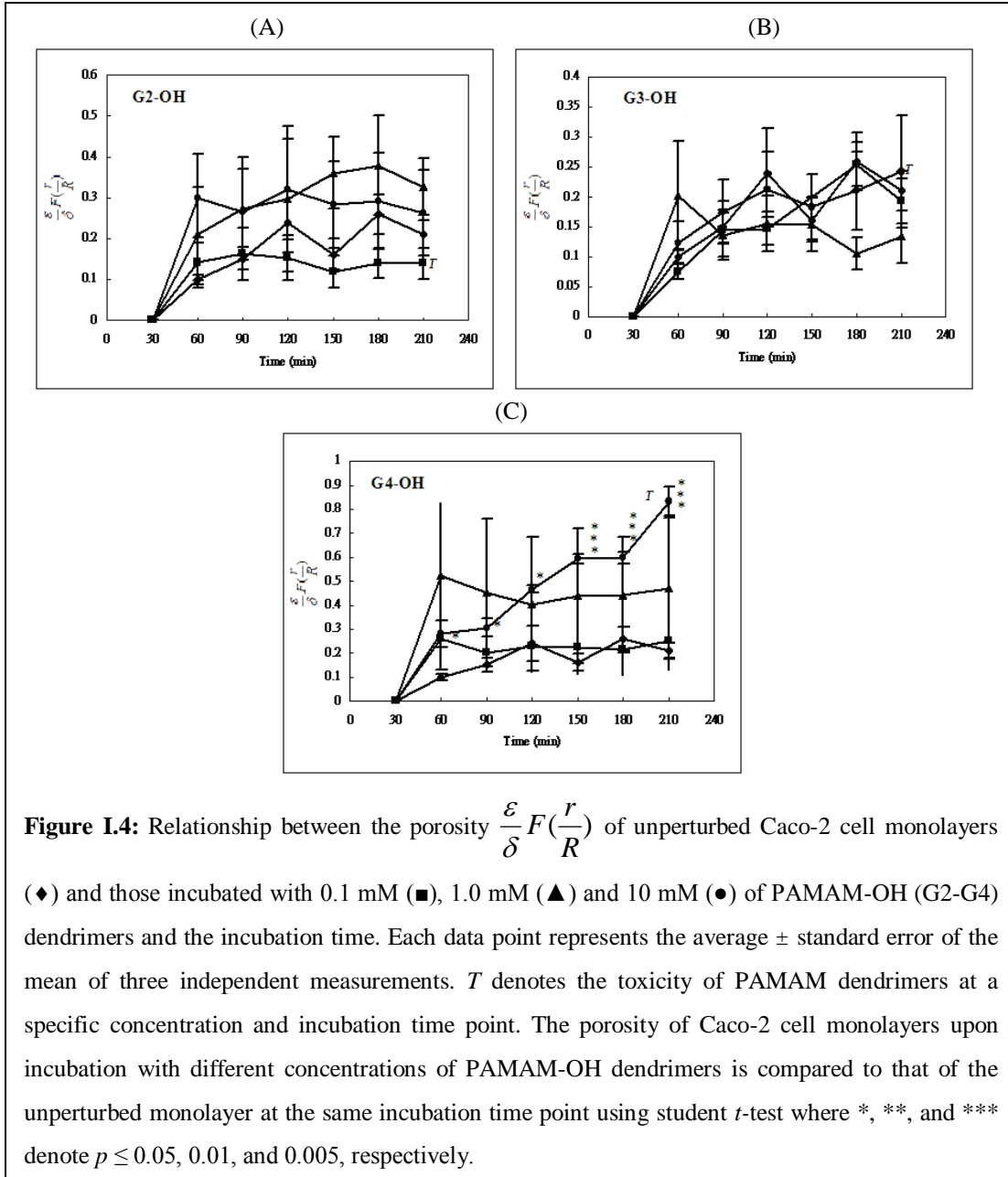


Figure I.3: Relationship between the porosity $\frac{\varepsilon}{\delta} F\left(\frac{r}{R}\right)$ of unperturbed Caco-2 cell monolayers (\diamond) and those incubated with 0.1 mM (\blacksquare), 1.0 mM (\blacktriangle) and 10 mM (\bullet) of PAMAM-COOH (G-0.5-G4.5) dendrimers and the incubation time. Each data point represents the average \pm standard error of the mean of three independent measurements. T denotes the toxicity of PAMAM dendrimers at a specific concentration and incubation time point. The porosity of Caco-2 cell monolayers upon incubation with different concentrations of PAMAM-COOH dendrimers is compared to that of the unperturbed monolayer at the same incubation time point using student t -test where *, **, and *** denote $p \leq 0.05$, 0.01, and 0.005, respectively.

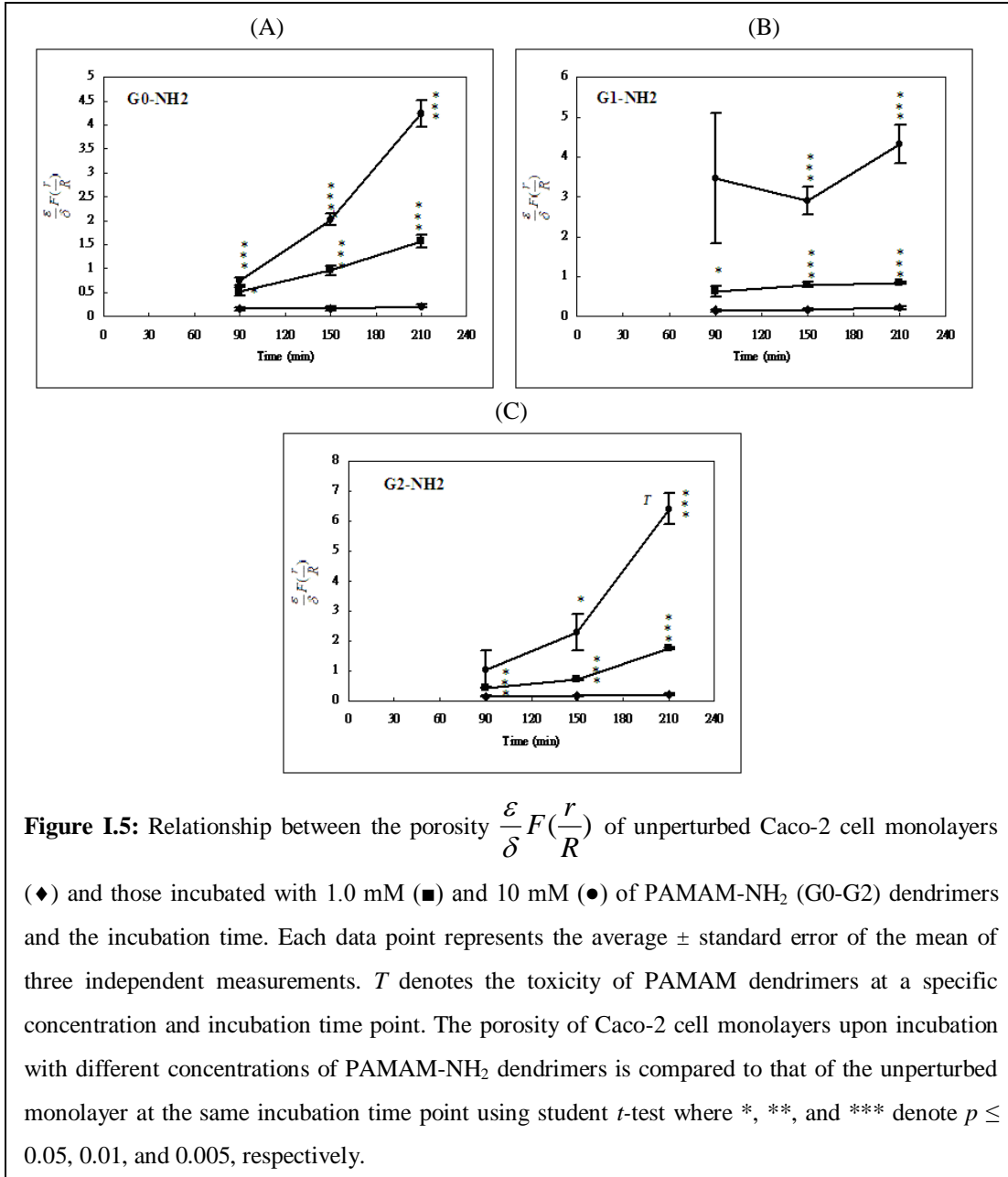
Surface chemistry and the associated charge density of PAMAM dendrimers affect the effective porosity of Caco-2 cell monolayers. Despite the similarity in size and molecular weight of G2-G4 PAMAM-OH dendrimers and PAMAM-NH₂ dendrimers, the change from NH₂ to OH surface groups affect the nature of their interaction with Caco-2 cell monolayers. At physiologic pH of 7.4, approximately 22% of the primary NH₂ surface groups will be ionized and carry a positive charge (**Table I.1**) resulting in an electrostatic interaction with the negatively charged epithelium of Caco-2 cells, which could have resulted in modulation of the tight junctions and the observed increase in monolayer's effective porosity. In comparison, neutral PAMAM-OH dendrimers (G2-G4) caused no significant changes on the effective porosity of Caco-2 cell monolayers (**Figure I.4**). These results collectively indicate that the interaction of PAMAM dendrimers with Caco-2 cell monolayers is generation size, molecular weight, and charge dependent.



I.3.2 Calculation of porosity of Caco-2 cell monolayers based on permeability of PAMAM-NH₂ dendrimers

Results show that the incubation of Caco-2 cell monolayers with 1.0 and 10.0 mM solutions of cationic PAMAM-NH₂ dendrimers (G0-G2) increased monolayer's effective

porosity in a concentration- and incubation time-dependent fashion (**Figure I.5**). G0-NH₂ caused a significant increase in effective porosity compared to that observed with mannitol, which increased with the increase in dendrimers concentration and incubation time (**Figure I.5A**). Similarly, G1-NH₂ caused an increase in monolayer's effective porosity that increased with the increase in dendrimers concentration from 1.0 to 10.0 mM (**Figure I.5B**). G2-NH₂ increased monolayer's effective porosity with the increase in dendrimers concentration and incubation time (**Figure I.5C**). By comparing the observed changes in monolayer's effective porosity with cationic G0-G2 dendrimers, the increase in generation number did not result in a parallel increase in effective porosity. This can be attributed to the fact that PAMAM dendrimers permeate across Caco-2 cell monolayers by a combination of paracellular and transcellular transport mechanisms compared to mannitol, which is transported exclusively via the paracellular route.^{14c,16}



I.4 Conclusions

Selected cationic PAMAM-NH₂ (G0-G2) and anionic PAMAM-COOH (G1.5 and G2.5) dendrimers increase the effective porosity of Caco-2 cell monolayers in a concentration-, incubation time-, surface charge, and generation-dependent fashion. This increase in

monolayer's effective porosity appears to be the primary reason for the observed increase in their permeability across Caco-2 cell monolayers. This quantitative estimation of the effect of PAMAM dendrimers on Caco-2 cell monolayers further emphasizes the potential of these selected PAMAM generations to serve as carriers for controlled oral drug delivery.

References

- (1) Lavelle, E. C. *Crit Rev Ther Drug* **2001**, *18*, 341.
- (2) (a) Delie, F.; Blanco-Prieto, M. J. *Molecules* **2005**, *10*, 65. (b) Leone-Bay, A.; Paton, D. R.; Weidner, J. J. *Medicinal Research Reviews* **2000**, *20*, 169.
- (3) Brayden, D. J.; Baird, A. W. *Adv Drug Deliver Rev* **2004**, *56*, 721.
- (4) Norris, D. A.; Puri, N.; Sinko, P. J. *Adv Drug Deliver Rev* **1998**, *34*, 135.
- (5) Tomalia, D. A.; Frechet, J. M. J. *J Polym Sci A1* **2002**, *40*, 2719.
- (6) Esfand, R.; Tomalia, D. A. *Drug Discov Today* **2001**, *6*, 427.
- (7) Tripathi, P. K.; Khopade, A. J.; Nagaich, S.; Shrivastava, S.; Jain, S.; Jain, N. K. *Pharmazie* **2002**, *57*, 261.
- (8) (a) D'Emanuele, A.; Jevprasesphant, R.; Penny, J.; Attwood, D. *J Control Release* **2004**, *95*, 447. (b) Najlah, M.; Freeman, S.; Attwood, D.; D'Emanuele, A. *Bioconjugate Chem* **2007**, *18*, 937.
- (9) (a) Najlah, M.; Freeman, S.; Attwood, D.; D'Emanuele, A. *Int J Pharm* **2006**, *308*, 175. (b) Najlah, M.; Freeman, S.; Attwood, D.; D'Emanuele, A. *Int J Pharm* **2007**, *336*, 183.
- (10) Weilun Ke, Y. Z., Rongqin Huang, Chen Jiang, Yuanying Pei *J Pharm Sci* **2007**.
- (11) Dubin, P. L.; Edwards, S. L.; Kaplan, J. I.; Mehta, M. S.; Tomalia, D.; Xia, J. L. *Anal Chem* **1992**, *64*, 2344.
- (12) El-Sayed, M.; Kiani, M. F.; Naimark, M. D.; Hikal, A. H.; Ghandehari, H. *Pharm Res* **2001**, *18*, 23.
- (13) Adson, A.; Raub, T. J.; Burton, P. S.; Barsuhn, C. L.; Hilgers, A. R.; Audus, K. L.; Ho, N. F. H. *J Pharm Sci* **1994**, *83*, 1529.
- (14) (a) El-Sayed, M.; Ginski, M.; Rhodes, C.; Ghandehari, H. *J Control Release* **2002**, *81*, 355. (b) El-Sayed, M.; Ginski, M.; Rhodes, C. A.; Ghandehari, H. *J Bioact Compat Pol* **2003**, *18*, 7. (c) El-Sayed, M.; Rhodes, C. A.; Ginski, M.; Ghandehari, H. *Int J Pharm* **2003**, *265*, 151.
- (15) Kitchens, K. M.; Kolhatkar, R. B.; Swaan, P. W.; Eddington, N. D.; Ghandehari, H. *Pharm Res* **2006**, *23*, 2818.
- (16) Kitchens, K. M.; Kolhatkar, R. B.; Swaan, P. W.; Ghandehari, H. *Mol Pharm* **2008**.
- (17) (a) Adson, A.; Burton, P. S.; Ruab, T. J.; Barsuhn, C. L.; Audus, L.; Ho, N. F. H. *Pharmaceutical Research* **1995**, *84*, 1197. (b) Knipp, G. T.; Ho, N. F. H.; Barsuhn, C. L.; Borchardt, R. T. *Journal of Pharmaceutical Sciences* **1997**, *86*, 1105. (c)

- Saitoh, R.; Sugano, K.; Takata, N.; Tachibana, T.; Higashida, A.; Nabuchi, Y.; Aso, Y. *Pharmaceutical Research* **2004**, *21*, 749.
- (18) Powell, D. W. *Am J Physiol* **1981**, *241*, G275.
- (19) Curry, F. E. In *Handbook of Physiology, Section 2, The Cardiovascular System*, 1984; Vol. IV.

Appendix II.

Visualizing the attack of RNase enzymes on dendriplexes and naked siRNA using atomic force microscopy

II.1 Introduction

Preclinical investigations showed the potential of small interfering RNA (siRNA) molecules in selectively silencing the expression of the genes implicated in the development of cancer, cardiovascular, neurodegenerative, and infectious diseases indicating their therapeutic potential.¹ siRNA molecules bind to the RNA-induced silencing complex (RISC) revealing the antisense RNA strand that selectively binds to the complementary sequence in the targeted mRNA, which triggers mRNA cleavage by the endonuclease RNase H enzymes and suppression of the translation process.² Delivery of siRNA molecules requires a biocompatible carrier to protect and shuttle the cargo into the cytoplasm of the diseased cells to produce the desired therapeutic activity both *in vitro* and *in vivo*. Many cationic peptides, lipids, and polymers have been used to condense siRNA via electrostatic interaction forming ionic complexes with variable size and surface charge, which proved effective in delivering the RNA cargo into the cytoplasm of mammalian cells *in vitro*.³ However, successful *in vivo* delivery of siRNA required the use of excess cationic carrier to shield and protect the RNA cargo against nucleases leading to non-specific distribution of the formed complexes to the reticular

endothelial system (liver, spleen, and bone marrow)⁴ and induction of toxicity,⁵ which hampered the translation of these particles into the clinic.

Poly(amidoamine), PAMAM, dendrimers are a family of water-soluble polymers that is characterized by a unique, highly-ordered, three dimensional, tree-like branching architecture with a large number of primary, secondary, and tertiary amine groups embedded in their structure, which become ionized at physiologic pH conferring a high positive charge density.⁶ PAMAM dendrimers show a controlled incremental increase in the size, molecular weight, and number of surface amine groups with the increase in their generation number (G). Steric crowding of the surface groups affects the molecular shape of PAMAM dendrimers where G0-G4 adopt an open planar and elliptical conformation whereas higher generations ($\geq G5$) are robust, non-deformable, spheroids.⁷ PAMAM dendrimers have been used to complex plasmid DNA (pDNA), antisense oligonucleotides (ASODN), and siRNA molecules into compact nanoparticles that proved to successfully escape the endosomal/lysosomal trafficking pathway through their endosomal buffering capacity known as the “proton sponge” mechanism.⁸ However, stabilization of nucleic acid cargo and successful intracellular delivery requires the use of high PAMAM dendrimer (+) to nucleic acid (-) ratio,⁹ which is often associated with destabilization of the cell membrane and non-specific toxicity.¹⁰ We are interested in formulation of compact dendriplexes that resist degradation by RNase enzymes without using excess PAMAM dendrimers to eliminate the associated toxicity.

Earlier studies showed that DNA condensation has two kinetic phases starting with an initial rapid binding (within 15 seconds) of DNA to multivalent cations followed by slower structural rearrangement that reaches an apparent equilibrium typically within 1–2

hours and exhibit insignificant changes at longer incubation times.¹¹ The effect of incubation time of cationic PAMAM dendrimers with pDNA molecules on the morphology and stability of the formed dendriplexes has been reported.¹² Briefly, incubation of G4 dendrimers with pDNA for 15 minutes resulted in formation of incomplete toroidal complexes or multimeric intermediates that resisted degradation by DNase I enzymes for 1 hour.¹² In comparison, increasing the incubation time of G4 dendrimers with pDNA to 2 hours resulted in the formation of ring-like toroidal complexes that resisted degradation by DNase I enzymes for up to 10 hours.¹² These results indicate that increasing the incubation time of cationic PAMAM dendrimers with pDNA results in formation of more compact particles that better shield the complexed DNA molecules and protect them against degradation by nuclease enzymes.

It is important to note that pDNA molecules exist in solution as long flexible chains with an average length of $\sim 1.2 \mu\text{m}$, which allow them to wrap around cationic carriers forming compact particles that resist degradation by DNase enzymes and achieve high transfection.^{5,13} In comparison, siRNA molecules are much shorter ($\sim 6 \text{ nm}$) rigid rods in solution that exhibit weak electrostatic interaction with cationic carrier, which increases their susceptibility to enzymatic attack, reduces their internalization by mammalian cells, and diminishes their net transfection.^{5,13} Further, flexibility of the cationic carrier play a critical role in governing its electrostatic binding to siRNA molecules.¹⁴ Previous computational studies showed that flexible cationic carriers assume a spherical shape with a compact core and strong orientation of the cationic surface groups toward the polynucleotides (e.g. DNA, RNA) present in solution forming individual binding points characterized by high binding strength.¹⁴ On the other hand, rigid cationic carriers form

more contact points with polynucleotides present in solution.¹⁴ These studies collectively show that both carrier flexibility and incubation time affect the morphology and enzymatic stability of the formed complexes.

In this article, we describe the complexation of anti-GAPDH siRNA molecules with G4 (flexible) and G5 (rigid) dendrimers based on the size and morphology of the formed dendriplexes at different incubation times (20 minutes and 24 hours). We also investigate the stability of the formed dendriplexes upon incubation with RNase V1 enzymes compared to naked siRNA molecules as a function of exposure time. We used atomic force microscopy (AFM) to visualize the morphology of the formed complexes and monitor the attack of RNase V1 enzymes in solution as a function of time. We relied on established AFM protocols used to study the dynamics of DNA binding to PAMAM dendrimers,^{12,15} polyethylenimine,¹⁶ and polylysine¹⁷ forming nanoparticles with different morphologies. AFM has also been used to investigate the degradation of free DNA by endonuclease and exonuclease enzymes in solution,¹⁸ which supports our study.

II.2 Experimental section

II.2.1 Materials

G4 (formula weight 14,215 Da) and G5 (formula weight 28,826 Da) with ethylene diamine cores were purchased from Dendritic Nanotechnologies, Inc. (Mount Pleasant, MI) as 10% w/v solutions in methanol. G4 and G5 solutions were dialyzed using Slide-A-Lyzer dialysis cassettes with a 7 kDa MWCO (Thermo Scientific Inc., Rockford, IL) against DI water for 24 hours to remove polymer debris. The aqueous solutions of G4 and

G5 were lyophilized and stored at 4 °C till used. Anti-GAPDH siRNA and RNase V1 enzyme were purchased from Ambion Inc. (Austin, TX).

II.2.2 Formulation of Dendriplexes

G4 and G5 dendrimers were dissolved in RNase-free water and mixed with 0.7 µg of anti-GAPDH siRNA molecules dissolved in 1 µl of RNase-free water at a nitrogen/phosphate (N/P, +/-) ratio of 2/1. Each mixture was vortexed and allowed to stand at room temperature for 20 minutes or 24 hours before loading onto a 1% w/v agarose gel containing ethidium bromide (EtBr). The gel was immersed in a Tris-acetate-EDTA (TAE) buffer and run at 60 V for 1 hour and visualized under UV exposure (Fotodyne Incorporated, Hartland, WI).

II.2.3 AFM Imaging of Dendriplexes and Naked siRNA

All AFM images were acquired using Nanoscope III MultiMode AFM with a sharp nitride lever (Veeco, Santa Barbra, CA) in the tapping mode at a 256 x 256 pixel resolution. Selected fields were scanned at scan rates ranging from 3-4 Hz where each image was acquired within 90 seconds and tapping frequencies ranged from 8-10.5 kHz in solution. Images were flattened to account for Z offsets and sample tilts. Tapping set points were selected close to the free oscillation amplitude to reduce forces exerted on the interfacial species. All imaging experiments started with scanning the mica substrate in DI water to confirm the absence of any adsorbed contaminants. Naked anti-GAPDH siRNA was imaged using 30 µl of siRNA solution (3.92 µg/ml) in 1mM PBS containing 2mM MgCl₂ where MgCl₂ ions would allow weak adsorption of anionic siRNA molecules to the negatively charged mica surface through electrostatic interaction following established protocols.¹⁹ Similarly, 30 µl of G4 and G5 dendriplexes were added

to freshly cleaved mica and covered with the liquid cell. A 20 μ l aliquot of the solution in the liquid cell was replaced with 20 μ l of RNase V1 enzyme (6.6 U/ml) diluted with 1 mM PBS of pH 7.4 to examine the effect of RNase enzyme on free siRNA and the dendriplexes. Imaging of naked siRNA and the dendriplexes started immediately after adding their solutions to mica surface with continuous recording for at least 5 minutes after visualizing each subject to allow thorough investigation of the morphology before the treatment with RNase V1 enzymes. Naked siRNA and dendriplexes were also imaged after the addition of RNase V1 enzymes as a function of time.

II.3 Results

II.3.1 Formulation of G4 and G5 Dendriplexes

Both G4 and G5 dendrimers successfully complexed the loaded anti-GAPDH siRNA molecules (0.7 μ g) at an N/P (+/-) ratio of 2/1 via the electrostatic interaction between the cationic amine groups (N) and the anionic phosphate groups (P). The gel image shows that siRNA molecules were retained in the wells after mixing with G4 and G5 dendrimers for 20 minutes and 24 hours indicating rapid condensation of the loaded siRNA molecules by the cationic carriers (**Figure II.1**).

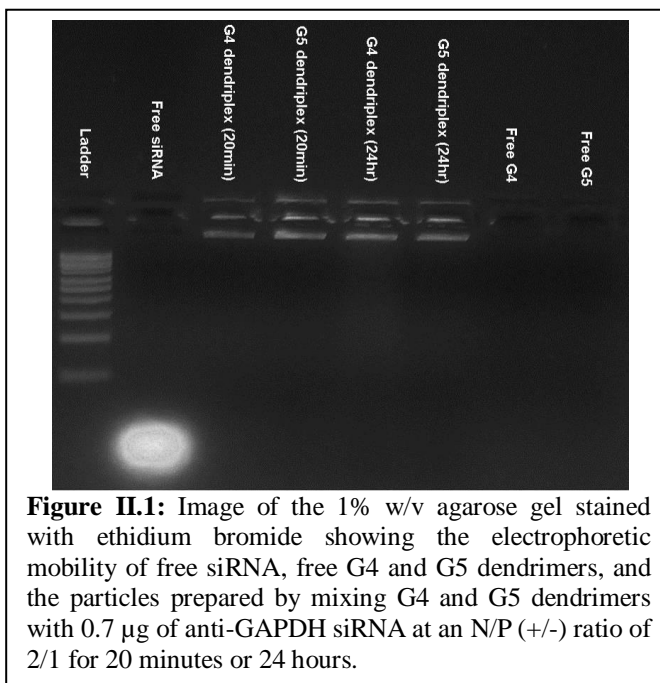
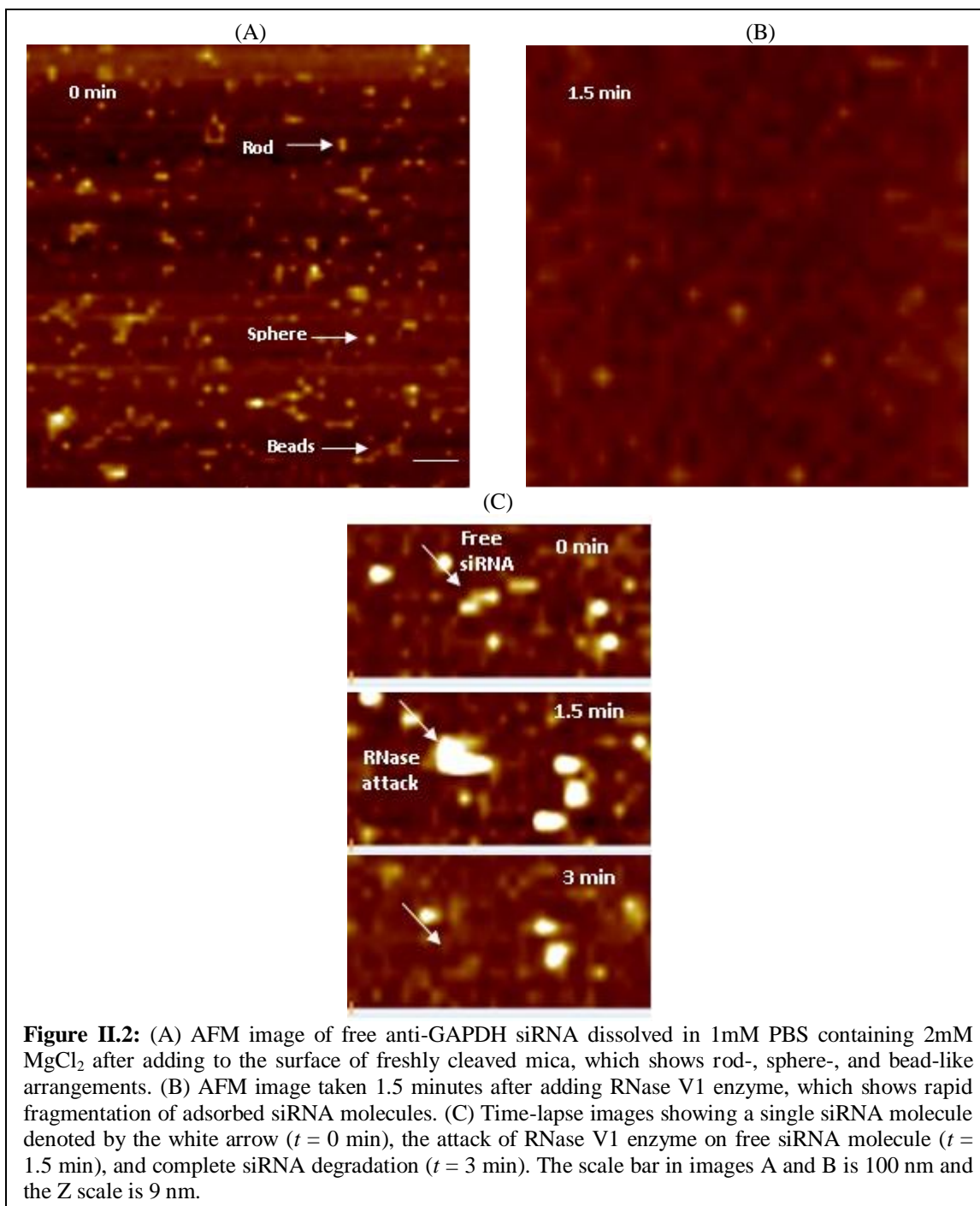


Figure II.1: Image of the 1% w/v agarose gel stained with ethidium bromide showing the electrophoretic mobility of free siRNA, free G4 and G5 dendrimers, and the particles prepared by mixing G4 and G5 dendrimers with 0.7 μ g of anti-GAPDH siRNA at an N/P (+/-) ratio of 2/1 for 20 minutes or 24 hours.

II.3.2 Effect of RNase Enzyme on Free siRNA

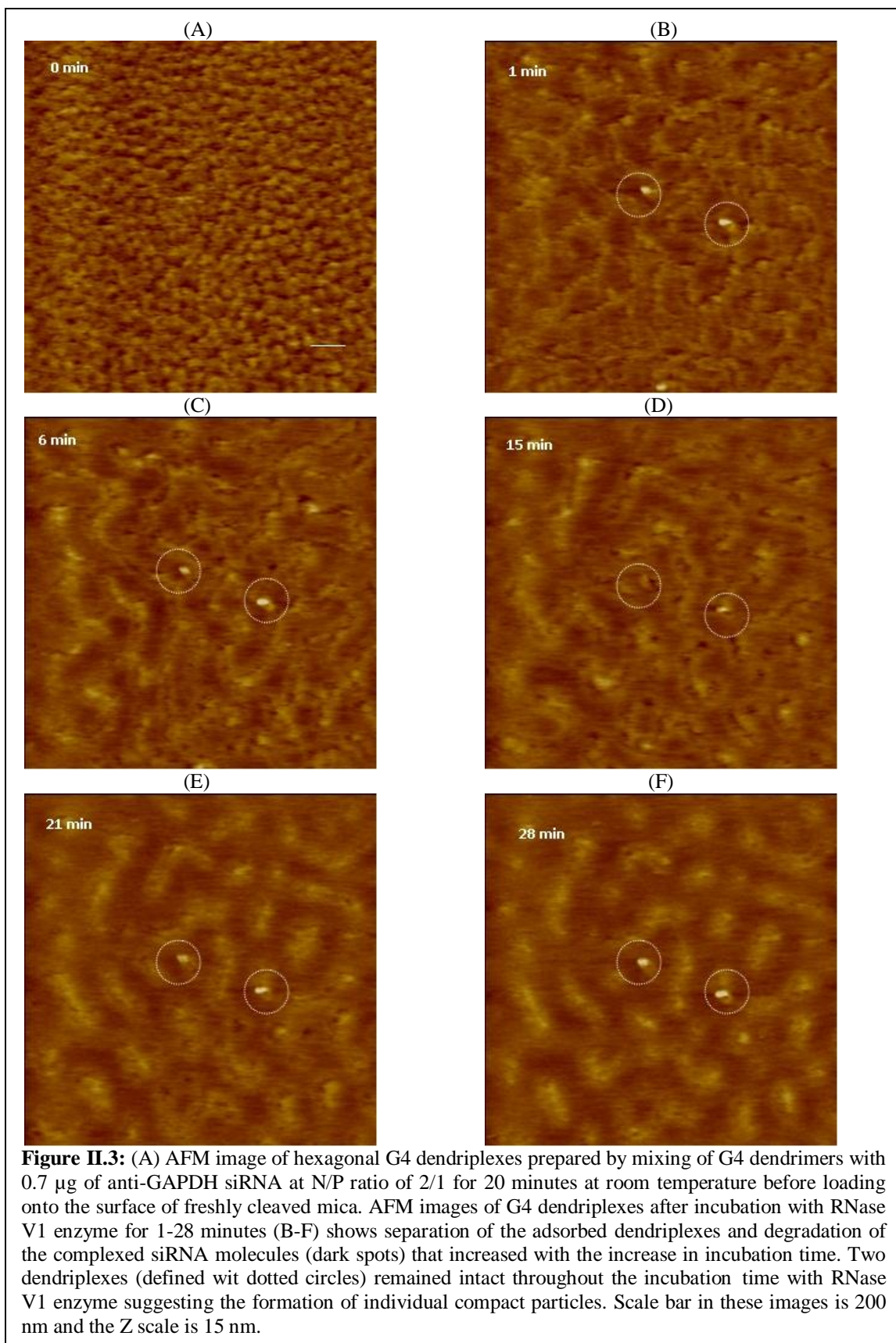
AFM images show that free siRNA molecules added to freshly cleaved mica appear as short rods, spheres, or threaded beads (**Figure II.2A**). The average diameter of siRNA spheres is 18.3 ± 3.1 nm while the average length of the rod- and bead-like features is 12.1 ± 0.6 and 51 ± 12.4 nm, respectively. These rod-, sphere-, and bead-like particles are probably formed via electrostatic interaction between cationic Mg^{+2} ions and multiple anionic siRNA molecules.¹² AFM images show that treatment of free siRNA molecules adsorbed to mica surface with RNase V1 enzyme results in their fragmentation within 1.5 minutes due to rapid and unrestricted access of the enzyme to RNA surface (**Figure II.2B**). Time-lapse images clearly show individual siRNA molecule adsorbed to mica surface denoted by the white arrow before the addition of RNase V1 enzyme (i.e. $t = 0$ minutes) (**Figure II.2C**). RNase V1 enzyme was visualized after 1.5 minutes of adding the enzyme solution to free siRNA, which caused complete degradation of adsorbed siRNA molecule within 3 minutes (**Figure II.2C**). These images clearly show rapid accessibility of RNase V1 enzyme to free siRNA molecules leading to their degradation, which is consistent with earlier results.^{12,20}



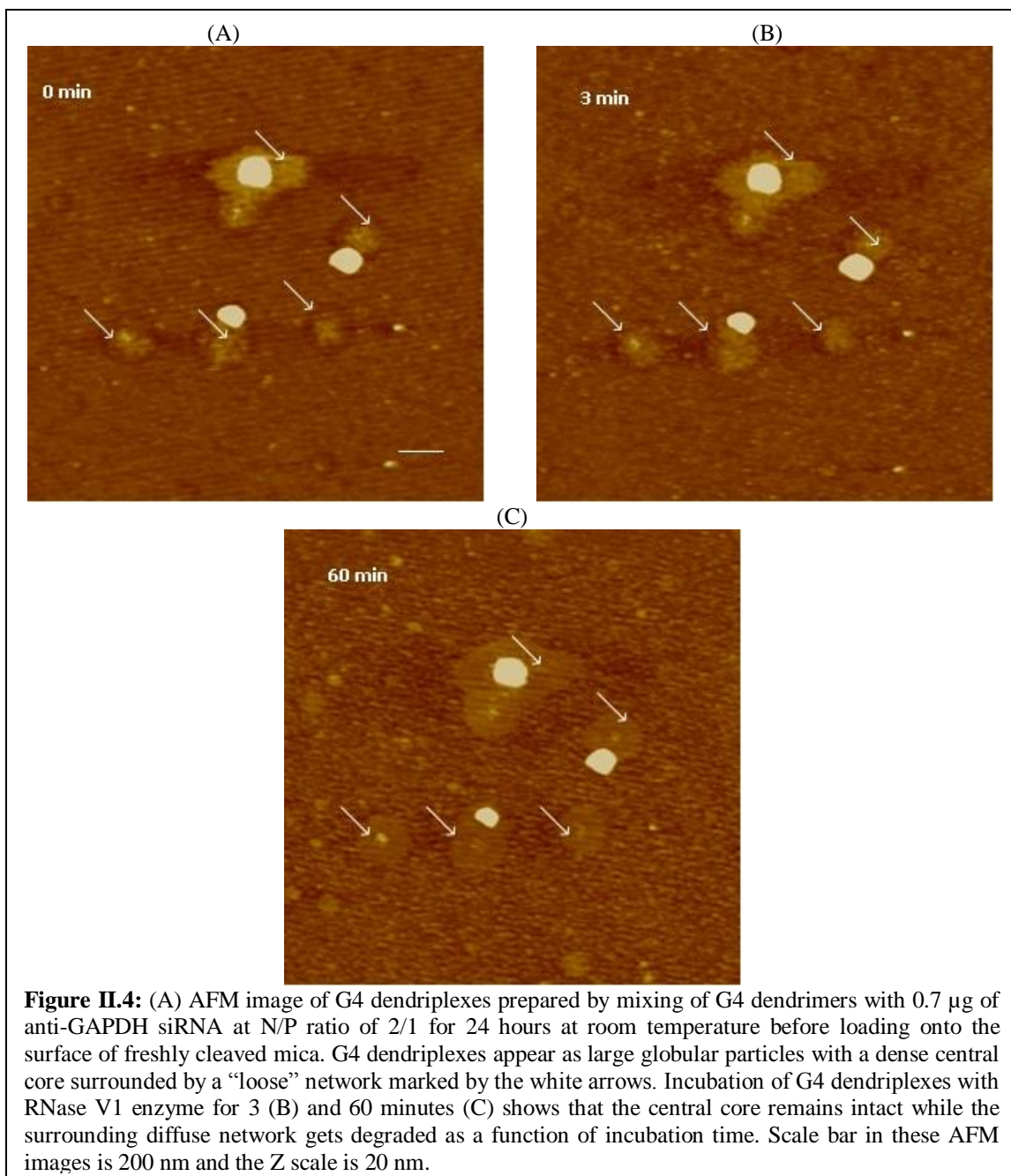
II.3.3 Effect of RNase Enzyme on G4 Dendriplexes

Incubation of G4 dendrimers with anti-GAPDH at an N/P ratio of 2/1 for 20 minutes yielded dendriplexes that were visualized using AFM (**Figure II.3**). AFM images show

that G4 dendriplexes are compact hexagonal particles with an average full width of 43 ± 19.3 nm at half the maximum height and an average height of 0.63 ± 0.025 nm (Figure II.3A). Our preliminary studies indicated the difficulty in imaging individual G4 dendriplexes and individual siRNA fragments released upon incubation with RNase V1 enzyme at different time points. Therefore, we investigated the effect of RNase V1 enzyme on a monolayer of G4 dendriplexes covering an entire AFM imaging field before and after enzyme addition instead of trying to image an individual particle. AFM images show that G4 dendriplexes formed a densely packed monolayer on freshly cleaved mica surface before the addition of RNase V1 enzyme (Figure II.3A). However, addition of RNase V1 enzyme separated the imaging field into bright spots where intact hexagonal G4 dendriplexes were located and dark spots where the particles got detached and the complexed siRNA was degraded within 1 minute (Figure II.3B). AFM images show that increasing the incubation time (6, 15, 21, and 28 minutes) with RNase enzyme increased siRNA degradation shown by the increase in the fraction of dark spots in the imaging field (Figure II.3C-F). Figure 3, Panels B-F show two large G4 dendriplexes marked by the dashed circles with heights of 9.4 and 7.6 nm and diameters of 151 and 110 nm from left to right. These complexes remained intact throughout the incubation time (28 minutes) with RNase V1 enzyme indicating better shielding of their RNA cargo compared to the bulk of G4 dendriplexes.



In comparison, G4 dendriplexes prepared by mixing of G4 dendrimers with anti-GAPDH siRNA at an N/P ratio of 2/1 for 24 hours appeared as large globular particles with a dense central core surrounded by “loose” network (**Figure II.4**). AFM images show that the average diameter of the tightly-packed core is 263 ± 60 nm with an average height of 35.3 ± 8.6 nm (**Figure II.4A**). Time-lapse AFM images show that incubation of these G4 dendriplexes with RNase V1 enzyme did not affect the compact central core for up to 60 minutes (**Figure II.4B & C**). However, the network surrounding the core fragmented gradually with the increase in incubation time with RNase V1 enzyme indicated by the reduction in their height from 12.3 ± 1.2 nm to 3.4 ± 1.5 nm (**Figure II.4B & C**). These results clearly show that increasing the incubation time of anti-GAPDH siRNA with G4 dendrimers from 20 minutes to 24 hours results in the formation of larger and more tightly-packed complexes that resist enzymatic degradation by RNase enzymes. These results are supported by previous studies indicating that complexation of siRNA molecules with G4 dendrimers is a biphasic process that starts with an initial exothermic binding process followed by secondary endothermic formation of larger dendriplex aggregates.²¹



II.3.4 Effect of RNase Enzyme on G5 Dendriplexes

Similarly, incubation of G5 dendrimers with anti-GAPDH at an N/P ratio of 2/1 for 20 minutes yielded compact hexagonal dendriplexes that formed a densely packed monolayers on the surface of freshly cleaved mica with an average full width of 62 ± 8.3 nm at half the maximum height and an average height of 1.1 ± 0.05 nm (**Figure II.5A**).

Addition of RNase V1 enzyme to the dendriplexes monolayer separated the imaging field into bright spots where intact hexagonal G5 complexes were located and dark spots where the particles got detached and the complexed siRNA was degraded (**Figure II.5B-D**). AFM images show that increasing the incubation time (1, 4, and 16 minutes) with RNase enzyme increased siRNA degradation shown by the increase in the fraction of dark spots in the imaging field (**Figure II.5B-D**). Increasing G5 incubation time with anti-GAPDH siRNA to 24 hours increased the width of the formed complexes to 48.3 ± 2.5 nm at half the maximum height and the average height to 2.1 ± 0.2 nm (**Figure II.6A**). Despite of the smaller size of G5 dendriplexes, they remained intact upon incubation with RNase V1 enzyme for up to 60 minutes (**Figure II.6B & C**) confirming that longer incubation time results in formation of tightly packed and more stable complexes.

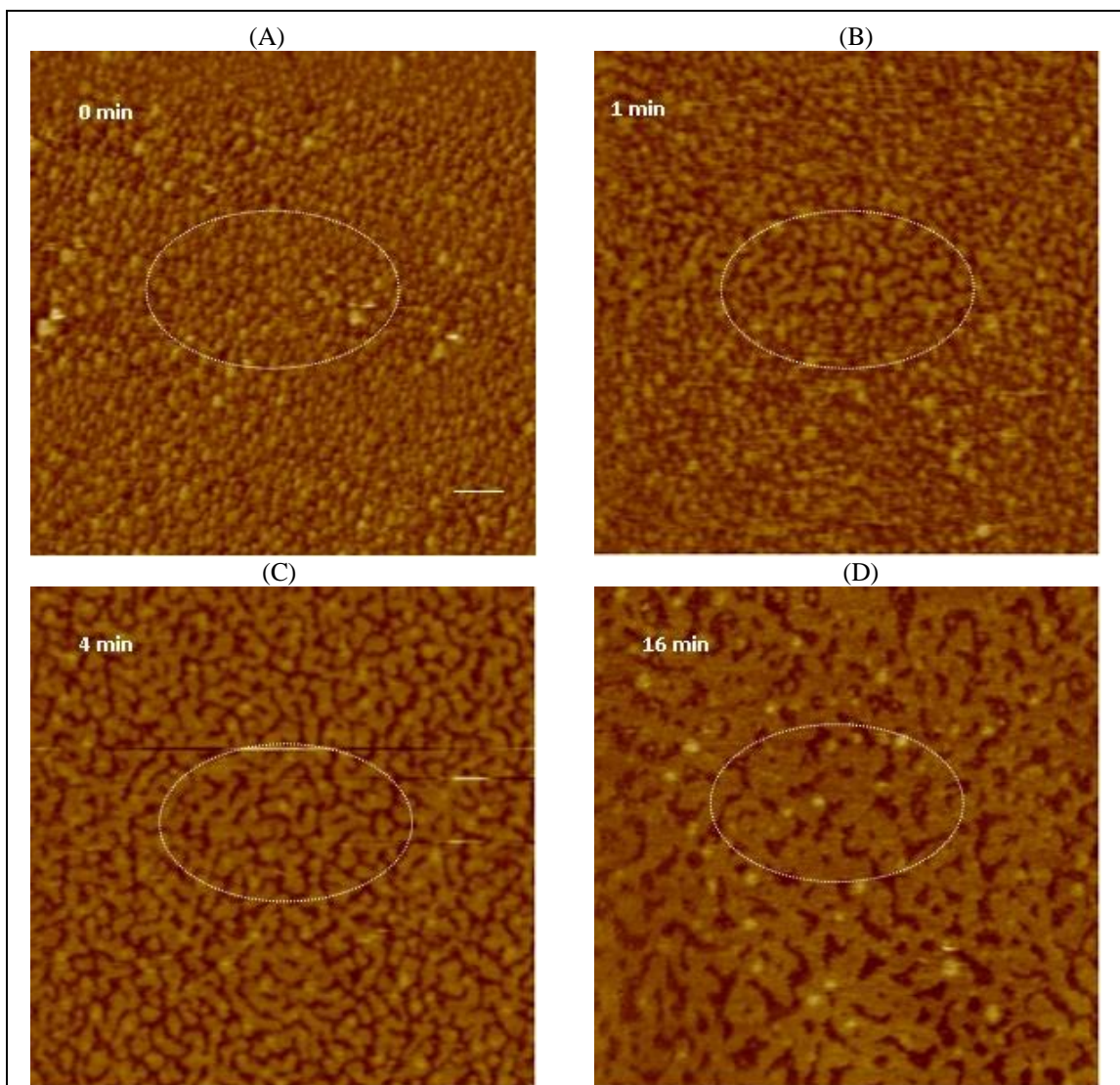
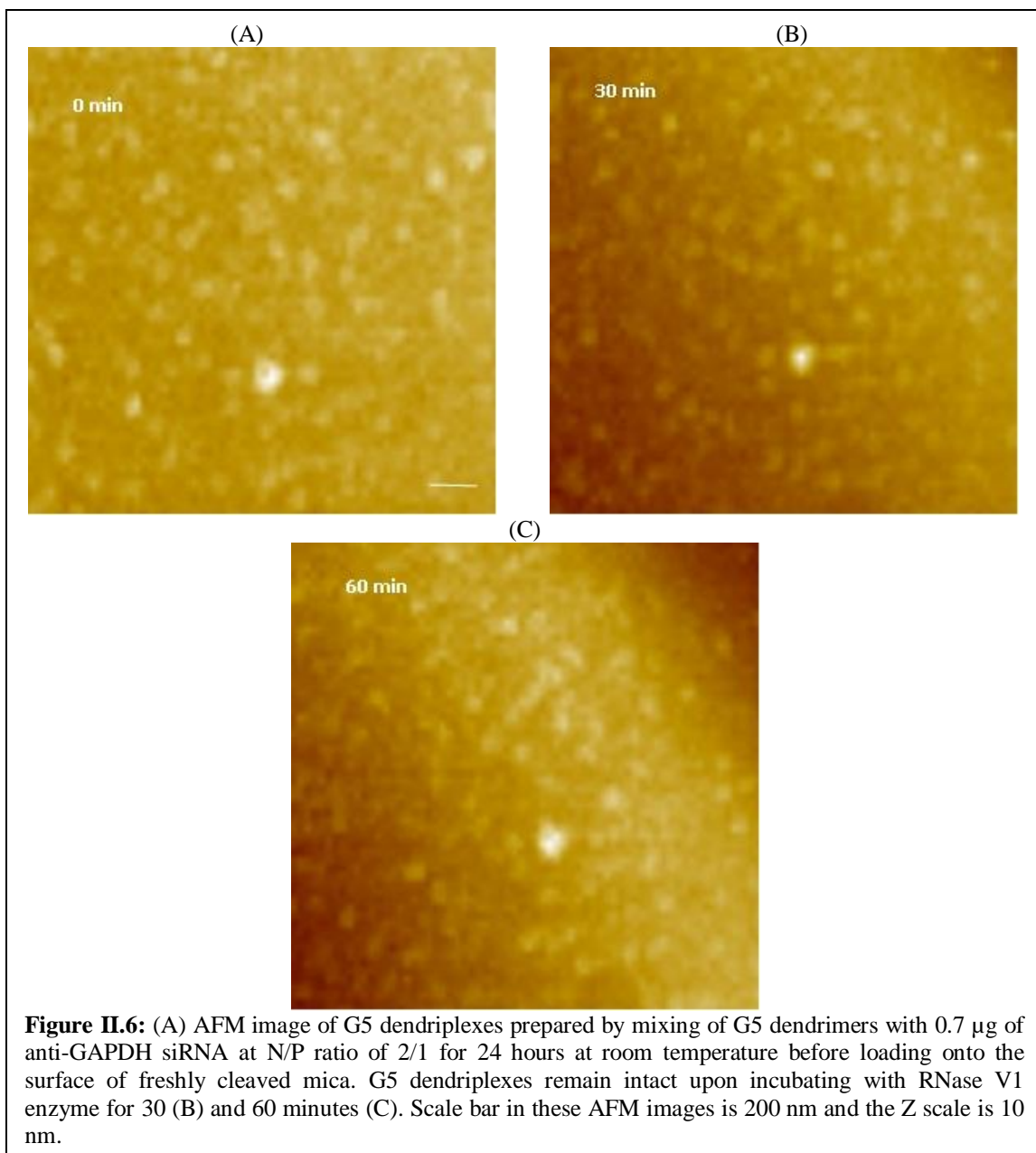


Figure II.5: (A) AFM image of hexagonal G5 dendriplexes prepared by mixing of G5 dendrimers with 0.7 μg of anti-GAPDH siRNA at N/P ratio of 2/1 for 20 minutes at room temperature before loading onto the surface of freshly cleaved mica. AFM images of G5 dendriplexes after incubation with RNase V1 enzyme for 1-16 minutes (B-D) shows separation of the adsorbed dendriplexes and degradation of the complexed siRNA molecules (dark spots) that increased with the increase in incubation time. Scale bar in these images is 200 nm and the Z scale is 17 nm.



II.4 Discussion

Particles prepared by ionic complexation of PAMAM dendrimers with siRNA molecules were examined using AFM under air-dry conditions.²⁰ However, it is critical to evaluate the morphology of such complexes under physiologically-relevant conditions, which will impact complex stability against enzymatic attack, interaction with different cells,

internalization mechanism, and overall transfection capacity. Therefore, we decided to visualize naked siRNA and G4 and G5 dendriplexes in solution using AFM, which will eliminate the destructive effect observed upon imaging biological samples in air.^{12,22} Imaging naked siRNA or G4 and G5 dendriplexes in solution in presence or absence of RNase V1 enzyme proved challenging due to free mobility of these particles in solution. To address this issue, we used small divalent Mg^{+2} cations to allow weak electrostatic adsorption of free siRNA and G4/G5 particles to mica's surface following previously published protocols.¹⁹ We applied weak forces (pico Newtons) by the tip of the AFM imaging probe to avoid delocalizing the examined samples coupled with changing the X and Y offsets as needed to track the moving features within the imaging field as previously reported.^{12,23} We also used a fast scanning speed (90 seconds/image) to avoid repelling the imaging tip by the examined sample.^{12,23} These settings allowed us to visualize free siRNA molecules, G4 and G5 dendriplexes, and the attack by RNase V1 enzyme in solution.

AFM images show that despite the difference in size, number of cationic amine groups, and flexibility of G4 and G5 dendrimers, they formed similar hexagonal particles when incubated for 20 minutes with anti-GAPDH siRNA (Figure II.3A & Figure II.5A). Increasing the incubation time of G4 and G5 dendrimers with anti-GAPDH siRNA to 24 hours produced larger dendriplexes compared to those observed at shorter incubation time point (Figure II.4A & Figure II.6A). However, G5 formed smaller dendriplexes compared to G4, which can be explained by the fact that G5 has twice the number of cationic amine groups (+) compared to G4. Therefore, the number of G5 particles used to complex 0.7 μ g of anti-GAPDH siRNA is half the number of G4 particles used to

complex the same amount of RNA. The relatively smaller number of G5 particles coupled with their established rigidity compared to G4 makes it harder for siRNA molecules to form intra-molecular bridges between multiple G5 particles via electrostatic interaction, which reduced the size of the formed dendriplexes. This is further confirmed by the absence of the loose network observed with G4 dendriplexes (Figure II.4A). These images indicate that complexation of anti-GAPDH siRNA to G4 and G5 dendrimers is a biphasic process that starts with a rapid exothermic binding forming “loose” dendriplexes followed by a slow endothermic formation of highly compacted complexes similar to previous reports.^{12,14,21,24} Further, the observed rapid degradation of G4 and G5 dendriplexes prepared within a short incubation time (20 minutes) indicates the G4 and G5 dendrimers could not “shield” the cleavage sites of the complexed RNA molecules from the RNase V1 enzyme (Figure II.3B-D& Figure II.5B-D). In comparison, formation of compact particles at longer incubation time proved effective in shielding and protecting the loaded RNA from the attack of RNase V1 enzyme (**Figure II.4 & Figure II.6**).

II.5 Conclusions

AFM images show that increasing the incubation time of G4 and G5 dendrimers with siRNA molecules to 24 hours results in formation of ionic complexes that can protect the loaded RNA cargo against enzymatic degradation without using excess cationic dendrimers. Further, the size of the formed complexes can be tuned by controlling the flexibility of the cationic carrier with flexible G4 forming larger particles than the more rigid G5 dendrimers while maintaining the desired enzymatic stability. These findings provide insight on potential formulation strategies to develop enzymatically-resistant complexes with tunable size for enhanced intracellular delivery of therapeutic siRNA

molecules without inducing undesirable side effects due to the use of excess cationic carrier.

References

- (1) (a) de Fougerolles, A.; Vornlocher, H. P.; Maraganore, J.; Lieberman, J. *Nat Rev Drug Discov* **2007**, *6*, 443. (b) Hassan, A. *Recent Pat Cardiovasc Drug Discov* **2006**, *1*, 141. (c) Koutsilieri, E.; Rethwilm, A.; Scheller, C. *J Neural Transm Suppl* **2007**, 43. (d) Zhang, J.; Wu, Y. O.; Xiao, L.; Li, K.; Chen, L. L.; Sirois, P. *Mol Biotechnol* **2007**, *37*, 225.
- (2) (a) Eccleston, A.; Eggleston, A. K. *Nature* **2004**, *431*, 337. (b) Elbashir, S. M.; Harborth, J.; Lendeckel, W.; Yalcin, A.; Weber, K.; Tuschl, T. *Nature* **2001**, *411*, 494. (c) Riddihough, G. *Science* **2005**, *309*, 1816.
- (3) (a) El-Sayed, M. E. H.; Hoffman, A. S.; Stayton, P. S. *Expert Opin Biol Th* **2005**, *5*, 23. (b) Fattal, E.; Nir, S.; Parente, R. A.; Szoka, F. C., Jr. *Biochemistry* **1994**, *33*, 6721. (c) Funhoff, A. M.; van Nostrum, C. F.; Lok, M. C.; Kruijtzter, J. A.; Crommelin, D. J.; Hennink, W. E. *J Control Release* **2005**, *101*, 233. (d) Lee, H.; Jeong, J. H.; Park, T. G. *J Control Release* **2001**, *76*, 183. (e) Yessine, M. A.; Leroux, J. C. *Adv Drug Deliver Rev* **2004**, *56*, 999.
- (4) Forrest, M. L.; Koerber, J. T.; Pack, D. W. *Bioconjugate Chem* **2003**, *14*, 934.
- (5) Gary, D. J.; Puri, N.; Won, Y. Y. *J Control Release* **2007**, *121*, 64.
- (6) (a) Frechet, J. M. J. *Science* **1994**, *263*, 1710. (b) Ottaviani, M. F.; Turro, N. J.; Jockusch, S.; Tomalia, D. A. *J Phys Chem-US* **1996**, *100*, 13675.
- (7) (a) Naylor, A. M.; Goddard, W. A.; Kiefer, G. E.; Tomalia, D. A. *J Am Chem Soc* **1989**, *111*, 2339. (b) Zeng, F. W.; Zimmerman, S. C. *Chem Rev* **1997**, *97*, 1681.
- (8) (a) Haensler, J.; Szoka, F. C., Jr. *Bioconjug Chem* **1993**, *4*, 372. (b) Kukowska-Latallo, J. F.; Bielinska, A. U.; Johnson, J.; Spindler, R.; Tomalia, D. A.; Baker, J. R., Jr. *Proc Natl Acad Sci U S A* **1996**, *93*, 4897. (c) Kukowska-Latallo, J. F.; Raczka, E.; Quintana, A.; Chen, C.; Rymaszewski, M.; Baker, J. R., Jr. *Hum Gene Ther* **2000**, *11*, 1385.
- (9) Wagner, E.; Kloeckner, J. *Adv Polym Sci* **2006**, *192*, 135.
- (10) Boeckle, S.; von Gersdorff, K.; van der Piepen, S.; Culmsee, C.; Wagner, E.; Ogris, M. *J Gene Med* **2004**, *6*, 1102.
- (11) Bloomfield, V. A. *Biopolymers* **1997**, *44*, 269.
- (12) Abdelhady, H. G.; Allen, S.; Davies, M. C.; Roberts, C. J.; Tendler, S. J. B.; Williams, P. M. *Nucleic Acids Res* **2003**, *31*, 4001.
- (13) Spagnou, S.; Miller, A. D.; Keller, M. *Biochemistry* **2004**, *43*, 13348.
- (14) Pavan, G. M.; Mintzer, M. A.; Simanek, E. E.; Merkel, O. M.; Kissel, T.; Danani, A. *Biomacromolecules* **2010**, *11*, 721.
- (15) Bielinska, A. U.; KukowskaLatallo, J. F.; Baker, J. R. *Bba-Gene Struct Expr* **1997**, *1353*, 180.
- (16) Shim, M. S.; Wang, X.; Ragan, R.; Kwon, Y. J. *Microsc Res Techniq* **2010**, *73*, 845.
- (17) Hansma, H. G.; Golan, R.; Hsieh, W.; Lollo, C. P.; Mullen-Ley, P.; Kwoh, D. *Nucleic Acids Res* **1998**, *15*, 2481.
- (18) (a) Bezanilla, M.; Drake, B.; Nudler, E.; Kashlev, M.; Hansma, P. K.; Hansma, H. G. *Biophys J* **1994**, *67*, 2454. (b) Hori, K.; Takahashi, T.; Okada, T. *Eur biophys j* **1998**, *27*, 63.
- (19) Hansma, H. G.; Laney, D. E. *Biophys J* **1996**, *70*, 1933.

- (20) Perez, A. P.; Romero, E. L.; Morilla, M. J. *Int J Pharmaceut* **2009**, *380*, 189.
- (21) (a) Jensen, L. B.; Mortensen, K.; Pavan, G. M.; Kasimova, M. R.; Jensen, D. K.; Gadzhyeva, V.; Nielsen, H. M.; Foged, C. *Biomacromolecules* **2010**, *11*, 3571. (b) Jensen, L. B.; Pavan, G. M.; Kasimova, M. R.; Rutherford, S.; Danani, A.; Nielsen, H. M.; Foged, C. *Int J Pharmaceut* **2011**, *416*, 410.
- (22) (a) Ellis, J. S.; Abdelhady, H. G.; Allen, S.; Davies, M. C.; Roberts, C. J.; Tandler, S. J. B.; Williams, P. M. *J Microsc-Oxford* **2004**, *215*, 297. (b) Putman, C. A. J.; Vanderwerf, K. O.; Degrooth, B. G.; Vanhulst, N. F.; Greve, J. *Appl Phys Lett* **1994**, *64*, 2454.
- (23) Abdelhady, H. G.; Allen, S.; Ebbens, S. J.; Madden, C.; Patel, N.; Roberts, C. J.; Zhang, J. X. *Nanotechnology* **2005**, *16*, 966.
- (24) (a) Karatasos, K.; Posocco, P.; Laurini, E.; Pricl, S. *Macromol Biosci* **2012**, *12*, 225. (b) Merkel, O. M.; Mintzer, M. A.; Librizzi, D.; Samsonova, O.; Dicke, T.; Sproat, B.; Garn, H.; Barth, P. J.; Simanek, E. E.; Kissel, T. *Mol Pharmaceut* **2010**, *7*, 969.